

Understanding and ameliorating perturbations of human cerebral energy metabolism after major trauma



Matthew George Stovell
Christ's College

Division of Neurosurgery,
Department of Clinical Neurosciences
University of Cambridge

This thesis is submitted for the degree of Doctor of Philosophy

January 2020

Declaration

This dissertation is my own work and contains nothing which is the outcome of work done in collaboration with others, except as specified in the text and Acknowledgements.

It is not substantially the same as any that I have submitted, or, is being concurrently submitted for a degree or diploma or other qualification at the University of Cambridge or any other University or similar institution except as declared in the Preface and specified in the text. I further state that no substantial part of my dissertation has already been submitted, or, is being concurrently submitted for any such degree, diploma or other qualification at the University of Cambridge or any other University or similar institution except as declared in the Preface and specified in the text

It does not exceed the prescribed word limit for the School of Clinical Medicine.

Research dissertation

Understanding and ameliorating perturbations of human cerebral energy metabolism after major trauma

Matthew George Stovell

Christ's College, Cambridge

Summary

After sustaining a severe traumatic brain injury (TBI) dysfunction of cerebral energy metabolism can cause further injury to the traumatised brain – resulting in worse patient morbidity, or death. Using the modalities of cerebral microdialysis, ^{13}C labelled high-resolution nuclear magnetic resonance (NMR) and *in-vivo* ^{31}P magnetic resonance spectroscopy (MRS) I have furthered our understanding of perturbations in human brain energy metabolism in the acute phase of a major traumatic brain injury. Furthermore, I have explored whether increasing the amount or changing the type of substrate available to the traumatised brain improves its energy metabolism.

Study I (Chapter 3): I studied the effect of supplementing the traumatised human brain with glucose at high-physiological and supra-physiological concentrations.

Study II (Chapter 4): I defined the optimum parameters for acquiring and analysing *in-vivo* ^{31}P magnetic resonance spectra in acute TBI patients.

Study III (Chapter 5): I studied the effect of acute major TBI on brain energy state and 'whole brain' pH using ^{31}P magnetic resonance spectroscopy, and how this relates to patient outcome.

Study IV (Chapter 6): I studied the effect of sodium succinate supplementation to the traumatised brain's energy state using ^{31}P magnetic resonance spectroscopy, and how this relates to the brain's extracellular ratio of lactate to pyruvate.

Study V (Chapter 7): I studied the diffusion of small molecules from cerebral microdialysis catheters in the human brain using a gadolinium-based contrast agent and magnetic resonance imaging.

The findings of these studies change our understanding of energy metabolism in the acutely traumatised human brain, which may also translate to that of the healthy human brain. They prompt the development of new clinical tools to aid prognostication, and guide potential clinical trials of metabolic therapies in the future.

Dedicated to Carolina for her support and patience

List of publications

Stovell MG, Mada MO, Carpenter TA, Yan JL, Guilfoyle MR, Jalloh I, Welsh KE, Helmy A, Howe DJ, Grice P, Mason A, Giorgi-Coll S, Gallagher CN, Murphy MP, Menon DK, Hutchinson PJ, Carpenter KL. Phosphorus spectroscopy in acute TBI demonstrates metabolic changes that relate to outcome in the presence of normal structural MRI. *J Cereb Blood Flow Metab.* 2020; 40: 67–84.

Stovell MG, Mada MO, Helmy A, Carpenter TA, Thelin EP, Yan JL, Guilfoyle MR, Jalloh I, Howe DJ, Grice P, Mason A, Giorgi-Coll S, Gallagher CN, Murphy MP, Menon DK, Hutchinson PJ, Carpenter KLH. The effect of succinate on brain NADH/NAD⁺ redox state and high energy phosphate metabolism in acute traumatic brain injury. *Sci Rep.* 2018 Jul 24;8(1):11140.

Stovell MG, Yan JL, Sleigh A, Mada MO, Carpenter TA, Hutchinson PJA, Carpenter KLH. Assessing Metabolism and Injury in Acute Human Traumatic Brain Injury with Magnetic Resonance Spectroscopy: Current and Future Applications. *Front Neurol.* 2017 Sep 12;8:426.

Acknowledgements

Funders

Medical Research Council (Grant No G1002277 ID98489).

National Institute for Health Research Biomedical Research Centre, Cambridge (Neuroscience Theme; Brain Injury and Repair Theme) and NIHR Brain Injury Healthcare Technology Co-operative (Supported Project 2016/17).

I would like to thank the following individuals for their guidance and support in the relevant aspects of this thesis.

Supervisors

I thank my supervisors for the opportunity to pursue this work, and their guidance, teaching and support throughout it.

[1] Prof P.J.A. Hutchinson

[2] Dr K.L.H. Carpenter

Collaborators

Dr M.O. Mada	MR imaging and spectroscopy, MR acquisition
Dr J.L. Yan	MR imaging co-registration
Dr T.A. Carpenter	MR imaging and spectroscopy
Mr P.P. Ruetten	MR imaging and spectroscopy
Dr D.J. Tozer	MR imaging and spectroscopy
Dr A. Sleigh	MR imaging and spectroscopy
Prof G.F. Mason	MR imaging and spectroscopy
Prof D.K. Menon	Neurocritical care, metabolism and MR spectroscopy
Dr E.P. Thelin	Neurocritical care and metabolism
Mr M.R. Guilfoyle	Statistical advice
Mr A.E. Helmy	Neurosurgery and metabolism
Dr S. Giorgi-Coll	Neurochemistry
Mr M. Cabaleira	ICM+
Ms V. Lupson	MR acquisition
Ms K.E. Welsh	MR acquisition
Mr C. Zimphango	MR acquisition

Other acknowledgements

I would like to express my gratitude to the patients, relatives, and staff on the Neurosciences Critical Care Unit, Addenbrooke's Hospital; the Research and Development Department, Addenbrooke's Hospital; and the University Department of Anaesthesia, University of Cambridge.

List of abbreviations and acronyms

Metabolism

ADP	Adenosine diphosphate	NADH	Nicotinamide adenine dinucleotide (reduced)
ATP	Adenosine triphosphate	NADP ⁺	Nicotinamide adenine dinucleotide phosphate (oxidised)
Cr	Creatine	NADPH	Nicotinamide adenine dinucleotide phosphate (reduced)
FADH	flavin adenine dinucleotide (oxidised)	PCr	Phosphocreatine
FADH ₂	flavin adenine dinucleotide (reduced)	PDE	Phosphodiesterases
GABA	γ -aminobutyric acid	Pi	Inorganic phosphate
GLUT	Glucose transporter	PME	Phosphomonoesters
L/P	Lactate/pyruvate	PPP	Pentose phosphate pathway
LDH	Lactate dehydrogenase	TCA	Tricarboxylic acid cycle
NAD ⁺	Nicotinamide adenine dinucleotide (oxidised)		

Clinical

ASDH	Acute subdural haematoma	ICH	Intracerebral/parenchymal haemorrhage
CAD	Cranial access device (bolt)	ICM+	ICP software
CT	Computerised tomography	ICP	Intracranial pressure
DAI	Diffuse axonal injury	M(<i>sex</i>)	Male
EDH	Extradural/Epidual haematoma	MD	Microdialysis
F(<i>sex</i>)	Female	NCCU	Neurocritical care unit
GCS	Glasgow coma scale	PbtO ₂	Partial pressure of Oxygen
GM	Grey matter (cerebral)	RTC	Road traffic collision
GOS	Glasgow Outcome Scale	TBI	Traumatic brain injury
GOS-E	Extended Glasgow outcome Scale	WM	White matter (cerebral)
HC	Healthy control		

Magnetic resonance/Imaging

DSS	4,4-dimethyl-4-silapentane-1-sulfonate sodium salt internal reference standard	NA	Number of averages
FID	Free induction decay	NMR	Nuclear magnetic resonance
FID	Free induction decay	PET	Positron emission tomography
FLAIR	Fluid attenuated inversion recovery	ppm	Parts per million
Gad	Gadolinium contrast agent	RF	Radiofrequency
MP-RAGE	Magnetization-prepared rapid gradient echo	SNR	Signal to noise ratio
MRI	Magnetic resonance imaging	SWI	Susceptibility weighted imaging
MRS	Magnetic resonance spectroscopy	T1W	T1 weighted
		T2W	T2 weighted

Statistics

<i>glht</i>	Generalised linear hypothesis test	<i>lmer</i>	Linear mixed effects model within R package 'lme4'
IQR	Interquartile range	SD/s.d.	Standard deviation
<i>lme</i>	Linear mixed effects model within R package 'nlme'		

Contents, Overview of Chapters and Hypotheses

Chapter 1. Introduction

In this chapter I introduce traumatic brain injury as a disease, 'normal' energy metabolism of the human brain, the principles of cerebral microdialysis, and the principles of nuclear magnetic resonance (MR).

Chapter 2. Generic Materials and Methods

This chapter covers the experimental methods used in the thesis common to different studies, including patient recruitment, cerebral microdialysis, high resolution NMR analysis of microdialysis samples, clinical monitoring and *in-vivo* MR imaging and spectroscopy.

Chapter 3 (Study I). High-physiological and supra-physiological 1,2-¹³C₂ glucose supplementation to the traumatised human brain

Hypothesis 1: *“Supplementing the brain with glucose directly will increase extracellular lactate and pyruvate as a sign of increased glycolytic metabolism, with evidence of further metabolism by the tricarboxylic acid cycle.”*

In this study I have delivered glucose directly to the traumatised human brain to ascertain if additional substrate can be metabolised if provided, using changes in microdialysis analytes and high-resolution NMR analysis of pooled samples to investigate the fate of supplemented glucose.

Chapter 4. Development of in-vivo ³¹P MRS

In this chapter I describe how the acquisition parameters were chosen for acquiring *in-vivo* ³¹P MR spectra in patients suffering from acute severe traumatic brain injury, and how the technique of spectra processing and analysis was decided; which was used in **Chapters 5 and 6**.

Chapter 5 (Study II). Phosphorus spectroscopy in acute TBI demonstrates metabolic changes that relate to outcome in the presence of normal structural MRI

Hypothesis 2: *“The PCr/ATP ratio of the acutely traumatised brain is lower than that of healthy controls, signifying a lower energy reserve.”*

Hypothesis 3: *“The pH of the acutely traumatised brain is lower (more acidic) than that of healthy controls due to impairment of mitochondrial respiration and accumulation of lactate and H⁺ ions.”*

In this study I examine the changes that occur in high energy phosphate ratios and brain pH using *in-vivo* ³¹P MRS in the acute phase after injury in 13 patients after major traumatic brain injury, comparing them

to 10 healthy control subjects. How these changes relate to functional outcome and whether they are evident in radiologically normal brain are also explored.

Chapter 6 (Study III). The effect of succinate on brain NADH/NAD⁺ redox state and high energy phosphate metabolism in acute traumatic brain injury

Hypothesis 4: “Succinate improves (lowers) the L/P ratio of the traumatised human brain”

Hypothesis 5: “Succinate leads to an increase in brain PCr/ATP ratio, measured by *in-vivo* ³¹P MRS, signifying it improves brain energy state.”

In this study I attempt to corroborate my group’s previous finding that succinate supplementation improves the NADH/NAD⁺ redox status of the traumatised brain, then investigate whether succinate has any effect on brain high energy phosphate metabolism using ³¹P MRS, and if these phenomena are linked.

Chapter 7 (Study IV). The diffusion of small molecules delivered focally to the human brain via microdialysis catheters

Hypothesis 6: “Small molecules perfused via microdialysis catheters for 24 hours will diffuse in the human brain to infiltrate a 25 mm x 25 mm x 25 mm voxel of tissue (used in preceding studies).”

In this study I determine the diffusion distance of a small MR-visible molecule (gadolinium contrast agent) in the traumatised human brain using *in-vivo* MRI, to determine if the ³¹P MRS voxels chosen in Chapter 4 are an appropriate size for the study in Chapter 6. Diffusion and NMR relaxation constants of the contrast agent are also estimated.

Chapter 8. Overall conclusions

This chapter summarises the work, provides overall conclusions and the direction of further work.

Chapter 9. References

Appendix - Interrogating metabolism kinetics in the traumatised human brain.

In this chapter I include my clinical study protocol and application for ethical approval to study human brain metabolism kinetics using *in-vivo* ¹³C MRS as described in **Chapter 8, Future Work.**

Chapter 1

Introduction

1.1	Introduction	2
1.2	Traumatic Brain Injury.....	2
1.2.1	Relevance	2
1.2.2	Heterogeneity	2
1.2.3	Severe TBI & Secondary Brain Injury	3
1.2.3.1	Assessment of severe brain injury	4
1.2.4	Prognosis and outcome assessment.....	4
1.3	Cerebral Metabolism.....	5
1.3.1	Glycolysis and the Pentose Phosphate Pathway	6
1.3.2	Lactate Dehydrogenase	6
1.3.3	The tricarboxylic acid (TCA) cycle.....	7
1.3.4	Oxidative phosphorylation and the electron transport chain	8
1.3.5	Adenosine triphosphate.....	10
1.3.6	Creatine kinase system: creatine and phosphocreatine.....	10
1.3.7	Metabolic fuels other than glucose: acetate, β -hydroxybutarate and lactate.....	11
1.3.8	Inter-cellular metabolic pathways	14
1.3.9	Neuroinflammation.....	16
1.4	Cerebral Microdialysis.....	17
1.4.1	Catheter structure.....	17
1.4.2	Catheter insertion	19
1.4.3	Microdialysis sampling and bedside analysis.....	19
1.4.4	Role in clinical care.....	19

1.4.5	Retromicrodialysis.....	20
1.4.6	Microdialysis and imaging.....	21
1.4.7	Limitations and potential issues of cerebral microdialysis	23
1.5	Magnetic Resonance	23
1.5.1	Nuclear magnetism	23
1.5.2	Classical mechanical description.....	24
1.5.3	Quantum mechanical explanation	29
1.5.4	Chemical shift.....	31
1.5.5	Scalar coupling / J-coupling.....	33
1.5.6	Acquisition and processing	33
1.5.7	Signal localisation.....	35

1.1 Introduction

This chapter introduces human traumatic brain injury (TBI) as a disease, our current understanding of energy metabolism in the healthy human brain, and the principles of cerebral microdialysis monitoring and magnetic resonance spectroscopy – to provide an appropriate context for the work carried out in this thesis. Detailed methodology is described in **Chapter 2: General Methods**, and in the **Methods** section of **Chapters 2-7**. The effect of TBI on human brain metabolism is covered in the relevant results chapters.

1.2 Traumatic Brain Injury

1.2.1 *Relevance*

Traumatic brain injury is a common condition associated with significant morbidity that affects patients, their families, and carers. It remains a significant burden to society; being the leading cause of death and disability in young people in the developed world, and is increasingly important in the developing world as access to motorised vehicles increases. The overall mortality of severe TBI is around 30-40 % (Rosenfeld *et al.*, 2012).

1.2.2 *Heterogeneity*

Human TBI is a heterogeneous disease of a complex organ; most commonly classified by the severity of neurological disruption, the mechanism of injury, or pattern of injury to the brain. Severity is measured

using the Glasgow Coma Scale (GCS) (Teasdale and Jennett, 1974). An initial post-resuscitation GCS of less than 9 is considered a severe TBI (**Table 1.1**). Pattern of injury may be focal or diffuse: focal brain injury caused by direct mechanical force will typically cause macroscopically visible cerebral contusions and/or haemorrhagic mass lesions such as subdural and extradural haematomas. Diffuse brain injury is more commonly the result of rapid rotational or acceleration/deceleration forces that cause microscopic disruption of cellular and tissue architecture, such as neuronal axons in 'diffuse axonal injury'. Furthermore, individuals may have very different responses to what may be a similar insult due to their medical comorbidities, or genetic factors.

Table 1.1: Glasgow Coma Scale (Teasdale and Jennett, 1974)

Severity	Glasgow Coma Scale
Mild	13-15
Moderate	9-12
Severe	3-8

1.2.3 Severe TBI & Secondary Brain Injury

In the hours, days and weeks following a severe TBI a series of pathophysiological processes occur that result in further damage to the brain. As these occur after the primary injury, they are referred to as 'secondary brain injury'. Key contributors to secondary brain injury include raised intracranial pressure (ICP), cerebral hypoperfusion, hypoxia, hypoglycaemia, neuroinflammation and metabolic dysfunction. These are inter-related in a complex manner (**Figure 1.1**). The role of neurosurgery and neurointensive care is to support the brain through this period and ameliorate the damaging effects of secondary brain injury.

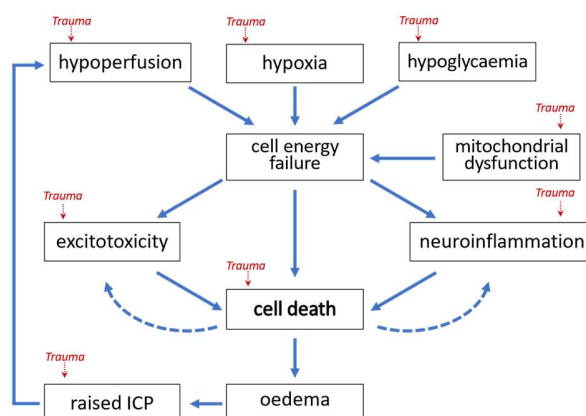


Figure 1.1. Simplified representation of mechanisms of secondary brain injury and their relationships to each other. Abbreviations: see table in *Precis*

1.2.3.1 Assessment of severe brain injury

The gold standard of brain injury assessment is clinical examination combined with imaging of the brain. The management of severe TBI includes sedation with powerful hypnotics to allow endotracheal intubation and mechanical ventilation to optimise gas exchange, limit further harm caused by the uncooperativeness of confused patients, and to reduce the metabolic requirement and intracranial pressure of the brain (Oddo *et al.*, 2016; Maas *et al.*, 2017). Sedation obscures clinical examination, so alternative assessment tools are required. This includes measurement of ICP and its derivative, the pressure reactivity index (Steiner *et al.*, 2002); measurement of brain tissue oxygen tension (PbtO₂) (Okonkwo *et al.*, 2017), brain chemistry and metabolism (Hutchinson *et al.*, 2015), and the temperature of the brain.

Computed tomography (CT) is the primary imaging modality used in the management of TBI as it detects the majority of clinically important traumatic lesions after a severe TBI – specifically those that require surgical intervention. As it can be acquired quickly, it can be performed repeatedly to monitor the evolution of lesions in the acute and subacute phases of illness. MRI is more sensitive at detecting parenchymal injury than CT, particularly in the posterior fossa of the skull (Mannion *et al.*, 2007); but it takes much longer and is more challenging to acquire in sedated patients than CT. Sequences such as fluid attenuated inversion recovery (FLAIR) are particularly sensitive at detecting cerebral oedema, and susceptibility weighted imaging (SWI) at detecting brain microhaemorrhages. However, microstructural and metabolic derangement can be invisible to these ‘structural’ MRI sequences, but detected with magnetic resonance spectroscopy (MRS) (Stovell *et al.*, 2017), used in **Chapters 5** and **6**.

In the last few decades the roles that raised intracranial pressure, hypoxia, cerebral perfusion pressure and hypoglycaemia play in secondary brain injury, and how they should be managed, have been increasingly understood (Teasdale and Jennett, 1974; Steiner *et al.*, 2002; Aries *et al.*, 2012; Le Roux *et al.*, 2014; Stocchetti *et al.*, 2015). However, the manifestation of cerebral metabolic dysfunction despite apparent control of these parameters is less understood, as is its management.

1.2.4 Prognosis and outcome assessment

A patient’s outcome after a TBI depends on the severity of the cranial and extra-cranial injury, their neurological function immediately after injury, the quality of medical and surgical care that they receive, and their social environment, comorbidities and age. Trauma affects the brain in many ways causing deficits in multiple domains that include consciousness, physical function, neuropsychological impairment, quality of life, and pain. These can be combined into a global assessment of patient

outcome, such as the Glasgow Outcome Scale (GOS) or Extended Glasgow Outcome Scale (GOS-E). The simplicity of the GOS and GOS-E (**Table 1.2**) has helped it become the most widely used outcome measure after TBI, but also means that it struggles to detect subtleties of specific deficits in different functional domains, particularly in patients with better outcomes. However, as patients who have sustained a severe TBI often have less favourable outcomes, this is less of a concern in this patient group.

Table 1.2: Glasgow Outcome Scale (GOS) and Extended Glasgow Outcome Scale (GOS-E)

GOS	GOS-E	Description
1 = Dead	1 = Dead	Dead
2 = Vegetative state	2 = Vegetative state	Absence of awareness of self and environment
3 = Severe dis.	3 = Lower Severe dis.	Needs full assistance in ADL
	4 = Upper severe dis.	Needs partial assistance in ADL
4 = Moderate dis.	5 = Lower moderate dis.	Independent, but cannot resume work/school or all previous social activities
	6 = Upper moderate dis.	Some disability exists, but can partly resume work or previous activities
5 = Good recovery	7 = Lower good dis.	Minor physical or mental deficits that affects daily life
	8 = Upper good dis.	Full recovery or minor symptoms that do not affect daily life

The Glasgow Outcome Scale (Jennett and Bond, 1975) and Extended Glasgow Outcome Scale (Jennett *et al.*, 1981) are summative measures of functional status, most often assessed at 6, 12 or 24 months after injury. *Abbreviations: dis., disability; ADL, activities of daily living.*

1.3 Cerebral Metabolism

Energy metabolism of the healthy human brain remains a subject of continued research as it is not fully understood. Concepts must be extrapolated from *in-vivo* animal and *in-vitro* cell culture studies, or limited to indirect and non-invasive research in humans.

It is thought that the brain is responsible for 20 – 25 % of the body's total carbohydrate energy expenditure (Jauch-Chara and Oltmanns, 2014) for neuronal firing and general 'housekeeping'. Cerebral metabolism includes general metabolic pathways ubiquitous to the human body, as well as metabolic pathways that appear unique to the brain. These may occur as multistep processes including complex interactions between different cell types, but for simplification, energy metabolism will be considered as

a linear sequence of events in the description below. The effect of TBI on these processes and how its deleterious effects may be ameliorated will be discussed in detail in **Chapters 3, 5 and 6**, but briefly indicated below where relevant.

1.3.1 Glycolysis and the Pentose Phosphate Pathway

Glucose is historically thought to be the principal metabolic fuel of the human brain (Prins *et al.*, 2013; Carpenter *et al.*, 2014; Hutchinson *et al.*, 2015). After uptake into cells via glucose transporters (Glucose Transporter (GLUT)-1 and GLUT-3), glucose is converted into glucose-6-phosphate. The majority of this is then metabolised via glycolysis (also known as the Embden–Meyerhof–Parnas pathway) into two molecules of pyruvate. As well as pyruvate, glycolysis yields a net production of two molecules of ATP and two molecules of NADH (discussed in below). Glycolysis is considered a relatively rapid method of energy production and importantly is anaerobic – able to support cellular energy in the absence of molecular oxygen. A smaller proportion of glucose is metabolised via the alternative, pentose phosphate pathway (PPP). The PPP is a complex pathway that reduces NADP^+ to NADPH and produces various intermediates including ribose-5-phosphate required for the synthesis of nucleotides and nucleic acids. NADPH participates in reductive reactions such as synthesis of fatty acids and the reduced form of glutathione, a cofactor for glutathione peroxidase which protects against oxygen free radicals. Like glycolysis, the PPP will anaerobically produce some pyruvate, but it does not generate energy; instead promoting synthesis of molecules for tissue repair and to combat oxidative stress. The ratio of glycolysis to the PPP may be affected by trauma (see **Chapter 3**).

1.3.2 Lactate Dehydrogenase

In the presence of molecular oxygen (aerobic conditions), pyruvate is transported into the mitochondria of the cell and combined with coenzyme-A by the enzyme pyruvate dehydrogenase to form acetyl-CoA for entry into the TCA cycle, after losing a molecule of CO_2 . Pyruvate dehydrogenase is inhibited by acetyl-CoA, NADH and ATP in a negative feedback loop that prevents excessive substrate metabolism. A scarcity of NAD^+ also inhibits glycolysis, which may occur if mitochondria are unable to oxidise the NADH produced by glycolysis or if there is insufficient molecular oxygen, both which may occur after TBI. In this instance, lactate dehydrogenase converts pyruvate to lactate, converting the NADH back into NAD^+ , freeing up NAD^+ to allow further glycolysis to occur. The conversion of pyruvate to lactate occurs very quickly in both directions, so that pyruvate and lactate are in continuous exchange, with the abundance of oxygen and mitochondrial function dictating the position of equilibrium. Hence, the ratio of lactate/pyruvate (L/P ratio) indicates the ratio of NADH/NAD^+ (NADH/NAD^+ redox state) of the cell

(Williamson *et al.*, 1967), and is thought to be a marker of mitochondrial function (Carpenter *et al.*, 2015a). Cerebral L/P ratio is an independent predictor of outcome after TBI (Timofeev *et al.*, 2011) and an important measurement in the experiments of **Chapters 3** and **6**. Glycolysis, the PPP and lactate dehydrogenase shunt are depicted in **Figure 1.2**).

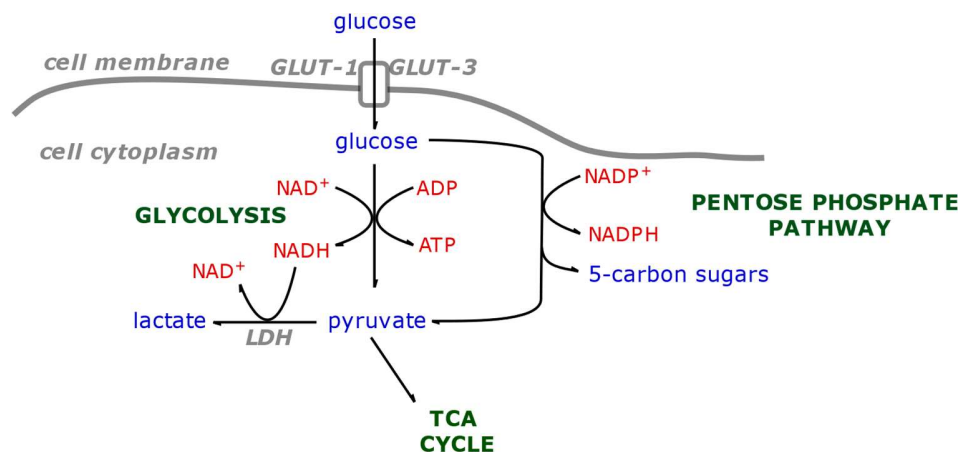


Figure 1.2. Schematic of glycolysis, the pentose phosphate pathway and lactate dehydrogenase shunt

Glucose enters the cell via GLUT-1 and GLUT-3 transporters where it is metabolised either via glycolysis or the pentose phosphate pathway, producing pyruvate. Pyruvate may then either enter the TCA cycle or be shunted to lactate by LDH, although the conversion of pyruvate to lactate is bidirectional and in free equilibrium. *Abbreviations: see table in **Precis**.*

1.3.3 The tricarboxylic acid (TCA) cycle

Under aerobic conditions acetyl-CoA is fed into the mitochondrial matrix and incorporated into the tricarboxylic acid (TCA) cycle, also called the citric acid, or Krebs's cycle. The full cycle consists of eight reactions that oxidise the acetyl group into CO₂, producing three molecules of the reducing agent NADH, one molecule of the reducing agent FADH₂, and a molecule of the high energy phosphate GTP.

An important alternative to the full cycle is the diversion of alpha-ketoglutarate (or oxo-glutarate) to produce glutamate by the enzyme glutamate dehydrogenase. This spin-out of carbons supplied by acetyl-CoA is particularly important for neurons, as glutamate is the principal excitatory neurotransmitter in the brain and the precursor for GABA, the principal inhibitory neurotransmitter in the brain. Thus, this cataplerosis represents a large proportion of TCA cycle activity in these cells (see **Chapter 3**).

As carbon is lost from the TCA cycle via cataplerosis, it can be 'topped-up' by anaplerotic reactions. In the human brain this either occurs through: glutamate's re-conversion to alpha-ketoglutarate; an alternative pyruvate entry via malate that forms oxaloacetate (catalysed by phosphoenolpyruvate-carboxykinase); the direct entry of additional malate (catalysed by malate dehydrogenase); or by aspartate's conversion to oxaloacetate by aspartate transaminase. A graphical representation of the TCA cycle and its cataplerosis and anaplerosis is in **Figure 1.3**.

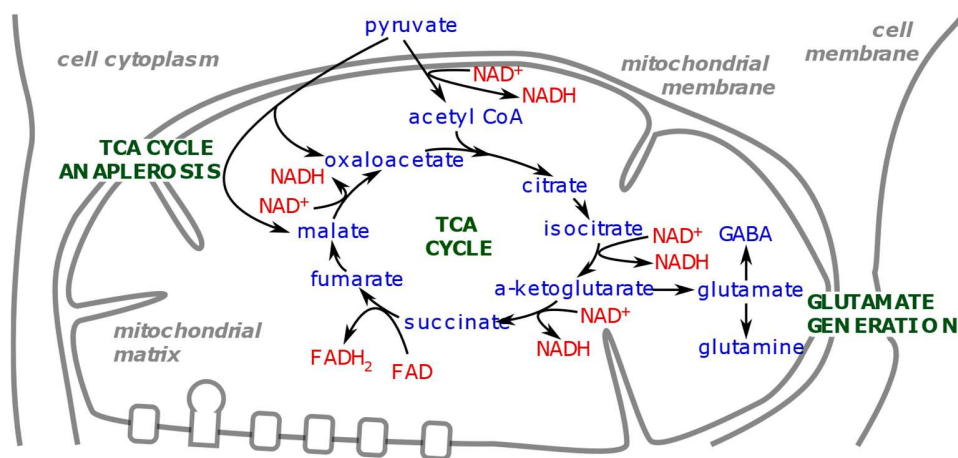


Figure 1.3. Schematic of the TCA cycle, anaplerosis and glutamate production

Pyruvate may enter the TCA cycle where it is metabolised, producing the reducing equivalents NADH and FADH_2 from NAD^+ and FADH. The TCA cycle may be anaplerotically 'topped-up' or have carbon skeletons drawn off in glutamate production. *Abbreviations: see table in **Precis**.*

1.3.4 Oxidative phosphorylation and the electron transport chain

The reducing agents NADH and FADH_2 are produced by glycolysis and the TCA cycle to drive the electron transport chain and oxidative phosphorylation: NADH and FADH_2 donate their electrons at the mitochondrial inner membrane through a series of mitochondrial protein complexes that terminates with oxygen in the mitochondrial matrix. This process provides energy for a flow of protons through the same mitochondrial complexes, that originates in the mitochondrial matrix, and terminates in the intermembrane space. This creates a powerful electrochemical gradient of protons across the inner mitochondrial membrane that is used to drive the enzyme ATP synthase (Complex V). ATP synthase uses

the energy potential of the protons travelling down their concentration gradient back across the inner membrane to combine inorganic phosphorus (Pi) with adenosine diphosphate (ADP), forming adenosine triphosphate (ATP).

The redox of NADH occurs through complexes I, III, IV and V (ATP synthase), whereas the redox of FADH₂ (using succinate) occurs through complex II, III, IV and V. The difference between the initial complex used by NADH and FADH₂ is important as complex II may be more resistant to injury than complex I, making it a potential therapeutic target (see **Chapter 6**) (Protti and Singer, 2006; Jalloh *et al.*, 2017). NADH generated by glycolysis cannot cross the mitochondrial membrane itself, so instead, the reducing equivalents NADH+H⁺ are transferred indirectly by the malate-aspartate shuttle. It is still debated how many molecules of ATP are generated by oxidative phosphorylation of a single molecule of glucose, but it is now generally accepted to be between 30 – 32 (Salway, 2004). This is a much greater yield per molecule of glucose than that produced by glycolysis alone, so although this occurs relatively more slowly than glycolysis, maintaining mitochondrial function is important to optimise cellular energy production. A schematic of oxidative phosphorylation and the electron transport chain is in **Figure 1.4**.

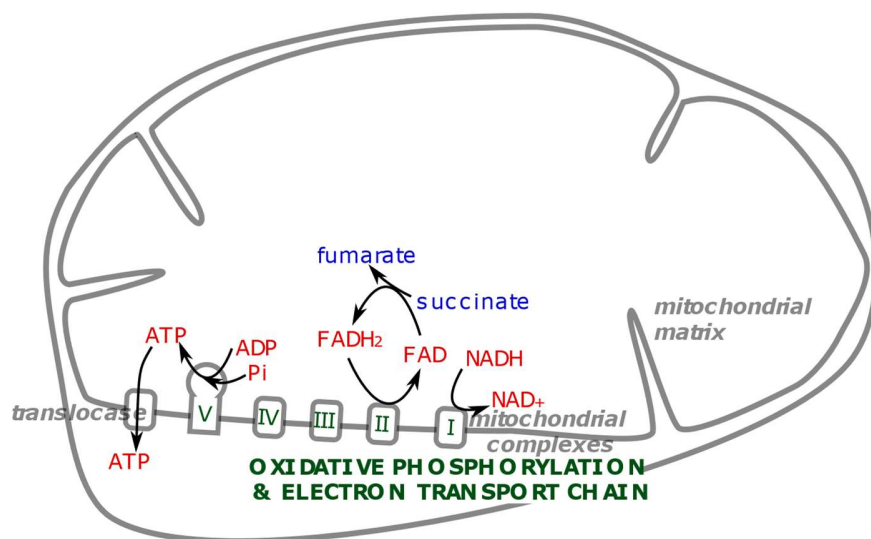


Figure 1.4. Schematic depicting oxidative phosphorylation and the electron transport chain

The reducing equivalents NADH and FADH₂ are used to drive the electron transport chain and oxidative phosphorylation through mitochondrial complexes I-V, which produces ATP from ADP and Pi.

*Abbreviations: see table in **Precis**.*

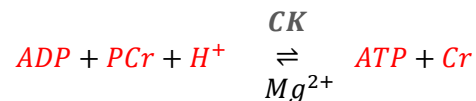
1.3.5 Adenosine triphosphate

ATP is the fundamental molecule of chemical energy in eukaryotic and prokaryotic organisms. The hydrolysis of ATP into ADP + Pi releases energy that is harnessed to drive cellular processes. In neurons, this includes the sodium potassium exchanger (Na⁺/K⁺ ATPase pump) that maintains the membrane potential. The brain maintains ATP at a concentration several fold higher than that of ADP (average 3 mmol/L vs 0.1 mmol/L (Erecinska and Silver, 1989; de Graaf, 2007; Komoroski *et al.*, 2008)) to power these processes, by continually recycling ADP back to ATP through oxidation of hydrocarbons (described above). The human brain, weighing about 1.2 kg, is thought to use and recycle an estimated 5.7 kg of ATP per day (Zhu *et al.*, 2012). As well as being used to drive cellular machinery, ATP is a constituent for ribonucleic acid (RNA) synthesis and is involved with extracellular signalling.

1.3.6 Creatine kinase system: creatine and phosphocreatine

On a cellular scale, the process of ATP regeneration via ATP synthase is relatively slow, so tissues that require energy in bursts such as the brain, skeletal muscle and cardiac muscle contain the high energy phosphate molecule phosphocreatine (PCr) and the enzyme creatine kinase (CK). Using magnesium as a cofactor, CK very rapidly transfers the high-energy phosphate group between ADP and PCr, producing ATP and creatine (Cr) in Equation 1.1.

Equation 1.1



In the brain, CK is found free in the cytoplasm as cyt-CK (BB-CK brain subtype), and as an octomer in the mitochondrial intermembrane space (Mt-CK isomer). The concentration of PCr is about double that of Cr, so that in times of high metabolic demand, PCr can act as a temporal energy buffer by donating its high energy phosphate group to ADP through cytoplasmic-CK, extremely rapidly recycling ATP for further work. During a period of lower metabolic demand, the phosphocreatine store is replenished by Mt-CK using newly generated ATP from oxidative phosphorylation in the mitochondrial intermembrane space.

As well as acting as a temporal energy buffer for ATP, PCr acts as a spatial energy buffer. The majority of ATP is produced in the mitochondrial intermembrane space but used in the cell cytoplasm. The free diffusion of ATP and ADP in cells is limited by their strong negative charges and relatively low cellular concentrations. PCr and Cr are able to diffuse more freely due to their smaller molecular size, less

overall charge, and relatively higher concentrations (5-10 mM, 2-5 mM respectively) (Wallimann *et al.*, 1992, 2011). The PCr-Cr system therefore acts as a shuttle, linking ATP production in the mitochondria to its use in the cytoplasm (Chance *et al.*, 1980; Jacobus, 1985; Yoshizaki *et al.*, 1990; Wallimann *et al.*, 2011). Measurements of relative concentrations of ATP, PCr and Pi can be performed in living tissue with ^{31}P MRS (discussed below in **Magnetic Resonance**), and form the principle results of **Chapters 5, 6 and 7**.

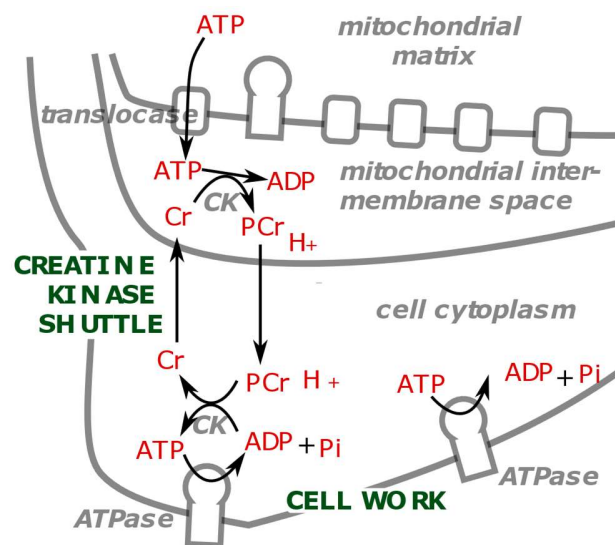


Figure 1.5. The creatine kinase system

The high energy phosphate charge from ATP is transferred to Cr by creatine kinase, producing PCr which diffuses to the cytoplasm and cell membrane where it is used to drive ATPases through creatine kinase regeneration of ATP from ADP. *Abbreviations: see table in **Precis**.*

1.3.7 Metabolic fuels other than glucose: acetate, β -hydroxybutyrate and lactate

Studies using a range of techniques have shown that the human brain will take up and directly metabolise alternative fuels to glucose including acetate, beta-hydroxybutyrate and lactate; which enter various points of the TCA cycle (Rothman *et al.*, 2011; Carpenter *et al.*, 2014; Glenn *et al.*, 2015b).

Acetate is almost exclusively metabolised by the brain's glia at normal serum concentrations, whereas beta-hydroxybutyrate is thought to be predominantly metabolised by neurons (Rothman *et al.*, 2011). In the brain, they are combined with CoA to form acetyl-CoA before being fed into the TCA cycle at the same point of entry as pyruvate. The brain's reliance on acetate and β -hydroxybutyrate is increased in fasting and prolonged strenuous exercise.

Lactate has been shown to be an important metabolic fuel for the brain (Gallagher *et al.*, 2009; Glenn *et al.*, 2015b; Hui *et al.*, 2017), rather than solely being a waste product of skeletal muscle metabolism as originally proposed (Hartree and Hill, 1923). The brain continually takes up and exports lactate from the blood (Glenn *et al.*, 2015a; Hui *et al.*, 2017), with neuron cell culture studies suggesting preferential metabolism of lactate over glucose (Pellerin and Magistretti, 1994; Bouzier-Sore *et al.*, 2003; Simpson *et al.*, 2007). In the presence of functioning mitochondrial electron transport chain/oxidative phosphorylation, available NAD⁺ can be used to convert lactate into pyruvate for entry into the TCA cycle for metabolism. Thus, elevated brain lactate levels do not suggest metabolic dysfunction or hypoxia *per se*, but rather it is an elevation of the ratio of lactate/pyruvate (L/P ratio), with reduced concentration of pyruvate, that implies a restriction of the mitochondrial NADH/NAD⁺ redox state. The role of lactate as a primary fuel may be influenced by TBI (Glenn *et al.*, 2015b) and has been proposed as an alternative metabolic therapy in TBI (Bouzat *et al.*, 2014; Quintard *et al.*, 2016). Lactate production and metabolism in the brain are further discussed in **Chapter 3**. An overview of metabolic fuels and their metabolism can be found in **Figure 1.6**.

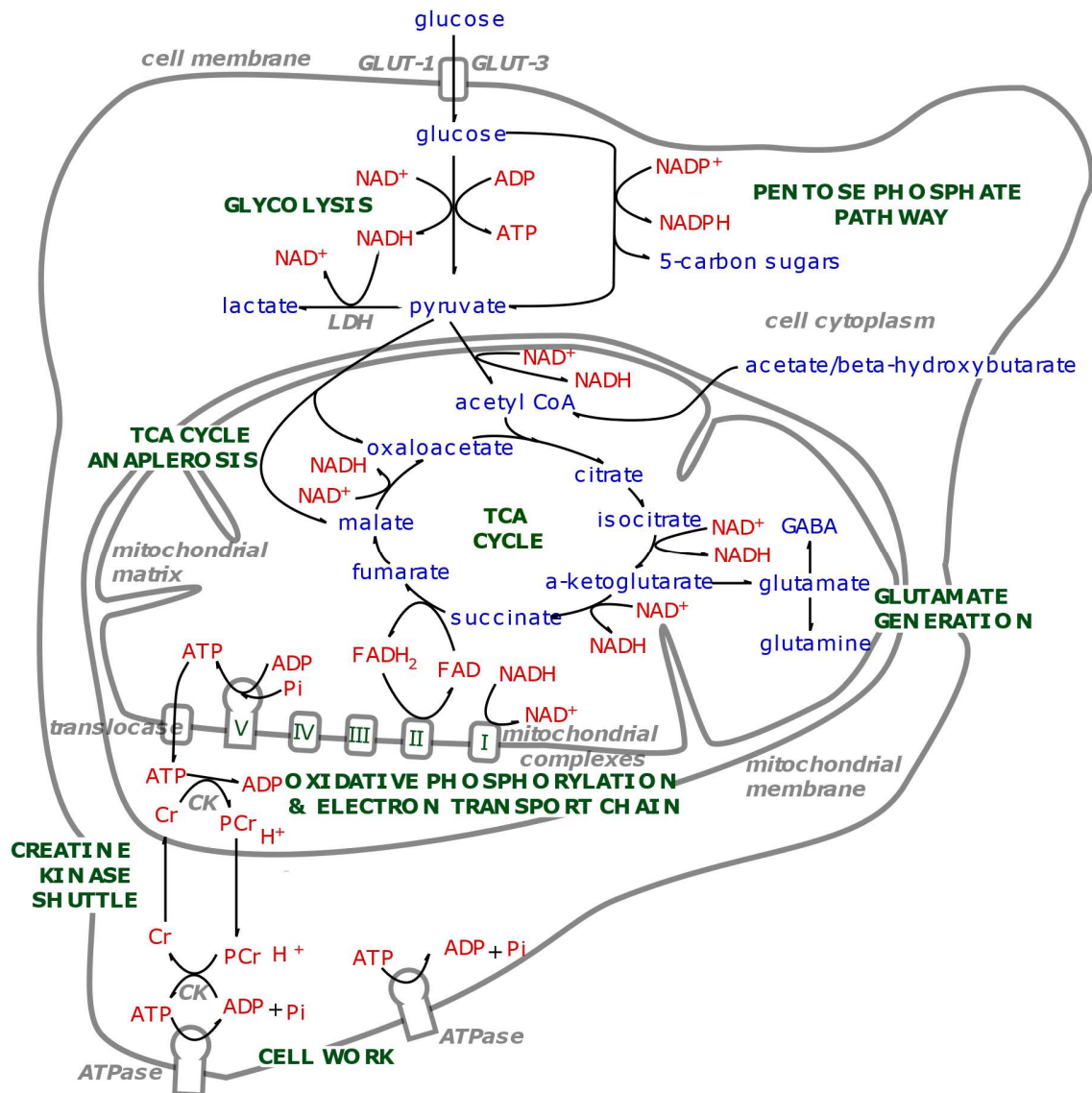


Figure 1.6. Overview of cerebral metabolic pathways, represented by single cell

Glucose enters the cell via GLUT1 and GLUT3 transporters where it is either metabolised via glycolysis, or the pentose phosphate pathway, producing pyruvate. Pyruvate may then either enter the TCA cycle where it is metabolised, producing the reducing equivalents NADH and FADH₂ from NAD⁺ and FAD. If insufficient NAD⁺ is available, pyruvate is shunted to lactate by LDH. The TCA cycle may also be anaplerotically 'topped-up' or have carbon skeletons drawn off in glutamate production. The reducing equivalents NADH and FADH₂ are used to drive the electron transport chain and oxidative phosphorylation through mitochondrial complexes I-V, which produces ATP from ADP and Pi. The high energy phosphate charge is transferred to Cr by creatine kinase, producing PCr which diffuses to the cytoplasm and cell membrane where it is used to drive ATPases by regenerating ATP from ADP by creatine kinase. *Abbreviations: see table in **Precis**.*

1.3.8 Inter-cellular metabolic pathways

The pathways above consider the energy metabolism of a hypothetical single, isolated cell (**Figure 1.6**), whereas the brain consists of a complex array of interacting neurons, glia, and cells of the neurovascular system.

Neurons are the main functional units of the brain; receiving chemical stimuli across synapses to their dendrites – causing their depolarisation and propagation of an electrical impulse to their cell bodies and then axons – terminating at a synapse where chemical neurotransmitters transmit the impulse to other neuron(s). Glutamate is the predominant synaptic excitatory neurotransmitter in the brain and GABA the predominant inhibitory neurotransmitter (Petroff, 2002). Glial cells support neurons and are more numerous: Oligodendrocytes contain myelin (fat) that envelope neurons, insulating them to increase their conduction velocity. Their abundance in cerebral white matter is responsible for its appearance (Jäkel and Dimou, 2017). Astrocytes support neurons; clearing 'spent' neurotransmitters at synapses, regulating the electrolyte concentration of brain's interstitium, providing structural support, and contributing the blood brain barrier neurovascular unit with their end-feet by holding together endothelial cells with tight junctions (Kimelberg, 2010; Jäkel and Dimou, 2017). Other cells of the neurovascular unit include pericytes and capillary endothelial cells (Sweeney *et al.*, 2016) (**Figure 1.7**). Ependymal cells are specialized epithelial cells that line the brain's ventricular system, playing a key role in the production of cerebrospinal fluid (Jäkel and Dimou, 2017). Microglia are neuroinflammatory cells that proliferate in response to CNS infection or damage, phagocytosing and clearing pathological and damaged cells in the brain (Killen *et al.*, 2019).

It is thought that the brain distributes steps of carbohydrate respiration between some of these different cell types (**Figure 1.7**). The most commonly described is the astrocyte-neuron lactate shuttle (ANLS) hypothesis, which suggests that glucose is primarily taken up from the vasculature and extracellular space by astrocytes, which metabolise it into lactate via glycolysis and lactate dehydrogenase. The lactate is then exported to adjacent neurons, converted to pyruvate, and fed into the neuronal TCA cycle for energy generation (Pellerin and Magistretti, 1994; Bouzier-Sore *et al.*, 2003). As an extension of this, the glutamate-glutamine shuttle proposes that lactate entering the neurons' TCA cycle is also spun out as glutamate. The glutamate is stored in neuronal vesicles before being released into the synaptic cleft where it can stimulate post-synaptic glutamate receptors for cell signalling. Astrocytes take up 'spent' glutamate from the synaptic cleft and convert it into glutamine, before exporting it back to neurons via the extracellular space (Gallagher *et al.*, 2009). This is currently a

widely-recognised description of multicell-organised brain energy metabolism (Carpenter *et al.*, 2015b), although it has been challenged and controversy exists (Patel *et al.*, 2014). My findings supplementing glucose to the human brain in **Chapter 3** support the proposed model of the astrocyte-neuron lactate shuttle and glutamate-glutamine shuttle model.

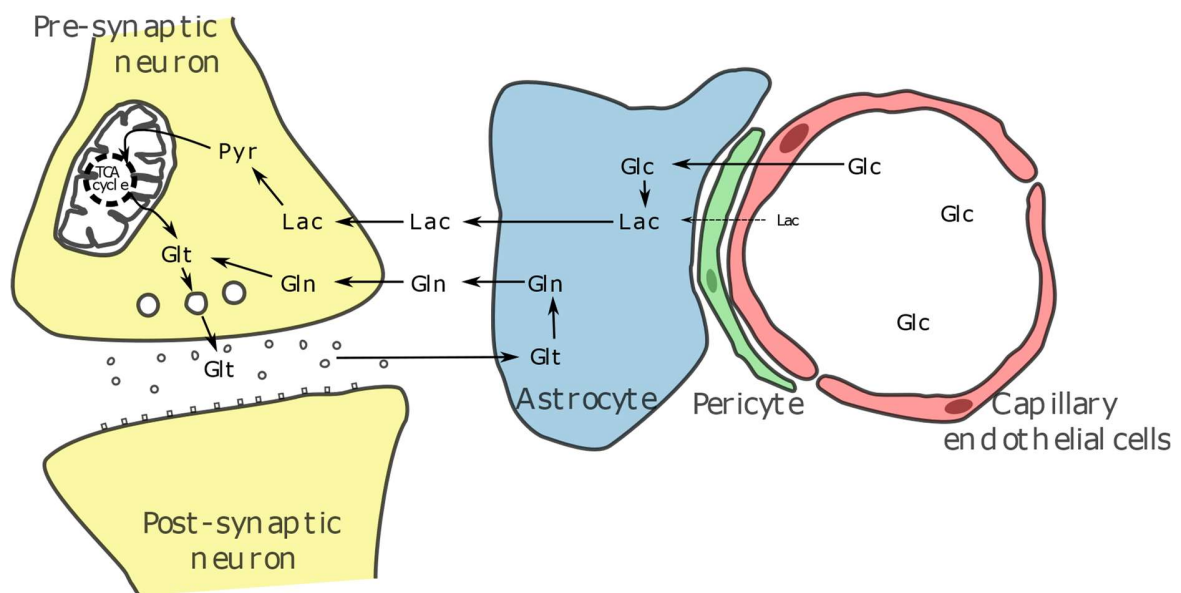


Figure 1.7. Intercellular metabolic pathways

Simplified schematic showing how different cell types divide metabolism of hydrocarbon skeletons, such as glucose and lactate, as proposed by the astrocyte-neuron lactate shuttle and glutamate-glutamine shuttling hypotheses. *Abbreviations: see table in **Precis**; Glc, glucose; Lac, lactate; Pyr, pyruvate; Glt, glutamate; Gln, glutamine.*

1.3.9 Neuroinflammation

Severe traumatic brain injury causes the release of free DNA, RNA, and alarmins such as HMGB1 from injured brain cells. These damage-associated molecular patterns (DAMPs) trigger neuroinflammatory cascades involving both resident immune cells (microglia), and migratory immune cells from the system circulation (Zhang *et al.*, 2010; Liesz *et al.*, 2019).

Microglia support cell survival and aid repair by phagocytosing unsalvageable injured cells and their elements – but this may conversely exacerbate injury due to excessive synaptic pruning (Helmy *et al.*, 2011). Pro-inflammatory microglia are classed as ‘M1’ and anti-inflammatory microglia as ‘M2’ (Italiani and Boraschi, 2014; Killen *et al.*, 2019), but the distinction between M1 and M2 subtypes is probably not clear-cut (Martinez and Gordon, 2014; Becher *et al.*, 2017), and switching between differentiated subtypes can occur (Simon *et al.*, 2017). Microglia recruit innate immune cells from the circulation: first neutrophils that peak within 24-48 hrs of injury, followed by a more sustained infiltration of activated macrophages derived from circulating monocytes, whose role and appearance seem almost identical to that of the resident microglia (Jäkel and Dimou, 2017; Killen *et al.*, 2019).

Microglia promote and control neuroinflammation through small extracellular signalling proteins called cytokines and chemokines. These are also released from activated, stressed, or dying cells (DiSabato *et al.*, 2016; Killen *et al.*, 2019). The extracellular cytokine profile changes with time after injury and ‘stage’ of inflammation: IL-1 β and TNF α are raised within the first 24 hrs post injury and are pro-inflammatory, promoting apoptosis (Cantaert *et al.*, 2010; Salim *et al.*, 2016; Becher *et al.*, 2017). Later, IL-10 and then IL-4 increase, supposedly with cell repair and survival roles (Ziebell and Morganti-Kossmann, 2010). IL-6 appears to be a general marker of inflammation (Singhal *et al.*, 2002). Many neuroinflammatory cytokines can be found at a higher concentration in contused brain compared to peri-contusional brain (Harish *et al.*, 2015).

The role of T cells and B cells of the adaptive immune system after TBI is less understood than that of the innate immune system (Thelin *et al.*, 2017). However, T cells are known to influence microglia differentiation and function (Simon *et al.*, 2017), and after TBI, B cell derived autoantibodies against brain specific proteins such as S100B (Marchi *et al.*, 2013) and glial fibrillary acidic protein (Wang *et al.*, 2016) have been found.

1.4 Cerebral Microdialysis

Cerebral microdialysis is an invasive monitoring technique increasingly used in neurocritical care to continuously monitor brain metabolism in patients who have sustained a severe TBI or poor-grade subarachnoid haemorrhage (Hutchinson *et al.*, 2015). In addition to its clinical role, it has important research applications that include substance delivery through retromicrodialysis that is integral to the studies of **Chapters 3** and **6**.

1.4.1 Catheter structure

Microdialysis catheters have a dual lumen of a channel-within-a-channel (**Fig. 3.1**). The terminal 10 mm (M Dialysis 71 high cut-off brain microdialysis catheter, used in experiments of this thesis) outer wall has a semi-permeable membrane through which small molecules (<100 kDa) can diffuse. As fluid (perfusate) is slowly pumped down the catheter and along the semi-permeable membrane, it exchanges solutes and fluid with the brain interstitium surrounding it. When fluid reaches the closed catheter tip it is forced to return via an inner, non-porous central channel where it is ultimately recovered in microdialysis vials. Dedicated microdialysis pumps drive the perfusion fluid slowly enough that the concentration of metabolites in the recovered fluid (microdialysate) has had time to equalise with that of the brain extracellular space. A variety of catheters exist that are designed for different tasks; possessing varying shaft length, membrane length and membrane pore size. Microdialysis pumps may also have varying flow rates, but 0.3 $\mu\text{L}/\text{min}$ is considered standard for cerebral studies, as higher perfusion rates cause greater net fluid loss and incomplete equalisation of metabolite concentration in the recovered fluid (Hutchinson *et al.*, 2015). ‘Standard’ perfusion fluid used for cerebral microdialysis is crystalloid (further details in **Chapter 2: General Methods**), but alternatives including human albumin solution and dextran are sometimes used (Hillman *et al.*, 2005; Helmy *et al.*, 2009).

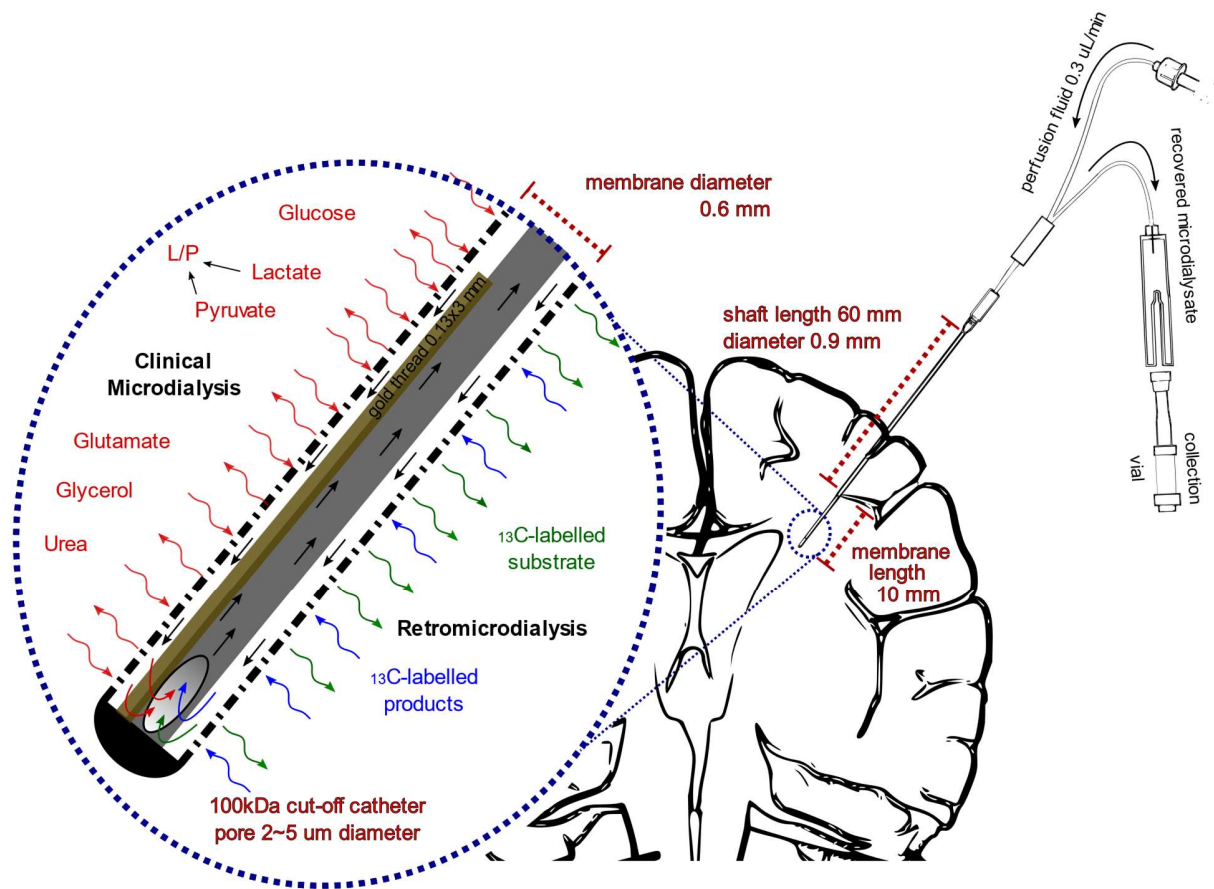


Figure 1.8. Schematic of cerebral microdialysis

100 kDa cut-off microdialysis catheter inserted into patient's brain, with magnified view of catheter tip demonstrating semipermeable membrane. A gold filament (0.13 mm x 3 mm) in the end of the catheter allows its identification on CT scans. The microdialysis perfusate is pumped slowly (0.3 uL/h) along the outer lumen, the final 10 mm of which is a semipermeable membrane (100 kDa cut-off, pore diameter \approx 2 – 5 μ m). Small molecules freely exchange with the brain interstitium, reaching equilibrium by the time they reach the recovery hole in the end of the central, non-porous channel, where the fluid passes back for collection in microdialysis vials. Glucose, lactate, pyruvate, glycerol, glutamate and urea may be used for clinical monitoring. Catheters can also be used to supplement the brain for research, displayed to the right side of magnification window. *Abbreviations: see table in **Precis**.*

1.4.2 Catheter insertion

Cerebral microdialysis (CMD) catheters can be inserted either via a single craniostomy burr hole (usually attached through a cranial access device ('triple-bolt')), or during open-surgery if the patient requires a craniotomy or craniectomy. Cerebral microdialysis is preferably used together with brain tissue oxygen pressure (PbtO₂) monitoring and intracranial pressure monitoring to provide multimodality monitoring from an equivalent region of brain, allowing differentiation of hypoxic elevation of L/P ratio from primary mitochondrial dysfunction elevation of L/P ratio. Catheters must be inserted with their whole membrane within the brain parenchyma, most commonly into frontal cortex white matter (centrum semiovale), avoiding eloquent regions of brain or non-viable regions of injury. However, studies do suggest that the ideal catheter location may be peri-lesional border zones, as these areas are at greatest risk of deterioration and will benefit most from monitoring and optimising therapy. However, these regions are more challenging to target, and if located too close to a lesion the detected metabolic pattern can be difficult to interpret clinically (Hutchinson *et al.*, 2015).

1.4.3 Microdialysis sampling and bedside analysis

Microdialysis vials are typically changed and analysed hourly in neurocritical care. An hour of perfusion will produce $\approx 18 \mu\text{L}$ of recovered microdialysate which is analysed using an automated enzymatic colorimetric analyser, such as an ISCUS (M Dialysis). Glucose, lactate, pyruvate, glycerol, glutamate and urea can be measured in this way, but as each metabolite only consumes $0.2 \mu\text{L} - 1.5 \mu\text{L}$ of microdialysate, a significant volume usually remains for further analysis, such as for high-resolution NMR analysis used in **Chapter 3**. Results of ISCUS analysis represent the physiology of patients from the previous hour of perfusion, with a ≈ 20 minute time lag due to the time it takes for fluid to return via the distal channel. On initial insertion of a catheter, a very high rate of perfusion is automatically run by the microdialysis pump as a 'flush' sequence for $2 \frac{1}{2} - 4$ minutes to expel the air from inside the catheter, so the recovered fluid for this period is discarded as it will not have had a chance to equalise with the surrounding brain. The result from the first hour of monitoring after catheter insertion is similarly discarded due to transient effects of micro-injury to the brain caused by catheter insertion.

1.4.4 Role in clinical care

Cerebral microdialysis allows patients' brain extracellular chemistry to be continually monitored, and attempts made to tailor treatment to patients' cerebral metabolism. By monitoring brain glucose, critical neuroglycopenia can be detected, and attempts made to reverse it with infusion of intravenous glucose (Hutchinson *et al.*, 2015), or loosening of glycaemic control (Vespa *et al.*, 2012; Plummer *et al.*,

2018). A patient's L/P ratio is perhaps the most important microdialysis biomarker as it reflects the NADH/NAD⁺ redox status of the brain – the balance between aerobic and anaerobic metabolism – and a value ≥ 25 in radiologically healthy brain is an independent predictor of poor patient outcome (Timofeev *et al.*, 2011). Furthermore, in the presence of low brain pyruvate and low PbtO₂, a high L/P ratio suggests brain ischemia which may be treated by increasing cerebral perfusion pressure and inspired oxygen concentration. However, if L/P ratio is high in the presence of a normal brain glucose concentration, normal cerebral perfusion pressure, and normal or high brain pyruvate and PbtO₂, the patient's brain is likely suffering from cellular mitochondrial dysfunction, for which there is currently no treatment. This was the rationale for performing the studies in **Chapter 6**, where more details can be found.

Microdialysis measurements of glucose, lactate, pyruvate and L/P ratio are usually considered more important markers than measurements of glutamate and glycerol (Hutchinson *et al.*, 2015). High brain glutamate is thought to represent harmful excitotoxicity (Hutchinson *et al.*, 2002, 2015; Hlatky *et al.*, 2004), but in my experience (and that of my group) the concentration of glutamate in the extracellular space is often under the detection limit of beside ISCUS analysis, so its results may be less reliable. The poor specificity of glycerol makes its significance even more questionable: it may represent cell membrane breakdown from oxidative stress (Hillered *et al.*, 1998), but is also a common metabolic intermediate of glucose (Lin, 1977; Nguyen *et al.*, 2007), and is even found in drugs used in the treatment of TBI. Thus, analysis of ISCUS results in **Chapters 3** and **6** did not focus on extracellular concentrations of glutamate and glycerol.

1.4.5 Retromicrodialysis

By adding study substrates to microdialysis perfusion fluid small regions of brain can be 'dosed' with agents that further interrogate the metabolism of the brain (Gallagher *et al.*, 2009; Jalloh *et al.*, 2015a) and/or attempt to ameliorate cellular metabolic crises (Jalloh *et al.*, 2017), such as the studies in **Chapters 3** and **6**. Whereas it is assumed that study substrates smaller than the cut-off size of a catheter's membrane will diffuse into the surrounding brain, it is not clear how far into the brain this diffusion reaches, and at what concentration (see **Chapter 7**). Nonetheless, the fluid recovered is from the same volume of brain that is perfused, so should represent the region 'dosed' by the study substrate.

Labelling study substrates with ^{13}C allows the fate of the study molecule to be ascertained from identifying the position that the ^{13}C ends up in within recovered metabolites, using high resolution NMR. Due to limitations of sample volumes and sensitivity multiple microdialysis vials must be pooled together for this type of analysis (see **Chapter 2, General Methods**).

1.4.6 *Microdialysis and imaging*

The microdialysis catheters used in the studies in this thesis contain a short gold filament at their tip which is visible on computerized tomography (CT) and some magnetic resonance imaging (MRI) sequences (**Figure 1.9**). Microdialysis catheters are otherwise invisible on these imaging modalities, and the importance of their localisation on patient imaging is particularly important for the experiments in **Chapter 7**. As a microdialysis pump battery is not MR compatible, the pump must be disconnected from the catheters during the MR study, but the catheters themselves can remain *in-situ* for reconnection after the scan. Thus, for the studies that involved combined microdialysis and imaging (**Chapters 6 and 7**), the time between disconnection and scanning must be performed swiftly.

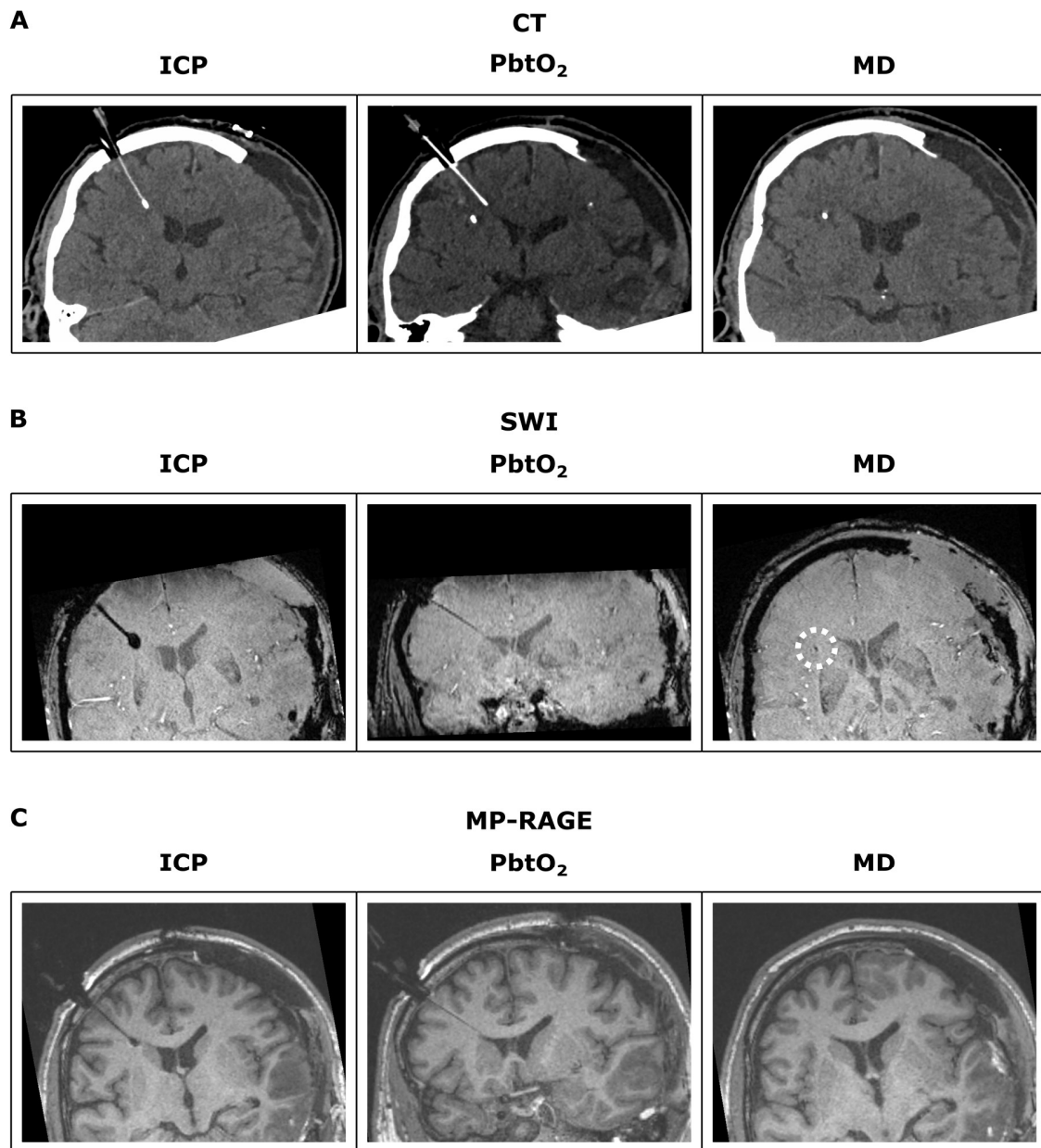


Figure 1.9. Multimodal monitoring appearance on CT and MR

Reformatted coronal slices demonstrate ICP, PbtO₂ and microdialysis probes in a patient's brain. *Panel A*: The ICP probe's thin shaft and bulbous end can be distinguished from the PbtO₂ probe's uniform shaft and tip. Only the gold filament at the end of the microdialysis catheter is visible on CT. *Panel B* and *C*: MRI MP-RAGE and SWI sequences reveal the same bulbous tip to the ICP probe and uniform PbtO₂ probe. The gold tipped microdialysis catheter is visible on SWI sequences (highlighted by white dashed circle in *Panel B*), but not MP-RAGE sequences (*Panel C*). *Abbreviations: see table in Precis.*

1.4.7 Limitations and potential issues of cerebral microdialysis

The 0.6 – 0.9 mm diameter channel-within-a-channel design of microdialysis catheters makes them inherently fragile – even more so than ICP and PbtO₂ probes. When inserted through triple-bolts, catheters may fail to pierce the dura, arachnoid or pia mater of the brain, so the extradural, subdural, or subarachnoid space is monitored, instead of the brain parenchyma. Furthermore, unlike static ICP and PbtO₂ monitoring, cerebral microdialysis requires continuous pumping of fluid past a delicate semipermeable membrane sited in living tissue. Pump batteries can fail or be depleted, and pumps may fail mechanically. Furthermore, over many days, a foreign body reaction is induced that leads to infiltration of the semipermeable membrane and potential pore obstruction (Helmy *et al.*, 2009). Vials must be changed and analysed on an ISCUS analyser hourly over days to weeks of monitoring. If the operator is busy with other aspects of patient care, then the changing of vials may be neglected, or the problems described above not identified. Modern ISCUS*flex* analysers can analyse multiple patients using a single machine, which unfortunately sometimes leads to vials being inserted in the wrong vial positions in the machine; causing it to fail or crash. Finally, microdialysis catheters can be accidentally dislodged during patient transfer or general nursing care. Whereas intermittent, obviously erroneous ISCUS results can be excluded without affecting a study's findings, long periods of failed monitoring may significantly hinder data analysis.

1.5 Magnetic Resonance

High-resolution *in-vitro* NMR analysis of microdialysis samples (**Chapter 3**), *in-vivo* ³¹P MRS and *in-vivo* ¹H MRI examinations of patients' brains (**Chapters 4-7**) rely on magnetic resonance. The terms NMR and MRS could be used interchangeably, but for the sake of clarity NMR will be used to refer to *in-vitro* analysis of microdialysis samples in NMR tubes, and MRS used to refer to *in-vivo* examination of the human brain. The principles of magnetic resonance will be described with both a classical mechanical explanation and a quantum mechanical explanation. As the focus of this thesis is acute brain metabolic dysfunction in clinical TBI, these concepts will be summarised briefly with an emphasis on aspects relevant to the experiments later described.

1.5.1 Nuclear magnetism

Protons, neutrons and electrons possess a fundamental property called 'nuclear spin', in which they rotate around their axis (**Figure 1.10**). Protons and neutrons tend to form pairs in nuclei so that their resultant net spins cancel out. For some isotopes this does not occur, such as ¹H, ¹³C and ³¹P – so their nuclei have a total net spin. As nuclei are positively charged, a tiny electrical current is generated by the

charge rotating around the nucleus. This tiny electrical current generates a small magnetic field at the nucleus, so that nuclei may be considered to be, and behave like, miniature bar magnets. The natural isotopic abundance of ^1H and ^{31}P approaches 100 %, so these nuclei can be detected without enrichment (**Chapters 4-7**), but only 1.1 % of naturally occurring carbon is isotope ^{13}C , so supplementation with substrates enriched with ^{13}C is most often required to study human metabolism with magnetic resonance.

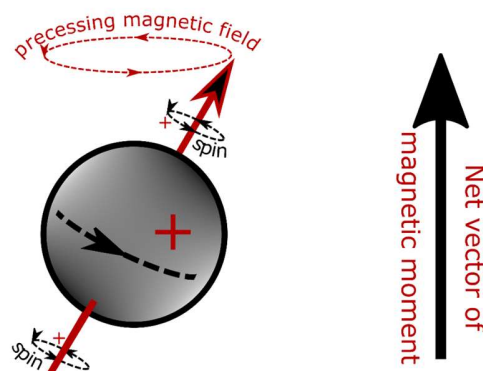


Figure 1.10. Nuclear magnetism

Charged hydrogen nuclei (protons) spin on their axis, and this rotating charge induces a magnetic field, or magnetic moment. The spinning nucleus itself also rotates (precesses) off axis. The net magnetic field vector of a very large number of nuclei precessing together out of phase is indicated by the arrow to the right. The same principle applies to ^{13}C and ^{31}P nuclei.

1.5.2 Classical mechanical description

The magnetic fields of individual nuclei are too small to be detected, and in the absence of an external magnetic field they point randomly in all directions. However, when they are subjected to a (strong) external magnetic field (B_0), there is a tendency for them to align more towards the direction of the B_0 , creating a net longitudinal magnetisation in line with the applied external magnetic field (**Fig. 1.11A**). A greater strength of B_0 creates a greater tendency to align, but the net magnetisation achieved with current equipment is invariably small due to random thermal motion and collision occurring at a much higher energy level that allows interactions between neighbouring nuclei's magnetic fields, resulting in their random reorientation through spin-spin relaxation (*see below*) (Hanson, 2008). Nonetheless, the strength of magnets used in high-resolution NMR are generally greater than that of *in-vivo* MRS, which partly explains the much better signal to noise of *in-vitro* ^{13}C spectra in **Chapter 3** compared to *in-vivo* ^{31}P spectra in **Chapters 4-6**.

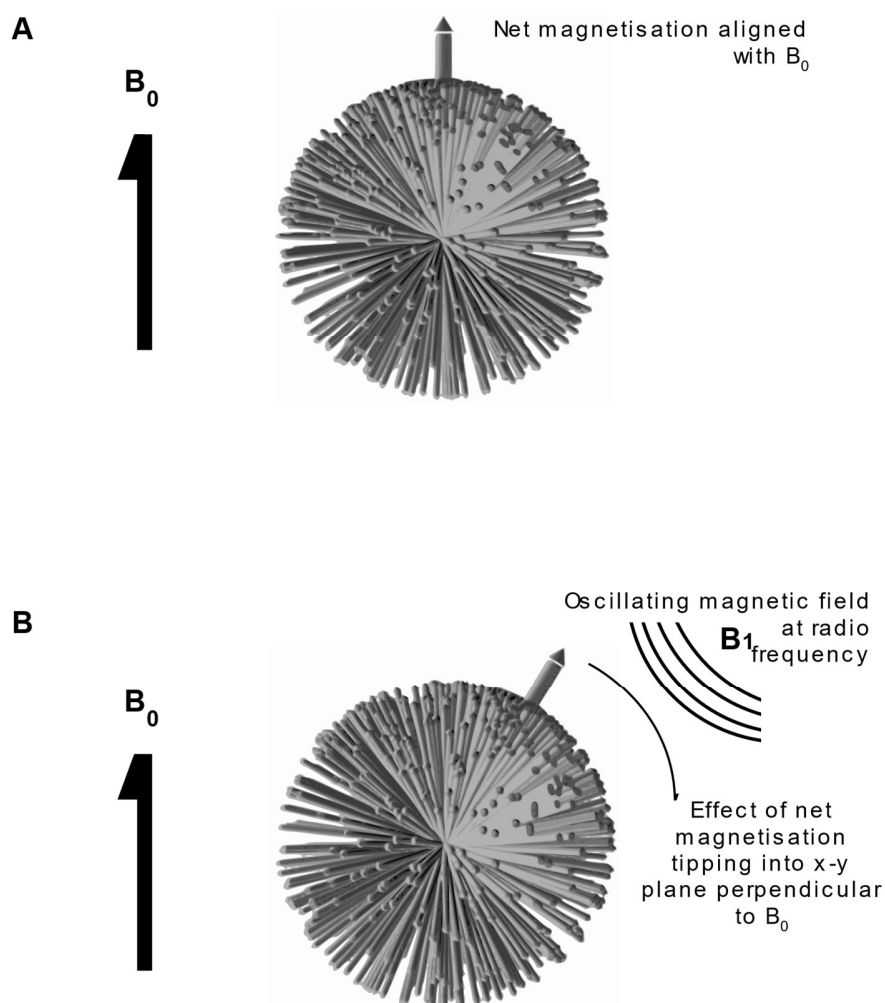


Figure 1.11. The effect of a static and oscillating magnetic field on a population of nuclear spins

Multiple nuclear spins are considered originating from a single point in space; each spin's direction indicated by a single arrow. *Panel A:* Application of an external magnetic field, (B_0) results in a tendency for the random direction of spin states to align with it (indicated by thicker arrow, labelled net magnetisation aligned with B_0). *Panel B:* When an external, oscillating magnetic field (B_1) is applied (perpendicular to B_0 in the rotating frame), then the net magnetization is tipped into the xy plane. Figure adapted from Hanson LG. Concepts in Magnetic Resonance Part A, Vol. 32A(5) 329-340 © 2008 Wiley Periodicals, Inc. (Hanson, 2008).

As nuclei spin off their central axis, their actual alignment precesses about the axis of the external field, like a spinning top that has been 'nudged' (see **Figure 1.10**). The frequency of this precession is important, and is given by the Larmor equation (Equation 1.2), where ω is the Larmor frequency of the nucleus in the external magnetic field B_0 , associated by the nucleus' gyromagnetic ratio (γ , a constant for each isotope).

Equation 1.2

$$\omega = \gamma \cdot B_0$$

Subjected to a constant B_0 , the precessional frequency of identical nuclei will be the same but at random phases of precession; thereby generating no net transverse magnetic field.

By briefly applying a second magnetic field (B_1) perpendicular to the spins aligned with B_0 , the phase of the precessing nuclei align in phase coherence, tipping the net magnetisation towards, or into, the transverse plane. The B_1 is generated by inducing a complex electrical current in an RF coil and must be at the Larmor frequency of the nucleus. For clinical scanners this is in the radiofrequency range (RF) for ^1H MR, and so the pulse is called an RF pulse. After cessation of the applied B_1 RF pulse the resultant rotating net transverse magnetisation can be detected as it induces an electric current in the RF coil, by Faraday's law.

With the spins continually precessing at a constant phase relative to B_0 , for simplification the system can be considered from their point of view, in the 'rotating frame of reference' (**Figure 1.11** is represented in the rotating frame of reference). This rotation is at the Larmor frequency of the nuclei, where z is in the direction of B_0 and B_1 is applied in the x - y plane. Consequently, the amount of magnetisation tipped into the transverse x - y plane can be expressed using a simplified Bloch equation, where the generation of transverse magnetisation over time is equal to the initial longitudinal magnetisation multiplied by the strength of the transverse magnetisation and the gyromagnetic ratio (Equation 1.3):

Equation 1.3

$$dM_{transvers} / dt = M_{longitudinal} \cdot B_1 \cdot \gamma$$

After cessation of the applied RF pulse, the induced transverse magnetisation dissipates, as longitudinal and transverse relaxation occur. With the application of the B_1 , the difference in population between spins aligned with and against the field is lost. The strong B_0 pulls the spins back into their resting alignment along the z axis, transferring energy from the spins to the surrounding lattice. Longitudinal T1

relaxation typically occurs in the order of seconds, and depends on the tissue or structure that the nucleus is in. If subsequent repeated RF pulses are applied before T1 relaxation has fully occurred, reduced signal will be acquired from molecules with longer T1s, as they have less longitudinal magnetisation at the start of each acquisition (Equation 1.3). This phenomenon is exploited to create tissue contrast in T1 weighted (T1W) imaging and used to generate the T1 maps of **Chapter 7**. However, this effect can lead to underestimation of ³¹P MRS phosphorus metabolite concentrations in **Chapters 5** and **6**, where it is referred to as 'T1 saturation'. If the RF pulse tips the spins into the x-y plane at time t_0 , the Bloch equation to calculate this recovery of longitudinal magnetisation (M_z) at time t is given by Equation 1.4:

Equation 1.4

$$M_z = M_0 (1 - e^{-t/T1})$$

Transverse T2 relaxation describes the process of adjacent spins exchanging energy between each other in so doing losing phase coherence. This is also called spin-spin relaxation and typically occurs much more rapidly than T1 relaxation, in the order of milliseconds. It is also dependent on the structure/tissue that the nucleus is in, but not in the same way as T1 relaxation. The remaining transverse magnetisation at time t is expressed at time t by Equation 1.5:

Equation 1.5

$$M_{xy} = M_0 \cdot e^{-t/T2}$$

As well as the spin-spin relaxation of T2, small inhomogeneities of the B_0 field caused by the sample or person being examined has an effect called T2* relaxation. Inhomogeneities in the magnetic field cause the nuclei to experience a different magnetic field, and hence different Larmor frequency. The rate of T2* is much faster than that of T2.

As the net magnetisation rotates around the laboratory frame of reference within the magnet it induces a current in the receiver coil wire due to electromagnetic induction. The frequency of the electrical current is equal to the precessional frequency of the nuclei, so dependent on the type of nucleus detected (¹H, ¹³C or ³¹P) and what external magnetic field it is subject to – either due to applied inhomogeneities in the B_0 , or local, chemical effects. The T2 and T2* relaxation (and to a lesser extent T1 relaxation) cause this rotating magnetic field to decay to zero, so the resultant electrical signal is called

the free induction decay (FID). The transverse magnetisation (rotating magnetic field) rotates in two dimensions over time (so three dimensions), but the current induced in a receiver coil wire (the FID) occurs in one dimension over time (so two dimensions). Hence, MR quadrature coils (such as the ones used in the experiments in this thesis) capture the signal (FID) in two orthogonal planes to determine its phase to appropriately represent it in two dimensions (represented graphically in **Figure 1.12**). Phase correction can be performed manually (as for the experiments in **Chapter 3**) and automatically by dedicated software (experiments in **Chapters 3-6**).

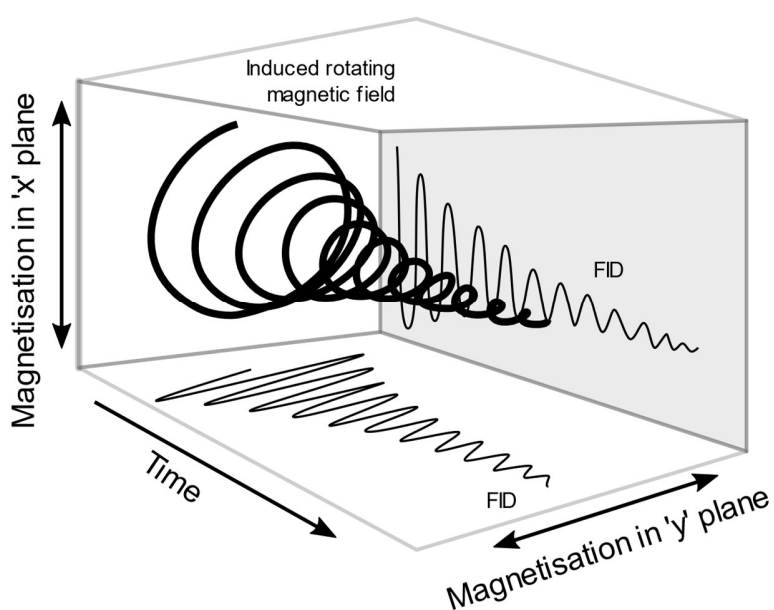


Figure 1.12. Signal free induction decay (FID) and phase

Figure representing the induced rotating magnetic field with its amplitude decaying over time (referenced from laboratory frame of view). When the signal is observed from plane 'x', it produces a decaying cosine wave, whereas when it is observed from an orthogonal plane 'y', it produces a decaying sine wave. These FIDs must be taken together to delineate negative and positive frequencies (as cosine 90 degrees = cosine -90 degrees), either by automated or manual phase adjustment. *Abbreviations: FID, free induction decay.* Figure adapted from de Graaf RA. In Vivo NMR Spectroscopy: Principles and Techniques, 2nd Edition Chapter 1, © 2007 John Wiley & Sons, Ltd (de Graaf, 2007)

1.5.3 Quantum mechanical explanation

The quantum mechanical explanation for NMR of the isotopes in this thesis (^1H , ^{13}C , ^{31}P) states that nuclear spin, described in **Nuclear Magnetism** (above), has two states of a fixed quantity, – either with or against the external magnetic field B_0 . Spins aligned with B_0 are in a lower energy state, given by Equation 1.6; and spins aligned against B_0 are in a higher energy state, expressed by Equation 1.7. It is thought that a single nucleus actually exists in a quantum combination of both states simultaneously in a probability distribution, adopting one or the other when observed macroscopically. The difference in the population observed between the two spin states is given by the Boltzmann distribution, in Equation 1.8.

Equation 1.6

$$E_- = -\frac{1}{2} \cdot \frac{B_0 \gamma h}{2\pi}$$

Equation 1.7

$$E_+ = +\frac{1}{2} \cdot \frac{B_0 \gamma h}{2\pi}$$

Equation 1.8

$$\frac{N_-}{N_+} = e^{(-B_0 \gamma h / 2\pi k T)}$$

Where h is Planck's constant, T is temperature in Kelvin and k is the Boltzmann constant. Normally the energy of thermal equilibrium is much greater than that of B_0 so the ratio is very small.

By applying an RF electromagnetic pulse at the Larmor frequency of the nucleus, which translates to the energy difference between the two states ($E = hf$), nuclei from the lower energy state will be pushed to the higher energy state. When the RF pulse is removed, nuclei relax back to the lower energy state, resulting in a transfer of energy at the Larmor frequency of the nuclei to a receiving coil (**Figure 1.13**). It is not agreed how to explain this transfer of energy using the quantum model (Hoult, 2009). However, the gyromagnetic ratio of a ^1H nucleus is greater than that of ^{31}P and ^{13}C nuclei, so ^1H 's precessional frequency is higher, and therefore the energy transferred or 'released' when it relaxes is greater than that of ^{31}P and ^{13}C (Equation 1.8, **Table 1.3**). Thus ^1H NMR is more sensitive than ^{31}P and ^{13}C NMR, explaining the different acquisition parameters for ^1H and ^{13}C in **Chapter 3**, and the choice of voxels size for ^{31}P MRS in **Chapters 4-6**.

Table 1.3: Gyromagnetic ratio

Isotope	Gyromagnetic ratio (MHz T ⁻¹)	Larmor frequency at 3 T (MHz)	Natural abundance (%)	Relative sensitivity
¹ H	42.58	127.74	99.99	1
³¹ P	17.24	51.72	100.00	0.0665
¹³ C	10.71	32.13	1.11	0.00018

¹H, ³¹P and ¹³C gyromagnetic ratio and Larmor frequency at 3 T, % natural abundance and relative sensitivity accounting for % natural abundance of isotope and Larmor frequency, but not natural concentration of nuclei in the brain or sample.

Spin system at rest, no external magnetic field applied.

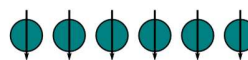


Application of strong external magnetic field B_0 allows spins to be in either a higher or lower energy state, with a slight preponderance to the lower energy state.

B_0



Higher Energy Level



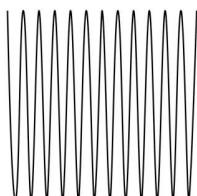
Lower Energy Level

Irradiation of system with electromagnetic energy at the appropriate frequency (energy that matches difference in energy states) shifts some spins from the lower energy to the higher energy state.

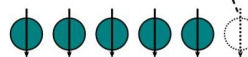
B_0



B_1 RF pulse



Higher Energy Level



Lower Energy Level

After irradiation the spins pushed into the higher energy level relax back to the lower energy level, releasing energy at the same frequency as that of RF excitation.

B_0



FID

Figure 1.13: Simplified quantum mechanical explanation of nuclear magnetic resonance.

Sequence read from top to bottom. Abbreviations: see table in *Precis*.

1.5.4 Chemical shift

From the Larmor equation, the resonant frequency of a nucleus depends on its gyromagnetic ratio (see **Table 1.3**), and the strength of the external magnetic field that is applied (B_0). In a chemical sample or living tissue, the magnetic field that the nuclei are actually subject to is influenced by its immediate chemical environment: Electrons, like protons, have charge and generate magnetic fields due to their motion around the nucleus. Their magnetic field is antiparallel to the B_0 , so 'shield' it, reducing the effective B_0 that the nucleus experiences. If the electrons of a ^1H nucleus are drawn away by an adjacent, more electronegative element such as oxygen, there is reduced electron shielding from the B_0 experienced by the ^1H nucleus. As the nucleus is exposed to a higher effective B_0 , its Larmor frequency is therefore fractionally higher than it would be in the absence of oxygen (graphical representation in **Figure 1.14**). This effect, called chemical shift, is relatively tiny; usually only measurable over a maximum of a few chemical bonds, and expressed in parts per million (ppm; Hz per MHz). It is the same at all field strengths and is the basis for identifying metabolites using MRS, used in results **Chapters 3-6**. In principle, a peak will be observed for every magnetically distinct nucleus in a molecule because nuclei that are not in identical structural situations do not experience the same shielding, and therefore experience slight differences in the external magnetic field that they are subject to.

Electronegative oxygen attracts electrons away from hydrogen bonded on other side of attached carbon

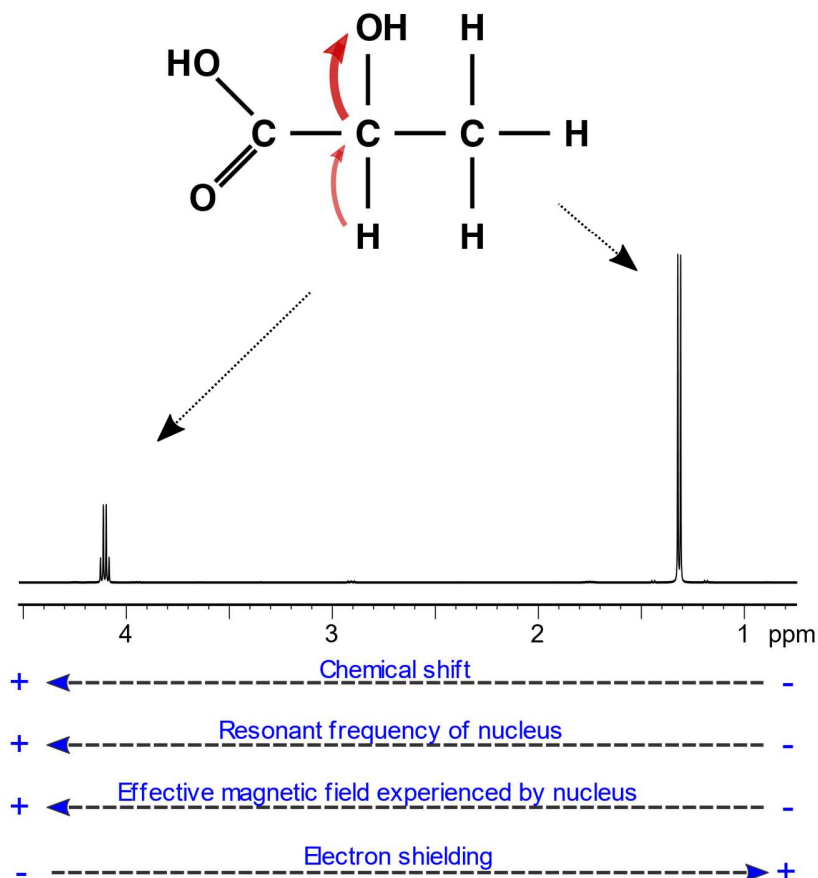


Figure 1.14. Graphical representation of chemical shift.

The electronegative oxygen draws electrons away from its bonded carbon, and the hydrogen on the other side (red arrows). This reduces the electron shielding of the hydrogen from the B_0 , increasing the effective magnetic field that it experiences, increasing its resonant frequency.

1.5.5 Scalar coupling / J-coupling

Scalar coupling is also caused by the interaction of electron spins with nuclei and occurs most strongly between magnetic nuclei that are bonded to each other, causing splitting of their spectral peaks. Fermi contact means that an s-orbital electron spin and nuclear spin favour an antiparallel orientation, but when a ^1H and ^{13}C are covalently bonded, the Pauli exclusion principle demands that the spins of the electron pair are antiparallel. Thus, two higher energy levels and two lower energy levels exist for each of the ^{13}C and ^1H nuclei, dependent on their electron spins being antiparallel or parallel with their nuclear spins. This yields two possible energy transitions, therefore two Larmor frequencies. Splitting can be more complex than a doublet, with the number of different frequencies equal to the number of coupled nuclei plus one for isotopes with a spin quantum number of $\frac{1}{2}$. The frequency difference between the split pairs is a constant, independent of field strength. J-coupling can reveal further information about the structure of a nucleus's molecular environment using high resolution NMR, and is used in **Chapter 3**, but in practice resolution is rarely sufficient with *in-vivo* MRS to fully separate a multiplet, and so the effect of peak splitting usually just broadens the signal and reduces peak height relative to baseline noise. Spectra can be simplified by ^1H decoupling, which is essential for some applications, and used, again in the experiments in **Chapter 3**.

1.5.6 Acquisition and processing

A typical RF excitation pulse is short, lasting milliseconds. In NMR and MRS experiments, often the delay between the end of the applied pulse and the opening of the receiver coil is kept to a minimum to detect as much induced transverse magnetisation as possible. However, MR sensitive nuclei that are bound up in large macromolecules or closely confined by cellular membranes exchange their spin states so quickly by spin-spin interaction that their transverse magnetisation decays by T2 decay before it can be detected. Only unbound molecules that are free to tumble, with slower spin-spin relaxation can be detected by NMR/MRS. This effect is sometimes exploited by purposefully delaying an acquisition's TE to simplify a complex spectrum by eliminating metabolites with relatively short T2.

As a single NMR/MRS experiment is a relatively insensitive technique, the acquisition is repeated multiple times and the acquired FID averaged together to increase signal to noise (SNR). The improvement in SNR is proportional to the square root of the number of averages (n). If the delay between acquisitions (TR) is repeated before a pause of more than five times the T1 of a nucleus within a molecule, the longitudinal magnetisation available for successive excitations is diminished and signal from that molecule will be artificially reduced. This is discussed briefly in **Chapter 5**.

After acquisition of the FID, which is acquired in the time domain, it is filtered (covered in **Chapters 2-4**), Fourier transformed, and phase corrected. The Fourier transformation converts a complex combination of decaying frequencies over time into a recognisable array of peaks over a frequency range (**Figure 1.15**).

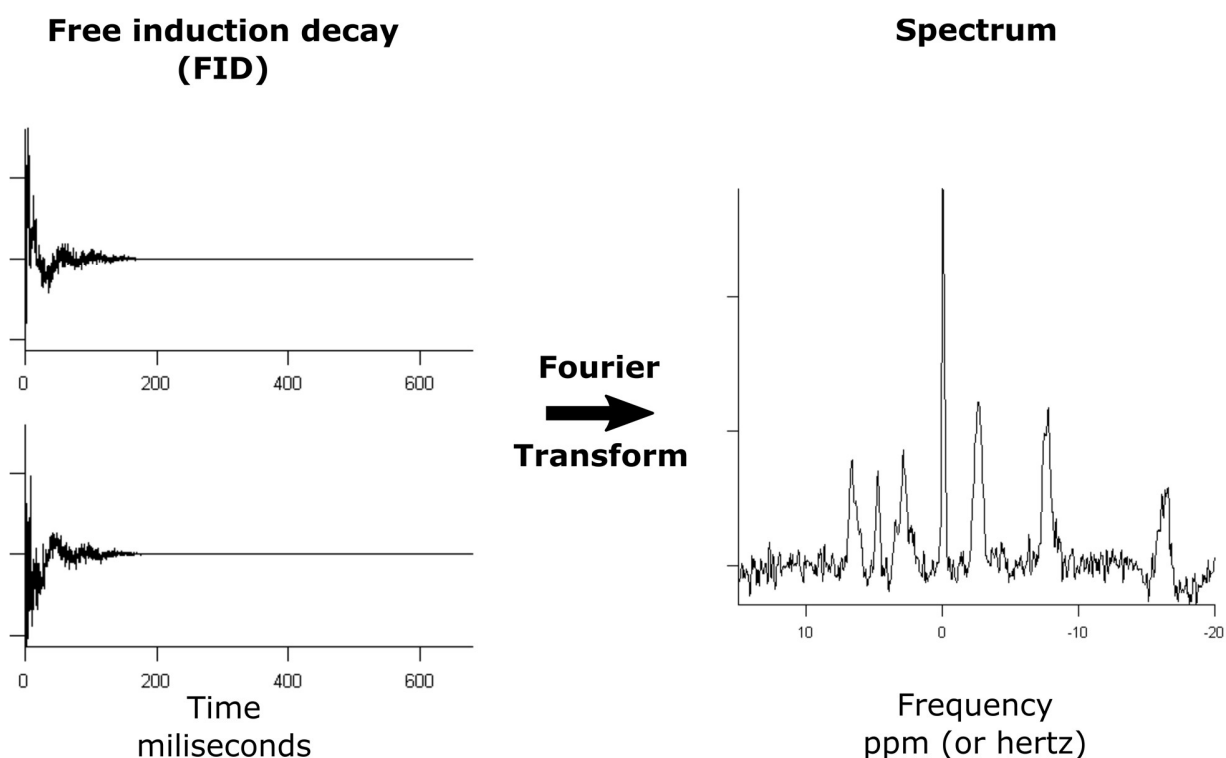


Figure 1.15. The time domain, frequency domain and Fourier transformation

The Fourier transform converts the complex combination of decaying waves in the time domain (the FID), into its individual frequencies, expressed in the frequency domain (the spectrum). Example FID and spectrum acquired on a healthy volunteer using a ^{31}P volume head coil on a 3T Siemens Trio scanner, 200 ms Hanning filter applied to spectrum. *Abbreviations: see table in **Precis**.*

Each frequency is identified by its chemical shift, expressed in parts per million (ppm) of a standard, set at 0 ppm. As described above, nuclei with extremely rapid spin-spin relaxation are not detected, but those with slightly less rapid relaxation can appear as a broad baseline hump in the spectrum. This is because the Fourier transformation of a fast decay gives an uncertain, wide frequency range.

Spectra are typically plotted with the chemical shift along the x-axis with increasing chemical shift (higher frequencies) reading from right to left. The y-axis represents signal intensity and can be quantified in high resolution NMR, but this is much more challenging when using *in-vivo* MRS.

A variety of commercially available software exists to analyse spectra with greater or lesser automation. The most commonly used for high-resolution NMR is Bruker's Topspin (Bruker, GmbH, Karlsruhe, Germany), which allows significant manual manipulation of spectra. For *in-vivo* MRS, the scanner manufacturer's built in software can be used, such as Syngo for Siemens (Siemens Medical Solutions), or third party programs such as LCModel (Provencher, 2001) and jMRUI (Stefan *et al.*, 2009). The methods of spectral analysis can be found in **Chapters 3** and **4**.

1.5.7 Signal localisation

High-resolution NMR of *in-vitro* samples does not require spatial encoding, as the sample within the NMR tube is considered homogenous. Where signal originates from in human brain is relevant and can be encoded using gradient coils that influence the magnetic field that the brain is subjected to. In classic MR imaging, a magnetic gradient (1) is applied during RF excitation that influences nuclei resonant frequency, meaning that only a single slice of tissue is excited by the RF pulse, thereby encoding one dimension (slice select gradient). Another magnetic gradient (2) is applied during signal detection, influencing precessional frequency of the nuclei during their detection, so encoding a second dimension (frequency encoding with readout gradient). The third dimension is encoded by applying varying magnetic gradients (3) in between these two gradients (1 and 2) that causes a change in the phase of the nuclei, rather than a change in their frequency (phase encoding gradients). These stepped phase encoding gradients are applied in successive iterations of the pulse-sequence, so the whole process (acquisition) must be repeated for each step of phase encoding (**Figure 1.16**), and then again for each slice.

As the frequency of a nucleus is the basis for its identification in MRS, frequency encoding gradients (2) are not used. Localisation of MRS signal can be achieved with: various single-voxel techniques that use sequentially applied RF-pulses with gradients, multivoxel chemical shift imaging (CSI) techniques that use extra phase encoding steps (3), or surface RF coils that only excite and detect signal from the small volume of tissue adjacent to the coil. The experiments in this thesis (**Chapters 4-6**) use the multivoxel CSI technique – also known as MR spectroscopic imaging (MRSI) (**Figure 1.16**). In CSI, 3D localisation of spectroscopy signal from a grid of voxels can be obtained using a slice select gradient (1) and a pair of variable, stepped phase encoding gradients (3) applied orthogonally to each other (Keevil, 2006; Skoch

et al., 2008). Alternatively, 3D localisation of signal from within a large cube (rather than a single grid) can be acquired using three phase encoding gradients (3) without a slice select gradient (1). However, this additional phase encoding step is often impractical as a pair of phase encoding steps is typically the limit of an acceptable scan duration.

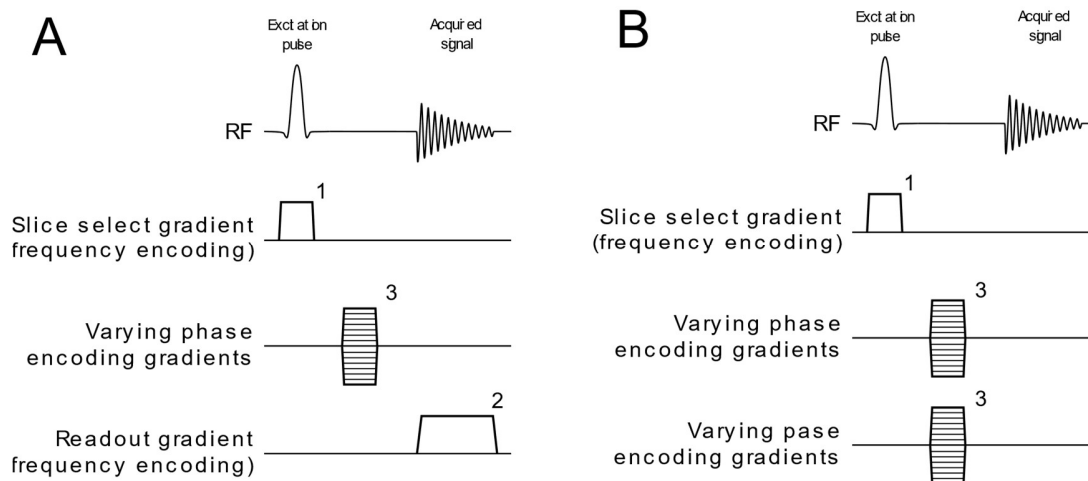


Figure 1.16. Simplified pulse-timing diagrams of 'standard' MRI and 2D CSI (with slice select gradient).

Panel A: Standard MRI acquisition with a slice select gradient (1) applied during the RF excitation pulse to localise one dimension, then a frequency encoding gradient (2) applied orthogonally during signal sampling to localise a second dimension. The third and final dimension is encoded by a phase encoding gradient (3) that is applied in between the two gradients (1 and 2) with different intensity for each iteration, resulting in different degrees of dephasing of spins. *Panel B:* A slice select gradient (1) is applied during the RF excitation pulse to localising a single slab of tissue, with stepped orthogonal frequency encoding gradients to encode two further dimensions, providing 3D localisation within the slab.

As phase encoding gradients are applied between the RF excitation and signal detection, the first few points of a potential FID cannot be acquired. Unlike MRI which deals with water at a single frequency, the different metabolites examined with MRS may have very different precessional frequencies that dephase at different rates, so phase coherence is lost by the time of sampling. Thus, the necessary loss of the first few points of the FID leads to uncertainty in phase correction of the spectra. Automated techniques exist to mitigate against this, but often result in some distortion of the baseline, as occurs partially in the results of **Chapters 4-6** (Saeed and Menon, 1993).

Chapter 2

Generic Materials and Methods

2.1	Patients	38
2.2	Microdialysis	38
2.2.1.1	Catheter insertion	38
2.2.1.2	Perfusate	39
2.2.1.3	Analysis of microdialysates	39
2.3	High-resolution NMR of microdialysis samples.....	40
2.4	Clinical monitoring	42
2.5	<i>In-vivo</i> MR imaging and MR spectroscopy	43
2.5.1	Timing of scans and multimodality monitoring	43
2.5.2	Acquisition of ^{31}P chemical shift imaging MR spectroscopy	44
2.5.3	Acquisition of ^1H MR Imaging	45
2.5.4	Co-registration of MR imaging data.....	45
2.5.5	Processing and analysis of ^{31}P chemical shift imaging MRS spectra	45
2.5.5.1	Selection of voxels	45
2.5.5.2	Processing of spectra	45
2.5.5.3	Analysis of spectra	46
2.5.6	Acquisition of ^1H T1 maps in gadolinium MR contrast agent study.....	46
2.5.7	Processing and analysis of ^1H T1 maps	47
2.6	Statistics	48
2.7	Declaration and specific acknowledgements.....	48

2.1 Patients

Adult patients (aged ≥ 16 years old) were recruited who had sustained moderate or severe TBI (defined as cranial trauma with consistent CT scan findings and a post-resuscitation Glasgow Coma Scale (GCS) ≤ 12), that required sedation and mechanical ventilation for intracranial hypertension and airway protection – which I define in this thesis as ‘major’ TBI. Patients were excluded with a pre-existing neurological condition, a previous significant head injury requiring hospitalisation, or if they were unlikely to survive more than 24 hours. Patients with non-MR compatible implants were excluded from *in-vivo* MR experiments and those with bleeding diathesis excluded from microdialysis studies. Patients were treated using the standard Neurocritical Care Unit (NCCU) TBI management protocols including: endotracheal intubation, ventilation, sedation, muscular paralysis and maintenance of blood sugar (serum glucose) concentration within the target range 4–10 mmol/L (Menon and Ercole, 2017). Targeted depth of sedation was not changed over patients’ inclusion in the studies. Sedation was achieved with propofol, with or without midazolam. Barbiturates were not used. Informed written assent was sought from the relatives of those patients who had suffered a TBI, or an independent medical practitioner if a relative could not be identified. Patients’ 6-month follow-up (**Chapter 5**) included Extended Glasgow Outcome Scale (Jennett *et al.*, 1981) (GOS-E) scoring, which was assessed without knowledge of study results. Outcome was dichotomised into upper severe disability or better (GOS-E ≥ 4 ; independent at home) and lower severe disability or worse (GOS-E ≤ 3 ; dependent at home, vegetative or dead), in accord with other recent studies.(Maas *et al.*, 2013; Hutchinson *et al.*, 2016).

Healthy control subjects were recruited from contacts in the academic department after obtaining informed, written consent.

The study was carried out in conformation with the spirit and the letter of the Declaration of Helsinki and the protocol was approved by the National Research Ethics Service, Committee East of England – Cambridge Central (REC Reference No. 11/EE/0463). Data from 4 patients in **Chapter 3** were taken from an existing dataset and published in pooled analysis in a previous publication (Jalloh *et al.*, 2015a), and not recruited by me.

2.2 Microdialysis

2.2.1.1 Catheter insertion

CMA 71 microdialysis catheters (shaft 60 mm, membrane length 10mm, membrane diameter 0.6 mm, nominal molecular weight cut-off 100 kDa) (MDialysis AB, Stockholm, Sweden) were directed into normal appearing frontal cortex white matter, neither into nor adjacent to lesions identified on CT. This

was either via a craniotomy for a traumatic lesion, or through a cranial access device (CAD) 'triple-bolt' (Technicam, Newton Abbot, UK) alongside an intracranial pressure monitor (Codman, Raynham, MA, USA) and, when available, a Licox brain tissue oxygen sensor (Integra LifeSciences Corporation, Plainsboro, NJ, USA). In patients with two catheters, one was inserted via a triple bolt and one via a craniotomy. Whereas I inserted many of the catheters, some were inserted by other neurosurgeons as part of routine clinical care in Addenbrooke's hospital neurocritical care unit.

2.2.1.2 Perfusate

Catheters were perfused at 0.3 $\mu\text{L}/\text{min}$ with unsupplemented CNS Perfusion Fluid (M Dialysis AB), consisting of an aqueous solution of NaCl (147 mmol/L), KCl (2.7 mmol/L), CaCl_2 (1.2 mmol/L), and MgCl_2 (0.85 mmol/L). Supplementation with study substrates (1,2- $^{13}\text{C}_2$ glucose in **Chapter 3**, 2,3- $^{13}\text{C}_2$ succinate in **Chapter 6**, and gadobutrol in **Chapter 7**) was achieved by changing the microdialysis pump syringe over to one containing pre-formulated study substrate. Study substrate perfusion was intended for ≈ 24 hours, but due to factors associated with patient care, occasionally it was perfused for a shorter or longer period of time. Microdialysis pump syringes were replaced with new syringes containing unsupplemented CNS Perfusion Fluid at the end of study substrate perfusion.

1,2- $^{13}\text{C}_2$ glucose (**Chapter 3**) and 2,3- $^{13}\text{C}_2$ succinate (**Chapter 6**) in CNS perfusion fluid were formulated by the Pharmacy Manufacturing Unit, Department of Pharmacy, Ipswich Hospital NHS Trust (Ipswich, UK) using high-grade ^{13}C substrates obtained from Cambridge Isotope Laboratories (Tewksbury, MA, USA) (isotopic enrichment 99 %, chemical purity 99 %). Formulations were tested to verify purity, sterility, freedom from endotoxins and absence of pyrogenicity, before release for use in patients. Formulation and testing was supervised by Mr John Harwood (Manufacturing Unit, Department of Pharmacy, Ipswich Hospital NHS Trust).

Gadolinium contrast agent supplementation in CNS perfusion fluid (**Chapter 7**) was prepared at the bedside as follows: Using a 1 ml 'insulin syringe', 0.1 ml of 1 mol/L concentration gadobutrol (Gadovist[®], Bayer AG, Germany) was diluted in 10 mls of CNS perfusion fluid in a sterile 10 ml universal container, then transferred to a microdialysis pump syringe, at a final gadobutrol concentration of 10 mmol/L.

2.2.1.3 Analysis of microdialysates

Microdialysis collection vials were changed every hour and the microdialysates analysed hourly on a bedside ISCUS analyser (M Dialysis AB); employing enzymatic colorimetric assays for glucose, lactate and pyruvate. Results from two hours of perfusion after changeover from NPF to study substrate, and

changeover from study substrate to NPF were discarded as 'run-in' and 'washout' periods, as per definitions in previous studies (Jalloh *et al.*, 2017). After analysis by ISCUS, the remaining microdialysate in vials from \approx 24 hours of substrate perfusion were pooled for NMR analysis. If NMR analysis could not be performed within 24 hours, vials were stored at -80 °C and later thawed and pooled for NMR analysis.

2.3 High-resolution NMR of microdialysis samples

Cerebral microdialysates perfused with 8 mmol/L 1,2- $^{13}\text{C}_2$ glucose were pooled by individual patient for NMR analysis. 180 μL of a patient's pooled sample was added to 20 μL of deuterium oxide (D_2O) and 50 μL of 24 mmol/L 2,2-dimethyl-2-silapentane-5-sulfonate sodium salt (DSS) internal reference standard (Sigma-Aldrich, Poole, Dorset, UK). NMR analysis was performed using 3mm NMR tubes (Hilgenberg GmbH, Malsfeld, Germany) in a Bruker Avance III HD 500 MHz spectrometer (Bruker BioSpin GmbH, Karlsruhe, Germany) using a dual $^1\text{H}/^{13}\text{C}$ cryoprobe (CP DUL500C/H, Bruker BioSpin GmbH) for ^{13}C and ^1H spectral acquisition. ^1H spectra were acquired using the water suppression pulse program *zgpr*, with 32 averages preceded by 2 dummy scans and a D1 (relaxation delay) of 32 seconds, to prevent T1 saturation effects. ^{13}C spectra were acquired using the pulse program *zgpg30*, with 4,096 (4 k) scans using a 30-degree flip angle on the carbon channel with a D1 of 3 seconds, digitizing 64 K points. Power-gated broadband ^1H decoupling was achieved using the 'WALTZ-16' supercycle. The receiver gain was set to a constant value in each experiment. NMR experiments were run by Mr Duncan Howe, Department of Chemistry, University of Cambridge.

Analysis of spectra was performed after exponential filtering (0.3 Hz for ^1H , 3.0 Hz for ^{13}C), Fourier transformation, phase correction (automatic and manual), and automatic polynomial baseline correction using TopSpin (Bruker GmbH, Germany). Peaks were identified referencing our own standards and online NMR databases (BMRB—Biological Magnetic Resonance Bank, University of Wisconsin (Ulrich *et al.*, 2008) and HMDB/HMDB—Human Metabolome Database, Genome Alberta (Wishart *et al.*, 2007)). Chemical shifts were referenced to DSS at zero ppm (Hz per MHz). Peak areas for DSS and lactate signals were integrated using Topspin at a standardised chemical shift range.

To quantify the lactate signals in the ^{13}C NMR spectra, peak areas of lactate relative to the internal standard DSS peaks were compared, using a series of known concentrations of standard (unenriched) lactate, containing naturally abundant 1.1 % ^{13}C (Jalloh *et al.*, 2018). These standards were prepared in

the same way as the microdialysates; using the same volumes and concentrations of D₂O and DSS internal standard and run under identical NMR conditions (see above). There was a linear relationship between the 3-¹³C lactate peak area (at 22.8 ppm) divided by the DSS internal standard peak area (at 0 ppm), relative to the concentration of the known unenriched lactate standard (assuming 1.1 % natural abundance of ¹³C in the standard) (**Figure 2.1, Panel A**). Calculating the concentration of lactate from ¹H NMR sequence *zgpr* does not require calibration, however the ¹H NMR-derived lactate concentration was nonetheless confirmed to be equal to its actual concentration calculated by weight of lactate in volume of sample (**Figure 2.1, Panel B**).

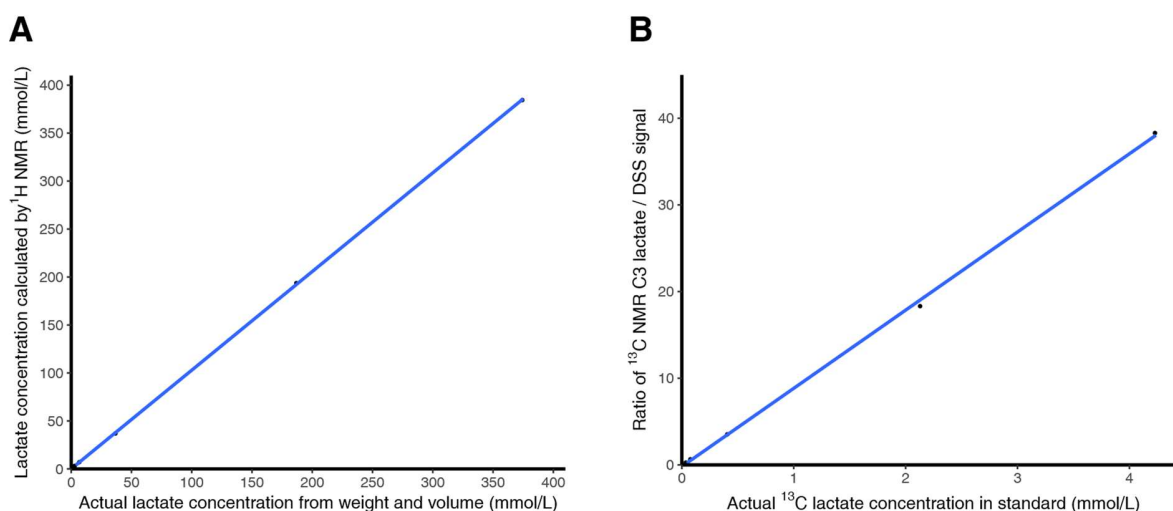


Figure 2.1 Standard ‘curves’ of lactate standards and their NMR signal

Panel A, ¹H NMR: Concentration of lactate calculated by ¹H NMR vs. actual lactate standard concentration. *y-axis* = lactate methyl signal (doublet at 1.32 ppm) divided by a third of the DSS signal (at 0 ppm, representing 3 methyl groups), multiplied by the known concentration (by weight) of DSS in the sample. In this calculation, the ¹H NMR lactate satellites of the 1.32 ppm peak split by natural abundance ¹³C were included to represent all lactate in the sample. These satellites were *not* used in later calculations (such as enrichment calculations), as ¹³C data were used instead. *x-axis* = Actual concentration of lactate in sample calculated from weight of DSS and volume of sample. The concentration calculated with ¹H NMR correlated closely with the known concentration of lactate standard (regression coefficient of 1.0068, $r^2 = 0.9998$). The pulse program *zgpr* was used with a long D1 of 32 s to avoid NMR saturation effects. *Panel B, ¹³C NMR:* Ratio of ¹³C NMR lactate/DSS signal, vs. actual lactate standard concentration. *y-axis* = ¹³C NMR signal of lactate C3 (at 22.8 ppm) divided by DSS signal (at 0 ppm, representing 3 methyl groups). *x-axis* = Actual concentration of 3-¹³C lactate (methyl group) in sample assuming ¹³C natural abundance of 1.1 %. The calculated correlation coefficient of 9.22 ($r^2 = 0.9995$) was used to calculate ¹³C lactate concentrations from ¹³C NMR lactate C3 / DSS signal ratios in later experiments.

The fractional enrichment (%) of ^{13}C lactate was defined as $100 \times [^{13}\text{C}] / ([^{13}\text{C}] + [^{12}\text{C}])$, where square brackets indicate concentrations of the relevant species (Equation 2.1). $[^{13}\text{C}]$ was determined from the calibrated ^{13}C NMR spectra (above). $[^{12}\text{C}]$ was determined from the ^1H spectra, measuring the peak areas of lactate C3 methyl protons that give an ^1H NMR doublet at 1.32 ppm (from protons attached to ^{12}C), relative to the peak area of DSS internal standard signal (at 0 ppm). The natural abundance of ^{13}C is 1.1 % of all carbon atoms, and ^{13}C results presented for the lactate ^{13}C singlet signals were expressed after subtracting this natural background. ^{13}C doublet signals were not background-subtracted because the probability of two ^{13}C atoms occurring next to each other naturally is 0.01 % (1.1 % x 1.1 %).

Equation 2.1

$$\text{Fractional enrichment} = \frac{[2,3-^{13}\text{C}_2 \text{ lactate}] + [3-^{13}\text{C} \text{ lactate}]}{[2,3-^{13}\text{C}_2 \text{ lactate}] + [3-^{13}\text{C} \text{ lactate}] + [^{12}\text{C} \text{ lactate}]} \times 100$$

Where **red** denotes data from ^{13}C NMR spectra and **blue** denotes data from ^1H NMR spectra.

The ratio of pentose phosphate pathway (PPP)-derived 3- ^{13}C lactate to glycolysis-derived 2,3- $^{13}\text{C}_2$ lactate was expressed in the form 1:N where N is the concentration of lactate derived from the ^{13}C doublet at 22.8 ppm, divided by the concentration of lactate represented by the ^{13}C singlet at 22.8 ppm (after first subtracting the singlet's ^{13}C natural abundance background) (Equation 2.2).

Equation 2.2

$$\frac{\text{PPP derived lactate}}{\text{glycolysis derived lactate}} = \frac{[3-^{13}\text{C} \text{ lactate}]}{[2,3-^{13}\text{C}_2 \text{ lactate}]} \times 100$$

2.4 Clinical monitoring

Patients received standard neurocritical care monitoring of Addenbrooke's NCCU; including mean arterial blood pressure (MAP), intracranial pressure (ICP), microdialysis and, where available, Licox PbtO₂ monitoring. Codman Microsensor intracranial pressure (ICP) probes (Codman Neuro, Johnson & Johnson, Wokingham, UK) and Licox brain tissue oxygen concentration (PbtO₂) monitoring probes (Integra LifeSciences Corporation, Plainsboro, NJ, USA) were inserted through triple lumen cranial access devices (Technicam, Newton Abbot, UK). Codman data were recorded and reviewed with ICM+ software

(Cambridge Enterprise Ltd., Cambridge, UK) (Smielewski *et al.*, 2005). CMA 71 microdialysis catheters were perfused at 0.3 $\mu\text{L}/\text{min}$ with unsupplemented CNS Perfusion Fluid (M Dialysis AB) and the recovered microdialysate vials analysed hourly using an ISCUS analyser (M Dialysis AB) (see above, **Microdialysis**). Routine arterial blood gas analysis (ABG) was performed, analysing PaCO_2 and pH of the arterial blood.

2.5 *In-vivo* MR imaging and MR spectroscopy

2.5.1 *Timing of scans and multimodality monitoring*

Scans were performed in the acute phase of injury, as soon as patients' intracranial pressure permitted them to be laid supine, but whilst they still required full sedation, ventilation and monitoring for control of intracranial hypertension. Patients were taken to the Wolfson Brain Imaging Centre (WBIC) scanner suite by me, an anaesthetist and a nurse. The location of the WBIC, directly adjacent to the neurosciences critical care unit, allows minimal disruption to clinical care during scan and transfer. The patients were maintained fully sedated and ventilated during the scans. Scans were acquired with the help of radiographer-physicist Dr Marius Mada.

During the scans ICP probes were coiled outside the RF head coil, as described previously (Newcombe *et al.*, 2008), to allow for continuous intracranial pressure monitoring. As microdialysis pump batteries are not MR compatible, the pumps must be disconnected from the catheters during the MR study, but the catheters themselves can remain *in-situ* for reconnection after the scan. Licox probes were similarly disconnected for scans and reconnected after return to NCCU. The time between disconnection of microdialysis and scanning in **Chapter 7** was kept to a minimum, with less than 15 minutes between disconnection and starting acquisition of ^{31}P spectra. An ABG sample was analysed immediately before and after patients in **Chapter 3** and **5** went for an MR scan, and the average of the two results used for analysis.

2.5.2 Acquisition of ^{31}P chemical shift imaging MR spectroscopy

Clinical 3 Tesla Siemens MR scanners (Trio and Verio) were used, with a custom ^{31}P head coil (PulseTeg Ltd., Chobham, UK) with a birdcage design that opens to facilitate use with our patients. Spectra were acquired using oblique 2-dimensional single slice chemical shift imaging (2D CSI) of 25 x 25 x 25 mm voxels in an 8 x 8 grid (**Figure 2.2**).



Figure 2.2. Example of a ^{31}P birdcage volume head-coil

The front of the coil can be opened, allowing to access a patient's head. The ^{31}P coil contains a ^1H channel for imaging, that allows localisation of the acquired spectra.

Flip angle was 90 degrees, TR 4000 ms, TE 2.3 ms, and band-width 3000 Hz. Repeats were performed for 30 (19 min) or 60 (35 min) averages (see **Chapter 4**). Weighted sampling of k-space was performed. In addition to the ^{31}P channel, the head coil contains a ^1H channel that allows an image of the brain to be acquired. Proton density and T2W scans were acquired before ^{31}P spectra so that the CSI grid could be appropriately positioned in subjects' brains.

For patients who had microdialysis catheters, CSI grids were positioned so that the microdialysis membrane was in the centre of a 25 x 25 x 25 mm voxel. CMA 71 microdialysis catheters contain a short gold filament at their tip (see **Figure 1.8**), visible on computerized tomography (CT) and the catheters are also visible on some magnetic resonance imaging (MRI) sequences (see **Chapter 4**). Catheters are otherwise invisible on MR and CT. To aid accurate positioning of the grid, patients' most recent CT scans were uploaded to the Siemens' terminal and co-registered with the proton density weighted and T2W sequences, so the position of the gold filament could be ascertained on the MRI sequences.

2.5.3 Acquisition of ^1H MR Imaging

After acquisition of ^{31}P MRS data using the above ^{31}P sequences, the subjects were withdrawn from the scanner, the ^{31}P head coil changed to a Siemens 12-channel ^1H head/neck coil, and further imaging acquired: 3D T1W gradient echo sequences (MP-RAGE; TE 2.98 ms, TR 2300 ms)(Brant-Zawadzki *et al.*, 1992) were acquired to assess subject anatomy, and fluid attenuated inversion recovery (FLAIR; TE 394 ms, TR 6000 ms) and susceptibility weighted imaging (SWI; TE 20 ms, TR 29 ms) sequences to detect injury.

2.5.4 Co-registration of MR imaging data

Image co-registration was performed in collaboration with Dr Jiun-Lin Yan. For a detailed description of this process, see **Appendix 1 (Chapter 10)**, but briefly: MP-RAGE, FLAIR and SWI sequences acquired with the 12-channel ^1H coil were co-registered with PD/T2 sequences acquired using the ^{31}P head coil. Voxel tissue-type (grey matter, white matter, and CSF) was segmented using FAST (FMRIB's Automated Segmentation Tool) processing of 3D T1W gradient echo sequences (MP-RAGE) in FSL (FMRIB software, Oxford, UK). Regions of FLAIR and SWI radiological injury were reviewed and manually mapped. Ratios of grey matter/white matter and radiologically-visible injury were then calculated for each voxel using Matlab software (MathWorks, Natick, MA). Voxels containing less than 90 % brain tissue were excluded. A sub-analysis of 'radiologically-normal' brain was performed by further excluding voxels that contained more than 5 % injury on FLAIR or SWI (further details in **Appendix 1 (Chapter 10)**).

2.5.5 Processing and analysis of ^{31}P chemical shift imaging MRS spectra

2.5.5.1 Selection of voxels

On the Siemens terminal, the 'central eight' voxels in each subject's brain were identified, and their position noted. Spectra were assessed visually and deemed acceptable if their signal to noise was sufficient for clear identification of the PCr, ATP and Pi peaks.

2.5.5.2 Processing of spectra

^{31}P spectra were filtered with a 200 ms Hanning filter, fitted, and peak areas (integrals) and chemical shifts computed using Siemens Syngo software. PCr, ATP and Pi peak integral, chemical shift and amplitude of the selected voxels were recorded. Each subject's spectral data were combined with their voxel tissue type and injury percent data (in their *Voxel_Percent_<<subject>>.csv* file – see **Chapter 10, Appendix**) using R (<http://www.R-project.org/>) for analysis. Voxels containing less than 90 % brain

volume (grey matter, white matter or CSF) were excluded. A subset of voxels that contained more than 5 % injury on FLAIR or SWI were defined.

2.5.5.3 Analysis of spectra

Absolute concentrations are difficult to accurately quantify with *in-vivo* clinical ^{31}P MRS, so the ratio of PCr to γATP signal intensities of the fitted spectra were used as our primary measure of high-energy phosphate metabolic status (Levine *et al.*, 1992; Mason *et al.*, 1998). γATP was employed as the ‘cleanest’ of the three ATP signals. The βATP peak was not used as it is not reliably excited due to being at the edge of the excitation bandwidth at 3T, and the αATP peak is incompletely resolved from NAD^+ and NADH . I did not attempt to adjust ATP values for the presence of ADP, as the latter is naturally much less abundant, e.g. $\text{ATP} \approx 3 \text{ mmol/L}$, $\text{ADP} < 100 \text{ micromol/L}$ (de Graaf, 2007), thus ADP only contributes around 3 % of total combined ATP and ADP. Moreover, ADP is mostly MR-invisible (Stubbs *et al.*, 1984; Takami *et al.*, 1988). To indicate whether variation in PCr/ γATP ratio was driven principally by changes in PCr or γATP , I assessed the ratio of PCr to total-mobile-phosphate (defined as the combined signals PCr + γATP + Pi) and the ratio of γATP to total-mobile-phosphate (Levine *et al.*, 1992; Mason *et al.*, 1998). The PCr, γATP and Pi resonances together represent the total mobile high energy phosphate pool involved directly with ATP metabolism. Intracellular pH was calculated from the chemical shift difference between PCr and Pi, using the established Equation 2.3 (Petroff *et al.*, 1985; Prichard and Shulman, 1986).

Equation 2.3

$$pH = 6.77 + \log_{10} \left(\frac{\Delta Pi - 3.29}{5.68 - \Delta Pi} \right)$$

Where ΔPi is the difference in chemical shift between the PCr and Pi peaks, in Hz / MHz.

2.5.6 Acquisition of ^1H T1 maps in gadolinium MR contrast agent study

T1 maps were acquired and analysed in collaboration with Dr Daniel Tozer and Mr Pascal Ruetten, using a clinical 3 Tesla Siemens Prismafit scanner. A Siemens 12-channel ^1H head/neck coil was used that was sufficiently large to accommodate a patient’s head with a protruding cranial access device.

Patients’ CMA 71 microdialysis catheters were perfused at 0.3 $\mu\text{L}/\text{min}$ with CNS Perfusion Fluid (M Dialysis AB) containing 10 mmol/L gadolinium MR contrast agent, gadobutrol (Gadovist[®], Bayer AG, Germany), for 24 hours prior to scanning (see **Microdialysis**, above).

Images were acquired with Siemens Syngo MapIt software at 1 mm isotropic resolution; using 3 flip angles (5 °, 15 °, 26 °), a TE of 2 ms, TR of 15 ms, field of view (FOV) of 224 x 224 mm, 88 slices in the axial plane, and 2 repeats (total scan time of 28 minutes). A B1 map was acquired to allow correction of B1 inhomogeneity. MapIt uses a spoiled gradient echo acquisition technique, fitting the acquired signal against flip angle into a model for each voxel (Equation 2.4). This allows T1 maps of brain volume to be acquired much faster than varying the timing of an inversion recovery pulse, an alternative technique.

Equation 2.4

$$S = M_0 \sin(\alpha) \left(\frac{1 - e^{-TR/T_1}}{1 - \cos(\alpha) e^{-TR/T_1}} \right)$$

Equation for acquired signal (S), given a resting magnetisation vector M_0 , flip angle α , repetition time TR and the tissue's T1 value (Cheng and Wright, 2006).

2.5.7 Processing and analysis of 1H T1 maps

T1 map volumes were aligned with microdialysis catheter trajectories by Dr Dan Tozer, using coordinates of catheter penetration into the brain and region of gadobutrol perfusion; that I identified on MP-RAGE sequences in 3D slicer (<https://www.slicer.org/>). Aligned volumes were imported into MATLAB (MathWorks, USA) by Mr Pascal Ruetten, and ≥ 4 profiles drawn in the 'axial plane' of the catheter, through the central point of maximum gadobutrol perfusion, avoiding grey matter and CSF spaces. Each subject's profile was averaged, and the concentration (C) of gadolinium calculated from Equation 2.5:

Equation 2.5

$$C = \frac{\left(\frac{1}{T1_{observed}} - \frac{1}{T1_{tissue}} \right)}{R}$$

Where $T1_{observed}$ is the T1 of the pixel (in seconds), $T1_{tissue}$ is the baseline T1 of each subject's cerebral white matter (seconds) and R is the relaxivity of gadobutrol ($3.6 \text{ L mmol}^{-1}\text{s}^{-1}$) (Pintaske *et al.*, 2006). Subjects' $T1_{tissue}$ was defined as the shortest value of T1 their white matter profiles.

2.6 Statistics

Data processing, statistical analysis, and graphical presentation of data were performed with the open source programming language R (www.r-project.org), using the RStudio interface (RStudio Team (2015), RStudio: Integrated Development for R. RStudio, Inc., Boston, MA URL <http://www.rstudio.com/>).

Details of data processing and analytical techniques used in each chapter can be found in the **Methods** section of the corresponding chapters. Statistical advice was kindly provided by Mr Mathew Guilfoyle.

2.7 Declaration and specific acknowledgements

In-vivo ^{31}P MR spectroscopy sequences were acquired in collaboration with radiographer-physicist Dr M.O. Mada. MR Image and MR Spectroscopy co-registration was performed in collaboration with PhD candidate, Dr J.L. Yan. High resolution NMR experiments were performed by NMR spectrometrist Mr D.J. Howe. T1 map analysis was performed in collaboration with Mr P.P.R. Ruetten, PhD candidate, and Dr D.J. Tozer, MR physicist. Mr M.R. Guilfoyle provided statistical advice.

Chapter 3

High-physiological and supra-physiological 1,2-¹³C₂ glucose supplementation to the traumatised human brain

Contents

3.1	Introduction	50
3.2	Methods.....	51
3.2.1	Patient recruitment.....	51
3.2.2	Microdialysis	52
3.2.3	Statistical Analysis.....	52
3.3	Results.....	53
3.3.1	Patients, monitoring and baseline characteristics.....	53
3.3.2	Evidence from ¹³ C labelling patterns.....	53
3.3.3	Glucose supplementation at 4 mmol/L: brain biochemistry compared to baseline	54
3.3.4	Glucose supplementation at 8 mmol/L: brain biochemistry compared to baseline	54
3.3.5	Glucose supplementation in the neuroglycopenic brain.....	56
3.3.6	NMR analysis of microdialysates from 8 mmol/L 1,2- ¹³ C ₂ glucose perfusion.....	59
3.4	Discussion.....	62
3.4.1	Significance of ¹³ C-labelling in metabolites.....	62
3.4.2	Effect on glycolytic activity – changes in extracellular lactate and pyruvate	62
3.4.2.1	Heterogeneity of patients’ baseline metabolites	63
3.4.2.2	Potential deleterious effect of supra-physiological glucose.....	64
3.4.3	Glycolysis and the pentose phosphate pathway – ¹³ C lactate.....	64

3.4.3.1	¹³ C lactate enrichment	65
3.4.3.2	Glycolysis and the pentose phosphate pathway	67
3.4.4	TCA cycle activity – absence of ¹³ C glutamine	68
3.4.4.1	Detection of ¹³ C glutamine in intravenous ¹³ C glucose studies	68
3.4.4.2	Absence of ¹³ C glutamine in previous microdialysis ¹³ C glucose studies	69
3.4.4.3	Presence of ¹³ C glutamine using microdialysis ¹³ C lactate, acetate and succinate.....	69
3.4.4.4	Mitochondrial dysfunction and hypoxia	70
3.4.5	Extracellular lactate as a key step in brain metabolism.....	71
3.4.6	Clinical relevance in TBI	74
3.4.6.1	Delivering glucose to the traumatised brain.....	74
3.4.6.2	Alternative fuels for cerebral energy metabolism.....	75
3.5	Conclusion.....	76
3.6	Declaration and specific acknowledgements	76
3.7	Supplementary Material	77

3.1 Introduction

While the brain may metabolise different metabolic fuels to generate energy, glucose is conventionally regarded as the primary substrate for brain energy metabolism (Prins *et al.*, 2013; Carpenter *et al.*, 2014; Hutchinson *et al.*, 2015) (see **Chapter 1, Introduction**). After TBI, various changes in brain glucose metabolism have been demonstrated: Typically, lower cerebral microdialysate (CMD) glucose concentrations occur in TBI patients (e.g. median 1.0 – 1.2 mmol/L across outcome groups) (Timofeev *et al.*, 2011; Jalloh *et al.*, 2015a) than in non-TBI control patients (mean 1.7 mmol/L (Reinstrup *et al.*, 2000) – median 1.9 mmol/L (Jalloh *et al.*, 2015a)). However, it is unclear whether low CMD glucose within TBI cohorts is pathological or adaptive. Furthermore, extremes of high and low CMD glucose are associated with worse outcomes (Timofeev *et al.*, 2011; Hutchinson *et al.*, 2015). Low CMD glucose (neuroglycopenia) may result from greater cellular uptake of glucose from the extracellular space, or else be due to ischaemia, although this is less likely with modern neuro-intensive care protocols targeting partial brain oxygen pressure (PbtO₂) and CPP thresholds. Inadequate cellular uptake may

explain high CMD glucose associated with unfavourable outcome in a large study of TBI patients (Timofeev *et al.*, 2011). However, studies that compare ‘tight’ and ‘loose’ control of serum glucose typically report that tight serum glucose control is associated with more frequent episodes of critically low CMD glucose (Oddo *et al.*, 2008; Vespa *et al.*, 2012; Plummer *et al.*, 2018), so more permissive serum glucose control is often advocated.

The changes in cerebral glucose metabolism after TBI are thus complex. Since both high and low brain glucose levels are statistically associated with unfavourable outcome (see above), an optimal range seems likely. However, there is currently insufficient data to define such a range (Hutchinson *et al.*, 2015) nor is it clear whether supplementing the traumatised human brain with additional glucose supports its metabolism with overall benefit (Hutchinson *et al.*, 2015). While serum glucose and glycaemic control influence brain glucose, this relationship may be lost in injured brain (Hutchinson *et al.*, 2015).

This study’s aim was to determine if the traumatised human brain could metabolise supplementary glucose when delivered directly and focally into the brain extracellular fluid. Additional glucose metabolism was expected to be expressed as an increase in its products of metabolism extracellularly: pyruvate and lactate in the recovered microdialysates (Hutchinson *et al.*, 2009). 1,2-¹³C₂ glucose was perfused at a ‘high-physiological’ concentration (4 mmol/L), and a ‘supra-physiological’ concentration (8 mmol/L) to study any potential dose response to supplementation that avoided systemic metabolism and the blood brain barrier. A key feature of this study was that the glucose delivered was stable-isotope labelled, in the form of 1,2-¹³C₂ glucose, which was employed to explore the pathways of glucose metabolism operating at high concentration, by means of ¹³C high-resolution nuclear magnetic resonance (NMR) analysis of the recovered microdialysates.

3.2 Methods

3.2.1 Patient recruitment

Twenty adults (aged ≥ 16 years) who had sustained TBI and required intracranial monitoring, sedation, muscular paralysis, intubation and mechanical ventilation were recruited. Patients were treated using our standard TBI management protocols, including maintenance of serum glucose concentration within the target range 4–10 mmol/L (Menon and Ercole, 2017). Data from 4 of the patients who received high-physiological (4 mmol/L) 1,2-¹³C₂ glucose by microdialysis were part of a previous study (Jalloh *et al.*, 2015a). The other patients were not part of any previous ¹³C studies.

3.2.2 Microdialysis

Microdialysis monitoring and glucose delivery were carried out as described in **Chapter 2 (General Materials & Methods)**, using M Dialysis 71 microdialysis catheters (membrane length 10 mm, nominal molecular weight cut-off 100 kDa) (**Figure 1.8**). The catheters were not directed into, nor adjacent to, lesions (e.g. contusions) identified on computerized tomography (CT). Catheters were perfused at 0.3 $\mu\text{L}/\text{min}$ with plain, unsupplemented CNS Perfusion Fluid (see above). Then, for a period of 24 hours, the perfusion fluid was changed to CNS perfusion fluid supplemented with either 4 mmol/L or 8 mmol/L 1,2- $^{13}\text{C}_2$ glucose (isotopic enrichment 99 %, chemical purity 99 %). After the 24-hour supplementation period, the perfusion fluid was changed back to plain, unsupplemented CNS perfusion fluid. Microdialysate collection vials were analysed hourly on a bedside ISCUS analyser (M Dialysis AB) and then pooled for NMR analysis (see **Chapter 2**).

3.2.3 Statistical Analysis

Statistical analysis of data was performed using the software package R (www.r-project.org). Demographics of patients who received 4 mmol/L and 8 mmol/L glucose were compared using Mann-Whitney U test. For ISCUS results, changes between baseline and glucose supplementation periods were excluded for two hours after changeover from pre-supplementation to glucose supplementation, and changeover from glucose supplementation to post supplementation, to allow for 'run-in' and 'washout' (Jalloh *et al.*, 2017). Each patient's pre- and post-supplementation data were combined as a baseline period for that individual, thereby making allowance for underlying trends in patient physiology. Heterogeneity (often seen in TBI cohorts) was accounted for by a linear mixed effects model ('lmer' in R package *lme4* (Bates *et al.*, 2015)) that allows for clustering of data, and has a different random effect for each patient. Also, Wilcoxon signed rank test (in R) was used for corroboration of results. Only those patients with microdialysates from *both* pre- and post-supplementation baseline periods were included in the data analysis. Detailed data analysis of ISCUS results focussed mainly on CMD glucose, lactate, pyruvate and lactate/pyruvate ratio, as the primary question was whether the traumatised brain could metabolise additional glucose. Regarding the other ISCUS analytes, interpretation of CMD glycerol is ambiguous (as it can be a glucose metabolite or a breakdown product of lipid), and several patients had incomplete glutamate CMD data.

3.3 Results

3.3.1 Patients, monitoring and baseline characteristics

Twenty TBI patients (14 M, 6 F) were recruited. Mean patient age was 39 years, and post resuscitation GCS 6. The causes of injury were mostly road traffic collisions (RTC) and falls. The most common surgical diagnoses were cerebral contusions and acute subdural haematomas. Detailed patient demography is in **Supplementary Table 3.1**. There were no complications from insertion of microdialysis catheters or related to the perfusion of study substrate; specifically, no cerebral haematomas or contusions were noted on CT imaging after catheter insertion. Microdialysis technique was in accord with the 2014 Consensus Statement guidelines (Hutchinson *et al.*, 2015), so catheters were never placed in lesions, and the first hour of microdialysate collected was never used for clinical monitoring (to eliminate any unreliable results from insertion trauma and the pump flush sequence). Throughout the study period adequate cerebral perfusion was maintained in all patients (> 60 mmHg) and no patients suffered from intractable raised ICP (> 25 mmHg). Brain tissue oxygen data was available for 7/20 patients, whose mean PbtO₂ was 27 mmHg (**Supplementary Table 3.1**). No patients suffered from cerebral ischaemia (PbtO₂ < 15 mmHg).

There were no significant differences (Mann-Whitney U, $p > 0.1$) between the two groups of patients – those who received 4 mmol/L or 8 mmol/L glucose – in terms of in baseline GCS, Extended Glasgow Outcome Scale (GOS-E) score, time interval between injury and period of supplementation (mean 2.9 days), or serum glucose and serum lactate during the period of 1,2-¹³C₂ glucose supplementation. However, there was a statistically significant difference ($p < 0.0001$, *Imer*) between the two patient groups for microdialysate glucose, lactate and pyruvate at baseline. Notably, microdialysate glucose was 32 % higher at baseline in the 8 mmol/L group compared with the 4 mmol/L group, while lactate and pyruvate were 21 % and 13 % lower respectively, conceivably representing slight inherent distinction between the two groups of patients, although the baseline L/P ratio was only 4 % lower in the 8 mmol/L than in the 4 mmol/L group (**Supplementary Table 3.2**).

3.3.2 Evidence from ¹³C labelling patterns

The appearance of doubly-labelled lactate (2,3-¹³C₂ lactate) in the recovered microdialysates shows unequivocally that the brain metabolised by glycolysis the exogenous 1,2-¹³C₂ glucose delivered via the microdialysis catheter. The 2,3-¹³C₂ lactate ‘signature’ of characteristic doublets in the ¹³C NMR spectrum is clear evidence that the ¹³C-¹³C bond stays intact (**Figure 3.1**), and the doublet signal is essentially free from endogenous lactate, because the probability of two ¹³C atoms occurring next to each other

naturally by chance (in the absence of exogenous double-labelling) is just one in ten thousand ($1.1\% \times 1.1\% = 0.01\%$). Thus, it is clear that the 8 mmol/L $1,2\text{-}^{13}\text{C}_2$ glucose delivered directly to the brain's extracellular space by microdialysis catheters was taken up by brain cells, metabolised by glycolysis as the main pathway into lactate, and ^{13}C -labelled lactate exported into the brain extracellular space. This is consistent with previous microdialysis studies using $1,2\text{-}^{13}\text{C}_2$ glucose at 2 mmol/L (Gallagher *et al.*, 2009) and 4 mmol/L (Jalloh *et al.*, 2015a). Also as previously, a lower enrichment in singly-labelled lactate ($3\text{-}^{13}\text{C}$ lactate) showed the pentose phosphate pathway to be a lesser contributor to lactate production than glycolysis ($2,3\text{-}^{13}\text{C}_2$ lactate) from the exogenously-supplied $1,2\text{-}^{13}\text{C}_2$ glucose (Jalloh *et al.* 2015a).

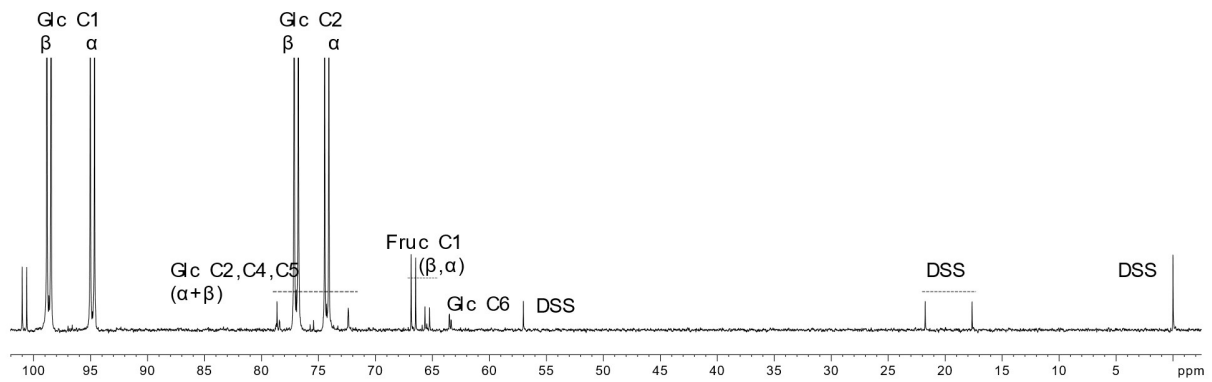
3.3.3 Glucose supplementation at 4 mmol/L: brain biochemistry compared to baseline

Eleven subjects, who received microdialysis perfusion supplemented with 4 mmol/L $1,2\text{-}^{13}\text{C}_2$ glucose, possessed complete baseline (*both* pre- and post- supplementation) ISCUS datasets. Mean baseline concentrations were: glucose 1.22 mmol/L, lactate 3.26 mmol/L and pyruvate 113 $\mu\text{mol/L}$. Compared to baseline, glucose supplementation resulted in a mean 19 % increase in extracellular lactate ($p < 0.0001$, *Imer*) and 17 % increase in extracellular pyruvate ($p < 0.0001$, *Imer*). There was a mean 5 % increase in L/P ratio ($p = 0.002$, *Imer*), unlikely to be of biological significance (**Figure 3.2**). Glycerol rose by a mean 8 % ($p < 0.0001$, *Imer*), but there was no significant change in extracellular glutamate.

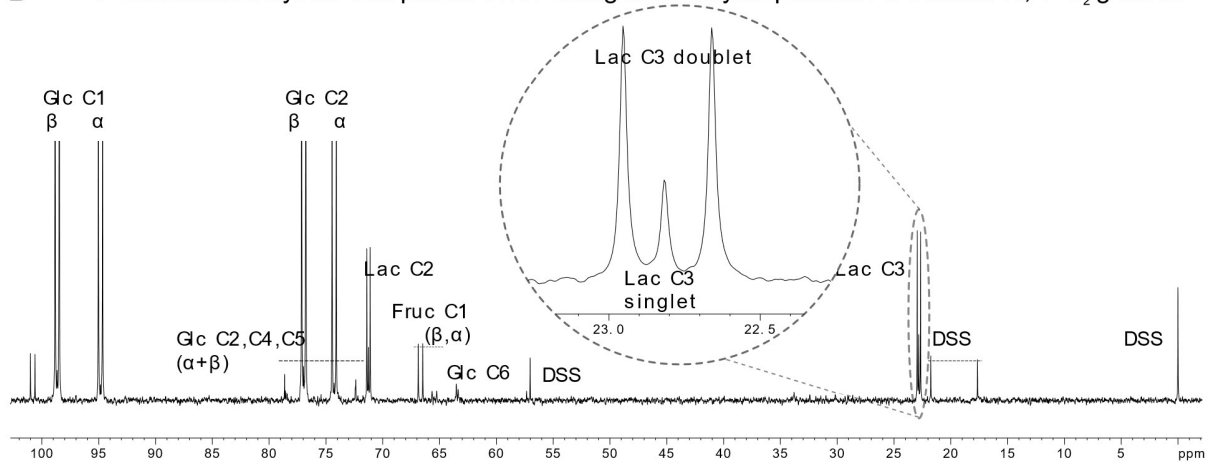
3.3.4 Glucose supplementation at 8 mmol/L: brain biochemistry compared to baseline

Twelve patients received microdialysis with CNS perfusion fluid supplemented with 8 mmol/L $1,2\text{-}^{13}\text{C}_2$ glucose. One of these 12 patients also had a second CMD catheter simultaneously supplemented with 5 mmol/L $1,2\text{-}^{13}\text{C}_2$ glucose. Eight of these 12 patients had complete ISCUS data-sets comprising pre-supplementation, during-supplementation, and post-supplementation. Mean baseline concentrations were: glucose 1.61 mmol/L, lactate 2.56 mmol/L and pyruvate 98 $\mu\text{mol/L}$. Compared to baseline perfusion with normal (un-supplemented) CNS perfusion fluid, glucose supplementation did not result in a statistically significant change (*Imer*) in extracellular lactate concentration (average 2 % decrease, $p = 0.17$) or pyruvate (average 2 % decrease, $p = 0.12$). Similarly, there was no significant change in L/P ratio (average 1.5 % increase, $p = 0.17$, *Imer*) (**Figure 3.2**). There was a statistically significant 15 % increase in glycerol ($p < 0.0001$, *Imer*) and 21 % fall in glutamate ($p < 0.0001$, *Imer*).

A Normal CNS perfusion fluid supplemented with 8 mmol/L $1,2\text{-}^{13}\text{C}_2$ glucose, prior to patient infusion



B Pooled microdialysate from patient GL-07 during microdialysis perfusion of 8 mmol/L $1,2\text{-}^{13}\text{C}_2$ glucose



C Spectrum of pooled microdialysate from an 'unlabelled' patient during perfusion with normal perfusion fluid without labelled substrate

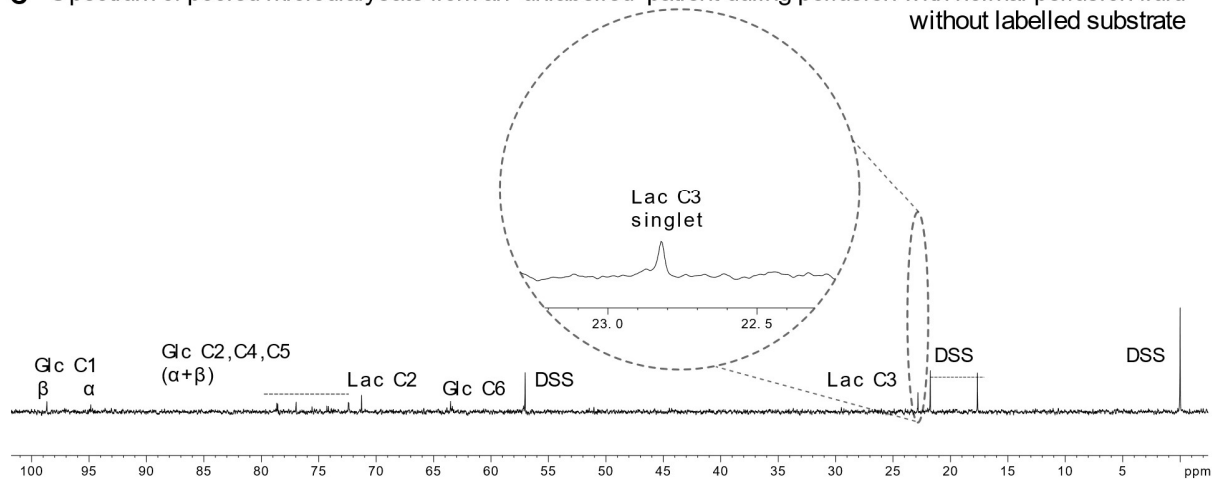


Figure 3.1 Example ^{13}C NMR spectra.

Panel A: CNS perfusion fluid supplemented with 8 mmol/L $1,2\text{-}^{13}\text{C}_2$ glucose, prior to infusion. The large α and β peaks (note that α and β denote two conformations of the glucose molecule) for ^{13}C at glucose position C1 and C2 can be seen dominating the spectrum, with small peaks representing natural abundance of ^{13}C at the unenriched positions within the molecule. *Panel B:* pooled microdialysate from patient GL-07 during their 24 hours of 8 mmol/L $1,2\text{-}^{13}\text{C}_2$ glucose supplementation. Lactate can be seen at 22.8 ppm (C3) and 71.2 ppm (C2). The C3 peak is expanded, showing in greater detail the ^{13}C labelled doublet and the small ^{13}C singlet inside the doublet. The doublet represents glycolytic metabolism of supplemented $1,2\text{-}^{13}\text{C}_2$ glucose, and the singlet a combination of pentose phosphate pathway-metabolised $1,2\text{-}^{13}\text{C}_2$ glucose supplement and the natural abundance background (1.1 %) of ^{13}C label in endogenous lactate. This singlet within a doublet was visible in all $1,2\text{-}^{13}\text{C}_2$ glucose-supplemented patients' microdialysates analysed with high resolution NMR. *Panel C:* pooled microdialysate from a patient during a period of 'baseline' perfusion with unsupplemented perfusion fluid. Small singlet peaks can be seen corresponding to lactate and glucose, representing the natural abundance background (1.1 %) of ^{13}C in these molecules. All spectra were analysed with Topspin (Bruker GmbH), referenced to internal standard DSS. Small peaks for ^{13}C -labelled fructose are visible in panels A and B, representing a small proportion of ^{13}C -labelled glucose that has undergone isomerisation which occurs spontaneously in solution. *Abbreviations: see table in **Precis**; Glc, glucose; Fruc, fructose; DSS, 4,4-dimethyl-4-silapentane-1-sulfonate sodium salt internal reference standard; Lac, lactate.*

3.3.5 Glucose supplementation in the neuroglycopenic brain

Seven subjects had a low baseline extracellular brain glucose, defined as ≤ 0.8 mmol/L (Stein *et al.*, 2012; Hutchinson *et al.*, 2015). Analysis of CMD (ISCUS) data from neuroglycopenic subjects - 3 patients supplemented with 8 mmol/L glucose and 4 patients supplemented with 4 mmol/L glucose - revealed a similar pattern as supplementation in the 4 mmol/L glucose group as a whole: there was a mean 15 % increase in lactate ($p < 0.001$), 15 % increase in pyruvate ($p < 0.001$), and only 4 % increase in L/P ratio ($p = 0.003$); although this effect appeared primarily driven by subjects who received 4 mmol/L (**Figure 3.3**).

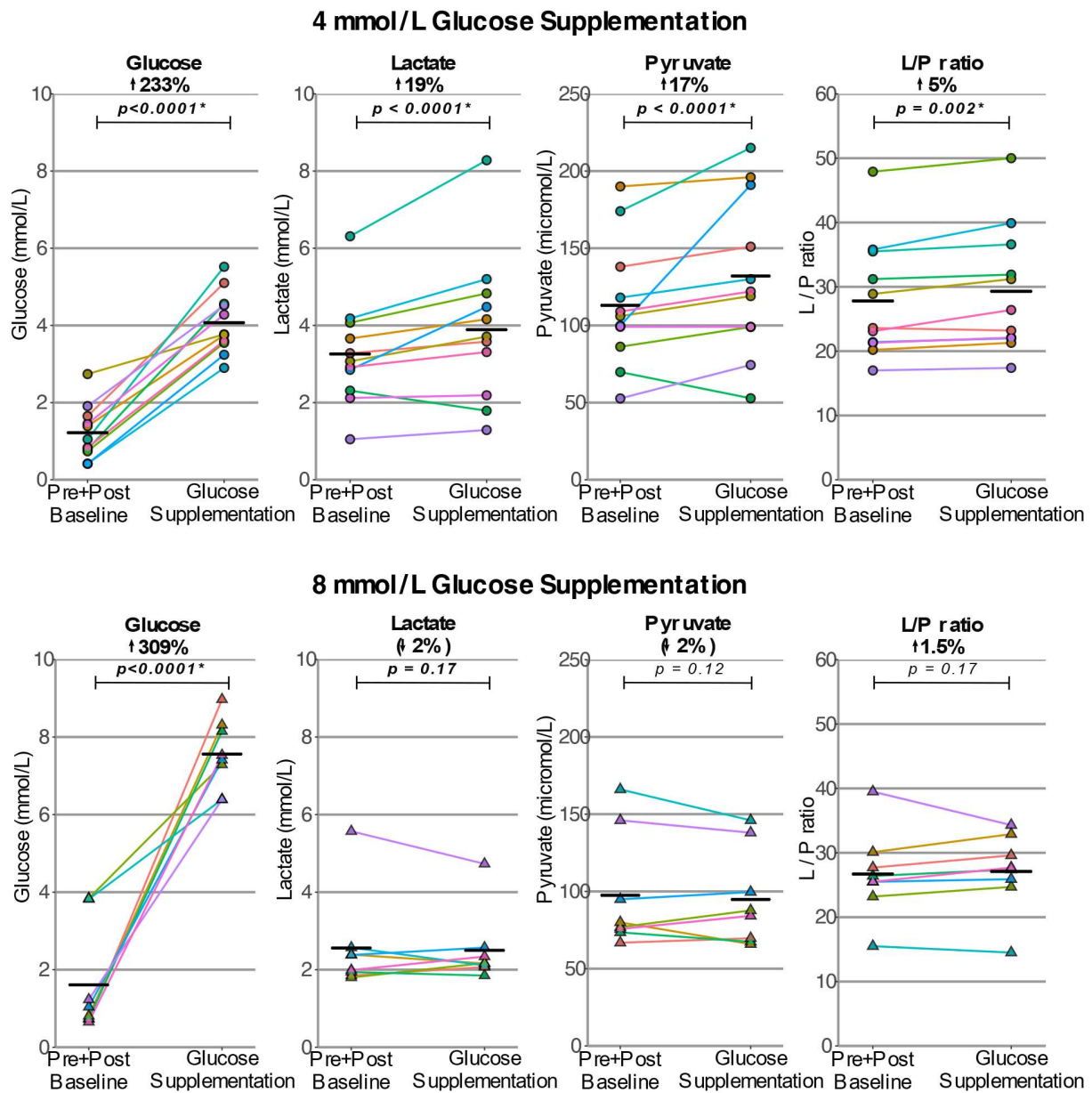


Figure 3.2 ISCUS bedside analyser measurements showing the effect of $1,2\text{-}^{13}\text{C}_2$ glucose supplementation via microdialysis on brain extracellular chemistry.

Each pair of data-points indicates mean levels at baseline and during succinate perfusion, respectively, for that patient. Supplementation was for ≈ 24 hours. Baseline denotes ≈ 24 hours of perfusion with plain (unsupplemented) CNS-perfusion fluid; the baseline value represents combined data pre- and post-supplementation (to account for any underlying trends). Circles (upper 4 panels) denote results from patients supplemented with $1,2\text{-}^{13}\text{C}_2$ glucose at 4 mmol/L, triangles (lower 4 panels) denote results from patients supplemented with $1,2\text{-}^{13}\text{C}_2$ glucose at 8 mmol/L, black crossbars on graphs denote averages of patient means. P-values calculated using linear mixed effects model in R. *Abbreviations: see table in Precis.*

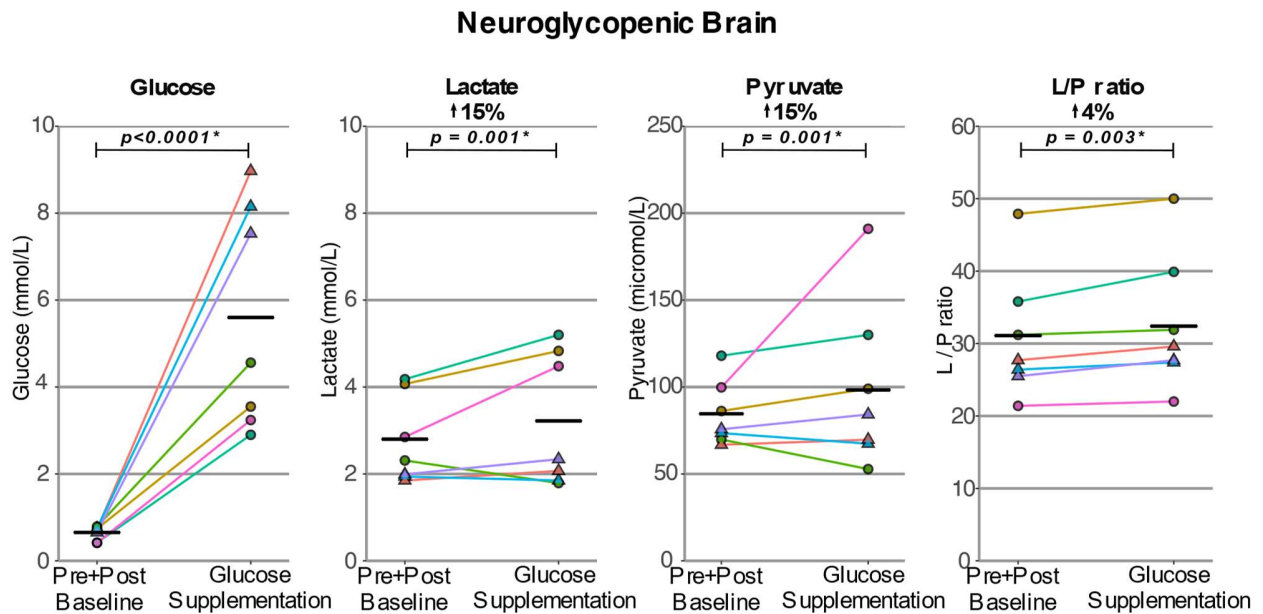


Figure 3.3 ISCUS bedside analyser measurements showing the effect of $1,2\text{-}^{13}\text{C}_2$ glucose supplementation via microdialysis on brain extracellular chemistry in a subset of patients with low baseline cerebral glucose (< 0.8 mmol/L).

Each pair of data-points indicates mean levels at baseline and during succinate perfusion, respectively, for that patient. Supplementation was for ≈ 24 hours. Baseline denotes ≈ 24 hours of combined data pre- and post- supplementation (to account for any underlying trends). Circles denote patients supplemented with glucose at 4 mmol/L, triangles denote patients supplemented with glucose at 8 mmol/L, black crossbars on graphs denote averages of patient means. P-values were calculated using linear mixed effects model in R. *Abbreviations: see table in Precis.* Summary results from ISCUS analysis of all subjects can be found in **Table 3.1**.

Table 3.1. Summary ISCUS results for microdialysates at baseline and during microdialysis supplementation with 1,2-¹³C₂ glucose.

	Supp. conc. (mmol/L)	Baseline mean	Supp. mean	% change mean	<i>Imer</i> <i>p</i>	Baseline median	Supp. median	% change median	<i>Wilcoxon</i> <i>p</i>
Glucose	4	1.22	4.07	↑233 %	0.0001	1.05	3.77	↑259 %	0.001
	8	1.61	7.56	↑309 %	0.0001	0.92	7.47	↑708 %	0.008
Lactate	4	3.26	3.89	↑19 %	0.0001	3.07	3.71	↑21 %	0.01
	8	2.56	2.50	↓2 %	0.17	2.18	2.16	↓1 %	0.8
Pyruvate	4	113	132	↑17 %	0.0001	106	122	↑15 %	0.04
	8	98	95	↓2 %	0.12	78	86	↑10 %	0.64
L/P ratio	4	27.8	29.3	↑5 %	0.002	23.6	26.4	↑12 %	0.007
	8	26.7	27.1	↑1.5 %	0.17	26.0	27.6	↑6 %	0.33
Glycerol	4	109	118	↑8 %	0.0001	110	88	↓20 %	0.2
	8	93	107	↑15 %	0.0001	85	101	↑19 %	0.2
Glutamate	4	3.24	8.06	↑149 %	0.3	2.35	6.75	↑187 %	0.9
	8	15.30	12.10	↓21 %	0.0001	3.89	1.90	↓51 %	0.016

Group means and medians from periods of baseline (pre- and post- supplementation) and during supplementation with 1,2-¹³C₂ glucose (Supp.). Significance determined by linear mixed effects model (*Imer*) and Wilcoxon signed rank of patient averages using R. Up- and down- arrows denote % change increases and decreases respectively.

3.3.6 NMR analysis of microdialysates from 8 mmol/L 1,2-¹³C₂ glucose perfusion

The mean percentage of lactate labelled with ¹³C at the C3 position in recovered microdialysates was 17.6 % (s.d. 5.4 %). This lactate comprised of 14.7 % (s.d. 4.9 %) doubly-labelled (2,3-¹³C₂ lactate, concentration 0.39 mmol/L) and 2.0 % (s.d. 0.7 %) singly-labelled (3-¹³C lactate, 0.03 mmol/L) after subtraction of 1.1 % ¹³C natural abundance from the singly-labelled lactate (**see Methods**). 2,3-¹³C₂ doubly labelled lactate arises from glycolysis of the 1,2-¹³C₂ glucose supplement, and 3-¹³C singly labelled lactate is derived from pentose phosphate pathway metabolism of the 1,2-¹³C₂ glucose supplement (**Figure 3.4**) (**Table 3.2**). The single-labelling results are presented after background subtraction to

remove the contribution from natural endogenous ^{13}C that is 1.1 % of all carbon atoms. Note that double-labelling results are not background-subtracted because the chance of two ^{13}C atoms occurring next to each other naturally is only 0.01 % (= 1.1 % x 1.1 %)

NMR spectroscopy showed no evidence for TCA cycle metabolism of 1,2- $^{13}\text{C}_2$ glucose supplemented at 8 mmol/L. Notably, doubly-labelled ^{13}C glutamine was not detected in microdialysates from any of the 12 subjects with NMR analysis, while only 2 of these subjects showed singly-labelled glutamine but this was not above background ^{13}C natural abundance.

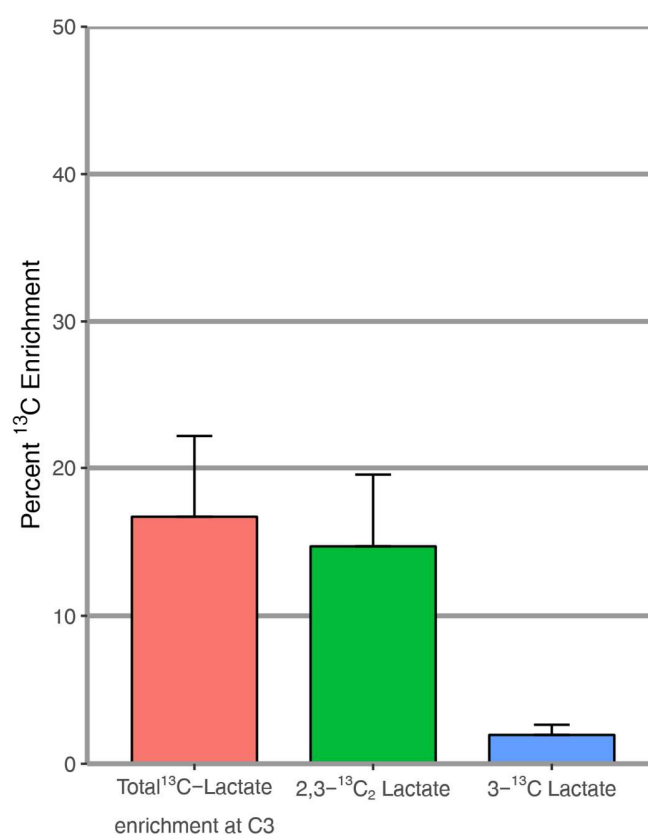


Figure 3.4. Bar charts showing mean percentage ^{13}C enrichment in lactate carbon position 3 in pooled recovered microdialysates from 12 TBI patients after supplementation with 8 mmol/L 1,2- $^{13}\text{C}_2$ glucose via cerebral microdialysis.

Error bars denote standard deviation. ^1H and ^{13}C high-resolution NMR analysed with Topspin. 'Total ^{13}C -Lactate' denotes total fractional ^{13}C enrichment at 3- ^{13}C lactate, which represents glycolytic and pentose phosphate pathway (PPP) metabolism of supplemented glucose. '2,3- $^{13}\text{C}_2$ Lactate' denotes percent of all lactate that is doubly-labelled (2,3- $^{13}\text{C}_2$ lactate doublet), representing glycolytic derived lactate. '3- ^{13}C Lactate (endog. subtracted)' denotes percent of all lactate that is singly labelled (3- ^{13}C lactate singlet) after subtraction of the natural abundance background ^{13}C .

Table 3.2. ^{13}C NMR results

ID	Glycolytic 2,3- $^{13}\text{C}_2$ lactate (calculated from C3 doublet)		PPP 3- ^{13}C lactate* (calculated from C3 singlet)		Total ^{13}C -lactate* C3 enrichment (calculated from C3 singlet + C3 doublet)		Percentage of total ^{13}C at C3 of lactate that is derived from PPP %	Ratio of PPP 3- ^{13}C lactate to glycolytic 2,3- $^{13}\text{C}_2$ lactate Ratio
	Conc. mol/L	FE %	Conc. mol/L	FE %	Conc. mol/L	FE %		
GL-01	0.15	8	0.015	0.8	0.17	8.8	9.1	1:10.0
GL-02	0.27	19	0.040	2.9	0.31	21.9	13	1:6.6
GL-05	0.61	13	0.081	1.7	0.69	14.7	12	1:7.4
GL-07	0.83	13	0.130	2.1	0.96	15.1	14	1:6.3
GL-08	0.24	14	0.020	1.2	0.26	15.2	8	1:12.0
GL-09	0.19	10	0.022	1.2	0.21	11.2	10	1:8.8
GL-11	0.22	13	0.031	1.8	0.25	14.8	12	1:7.0
GL-12	0.22	12	0.039	2.2	0.26	14.2	15	1:5.7
GL-13	0.38	18	0.053	2.5	0.43	20.5	12	1:7.3
GL-14	0.6	15	0.084	1.9	0.68	16.9	12	1:7.1
GL-15	0.63	27	0.073	3.1	0.7	30.1	10	1:8.6
GL-16	0.39	15	0.049	1.9	0.44	16.9	11	1:7.9

Results of high-resolution NMR analysis of microdialysate (each patient's NMR sample was a pool of 24 x 1h vials) during supplementation with 8 mmol/L 1,2- $^{13}\text{C}_2$ glucose. *Abbreviations: see table in Precis; FE, fractional enrichment – see Methods for details of calculation.* * The 3- ^{13}C lactate fractional enrichment results are presented after background subtraction to remove the contribution from natural abundance background ^{13}C that is 1.1 % of all carbon atoms. 2,3- $^{13}\text{C}_2$ lactate results are not background-subtracted as the probability of two natural ^{13}C atoms occurring next to each other by chance is only 0.01 % (= 1.1 % x 1.1 %).

3.4 Discussion

In this study I have shown that the traumatised human brain can metabolise additional glucose when delivered directly into the brain extracellular fluid via a microdialysis catheter to a limited degree, which may be a useful strategy in TBI patients in certain circumstances. Analysis of ^{13}C NMR data reveals that extracellular lactate is a key metabolic step in the appearance of brain extracellular glutamine.

3.4.1 Significance of ^{13}C -labelling in metabolites

The substrate 1,2- $^{13}\text{C}_2$ glucose was metabolised to 2,3- $^{13}\text{C}_2$ lactate, analysed by NMR in the recovered microdialysates, providing clear unambiguous evidence of glycolysis, as the probability of two natural ^{13}C atoms occurring next to each other by chance is only 0.01 %. A smaller amount of 3- ^{13}C lactate was found, indicating metabolism of the glucose via the pentose phosphate pathway (PPP) as a minor route for lactate production.

Despite this unambiguous evidence of glycolytic (and PPP) metabolism of 1,2- $^{13}\text{C}_2$ glucose, there was no evidence for further metabolism via the TCA cycle – notably no doubly-labelled glutamine was identified, while singly-labelled glutamine was only at natural-abundance background level, mirroring the results of previous studies (Gallagher *et al.*, 2009; Jalloh *et al.*, 2015a).

The lack of change in ISCUS-measured extracellular metabolites during perfusion with 8 mmol/L 1,2- $^{13}\text{C}_2$ glucose suggests that whereas supplemented ^{13}C glucose was metabolised, this occurred *instead of* metabolism of endogenous glucose in this group as a whole; rather than *in addition* to metabolism of endogenous glucose. Conversely, metabolism of 4 mmol/L 1,2- $^{13}\text{C}_2$ supplemented glucose appeared to occur *in addition* to that of endogenous glucose in some patients. I discuss several explanations below

3.4.2 Effect on glycolytic activity – changes in extracellular lactate and pyruvate

As a result of supplementation with 1,2- $^{13}\text{C}_2$ glucose, total microdialysate levels of glucose measured on an ISCUS bedside analyser (enzymatic colorimetric analysis) rose markedly and significantly as expected, from a mean 1.22 mmol/L and 1.61 mmol/L at baseline, to 4.07 mmol/L and 7.56 mmol/L during 4 mmol/L and 8 mmol/L supplementation respectively. Supplementation with 4 mmol/L resulted in a corresponding significant increase in lactate (19 %) and pyruvate (17 %), suggesting increased glycolytic activity. However, supplementation with 8 mmol/L glucose did not appear to increase glycolysis, as there was no significant change in microdialysis lactate or pyruvate. These findings do not fit with classic zero or first order metabolism kinetics, nor that of saturation of a metabolic pathway.

3.4.2.1 Heterogeneity of patients' baseline metabolites

It is more likely that the different response in extracellular lactate and pyruvate observed in subjects who received 8 mmol/L and 4 mmol/L glucose is due to patient differences: Baseline glucose was 32 % lower in the 4 mmol/L supplementation group (1.22 mmol/L) than the 8 mmol/L supplementation group (1.61 mmol/L); while lactate and pyruvate were 14 and 21 % higher. Supplementation of additional glucose is less likely to increase glycolysis in patients with an 'already-high' baseline glucose, in contrast to patients with lower baseline glucose. This is evident in the subgroup analysis of neuroglycopenic patients, who observed a statistically significant increase in extracellular lactate and pyruvate regardless of which supplementation concentration they received.

Also compatible with this scenario of glucose supplementation being dependent on baseline glucose is that in a subset of patients where ISCUS measurements identified low baseline brain glucose (neuroglycopenia), there were modest statistically significant increases in lactate, pyruvate and L/P ratio when supplemented with 1,2-¹³C₂ glucose via microdialysis, regardless of supplementation group. This 'neuroglycopenic' subgroup nevertheless showed a similar pattern of metabolite labelling to the study cohort as a whole, i.e. ¹³C labelling in lactate indicating glycolysis and PPP, but no detectable ¹³C labelling in glutamine.

The relatively high baseline lactate and pyruvate in patients who received 4 mmol/L glucose supplementation may indicate tissue that is able to metabolise glucose relatively freely – and thus can metabolise additional glucose when it is supplemented. In contrast, the relatively lower baseline lactate and pyruvate in patients who received 8 mmol/L glucose may represent some relative impairment of cerebral glycolysis (and PPP), which hinders their ability to increase their rate of glucose metabolism in the presence of excess substrate.

The behaviour pattern of patients who received 8 mmol/L glucose is consistent with earlier findings by Jalloh et al. where 1,2-¹³C₂ glucose supplementation (at 4 mmol/L) resulted in a proportionate rise in ISCUS-measured glucose but no significant changes in lactate or pyruvate, and only a minor (albeit statistically significant) increase in L/P ratio (Jalloh *et al.*, 2015a). However, this analysis relied on pooled data that does not adjust for underlying trends in patient biochemistry, nor heterogeneity between patients (Jalloh *et al.*, 2015a). Further examination of this data suggests there was a trend for lactate and pyruvate to increase with glucose supplementation in healthy controls' normal brain. This difference did not reach statistical significance, but that may be due to the small number of observations in this group. Conversely, there was no trend for increased lactate and pyruvate in TBI patients (Jalloh *et*

al., 2015a). Thus, the ability of the traumatised brain to metabolise additional glucose via glycolysis and the PPP may be dependent on its baseline metabolic 'health' and be limited in patients with greater metabolic injury.

3.4.2.2 *Potential deleterious effect of supra-physiological glucose*

However it is possible that the self-limiting mechanism of glycolysis is dysfunctional in the traumatised brain: cells take up glucose via specific transporters (Tomlinson and Gardiner, 2008; Jauch-Chara and Oltmanns, 2014), then hexokinase phosphorylates the glucose molecule in the first step of glycolysis, locking it in the cell, as glucose-6-phosphate does not get transported out. Normally, the numerous steps of glycolysis would follow, leading to pyruvate (and then lactate and/or acetate and TCA cycle). However if there is too much glucose, the hexokinase is product-inhibited by the glucose-6-phosphate and the cell stops taking up glucose and glycolysis slows down (Berg *et al.*, 2002). This may be relevant to the present study; if the product-inhibition of hexokinase in the traumatised human brain was irreversible after TBI. It is also possible that supplementation with glucose at such a high concentration as 8 mmol/L is deleterious to brain metabolism, thereby hindering cellular glycolysis (Berg *et al.*, 2002). The potential deleterious effect of severe hyperglycaemia in the brain after TBI has been reported in the past (Tomlinson and Gardiner, 2008; Jauch-Chara and Oltmanns, 2014), but previous studies have considered elevated serum glucose rather than increased brain interstitial glucose. Hyperglycaemic effects reported in these studies are likely to manifest, at least in part, through effects on brain vasculature, which is less relevant to this study. Nevertheless, a comprehensive study of graded hyperglycaemia in humans and rabbits found that more extreme hyperglycaemia may cause neuron injury and suppression of astrocyte activation in the frontal cortex, whereas moderate hyperglycaemia may not (Sonneville *et al.*, 2012).

A caveat is that glucose given directly into the brain extracellular fluid might differ in its subsequent processing compared to glucose delivered via the circulation (e.g. intravenous glucose, discussed below). Moreover, monitoring products by microdialysis only samples the extracellular compartment, and one cannot rule out increased glycolytic production of pyruvate and lactate, if these products remained within the intracellular compartment in those patients who received 8 mmol/L glucose supplementation.

3.4.3 *Glycolysis and the pentose phosphate pathway – ¹³C lactate*

Although there was no evidence that supplementing the brain extracellular space with 8 mmol/L 1,2-¹³C₂ glucose increased the *rate* of glucose metabolism, ¹³C labelled glucose was metabolised by glycolysis and

the pentose phosphate pathway *in-place* of endogenous unlabelled glucose, evidenced by recovered ^{13}C lactate in microdialysates. Thus, results of ^{13}C NMR analysis appear to reveal the baseline metabolism of this cohorts' brains.

3.4.3.1 ^{13}C lactate enrichment

When glycolysis breaks down one mole of $1,2\text{-}^{13}\text{C}_2$ glucose it produces 1 mole of $2,3\text{-}^{13}\text{C}_2$ lactate and 1 mole of unlabelled lactate, so in effect self-diluting the labelled lactate. The same is true of pyruvate: a 1:1 mixture of $2,3\text{-}^{13}\text{C}_2$ pyruvate and unlabelled pyruvate ensue from 1 mole of $1,2\text{-}^{13}\text{C}_2$ glucose. Thus, the theoretical maximum level of enrichment of lactate at the region of interest (ROI) addressed by the microdialysis catheter assuming exposure to $1,2\text{-}^{13}\text{C}_2$ glucose at 99 % enrichment is 49 %. However, when baseline extracellular unlabelled lactate is considered, this may be expected to fall to around 44 % (assuming an unlabelled baseline glucose concentration of 1 mmol/L). The mean level of enrichment observed in $2,3\text{-}^{13}\text{C}_2$ lactate in this study was under half this, at 19 %. The highest individual level of enrichment observed in $2,3\text{-}^{13}\text{C}_2$ lactate was 31 %, which is over three-fifths of the theoretical maximum level of enrichment of 49 % if the region of interest (ROI) addressed by the microdialysis catheter was exposed solely to $1,2\text{-}^{13}\text{C}_2$ glucose at 99 % enrichment.

Microdialysis delivery of glucose was used to create focal high-physiological and supra-physiological cerebral concentrations of glucose in the brain extracellular fluid. However, this might not entirely reproduce the situation with glucose delivery from the circulation. The brain has an extensive vascular supply, and astrocyte end-feet are firmly attached to the endothelial cells of the blood capillaries constituting the tight junctions of the blood-brain barrier. Glucose uptake from blood into brain is controlled via specific transporters (Tomlinson and Gardiner, 2008; Jauch-Chara and Oltmanns, 2014). Transfer of glucose from blood in the capillary into the astrocytes directly adjoining the endothelial cells might conceivably be more effective at feeding glucose into the astrocytes than direct uptake from the extracellular fluid (**Figure 3.5**), which might explain the discrepancy between observed and theoretical ^{13}C lactate enrichment.

Other likely sources of dilution include endogenous lactate, which may be influenced by factors such as diffusion within the brain (from the rest of the brain outside of the ROI of the catheter) and exchange with the circulation. It has already been shown, by arteriovenous difference measurements, that the brain undergoes periods of net uptake and net export of lactate (Jalloh *et al.*, 2013).

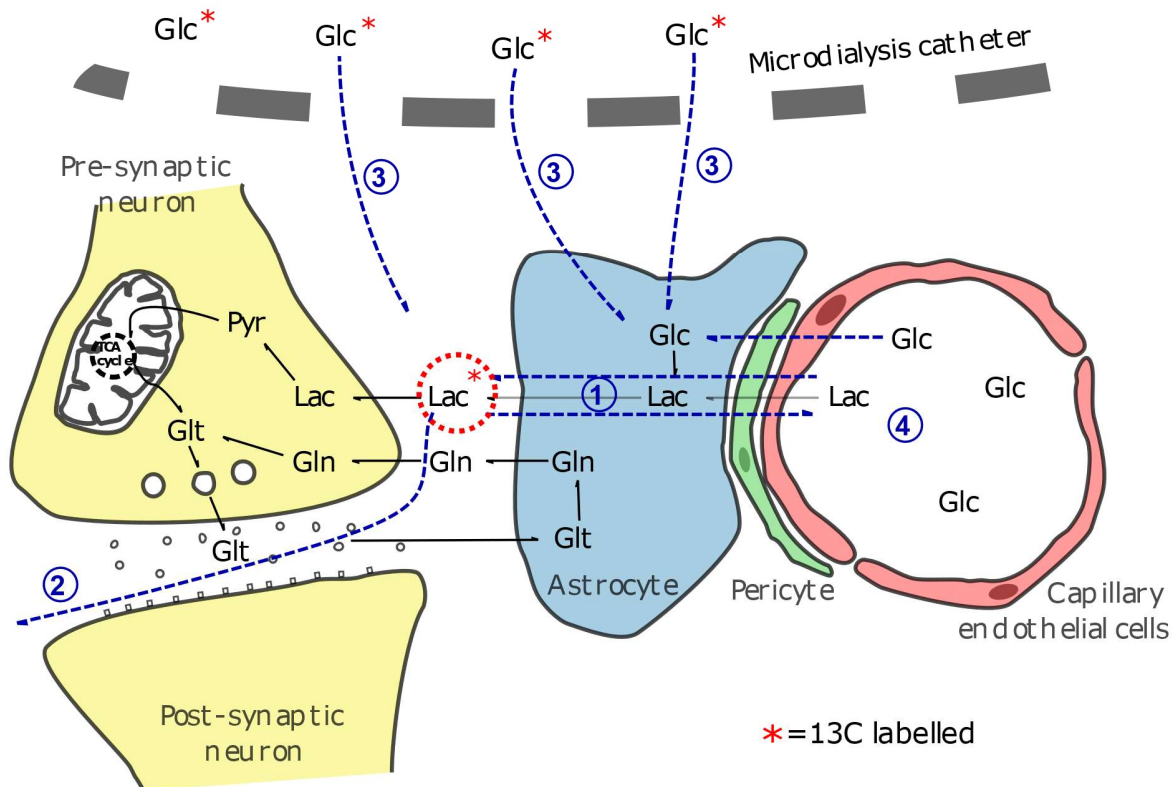


Figure 3.5. Schematic with potential explanations for relatively low ^{13}C lactate enrichment despite high concentration ^{13}C glucose supplementation.

(1) Exchange of ^{13}C lactate with unlabelled lactate from the systemic circulation. (2) Local diffusion of ^{13}C lactate away from the region surrounding the catheter. (3) Insufficient rate of delivery of ^{13}C glucose by catheter compared to the cellular metabolic rate of glucose. (4) Glucose may more readily be absorbed by glia and neurons from capillaries, its natural route, rather than through the extracellular space. Part of the dilution with unlabelled lactate originates from the $1,2\text{-}^{13}\text{C}_2$ glucose itself, as when a molecule of $1,2\text{-}^{13}\text{C}_2$ glucose undergoes glycolysis it breaks up to give a 1:1 mixture of $2,3\text{-}^{13}\text{C}_2$ pyruvate and unlabelled pyruvate - the unlabelled pyruvate comes from the unlabelled carbons at positions 4, 5 and 6 in the $1,2\text{-}^{13}\text{C}_2$ glucose molecule – and hence a 1:1 mixture of $2,3\text{-}^{13}\text{C}_2$ lactate and unlabelled lactate. Glycolysis can be self-limiting. Cells take up glucose via specific transporters. Then in the first step of glycolysis, hexokinase phosphorylates the glucose, locking it in the cell, as glucose-6-phosphate is not transported out. Normally, the other steps of glycolysis would follow, but if there is too much glucose, then hexokinase is product-inhibited by glucose-6-phosphate and the cell stops taking up glucose and glycolysis slows down. *Abbreviations: see table in Precis; Glc, glucose; Lac, lactate; Pyr, pyruvate; Glt, glutamate; Gln, glutamine.*

3.4.3.2 Glycolysis and the pentose phosphate pathway

Glycolysis is the principle metabolic path for glucose metabolism in the brain, generating 2 moles of ATP per mole of glucose, whereas the PPP is an alternative, minor route. This was confirmed in the 7.9:1 ratio of 2,3-¹³C₂ lactate to 3-¹³C lactate in this study. There was a close positive linear correlation between 2,3-¹³C₂ lactate and 3-¹³C lactate (Pearson's $r^2 = 0.94$ for concentrations and $r^2 = 0.84$ for fractional enrichments) (**Figure 3.6**) with a y-intercept close to zero. Thus, the minor PPP lactate production mirrored the major glycolytic lactate production. This concurs with the known biochemistry of the PPP being an 'alternative pathway' that is a complex detour bypassing several of the steps of glycolysis. The PPP is a complex biosynthetic network generating many other species besides lactate. The PPP neither consumes nor produces ATP, but sacrifices some of the brain's glucose for the sake of producing intermediates for protecting and repairing the brain (Carpenter *et al.*, 2014; Jalloh *et al.*, 2015a) as follows: The NADPH generated by the 'oxidative phase' of the PPP provides reducing equivalents for fatty acid synthesis (e.g. for repairing injured tissue) and for the formation of the reduced form of glutathione (GSH) and thioredoxin, which are cofactors for glutathione peroxidases and peroxiredoxins, respectively, for combating oxidative stress. The 5-carbon (pentose) sugar ribose-5-phosphate can be utilised in nucleic acid synthesis, providing reparative building blocks for the injured tissue, while the 4-carbon sugar erythrose-4-phosphate can be utilised in the synthesis of aromatic amino acids. The exit-points of the PPP involve the re-entry of products fructose-6-phosphate and glyceraldehyde-3-phosphate (these can alternatively be recycled back into the PPP to generate more NADPH) into the main stream of glycolysis, producing pyruvate, which can enter mitochondria, form acetate and enter the TCA cycle, or pyruvate can be converted to lactate in the cytosol and exit into the extracellular fluid. The PPP may be increased after TBI, evidenced by rodent studies of moderate-severe TBI (Bartnik *et al.*, 2005, 2007), but a microdialysis study in human healthy controls and TBI patients suggested a more varied response in the ratio of PPP to glycolytic metabolism, with the tendency for more patients to have a reduction in their relative PPP metabolism (Jalloh *et al.*, 2015a).

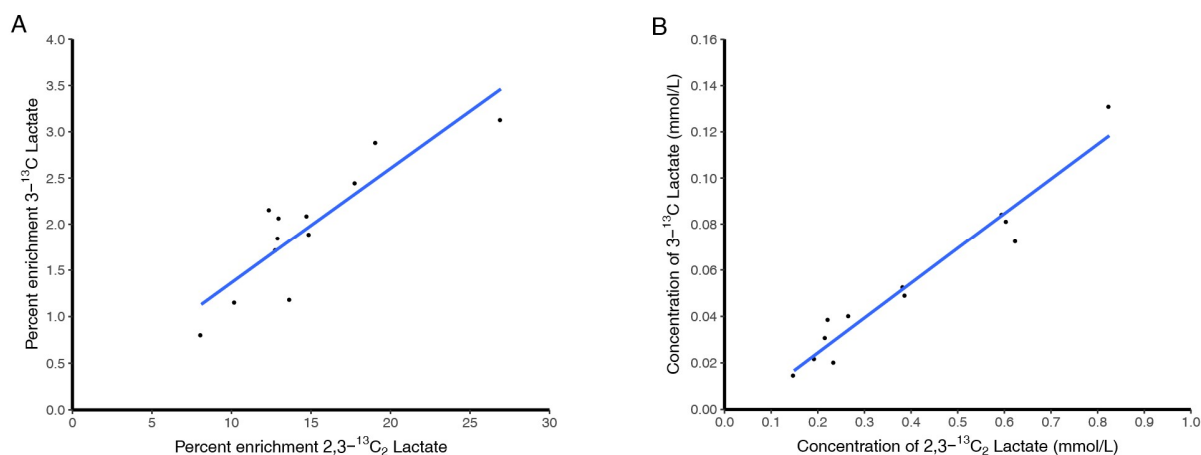


Figure 3.6. Correlation between glycolysis and PPP derived lactate

There was a strong linear correlation between glycolysis derived lactate (2,3- $^{13}\text{C}_2$ lactate) and pentose phosphate pathway (PPP) derived lactate (3- ^{13}C lactate, excluding natural abundance) with a y-intercept of effectively zero in patients who received 8 mmol/L 1,2- $^{13}\text{C}_2$ glucose, suggesting that these two metabolic pathways are up- and down-regulated in unison. Relationships expressed as percent ^{13}C enrichment (Panel A, Pearson's $r^2 = 0.94$) and ^{13}C concentration (mmol/L) (Panel B, Pearson's $r^2 = 0.84$).

3.4.4 TCA cycle activity – absence of ^{13}C glutamine

No evidence of 1,2- $^{13}\text{C}_2$ glucose metabolism via the TCA cycle was found using ^{13}C NMR analysis of microdialysis samples; as ^{13}C glutamine was only found at its natural-abundance background level. Besides being absent in the present study, ^{13}C labelling in glutamine was also absent in earlier studies of microdialysis delivery of ^{13}C -labelled glucose at lower concentrations (Gallagher *et al.*, 2009; Jalloh *et al.*, 2015a).

3.4.4.1 Detection of ^{13}C glutamine in intravenous ^{13}C glucose studies

There is much literature from magnetic resonance studies showing that intravenous supplements of ^{13}C -labelled glucose can be metabolised in brain *in-vivo* via the TCA cycle, evidenced by detection of ^{13}C -label in glutamine and glutamate. These studies address brain tissue, dominated by the *intracellular* compartment, thereby differing from microdialysis that samples *extracellular* molecules. Studies in healthy human volunteers, and animals, receiving intravenous ^{13}C -glucose have shown ample TCA cycle evidence by cerebral ^{13}C MRS *in-vivo* (de Graaf *et al.*, 2003; Rothman *et al.*, 2011). However, cerebral ^{13}C MRS *in-vivo* has not yet been performed in TBI patients. Animal studies, giving intravenous ^{13}C -glucose both in TBI-models and non-TBI animals, have shown TCA cycle evidence, by *ex-vivo* NMR analysis of ^{13}C in brain tissue extracts, showing ^{13}C labelling in glutamate and/or glutamine (Bartnik *et al.*, 2005, 2007).

3.4.4.2 Absence of ^{13}C glutamine in previous microdialysis ^{13}C glucose studies

Contrary to the above evidence from brain tissue studies, microdialysis evidence of TCA cycle seems consistently lacking when using ^{13}C -labelled glucose as the substrate in TBI patients and non-TBI surgical patients. Previous research studies using lower concentrations of ^{13}C -glucose ascribed this to dilution with endogenous material, particularly as many biosynthetic steps and intermediates are involved in the pathway between glucose and glutamate / glutamine (Gallagher *et al.*, 2009; Jalloh *et al.*, 2015a).

3.4.4.3 Presence of ^{13}C glutamine using microdialysis ^{13}C lactate, acetate and succinate

Notably, clear evidence of TCA cycle ^{13}C labelling in glutamine was found from microdialysis delivery (into TBI patients' brains) of three other substrates: 2,3- $^{13}\text{C}_2$ succinate, 2- ^{13}C acetate, and 3- ^{13}C lactate (Figure 3.7) (Gallagher *et al.*, 2009; Jalloh *et al.*, 2017, 2018). These three substrates are closer (in terms of the number of main biosynthetic steps) to the TCA cycle than glucose – succinate is itself a TCA cycle intermediate, acetate is one step from the TCA cycle, and lactate is three steps from the TCA cycle. Dilution of label may explain why production of ^{13}C -glutamine (as evidence of TCA cycle) is seen when the administered substrate is 3- ^{13}C lactate, but not when 1,2- $^{13}\text{C}_2$ -glucose is the substrate. Microdialysis delivery of 3- ^{13}C lactate (8 mmol/L) with a fractional enrichment of 99 % resulted in ^{13}C labelling in the product glutamine showing NMR singlets for C4, C3 and C2 with maximal fractional enrichments of 15.8 %, 11.9 % and 7.5 % respectively (Jalloh *et al.*, 2018). In contrast, in the present study, microdialysis administration of 1,2- $^{13}\text{C}_2$ glucose (8 mmol/L) with a fractional enrichment of 99 % only resulted in 2,3- $^{13}\text{C}_2$ lactate and 3- ^{13}C lactate with maximal fractional enrichments of 31 % and 3.6 % respectively and no detectable ^{13}C -labelling in glutamine. In an earlier study, microdialysis administration of 1,2- $^{13}\text{C}_2$ glucose (4 mmol/L) with a fractional enrichment of 99 % resulted in 2,3- $^{13}\text{C}_2$ lactate and 3- ^{13}C lactate with maximal fractional enrichments of 17 % and 2 % respectively and no detectable ^{13}C -labelling in glutamine (Jalloh *et al.*, 2015a). Comparisons of the above values suggests that even though 1,2- $^{13}\text{C}_2$ glucose was given by microdialysis at a supra-physiological high concentration and high ^{13}C fractional enrichment, there was simply not enough enrichment evident at the lactate stage, and consequently no detectable ^{13}C -labelling in glutamine.

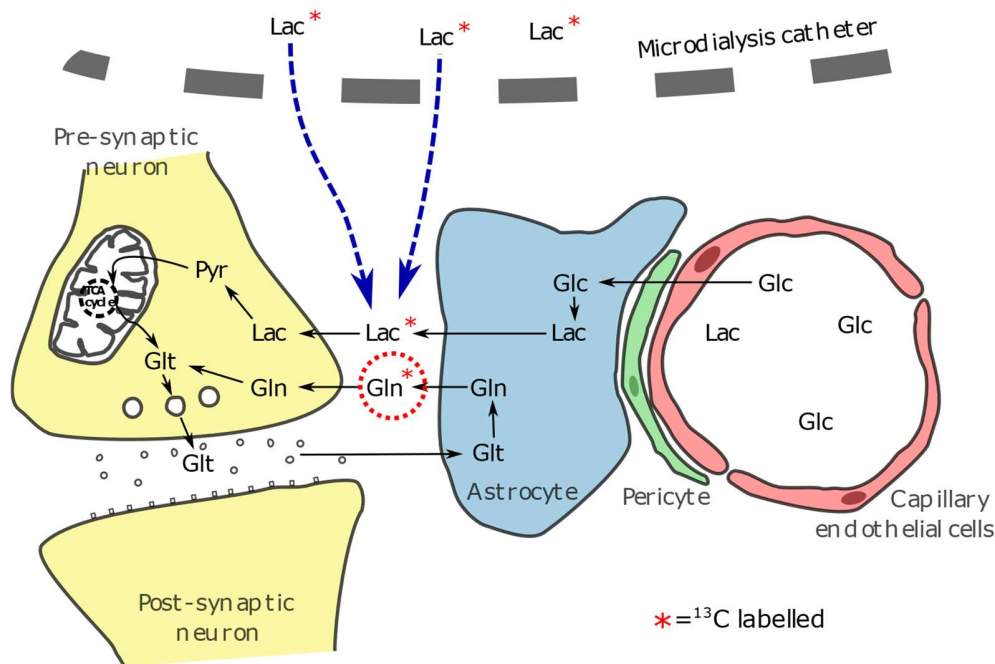


Figure 3.7. Microdialysis delivered ^{13}C labelled lactate produces ^{13}C labelled glutamine

Delivery of modest concentration ^{13}C lactate by microdialysis catheter results in ^{13}C labelling of glutamine. Abbreviations: see table in *Precis*; Glc, glucose; Lac, lactate; Pyr, pyruvate; Glt, glutamate; Gln, glutamine.

3.4.4.4 Mitochondrial dysfunction and hypoxia

Another possible explanation of lack of ^{13}C labelling in glutamine could be mitochondrial dysfunction. In an earlier study of 3- ^{13}C lactate (8 mmol/L) given by microdialysis, most of the patients showed TCA cycle metabolism evident from ^{13}C labelling in glutamine, but a few individuals were ‘non-responders’ who gave no ^{13}C -glutamine production, attributed to mitochondrial dysfunction (Jalloh *et al.*, 2018). However, I think it highly unlikely that *all* of the patients tested with 1,2- $^{13}\text{C}_2$ glucose in the present and previous study (Jalloh *et al.*, 2015a) would have been non-responders because of mitochondrial dysfunction, particularly as some of the patients had baseline L/P ratio below 25.

Another relevant factor is adequate oxygen supply essential for mitochondrial function. Patients with PbtO₂ monitoring had a mean PbtO₂ of 27 mmHg with none below 15 mmHg (**Supplementary Table 3.1**), thus not hypoxic, and all 20 of the patients in the present study were treated with the same

protocol-driven therapy aimed at adequate cerebral perfusion. Thus, the absence of ^{13}C labelling in glutamine is highly unlikely to be due to lack of oxygen. Hyperoxia may suppress cellular glycolysis (Das, 2013), but it demonstrates a variable effect on cerebral microdialysis lactate and L/P ratio, and may increase cerebral oxygen extraction in patients suffering from acute severe TBI (Nortje *et al.*, 2008). However, none of the patients in this study demonstrated cerebral hyperoxia (highest PbtO_2 38 mmHg; patient GL-13), nor were they exposed to extreme hyperoxaemia ($\text{PaO}_2 \leq 17$ kPa; except patient GL-05 whose mean PaO_2 was 19 kPa).

3.4.5 Extracellular lactate as a key step in brain metabolism

The lack of ^{13}C glutamine detected during supplementation of 1,2- $^{13}\text{C}_2$ glucose at 8 mmol/L, considering the presence of ^{13}C glutamine in studies supplementing ^{13}C lactate directly, suggests that extracellular lactate is an important intermediate step of brain glucose metabolism (**Figure 3.8**). Considering that an average 19 % enrichment of ^{13}C lactate was achieved by glycolysis of ^{13}C glucose, similar enrichment would be expected from 'independent' TCA metabolism of the intermediates within a single cell. However, if lactate was exported to the extracellular environment and metabolised to glutamine by a different cell population, the concentration of ^{13}C lactate (average 0.47 mmol/L) after further dilution with extracellular systemic lactate from the circulation may be insufficient to produce detectible concentrations of ^{13}C glutamine. However, when ^{13}C lactate is supplemented directly at concentrations of 4 mmol/L (Gallagher *et al.*, 2009) and 8 mmol/L (Jalloh *et al.*, 2018) ^{13}C glutamine is detected.

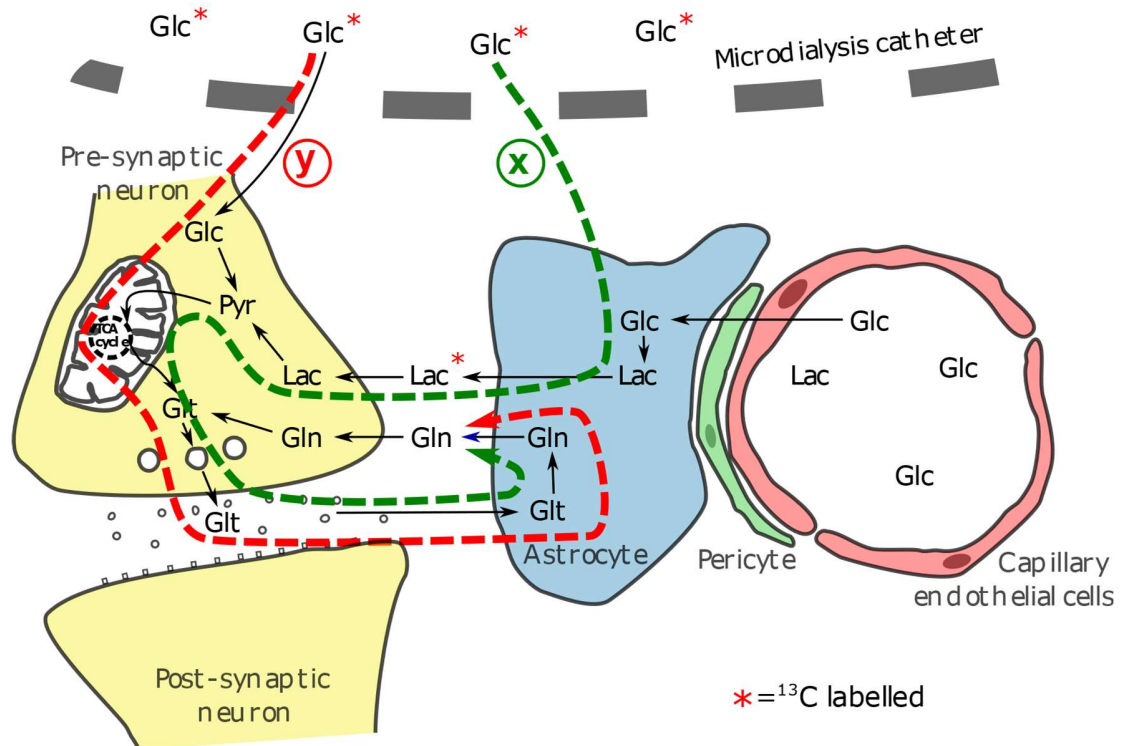


Figure 3.8. Extracellular lactate is an important step in the brain's production of glutamine

Delivery of ^{13}C glucose by microdialysis catheter does not result in ^{13}C labelling of glutamine but does produce low concentration ^{13}C lactate labelling. This suggests that additional dilution of the ^{13}C label occurs at the point of extracellular lactate, so pathway 'x' that shuttles lactate between cells (coloured green) is more likely to represent the dominant pathway of glutamine production than pathway 'y', coloured red in the traumatised human brain. Pathway 'y', that does not involve extracellular lactate, would expect to produce ^{13}C labelled glutamine when ^{13}C glucose is perfused at high concentrations, but not when ^{13}C lactate is perfused. *Abbreviations: see table in **Precis**; Glc, glucose; Lac, lactate; Pyr, pyruvate; Glt, glutamate; Gln, glutamine.*

Regarding supply routes of glucose, debate still exists whether astrocytic glycolysis-derived lactate is the preferred energy substrate for neurons as in the astrocyte-neuron shuttle hypothesis (ANLSH - see below), or whether both astrocytes and neurons independently metabolise glucose per their needs (Pellerin and Magistretti, 1994, 2012; Patel *et al.*, 2014). Schematic illustrations are in **Figures 1.6 & 1.7**. Supporting the 'independent model' (vs. ANLSH) is a kinetic metabolic modelling study in rats (Patel *et al.*, 2014).

In the ANLSH (Pellerin and Magistretti, 1994, 2012; Bouzier-Sore *et al.*, 2003), metabolic trafficking of molecules between astrocytes and neurons can be summarised as follows (Gallagher *et al.*, 2009): Glucose from the vasculature is taken up by astrocytes that metabolise it by glycolysis to form lactate that is exported out of the astrocyte and subsequently taken up by neurons that metabolise it via the TCA cycle. A portion of the TCA cycle intermediate alpha-ketoglutarate is converted into the spin-off product glutamate. The neuron's glutamate is predominantly stored intracellularly within vesicles. Brain tissue intracellular glutamate concentrations are typically of the order of millimoles/L (de Graaf, 2007). Glutamate molecules are released from the pre-synaptic neuron into the synaptic cleft where they can stimulate glutamate receptors on the post-synaptic neuron. Within the synaptic cleft, 'resting' glutamate concentrations are low (1–10 micromol/L), and reach 100–1000 micromol/L briefly during neurotransmission (McKenna, 2007). Leftover extracellular glutamate is taken up by astrocytes, converted into glutamine (by glutamine synthetase in the cytosol and endoplasmic reticulum) (Norenberg and Martinez-Hernandez, 1979) and exported into the extracellular fluid. Extracellular glutamine can then be taken up by neurons and converted back into glutamate, by glutaminase in the mitochondria and cytosol (Aoki *et al.*, 1991). Outside of the synaptic cleft, extracellular concentrations (as measured by microdialysis) of glutamate are typically low (1–20 micromol/L, rising to 100–200 micromol/L in ischaemia), while glutamine concentrations are typically 400–1000 micromol/L (Hutchinson *et al.*, 2002; Samuelsson *et al.*, 2007).

Notably, both glucose metabolic models – 'independent' and ANLSH - feature glutamate-glutamine cycling between neurons and astrocytes (Patel *et al.*, 2014). The lack of ^{13}C -labelling in glutamine when microdialysis-delivered 1,2- $^{13}\text{C}_2$ glucose is the substrate is compatible with the ANLSH – implying that lactate is the favoured substrate for the neuronal TCA cycle, and that when 1,2- $^{13}\text{C}_2$ glucose is the substrate (even when supra-physiological and highly enriched) the ensuing 2,3- $^{13}\text{C}_2$ lactate becomes too diluted with unlabelled lactate, particularly as the astrocytic glycolysis-derived lactate is not only self-diluted with the lactate from the unlabelled half of the glucose molecule (comprising C4, C5 and C6), but

also exits into the extracellular pool and then taken up by neurons to be processed by the TCA cycle to result in ^{13}C labelling in glutamine. A further consideration is that astrocytes / glia can themselves synthesise glutamate de novo via the TCA cycle alpha-ketoglutarate, and ensuing glutamate can be converted to glutamine by the same astrocytes / glia (Pardo *et al.*, 2013; Rose *et al.*, 2013).

3.4.6 Clinical relevance in TBI

Taken together, the ISCUS and ^{13}C results of this and previous (Jalloh *et al.*, 2015a) studies suggest that glucose supplementation may be of limited use in brain injury – in that labelling evidence for glycolysis (and minor PPP), rather than TCA cycle were found, but no shift towards oxidative TCA cycle metabolism (no decrease in L/P ratio and no detectable ^{13}C glutamine). Furthermore glycolytic activity, which in itself only produces 2 moles of ATP per mole of glucose metabolised, appeared to be increased in patients with either low baseline glucose, or evidence of functioning metabolism producing higher concentrations of extracellular lactate and pyruvate at baseline. The TCA cycle and oxidative phosphorylation produces a (theoretical) yield of 36-38 moles of ATP per mole of glucose, which is much greater than that of glycolysis alone. However, although no evidence of increased TCA cycle activity was found, the changes in L/P ratio associated with glucose supplementation were insignificant, suggesting no decrease in mitochondrial metabolism.

3.4.6.1 Delivering glucose to the traumatised brain

A caveat to this study is that glucose was delivered directly into the brain extracellular fluid, rather than by its 'natural' route via the circulation. Microdialysis delivery might conceivably be a less effective way (versus intravenous administration) of getting glucose into brain cells, and may alter its subsequent processing. Blood glucose concentration and glycaemic control normally influence brain glucose though this relationship may be less clear in injured brain (Vespa *et al.*, 2006, 2012; Oddo *et al.*, 2008; Schlenk *et al.*, 2008; Rostami and Bellander, 2011; Zetterling *et al.*, 2011; Magnoni *et al.*, 2012; Schmidt *et al.*, 2012). In the present study during the microdialysis supplementation period there was a weak positive trend (*Pearson* $r = 0.41$, $p = 0.08$) between blood glucose and brain microdialysate (ISCUS) glucose concentrations during the microdialysis supplementation period, but no significant relationships between blood glucose concentrations and brain microdialysate (ISCUS) concentrations of lactate, pyruvate or L/P ratio. Other studies reported that blood glucose levels appear to influence brain metabolism in TBI patients, evidenced by arterial-jugular venous difference measurements (Holbein *et al.*, 2009) and cerebral microdialysis (Diaz-Parejo *et al.*, 2003; Meierhans *et al.*, 2010). These showed that blood glucose levels within the range 6–9 mM and brain microdialysate glucose 1–5 mM were

associated with minimizing the corresponding microdialysate L/P ratio and glutamate concentration. High microdialysate glucose > 5mM was associated with high glutamate, while low microdialysate glucose < 1 mM was associated with high L/P ratio, albeit in a small study (Meierhans *et al.*, 2010). Moreover, my research group's data from 619 TBI patients also suggests high microdialysate L/P ratio is associated with low microdialysate glucose [Guilfoyle *et al.*, manuscript in preparation]. In the present small study, there was no significant relationship between microdialysate L/P ratio and microdialysate glucose.

Delivering additional glucose to the whole brain using intravenous infusions to achieve iatrogenic hyperglycaemia may be associated with additional risk. A large study of the general critical care population (mainly non-TBI) revealed worse outcome in patients who had loose control of serum glucose (van den Berghe *et al.*, 2001), although this was not confirmed in a later, similar study (NICE-SUGAR Study Investigators *et al.*, 2009). A more recent meta-analysis of tight versus loose glucose control in TBI patients found that tight control was associated with better neurological outcome (Hermanides *et al.*, 2018). Furthermore, an observational study of 86 TBI patients (Donnelly *et al.*, 2015) whose blood glucose was targeted between 6-8 mmol/L using an insulin sliding scale (achieving a mean of 6.6 (SD 1.1) mmol/L) concluded that increased blood glucose may impair cerebrovascular reactivity, potentially indicating a mechanistic link between increased blood glucose and poorer outcome after TBI. Defining the optimal ranges of both cerebral and blood glucose requires further study.

3.4.6.2 *Alternative fuels for cerebral energy metabolism*

There is a growing discussion in the literature on whether substrates other than glucose have a therapeutic role in TBI. Debate exists (Dienel *et al.*, 2016) on the suitability of administering exogenous intravenous lactate as therapy for TBI (Ichai *et al.*, 2009, 2013; Bouzat *et al.*, 2014), although it is clearly metabolised via the TCA cycle (Jalloh *et al.*, 2018), and its metabolism does not appear to be suppressed after TBI (Glenn *et al.*, 2015b). Also in TBI patients, microdialysis-delivered 2,3-¹³C₂ succinate not only produced ¹³C-labelling in glutamine but also lowered the L/P ratio suggesting that oxidative metabolism was boosted (Jalloh *et al.*, 2017). Further evidence comes from a combined study of *in-vivo* ³¹P MRS and microdialysis in TBI patients, where succinate delivery by microdialysis resulted in an inverse relationship between the relative changes in the phosphocreatine/gammaATP ratio (a measure of brain energy status) and the L/P ratio, suggesting that the succinate may be able to support brain energy metabolism (Stovell *et al.*, 2018) (see **Chapter 6**). Whether such alternative substrates have a role therapeutically will need more extensive and larger studies, comparing with glucose.

3.5 Conclusion

By a reductionist approach of direct glucose delivery focally into the extracellular space I have shown a limited utilisation of supplementary glucose by the injured brain; with greater effect supplementing high-physiological (4 mmol/L) glucose than supra-physiological (8 mmol/L) glucose – although the effect of glucose supplementation is likely principally determined by whether an underlying disturbance exists in the brain's ability to metabolise glucose. Using ^{13}C -labelling, clear evidence of the rapid but low ATP-yielding glycolysis and the potentially neuroprotective and reparative PPP (that yields no ATP) were found. The lack of ^{13}C evidence for TCA cycle metabolism of the glucose may be due to limitations such as: microdialysis being limited to extracellular sampling, dilution of metabolites with unlabelled molecules (by endogenous species and by self-dilution with the products of the unlabelled C4,C5,C6 moiety of the 1,2- $^{13}\text{C}_2$ glucose molecule), diffusion within the brain, and exchange with the circulation. Even so, the ISCUS bedside readings also suggest that the glucose supplementation did not produce a shift away from 'non-oxidative' (glycolytic) metabolism, as the L/P ratio did not fall. Furthermore, these findings, taken in context of previous studies that demonstrate glutamine production from extracellular lactate in 'normal' and traumatically injured brain (Gallagher *et al.*, 2009; Jalloh *et al.*, 2018) suggest that extracellular lactate is an important step in glutamine production by the traumatised brain. The modest significant rises in lactate and pyruvate production in neuroglycopaenic individuals suggest potential utility of glucose supplementation in this group. Further studies in TBI patients with intravenous ^{13}C -labelled glucose and monitoring by *in-vivo* MRS and cerebral microdialysis are warranted, to address respectively the intracellular and extracellular compartments.

3.6 Declaration and specific acknowledgements

In-vitro NMR experiments of prepared samples were run by NMR spectroscopist Mr D.J. Howe in the Department of Chemistry, but the resultant spectra analysed by me.

3.7 Supplementary Material

Supplementary Table 3.1. Patient demographics

ID	Age	Sex	Mechanism Injury	GCS	Brain Injury	ICP mmHg	CPP mmHg	PbtO ₂ mmHg	4 mmol/ISCUS	8 mmol/ISCUS	8 mmol/NMR	Days from TBI	Cath Latr
GL-01	65	M	Assault	E1V1M2	ASDH	14	68	NA	X	X	X	1	Ipsi
GL-02	39	M	Assault	E1V2M3	ICH/EDH/contusions	NA	NA	NA			X	3	Ipsi
GL-03	33	F	RTC (ped-car)	E1V2M2	Contusions	13	77	NA	X			11	Ipsi
GL-04	37	M	Fall	E1V1M4	ASDH/contusions	11	75	43	X			2	Cont
GL-05	23	M	RTC (car-wall)	E1V1M5	Contusions	19	84	20	X		X	9	Ipsi
GL-06	19	F	Fall (horse)	E1V1M3	Contusions	9	75	38	X			2	Cont
GL-07	39	M	Fall	E1V1M5	Contusions	NA	NA	NA	X		X	4	Cont
GL-08	44	M	RTC (cycl/car)	E1V1M2	ASDH/contusions	22	79	NA		X	X	1	Ipsi
GL-09	55	F	RTC (cycl/car)	E1V1M5	ASDH	6	80	30		X	X	2	Cont
GL-10	41	F	RTC (ped-car)	E2V2M5	EDH/ASDH/contusions	7	81	24	X			5	Cont
GL-11	32	M	RTC (car-wall)	E1V2M5	ASDH/contusions	5	80	NA		X	X	1	Cont
GL-12	16	F	RTC (car-wall)	E1V1M2	DAI	9	71	NA		X	X	1	Ipsi
GL-13	32	M	Assault	E2V1M4	ASDH	13	74	NA		X	X	2	Ipsi
GL-14	32	M	RTC	E1V2M4	ASDH	19	73	16		X	X	2	Ipsi
GL-15	19	M	Fall	E1V1M2	ASDH	9	76	NA		X	X	2	Cont
GL-16	40	M	Fall	E4V1M5	ASDH/EDH/contusions	NA	NA	NA			X	2	Cont
GL-17	27	M	RTC	7	Contusions	NA	NA	NA	X			1	Cont
GL-18	53	F	RTC	6	DAI	NA	NA	NA	X			1	Ipsi
GL-19	37	M	RTC	8	Contusions	NA	NA	NA	X			2	Ipsi
GL-20	28	M	RTC	3	ASDH/contusions	NA	NA	NA	X			4	Ipsi

Table indicates whether full ISCUS and/or high-resolution NMR data were available, and hence used for analysis ('x' indicates available data). ICP, CPP and PbtO₂ data represents supplementation period median values. Days from TBI denotes time interval between injury and period of supplementation in days. Cath Latr indicates whether microdialysis catheter was placed ipsilateral or contralateral to the cerebral hemisphere with greatest injury burden on CT. *Abbreviations: see table in Precis; NA, not available; Ipsi, ipsilateral; Cont, contralateral.* Patients GL-17, GL-18, GL-19 and GL-20 were part of a previous study (Jalloh *et al.*, 2015a).

Supplementary Table 3.2. ISCUS clinical microdialysis analyser individual results

ID	Age	Sex	Conc. Glucose Suppl. (mmol/L)	Unsupp. perfusion Glucose (mmol/L)	Suppl. perfusion Glucose (mmol/L)	Unsupp. perfusion Lactate (mmol/L)	Suppl. perfusion Lactate (mmol/L)	Unsupp. perfusion Pyruvate (μ mol/L)	Suppl. perfusion Pyruvate (μ mol/L)	Unsupp. perfusion L/P ratio	Suppl perfusion L/P ratio	Serum glucose† (mmol/L)	Serum lactate† (mmol/L)	Injury-Supp. Interval (hours)
GL-01	65	M	4	1.65	5.10	3.28	3.58	138	151	23.6	23.2	11.5	1.40	46
GL-01	65	M	8	0.73	8.97	1.85	2.07	66.8	69.7	27.7	29.6	11.5	1.40	46
GL-03	33	F	4	1.39	3.75	3.66	4.16	190	196	20.2	21.3	7.8	1.05	270
GL-04	37	M	4	2.74	3.77	3.07	3.71	106	119	28.9	31.2	7.8	0.95	66
GL-05	23	M	4	0.74	3.55	4.07	4.83	86.2	99	47.9	50	7.5	0.65	217
GL-06	19	F	4	0.79	4.56	2.31	1.79	69.8	52.8	31.2	31.9	7.9	1.10	57
GL-07	39	M	4	1.05	5.52	6.31	8.28	174	215	35.5	36.6	7.8	1.05	115
GL-08	44	M	8	0.81	8.31	2.39	2.16	80	65.9	30.1	32.9	7.6	1.25	47
GL-09	55	F	8	3.84	7.29	1.8	2.17	76.9	87.7	23.2	24.7	10.9	0.90	55
GL-10	41	F	4	0.42	2.90	4.18	5.2	118	130	35.8	39.9	6.6	0.65	138
GL-11	32	M	8	0.75	8.15	1.94	1.85	73.5	67.4	26.4	27.4	6.9	1.10	35
GL-12	16	F	8	3.82	6.39	2.57	2.11	166	146	15.5	14.5	6.1	0.70	41
GL-13	32	M	8	1.04	7.41	2.38	2.57	94.9	99.6	25.5	25.9	6.7	1.10	48
GL-14	32	M	8	1.23	6.39	5.57	4.73	146	138	39.5	34.3	9.6	1.45	67
GL-15	19	M	8	0.65	7.53	1.99	2.34	75.7	84.2	25.5	27.7	10.9	1.00	66
GL-17	27	M	4	0.42	3.24	2.85	4.48	99.8	191	21.4	22	6.6	NA	45
GL-18	53	F	4	1.91	4.52	1.05	1.29	52.7	74.4	17	17.4	5.7	NA	41
GL-19	37	M	4	1.45	4.28	2.12	2.19	99.1	99.1	21.3	22.1	6.9	NA	49
GL-20	28	M	4	0.83	3.60	2.92	3.31	109	122	23.1	26.4	8.3	NA	104
mean			4	1.22*	4.07	3.26*	3.89	113*	132	27.8	29.3	7.6	0.98	105
mean			8	1.61*	7.56	2.56*	2.50	98*	95	26.7	27.1	8.8	1.11	51

Table shows each patient's mean results, from baseline period (pre- and post- supplementation) and supplementation period (Supp.) respectively, with either 4 mmol/L or 8 mmol/L 1,2-¹³C₂ glucose (via the microdialysis catheter) as indicated. *There was a statistically significant difference in baseline (unsupplemented) glucose, lactate and pyruvate between patients who received 4 mmol/L and 8 mmol/L 1,2-¹³C₂ glucose ($p < 0.001$, *lmer* in R). †Serum glucose and lactate concentration shown was measured during the period in which 1,2-¹³C₂ glucose was perfused via the microdialysis catheter measured in either arterial or venous blood. *Abbreviations: see table in Precis; Conc., concentration; Suppl., supplemented; Unsupp., unsupplemented.* The bottom two rows show group means in bold type.

Chapter 4

Development of *in-vivo* ^{31}P MR Spectroscopy

Contents

4.1	Introduction	80
4.2	Methods.....	80
4.2.1	Subject recruitment	80
4.2.2	Acquisition parameters.....	81
4.2.2.1	CSI voxel grid size and position	81
4.2.2.2	Sampling of K-space	81
4.2.2.3	Number of averages (NAs).....	81
4.2.2.4	Assessment of spectra signal to noise (SNR)	81
4.2.3	Analysis methodology	82
4.2.3.1	Analysis with Siemens Syngo	82
4.2.3.2	Analysis with LCMoel	82
4.2.3.3	Comparison of Syngo and LCMoel.....	82
4.3	Results.....	82
4.3.1	Subject demographics.....	82
4.3.2	Acquisition Parameters.....	83
4.3.2.1	Voxel size, sampling of k-space and scan time	88
4.3.2.2	Number of averages and scan time	88
4.3.3	Analysis methodology	90
4.3.3.1	Siemens Syngo vs LCMoel.....	90
4.4	Discussion.....	92
4.4.1	Acquisition Parameters.....	92

4.4.1.1	Scan ‘time’ and assessment of SNR	92
4.4.1.2	Voxel size and position.....	93
4.4.1.3	Sampling k-space and number of averages (NA)	93
4.4.1.4	Chemical Shift Imaging.....	94
4.4.2	Analysis methodology	95
4.4.2.1	Siemens Syngo	95
4.4.2.2	LCModel	95
4.4.2.3	Comparison of Syngo and LCModel results	96
4.5	Conclusions	97
4.6	Declaration and specific acknowledgements	97

4.1 Introduction

³¹P MRS experiments were performed in the Wolfson Brain Imaging Centre on Siemens 3T scanners, employing 2D chemical shift imaging (CSI) using a custom ³¹P head coil. As this was the first time this technique had been used on patients in the acute phase of TBI, the acquisition parameters required optimising to achieve spectra with sufficient signal to noise in an appropriately sized voxel within an acceptable timeframe, described in the **Acquisition Parameters** sections of this chapter. The spectra were analysed using the dedicated software on the Siemens terminal ‘Siemens Syngo’ (Siemens AG, Erlangen, Germany); and a third party software, the Linear Combination Model (LCModel) (Provencher, 1993). Results of analyses with Syngo and LCModel were compared, described in the **Analysis Methodology** sections of this chapter.

4.2 Methods

4.2.1 Subject recruitment

A single, 30-year-old male healthy control (HC-00) was recruited for development of **Acquisition Parameters**. Development of **Analysis Methodology** relied on the dataset used in results **Chapters 5 and 6**: 10 further healthy control subjects and 15 sedated, ventilated TBI patients in the acute phase of their illness. Further details of subject recruitment are in **Chapter 2, Generic Materials and Methods**.

4.2.2 Acquisition parameters

Oblique 2-dimensional single slice chemical shift imaging (2D-CSI) was acquired using Siemens 3T Trio and Verio MR scanners using a custom ^{31}P head coil (PulseTeq Ltd., Chobham, UK). Flip angle was 90 degrees, band-width 3000 Hz, TR 4000 ms, and TE 2.3 ms. Further details in **Chapter 2, Generic Materials and Methods**.

4.2.2.1 CSI voxel grid size and position

The first two scans of HC-00's brain (scans 1 and 2) were acquired with a steep gantry angle, but this was reduced to neutral in subsequent scans (scans 3-6). Scans of the lower limb were performed in the oblique axial plane, accommodating the subject's leg directed through the apertures in the head coil. Voxel size was either 30 x 30 x 30 mm, or 25 x 25 x 25 mm.

4.2.2.2 Sampling of K-space

Data was acquired either filling all of k-space (standard), or with weighted sampling of k-space. Weighted sampling of k-space measures the central points of the k-space the same number of times as the 'number of averages' (NAs), and points on the elliptical boundary are measured at least once, with the frequency of measurement of points in between dependent on the radial distance of the voxel from the centre of k-space.

4.2.2.3 Number of averages (NAs)

The number of averages (NAs) varied from 10 to 120.

4.2.2.4 Assessment of spectra signal to noise (SNR)

Spectra were reviewed on the scanner terminal immediately after acquisition using Siemens Syngo software, and a qualitative assessment made of how well the key peaks (PCr, γATP and Pi) could be delineated from the baseline noise. This determined the parameters of subsequent experiments.

Spectra were then analysed offline: screenshots of individual spectra were taken and the peak height of PCr, γATP and the baseline noise were measured from the centre of the baseline in pixels for semi-quantitative assessment using a drawing program (GIMP; GNU Image Manipulation Program, www.gimp.org).

4.2.3 Analysis methodology

4.2.3.1 Analysis with Siemens Syngo

Patients' spectra were filtered with a 200 ms Hanning filter, zero-filled from 1024 to 2048 datapoints, and Fourier transformed. Correction of frequency shift, phase and baseline was performed automatically before curve fitting. Peak integrals, chemical shifts and peak widths (full width at half maximum height) of PCr, γ ATP and Pi for the central eight voxels of each subject were recorded from the terminal into an Excel spreadsheet.

4.2.3.2 Analysis with LCModel

A basis set was kindly provided by Dr D. Deelchand, University of Minnesota, USA to analyse ^{31}P spectra in LCModel (Deelchand *et al.*, 2015). Spectra were imported in *.rda* format and analysed with LCModel; computing peak integrals and estimates of peaks' standard deviations, as a percentages of the calculated metabolite concentration (%SD) (Provencher, 1993). Chemical shift data were extracted from the 'detailed output' of LCModel by adding "LPRINT = 6" to control parameters in advanced settings (Provencher, 2018).

4.2.3.3 Comparison of Syngo and LCModel

PCr, γ ATP and Pi integrals and pH calculated by Syngo and LCModel from the central eight voxels of each TBI patient (13) and healthy control subject (10) were imported into R (R Core Team, 2018). Correlations between Syngo and LCModel were assessed using Pearson correlation coefficient ('cor.test') and scatter plots plotted with lines of best fit using ('ggplot2'). Three cut-offs of LCModel fitting were used: strict criteria (< 15 %SD), modest criteria (< 20 %SD), and no criteria (inclusion of all central eight voxels).

4.3 Results

4.3.1 Subject demographics

Subject HC-00, used for development of acquisition parameters, was a healthy 32 year old male. Demographics for the 10 other healthy controls used for development of analysis methodology and the experiments in **Chapter 5** can be found in **Table 4.1**. Fifteen acute phase TBI patients were recruited for the studies in **Chapters 5** and **6**, but acceptable ^{31}P MRS spectra were not achieved in two patients: one patient's spectra had insufficient SNR, and another patient's scan had to be abandoned for clinical reasons. Demographics of the remaining 13 ventilated TBI patients (9 male, 4 female, median age 42 years, range 24-65 years) can be found in **Table 4.2**. No clinical complications resulted from acquisition of MRS spectra.

Table 4.1 Healthy control subject demographics

Subject no.	Age group	Sex
<i>HC-00</i>	<i>20-34</i>	<i>M</i>
HC-01	50-65	M
HC-02	20-34	F
HC-03	50-65	M
HC-04	35-49	F
HC-05	20-34	F
HC-06	20-34	M
HC-07	20-34	M
HC-08	35-49	F
HC-09	35-49	M
HC-10	50-65	F

Age group in years. *Abbreviations: see table in **Precis.***

4.3.2 Acquisition Parameters

Scan acquisition date, number of averages acquired (NAs), k-space sampling, scan duration, and calculated SNR of PCr and γ ATP peaks in the central 4 voxels of HC-00's brain are shown in **Table 4.3**. Examples of spectra from each scan are shown in **Figure 4.1**.

Table 4.2, TBI patient demographics.

Subject no.	Age group	Sex	Injury Mechanism	Brain Injury	GCS total	GCS EVM	Days from TBI	GOS-E 6-month	Outcome
TBI-01	20-34	M	Assault	EDH, brain contusions	8	E1V2M5	5	3	Unfav
TBI-02	50-65	F	Fall from height	ASDH, ICH	7	E2V1M4	3	5	Fav.
TBI-03	35-49	M	Assault	DAI, hypoxia	8	E3V4M1	10	2	Unfav
TBI-04	50-65	M	RTC	EDH, ICH	3	E1V1M1	4	1	Unfav
TBI-05	50-65	M	Presumed assault	ASDH, brain contusions	10	E4V2M6	7	2	Unfav
TBI-06	20-34	M	RTC	brain contusions	6	E1V1M4	4	5	Fav.
TBI-07	35-49	M	Fall from height	ASDH, brain contusions	8	E2V1M5	5	5	Fav.
TBI-08	35-49	M	RTC	ASDH	6	E1V1M4	11	5	Fav.
TBI-09	35-49	M	Assault	ASDH, EDH, brain contusions	6	E1V2M3	4	1	Unfav
TBI-10	50-65	F	RTC	EDH, brain contusions	10	E3V1M6	6	1	Unfav
TBI-11	20-34	F	RTC	brain contusions	5	E1V2M2	14	4	Fav.
TBI-12	20-34	M	RTC	brain contusions	7	E1V1M5	13	5	Fav.
TBI-13	50-65	M	Assault	ASDH, brain contusions	4	E1V1M2	4	5	Fav.

Patients TBI-05 and TBI-10 presented as only moderately drowsy but then rapidly deteriorated; requiring sedation, intubation, ventilation and surgery, followed by a period of intracranial multimodality monitoring and treatment for intracranial hypertension. Patients TBI-03, TBI-08, TBI-11 and TBI-12 had persistently high ICP that was difficult to control and were scanned as soon as they could tolerate lying flat. At the time of the scans they still required sedation, ventilation and active ICP control, thus still representing the 'acute phase' after TBI. Age group in years, GCS denotes highest GCS at presentation to emergency services. *Abbreviations: see table in **Precis**; RTC, road traffic collision; GCS, Glasgow Coma Scale score; E, eye response; V, verbal response; M, motor response; L, left; R, right. GOS-E, Extended Glasgow Outcome Scale; Fav., favourable outcome GOS-E \geq 4; Unfav., unfavourable outcome GOS-E \leq 3.*

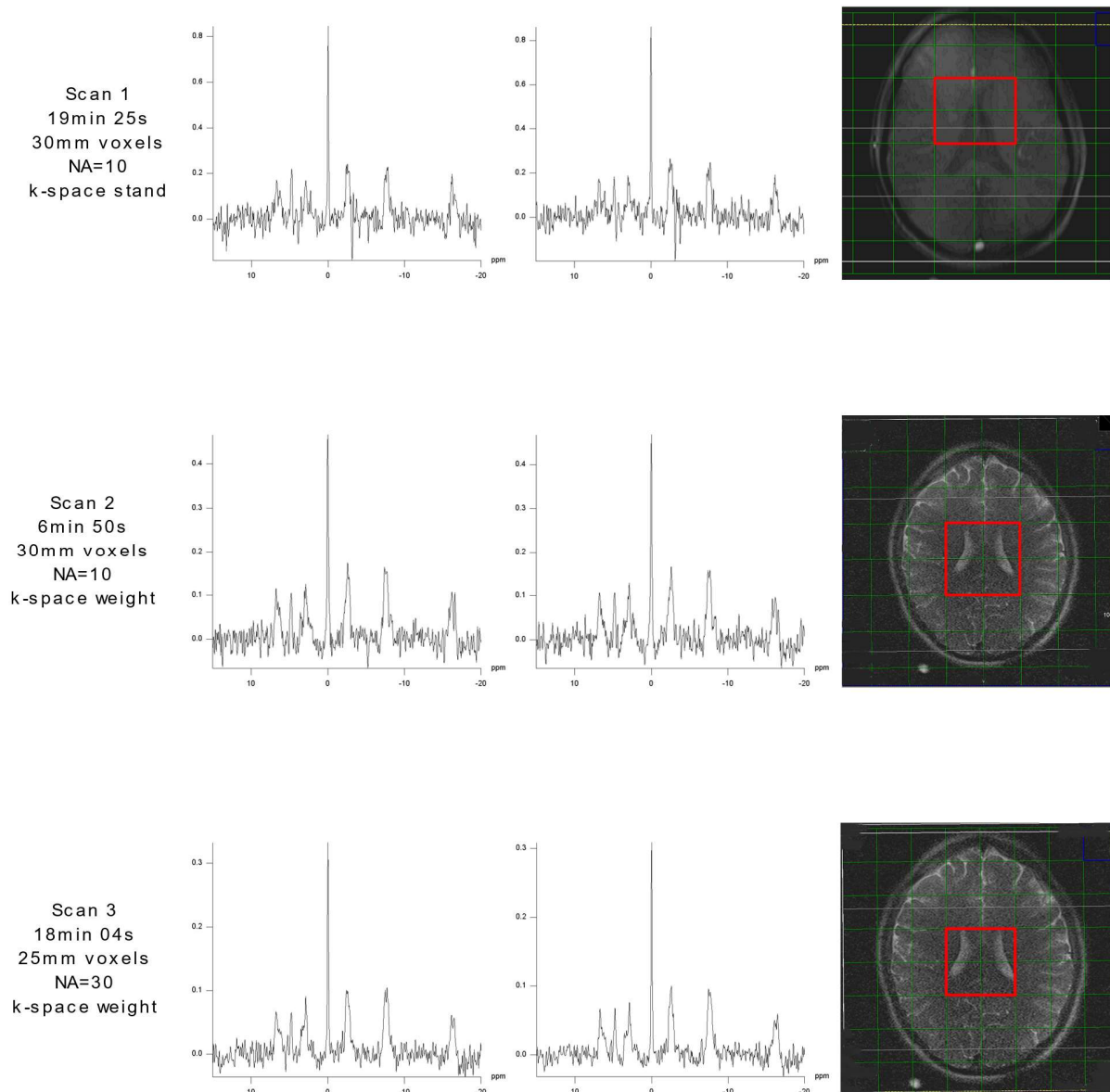
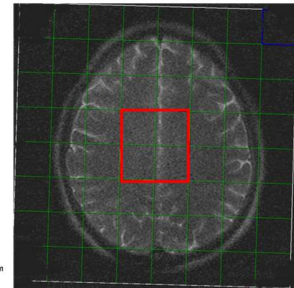
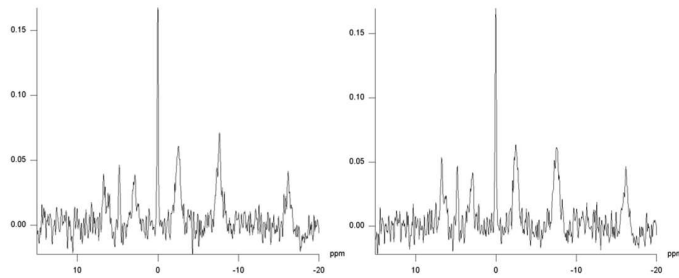


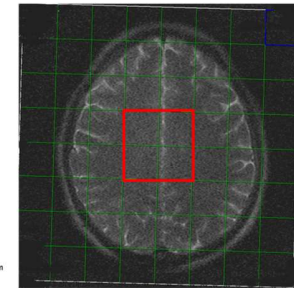
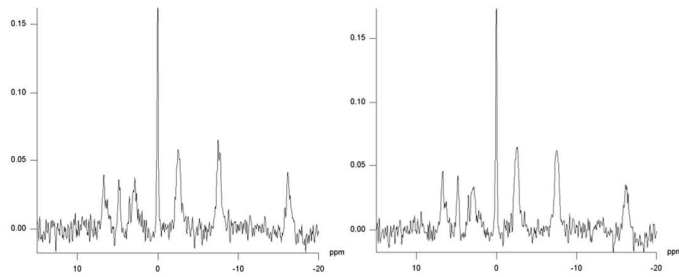
Figure 4.1 Example ^{31}P CSI spectra with localisation in subject HC-00

Spectra from subject HC-00's brain used for development of acquisition parameters (scans 1-6), and lower legs (scan 7), to compare ^{31}P MRS SNR of brain to that of skeletal muscle. Axial ^1H MRI T2 weighted sequences are shown on the right, with the ^{31}P CSI grid overlaid in green. The central four voxels used for analysis of signal to noise are highlighted in red. Spectra from the frontal (superior in image) two of these central voxels are displayed on the left side of the anatomical image. Faint yellow, white and blue lines are artefactual. Scan parameters noted on left. *Abbreviations: see table in **Precis**; NA, number of averages; stand, standard (unweighted) sampling of k-space; weight, weighted sampling of k-space; ppm, parts per million chemical shift.*

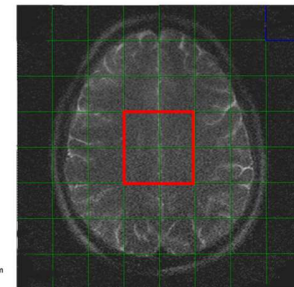
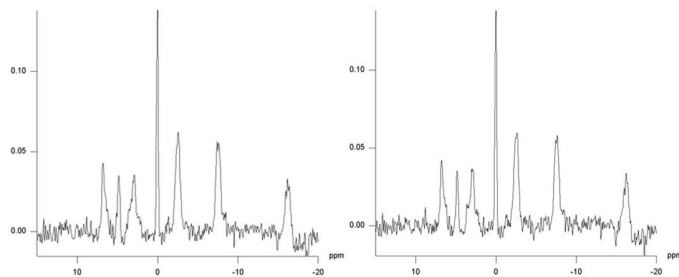
Scan 4
18min 04s
30mm voxels
NA=30
k-space weight



Scan 5
35min 04s
25mm voxels
NA=60
k-space weight



Scan 6
69min 05s
25mm voxels
NA=120
k-space weight



Scan 7
18min 04s
25mm voxels
NA=30
k-space weight

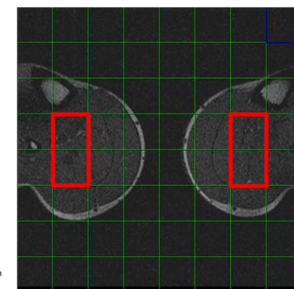
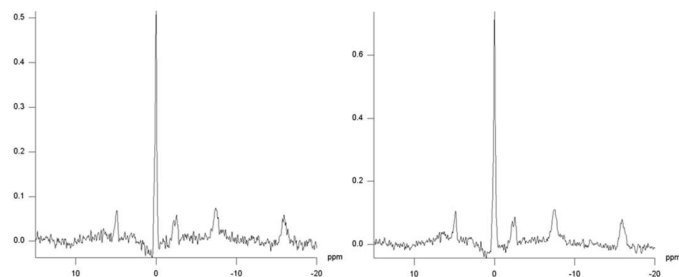


Table 4.3 Signal to noise of PCr and γ ATP peaks using different parameters

Scan	Scan date	Voxel size	K-space sampling	NA	Scan time	Voxel no.	Amplitude	Amplitude	Amplitude	SNR	SNR	Qual.
							PCr	γ ATP	Noise	PCr	γ ATP	
1	2014.11.06	30	standard	10	19:25	28	528	151	35	15.09	4.31	Acceptable
	2014.11.06	30	standard	10	19:25	29	516	160	56	9.21	2.86	
	2014.11.06	30	standard	10	19:25	36	555	142	36	15.42	3.94	
	2014.11.06	30	standard	10	19:25	37	554	156	38	14.58	4.11	
	mean						538.25	152.25	41.25	13.57	3.81	
2	2015.02.11	30	weighted	10	6:50	28	553	203	51	10.84	3.98	Acceptable
	2015.02.11	30	weighted	10	6:50	29	560	196	50	11.20	3.92	
	2015.02.11	30	weighted	10	6:50	36	559	182	49	11.41	3.71	
	2015.02.11	30	weighted	10	6:50	37	554	180	53	10.45	3.40	
	mean						556.50	190.25	50.75	10.98	3.75	
3	2015.02.11	25	weighted	30	18:04	28	570	169	32	17.81	5.28	Acceptable
	2015.02.11	25	weighted	30	18:04	29	581	189	38	15.29	4.97	
	2015.02.11	25	weighted	30	18:04	36	575	168	40	14.38	4.20	
	2015.02.11	25	weighted	30	18:04	37	582	182	47	12.38	3.87	
	mean						577.00	177.00	39.25	14.96	4.58	
4	2015.09.03	25	weighted	30	18:04	28	555	195	41	13.54	4.76	Acceptable
	2015.09.03	25	weighted	30	18:04	29	556	203	52	10.69	3.90	
	2015.09.03	25	weighted	30	18:04	36	554	224	51	10.86	4.39	
	2015.09.03	25	weighted	30	18:04	37	574	208	42	13.67	4.95	
	mean						559.75	207.50	46.50	12.19	4.50	
5	2015.09.03	25	weighted	60	35:04	28	571	203	33	17.30	6.15	Good
	2015.09.03	25	weighted	60	35:04	29	577	218	39	14.79	5.59	
	2015.09.03	25	weighted	60	35:04	36	570	200	33	17.27	6.06	
	2015.09.03	25	weighted	60	35:04	37	580	196	34	17.06	5.76	
	mean						574.50	204.25	34.75	16.61	5.89	
6	2015.09.04	25	weighted	120	69:05	28	573	256	25	22.92	10.24	Excellent
	2015.09.04	25	weighted	120	69:05	29	555	235	25	22.20	9.40	
	2015.09.04	25	weighted	120	69:05	36	564	247	30	18.80	8.23	
	2015.09.04	25	weighted	120	69:05	37	576	247	27	21.33	9.15	
	mean						567.00	246.25	26.75	21.31	9.26	
7	2015.09.08	25	weighted	30	18:04	26	583	65	8	72.88	8.13	Excellent
	2015.09.08	25	weighted	30	18:04	31	600	69	11	54.55	6.27	
	2015.09.08	25	weighted	30	18:04	34	591	80	14	42.21	5.71	
	2015.09.08	25	weighted	30	18:04	39	605	71	15	40.33	4.73	
	mean						594.75	71.25	12.00	52.49	6.21	

Data from healthy control HC-00 brain (scans 1-6) and lower legs (scan 7). Voxel-size in millimetres, scan time in minutes and seconds, amplitude is peak height measured in image pixels, SNR represents species peak height divided by noise height. Weighted sampling of k-space improves SNR, as does increasing the NA. Abbreviations: see table in *Precis*; NA, number of averages; PCr, phosphocreatine peak; γ ATP, gamma-adenosine triphosphate peak; Qual., assessment of spectra quality.

4.3.2.1 Voxel size, sampling of k-space and scan time

The SNR of spectra acquired with 10 averages and standard sampling of k-space using 30 mm voxels was considered acceptable (scan number 1). Using weighted sampling of k-space led to a slight reduction in SNR (scan number 2) (**Figure 4.2**), but a marked decrease in scan time. Weighted sampling of k-space allowed spectra with an even greater SNR than the spectra in scan 1 to be acquired from 25 mm voxels in the same amount of time, by increasing the NAs (scan 3).

4.3.2.2 Number of averages and scan time

Increasing the NAs from 30 (scan number 4) to 60 (scan number 5) improved SNR of the PCr and γ ATP peaks but doubled the scan time from 18 minutes to 35 minutes. Increasing the NAs to 120 improved the SNR a similar factor again, but almost quadrupled the scan time to 69 minutes. Both 18 minutes and 35 minutes were considered acceptable scan times, but 69 minutes was too long, as patients required ^1H MRI sequences for their clinical care and other ^1H MRI research studies to which they had been recruited. The relationship between number of averages and SNR is represented in **Figure 4.3**.

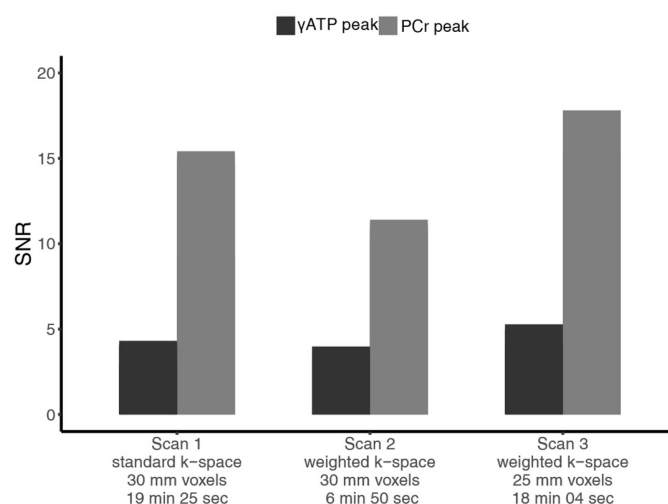


Figure 4.2 Effect of k-space sampling and voxel size on signal to noise (SNR)

Bar charts representing signal to noise (SNR) of the γ ATP peaks (dark grey) and PCr peaks (lighter grey) in scans 1-3 of subject HC-00. Performing weighted sampling of k-space caused a slight reduction in PCr peak SNR (scan 2), but greatly reduced the duration of the scan. This allowed 25 mm voxels to be acquired (scan 3) in the same amount of time that 30 mm voxels were acquired with standard sampling of k-space (scan 1). Abbreviations: see table in *Precis*.

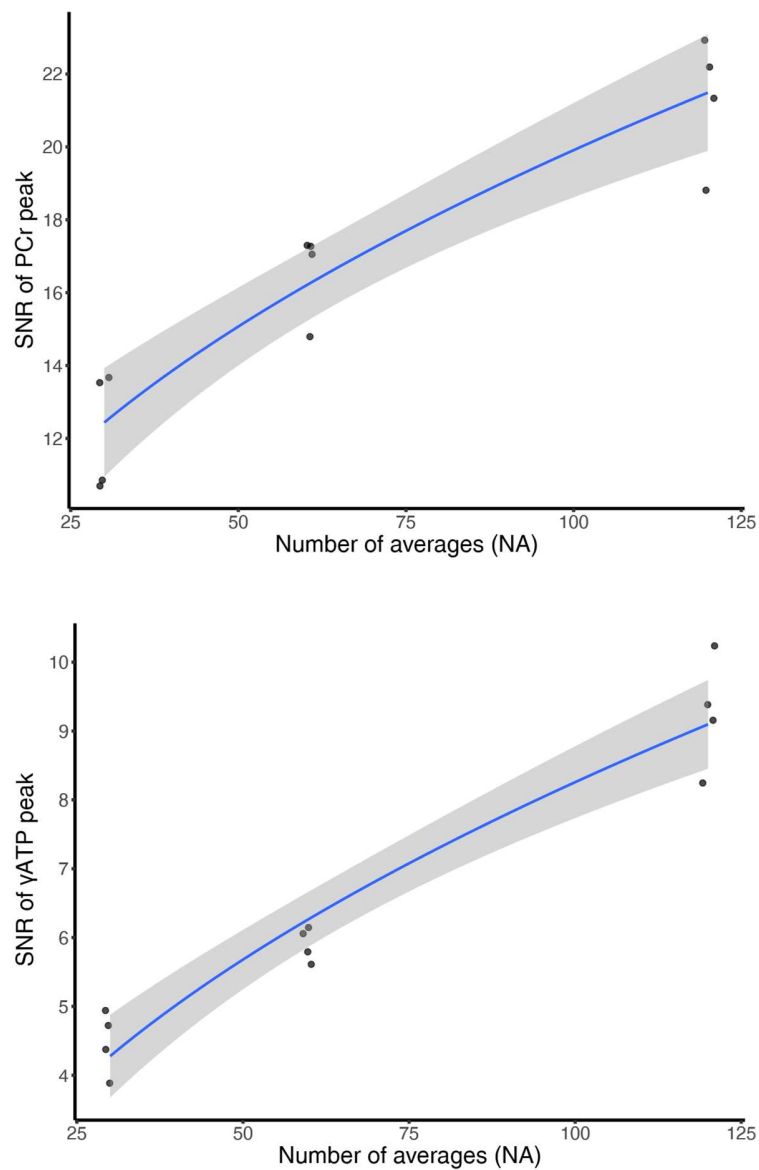


Figure 4.3 Effect of number of averages (NA) on signal to noise (SNR)

Scatter plot with small amount of random variation ('geom_jitter' in R) showing relationship between the number of averages (NA) acquired and the signal to noise (SNR) of the acquired spectra in scans 4-6. The SNR increases proportionally to the square root of NA, represented by blue regression lines, 95 % confidence intervals represented by shaded grey area. $SNR_{PCr} = 1.65 (\sqrt{NA}) + 3.4 ; r^2 = 0.84$.

$SNR_{ATP} = 0.88 (\sqrt{NA}) - 0.54 ; r^2 = 0.93$. Abbreviations: see table in **Precis**

4.3.3 Analysis methodology

4.3.3.1 Siemens Syngo vs LCModel

Siemens Syngo calculated individual peak integral, height, width (full width half maximum – FWHM) and chemical shift, but not fit errors of individual peaks. LCModel calculated individual peak integral and chemical shift, but unlike Syngo, it did not compute individual peak width (FWHM). LCModel did estimate the fit error of individual peaks, which it calls “%SD”.

As expected, a correlation existed in spectroscopy results calculated by Siemens Syngo and LCModel. This correlation was highly statistically significant ($p < 0.0001$) using all subject data. The correlation was also statistically significant using subsets of data that met a minimum %SD in LCModel, with the exception of the integral of Pi using a < 15 %SD cut-off ($p = 0.08$). There was an expected greater variability and a weaker correlation of the integral of Pi peaks than the peaks of PCr and γ ATP, as a Pi peak is much smaller than that of PCr γ ATP. A lower threshold of < 30 %SD was used for estimates of pH, as this uses the position (chemical shift) of the Pi peak, which is more reliably calculated than peak area in peaks with lower SNR. LCModel’s analysis of γ ATP, Pi and pH appeared to produce more outliers than Syngo’s analysis. Individual correlation coefficients are listed in **Table 4.4**, and scatter plots of PCr, γ ATP, Pi and pH values in **Figure 4.4**.

Table 4.4

%SD cut-off	PCr	γ ATP	Pi	pH
No cut-off	0.84	0.87	0.71	0.65
< 20 %SD	0.86	0.90	0.62	0.70
< 15 %SD	0.85	0.89	0.50	0.73

Spearman’s correlation coefficient (ρ) from results of Siemens Syngo analysis and LCModel analysis of the central 8 voxels of 13 TBI patients and 10 healthy controls. < 15 %SD and < 20 %SD denotes inclusion of LCModel values whose estimated standard deviations are < 15 % and < 20 % of their calculated concentrations, respectively. All correlations were statistically significant ($p < 0.001$), except for Pi at < 15 %SD ($p = 0.08$).

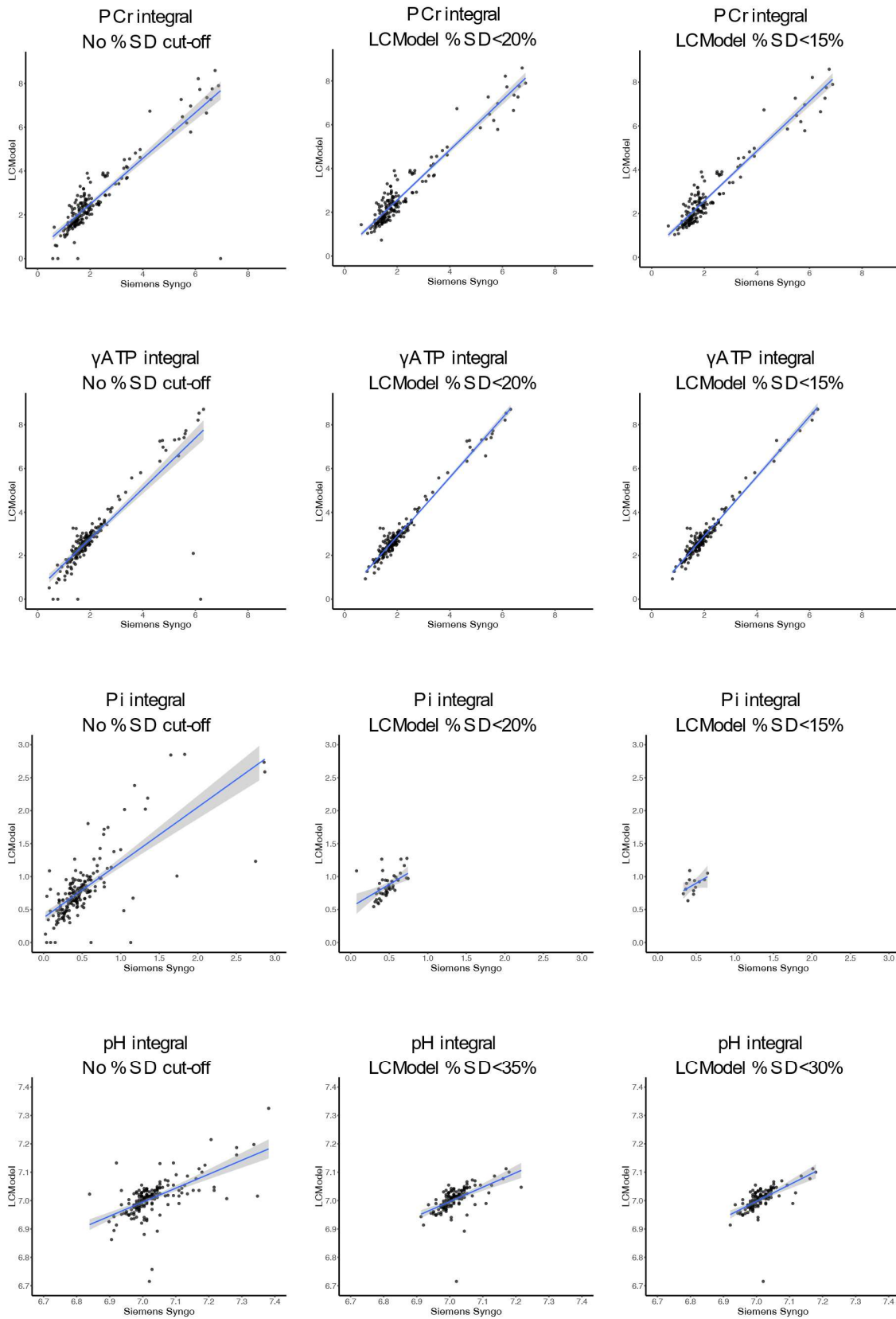


Figure 4.4 Correlation between LCMoDel and Siemens Syngo

Scatterplots showing correlations between Siemens Syngo and LCMoDel analysis of voxel spectra: Left panels represent all data, without an LCMoDel %SD cut-off applied; central panels represent LCMoDel data whose estimated standard deviations are less than 20 % of the calculated concentration (%SD < 20 %); right panels represent LCMoDel data whose estimated standard deviations are less than 15 % of the calculated concentration (< 15 %SD). For calculation of pH, a less strict < 35 %SD was used for middle panels and < 30 %SD for panels on the right. Linear regression lines in blue, with 95 % confidence intervals shaded grey. *Abbreviations: see table in **Precis**.*

4.4 Discussion

4.4.1 Acquisition Parameters

4.4.1.1 Scan 'time' and assessment of SNR

Choosing the acquisition parameters of an *in-vivo* MRS experiment requires 'trading-off' scan parameters to acquire spectra with acceptable SNR within an acceptable scan 'time' (duration). The WBIC scanner suite is optimised for transferring and scanning critically ill patients: it is located adjacent to NCCU and offers continuous ICP monitoring during scans. Furthermore, patients are transferred by an anaesthetist and critical care nurse – and for these experiments – a neurosurgeon. Nonetheless, TBI patients cannot tolerate lying flat for excessively long scans in the acute phase of their injury, and they require ¹H imaging to support clinical management. Many of the patients recruited were recruited to additional imaging studies (Maas *et al.*, 2015) that required ¹H imaging sequences of up to an hour total scan time. Thus, 20 minutes was decided as an initial time limit for ³¹P MRS sequences during early development of ³¹P MRS acquisition parameters (limiting total scan time to an hour and half). As the transfer and scanning team gained experience and confidence, the scan time was extended to a maximum of 40 minutes for ³¹P MRS acquisition, prompting the experimental parameters of scans 4-6.

Although the critical nature of patients' illness made scanning clinically challenging, patients' deep sedation meant that movement artefact – which is typically a challenge for long scan times – was not a problem (Zaitsev *et al.*, 2015; Havsteen *et al.*, 2017). Furthermore, the ¹H imaging acquired for imaging studies (MP-RAGE, FLAIR and SWI) was used in the analysis of experiments in **Chapter 5**.

Visual assessment of ³¹P spectra SNR on the scanner terminal allowed qualitative assessment of the principle peaks used in the studies of **Chapters 5** and **6**: the integral of PCr and γ ATP, and the chemical shift position of Pi. The Pi peak is comparatively small, so accurate assessment of its integral is challenging and thus was not considered an absolute requirement for acceptable SNR. However, the

accurate assessment of its chemical shift was considered a requirement as it is used to determine brain pH in the experiments of **Chapter 5** (for calculation of brain pH see **Chapter 2**).

To quantitatively corroborate qualitative assessment of SNR, screenshots of spectra were taken and analysed 'off-line' as Siemens Syngo does not calculate the height of the noise above baseline. Using the same method (height in pixels) to measure noise, PCr and γ ATP allowed a fair and reasonably accurate comparison. Bitmap screenshots were used as Syngo does not output spectra as vector diagrams.

4.4.1.2 Voxel size and position

The 30 mm default voxel size of the scanner's ^{31}P MRS CSI sequences was used for scans 1 and 2 (**Figure 4.1**). This was deemed too large to support the experiments in **Chapter 6**: the ^{31}P MRS assessment of brain metabolism around a microdialysis catheter perfused with succinate. Decreasing voxel size causes a reduction in SNR proportional to change in volume as there is less tissue in each voxel to release signal for detection by the MR coil. The voxel dimensions were reduced from 30 mm to 25 mm – a 42 % reduction in voxel volume (27 ml to 15.6 ml) – and hence a considerable reduction in expected SNR (expected 42 % reduction). However, the merging of varying cerebral biochemical profiles in different regions of the brain is reduced by reducing voxel size, as each voxel represents a more focal region of brain biochemistry.

The acute gantry angle relative to patients' brains of the CSI grid used for scans 1 and 2 were adjusted to the axial plane of patients' brains so that the largest number of voxels in the grid captured cerebral cortex, for the experiments in **Chapter 5**. This neutral gantry angle also facilitated acquiring a voxel surrounding a microdialysis catheter in **Chapter 6**.

4.4.1.3 Sampling k-space and number of averages (NA)

K-space is the data matrix in which MR frequency data and phase data are recorded, before transformation into an image or array of spectra. The 2-D CSI used in the experiments of this thesis employs phase encoding in two dimensions after application of a slice selection gradient. Datapoints in the centre of k-space contribute to most of the SNR of a spectrum in MR spectroscopy, or image contrast in the case of MR imaging. Datapoints in the periphery of k-space mainly encode spatial resolution of spectra in the grid, or pixels in an image. By weighting the collection of data into the central region of k-space, the scan time could be greatly reduced (scan 2 vs. scan 1), allowing a larger number of averages to be acquired in the same amount of time. Thus, an equivalent SNR using 25 mm voxels could be achieved to that using 30 mm voxels in a similar scan time by employing weighted

sampling of k-space (scan 3 vs. scan 1). Weighted sampling of k-space increases spectral line width and spectral contamination between voxels, but these effects are partially mitigated by post processing with the Hanning filter. Although some spatial resolution would have been lost using weighted sampling of k-space, it was deemed more important to acquire appropriately sized voxels with acceptable SNR for the experiments in **Chapter 6**.

Noise in an *in-vivo* MRS spectrum acquired using an appropriately RF-shielded 3T scanner principally originates from the subject's body, where thermal Brownian motion of solvated electrons and ions creates random RF currents which are picked up the receiver coil (Redpath, 1998). Noise also originates from electrical noise (Johnson noise) in the measurement chain of the scanner, particularly by the RF receive coil, preamplifier, and the connections between the two. When multiple scans are averaged, these random sources of noise begin to cancel each other out, but the spectral peaks are not random so remain constant. Increasing the number of averages (NAs) increases SNR by the number of repeats in Equation 4.1.

Equation 4.1

$$\uparrow \text{SNR} \propto \uparrow \sqrt{NA}$$

The SNR of scans 3 and 4, acquired with 30 averages (18 min, 4 s), was deemed acceptable (**Table 4.3**) and thus 30 averages was used in the TBI patients recruited at the beginning of the studies in **Chapters 5** and **6**. Doubling the NAs improved the SNR appreciably (expected increase 41 %; observed increase 36 %), but remained within an acceptable scan duration (35 min, 4 s) as the transfer and scan team experience improved. Quadrupling the NAs to 120 improved the SNR further, but the 69 min 5 s scan time required was impractical, and the improvement per unit time less marked, as expected from Equation 4.1 (expected increase 100 %; observed increase 75 %) (**Figure 4.3**). Thus, later TBI patients recruited to studies in **Chapters 5** and **6** had ³¹P spectra acquired with 60 averages.

Spectral noise may also originate from unshielded medical equipment releasing electromagnetic radiation from within the scanner's RF cage, and does not necessarily cancel itself out by increasing the number of averages acquired.

4.4.1.4 Chemical Shift Imaging

Chemical shift imaging (CSI), also called magnetic resonance spectroscopic imaging (MRSI), allows acquisition of spectra from multiple voxels in a subject's brain at the same time. Although an acquisition takes longer than single voxel MRS techniques, if data from more than one voxel is required, it is much

more time efficient than repeating a single voxel technique multiple times. The experiments of **Chapter 6** require the comparison of two voxels; if these voxels were acquired using a single voxel technique such as image-selected *in-vivo* spectroscopy (ISIS) data from the rest of subjects' brains would not have been available for analysis in **Chapter 5**. Nonetheless, a specific challenge of the CSI technique is the difficulty acquiring good shim over all voxels in the grid, potentially leading to lower quality spectra compared to single voxel techniques.

2D-CSI was used with a slice select gradient, which provided data in a 3D slab. Using 3D-CSI would have delivered a 3D cube of voxels spanning the entire brain, rather than a grid. However, this type of acquisition would have taken eight times as long as the current scans, so was considered impractical.

4.4.2 Analysis methodology

Programs that quantify *in-vivo* MRS data either fit the acquired data in the time domain before it is Fourier transformed (**Chapter 1, MRS**), or after transformation into the frequency domain as spectra.

4.4.2.1 Siemens Syngo

Siemens Syngo fits MRS data in the frequency domain. Filtering and zero-filling of time-domain data before Fourier transforming is customisable, but for these experiments a 200 ms Hanning filter and zero filling from 512 to 1024 datapoints were used. Correction of frequency shift, phase shift and baseline distortion are also customisable: the ability to customise these parameters is an advantage, but except for adjusting the Hanning filter frequency, the automatic parameters performed well and did not need to be changed. The technique of the final, fitting stage of the processed spectra is also customisable, but the mathematical technique that it uses is not described in the Siemens literature. The calculation of individual peaks' widths is a potential advantage of Siemens Syngo, but it does not quantify how reliable it considers the fit of each individual peak is, as LCModel does.

4.4.2.2 LCModel

LCModel, the Linear Combination Model uses unprocessed data in the time domain, but fits the data in the frequency domain (Provencher, 1993; Deelchand *et al.*, 2015). Pre-filtering (apodization) and zero-filling should not be performed as this "ruins the statistical tests in LCModel and usually destroys information" (Provencher, 2018), so Siemens raw data files (*.rda* files) were used for analysis in this chapter. LCModel automatically performs frequency, phase and baseline correction, but a disadvantage of this is that it cannot be customised by the user. The processed data is fitted as a linear combination of a basis set of complete modelled spectra, acquired from *in-vitro* phantoms of known metabolite

concentrations (Provencher, 1993). As LCMoDel was designed solely to analyse ^1H MRS spectra (Provencher, 2018), a 'custom-made' data base-set was acquired, developed by Deelchand et al. (Deelchand *et al.*, 2015).

An advantage of LCMoDel is that it calculates the reliability of each peak's fit as the '%SD', defined as "the estimated standard deviations (Cramer-Rao lower bounds) expressed in percent of the estimated concentrations(Provencher, 2018)." Typically, a cut-off of $< 15\%$ SD, or $< 20\%$ SD is used for analysis (Provencher, 1993; Cavassila *et al.*, 2000, 2001; Sidek *et al.*, 2016). A potential disadvantage of LCMoDel is the absence of individual peak width results.

4.4.2.3 Comparison of Syngo and LCMoDel results

LCMoDel analysis depended on the selection criteria, or cut-off used: whether voxels were included or excluded that had an uncertainty $< 20\%$ SD, or $< 15\%$ SD. The agreement (correlation) between calculated values by LCMoDel and Syngo was generally good for the PCr and γATP integrals, whose peaks are relatively large and well defined. However, there were several outlier PCr and γATP datapoints, interpreted as zero by LCMoDel analysis of 'all data' (without a %SD cut-off) (**Figure 4.4**).

The agreement between Syngo calculated and LCMoDel calculated results for Pi integral was less good (**Figure 4.4**). This is expected, as the median Pi peak integrals were about four-fold smaller than the PCr and γATP peaks in the dataset. This lower signal to noise caused greater uncertainty of the fits, reflected by the few datapoints remaining after LCMoDel cut-offs of $< 20\%$ SD and $< 15\%$ SD were applied. It is not completely clear which fitting program produces the more accurate result, but the greater number of zero-values output by LCMoDel may imply that it is unable to handle spectra with lower SNR as well as Syngo. Alternatively, Syngo may be generating over-smoothed 'artificial' values for these voxels. However, as LCMoDel is designed for ^1H MRS(Provencher, 2018), with ^{31}P MRS made possible using a yet-unestablished customised dataset provided by a third party(Deelchand *et al.*, 2015), it was thought that Syngo, which was originally designed to include ^{31}P MRS analysis, was more likely to be reliable.

Calculation of pH depends on the position of the Pi peak, which can be more confidently determined in a spectrum with borderline SNR than the magnitude of its integral. Thus, the chosen cut-off for determining the position of the Pi peak was less strict, at $< 30\%$ SD and $< 35\%$ SD, rather than $< 20\%$ SD and $< 15\%$ SD.

4.5 Conclusions

In-vivo ^{31}P MR spectroscopy was performed using 2D-CSI with 25 mm voxels to optimally support the studies in **Chapters 5** and **6**, requiring weighted sampling of k-space to accommodate a reasonable scan time. Thirty averages produced acceptable spectra in the early scans of **Chapters 5** and **6**'s studies, but were increased to 60 to optimise SNR as more scan time became available. Data were analysed with Siemens Syngo and LCModel with comparable results, but Syngo was selected for the MRS analysis in the studies of this thesis as a characteristic of its processing model was lower variance than LCModel, which may be an advantage in studies such as this; as well as it being designed for ^{31}P MRS analysis, unlike LCModel.

4.6 Declaration and specific acknowledgements

In-vivo ^{31}P MR spectroscopy sequences were acquired in collaboration with Dr M.O. Mada, diagnostic radiographer and MR physicist. Dr T.A. Carpenter customised LCModel's basis set with data provided by Deelchand et al.

Chapter 5

Phosphorus spectroscopy in acute TBI demonstrates metabolic changes that relate to outcome in the presence of normal structural MRI

Contents

5.1	Introduction	100
5.2	Materials & Methods	100
5.2.1	Study design, patients & healthy controls	100
5.2.2	Magnetic resonance spectroscopy	100
5.2.3	Statistical analysis	101
5.3	Results.....	102
5.3.1	³¹ P MRS: metabolic changes in acute TBI.....	105
5.3.2	³¹ P MRS: metabolic changes by outcome	108
5.3.3	³¹ P MRS: metabolic changes in the absence of visible tissue injury	110
5.4	Discussion.....	113
5.4.1	Change in PCr/ATP energy state following TBI	113
5.4.2	Brain alkalosis following TBI.....	116
5.4.3	Possible effects of sedation	118
5.4.4	Ventilation and alkalosis	119
5.4.5	Metabolic derangement in radiologically normal-appearing brain.....	119
5.4.6	³¹ P MRS and clinical outcome	120

5.4.7	Strengths and limitations	121
5.5	Conclusions	121
5.6	Declaration and specific acknowledgements	122
5.7	Supplementary Material	123

5.1 Introduction

Although changes in brain glucose metabolism and extracellular lactate/pyruvate ratio are well-known after TBI, it was hitherto unknown whether these translate to downstream changes in ATP metabolism and intracellular pH. Here, I have performed the first clinical voxel-based *in-vivo* phosphorus magnetic resonance spectroscopy (^{31}P MRS) in 13 acute-phase major TBI patients versus 10 healthy controls (HCs); reporting changes in brain energy metabolism and intracellular pH in the acute phase of major TBI. I evaluate how these data relate statistically to patients' clinical outcomes after six months, and identify altered brain metabolism in brain that appears uninjured on MRI sequences sensitive to pathology.

5.2 Materials & Methods

5.2.1 Study design, patients & healthy controls

Fifteen patients who had sustained moderate or severe TBI that required sedation and mechanical ventilation for intracranial hypertension and airway protection were recruited (see **Chapter 2, Materials & Methods and Chapter 4, ^{31}P MRS Development**). Of these 15, spectra of acceptable signal to noise were acquired in 13 (see **Table 4.2**). Scans were performed in the acute phase as soon as patients' intracranial pressure permitted them to be laid supine, whilst still requiring full sedation, ventilation and monitoring for control of intracranial hypertension. Of the 13 patients, 9 were scanned within a week of primary injury, and 4 within 2 weeks of injury because their persistent brittle intracranial hypertension precluded them from being laid supine for MR any sooner. Arterial blood samples were taken and analysed for pH and partial pressure of CO_2 (PaCO_2) before and after patients' scans, and the average of the two results calculated.

5.2.2 Magnetic resonance spectroscopy

Relative concentrations of ATP, PCr and Pi were measured in 2.5 x 2.5 x 2.5 cm voxels using Siemens 3 T scanners and a custom ^{31}P head-coil. Absolute concentrations are difficult to accurately quantify with *in-vivo* clinical ^{31}P MRS, so the ratio of PCr to γ ATP signal intensities of the fitted spectra were used as the primary measure of high-energy phosphate metabolic status (Levine *et al.*, 1992; Mason *et al.*, 1998). To

indicate whether variations in PCr/ γ ATP ratio was driven principally by changes in PCr or γ ATP, the ratio of PCr to total-mobile-phosphate and γ ATP to total-mobile-phosphate was assessed (Levine *et al.*, 1992; Mason *et al.*, 1998). Total-mobile-phosphate was defined as the combined signal from the mobile phosphorus species directly involved in ATP metabolism (PCr, γ ATP and Pi). The γ ATP peak was chosen as the 'cleanest' of the three ATP signals to represent ATP. The β ATP peak is unreliably excited at the edge of the excitation bandwidth used, and α ATP represents the same isotopes as γ ATP, but with the addition of NADH, so these were not included. I did not attempt to adjust ATP values for the presence of ADP, as the latter is naturally much less abundant in the brain, e.g. ATP \approx 3 mmol/L, ADP < 100 micromol/L (de Graaf, 2007) and mostly MR-invisible (Stubbs *et al.*, 1984; Takami *et al.*, 1988). Intracellular pH was calculated from the chemical shift difference between PCr and Pi, using an established equation (Petroff *et al.*, 1985; Prichard and Shulman, 1986).

Patients also received ^1H clinical MR imaging, including sequences sensitive for detecting injury (FLAIR and SWI). Voxel tissue-type (grey matter, white matter, and CSF) was segmented and regions of FLAIR and SWI radiological injury were mapped. The primary inclusion criterion for data analysis was that voxels contained at least 90 % brain tissue; voxels with less than 90 % brain tissue were excluded at the outset. A sub-analysis of 'radiologically-normal' brain was performed by further excluding voxels that contained more than 5 % injury on FLAIR or SWI. As part of the study in **Chapter 6**, nine voxels were supplemented (via a microdialysis catheter, prior to scan) with succinate or glucose, and so were excluded from data analysis in this Chapter.

5.2.3 Statistical analysis

Comparison of PCr/ γ ATP, PCr/total-mobile-phosphate, γ ATP/total-mobile-phosphate and pH between healthy controls and TBI patients was performed with subject-mean data, using Mann-Whitney U test, and repeated using a linear mixed effects model ('*lme*' in R package *nlme* (Pinheiro *et al.*, 2018)) of pooled data, which accounts for 'clustering' of data as each subject contributes multiple voxels. Further comparisons of high energy phosphate ratios and pH between TBI patients with 'favourable outcome' (GOS-E \geq 4) and 'unfavourable outcome' (GOS-E \leq 3) were also performed with Mann-Whitney U of subject-mean data and *lme* of individual voxels, using generalised linear hypothesis tests (*glht*) with Bonferroni correction when healthy controls were included in the model of patient outcome. Voxel grey matter/white matter ratio was included as a covariate in all mixed effect models. The relationship between brain pH and PCr/ATP ratio, arterial blood pH and PaCO₂ was assessed with Spearman's rank

correlation. Potential confounders/nuisance variables were explored using Spearman's rank correlation and Mann-Whitney U tests. Results quoted for outcome are group medians of within-patient means. Graphs were plotted with R and Origin.

5.3 Results

In-vivo ^{31}P MRS data were available for a total of 90 voxels from 13 sedated, ventilated TBI patients (9 male, 4 female), median age 42 years, range 24-65 years, and 80 voxels from 10 age-group and sex-matched healthy control subjects. Patients' demography is in **Table 4.2**, and healthy controls in **Table 4.1**. No clinical complications resulted from MRS. An example scan, and acquired spectra are shown in **Figure 4.1**. Summary ^{31}P MRS data are in **Table 5.1** and individual patient data in **Table 5.2**. Scans were performed as early after injury as clinically feasible, whilst patients still required deep sedation and neurocritical care, so were regarded as within the 'acute phase' of injury.

Table 5.1. ³¹P MRS results: group medians and interquartile ranges of within-subject means

	<i>Number subjects</i>	<i>Injured voxels</i>	<i>PCr/γATP median (IQR)</i>	<i>PCr/total median (IQR)</i>	<i>γATP/total median (IQR)</i>	<i>pH median (IQR)</i>
TBI: all patients	13	Including	1.09 (1.04-1.20)	0.47 (0.46-0.48)	0.44 (0.40-0.45)	7.04 (7.02-7.05)
		Excluding	1.07 (1.06-1.21)	0.47 (0.46-0.49)	0.44 (0.40-0.45)	7.03 (7.01-7.05)
Healthy controls	10	NA	0.93 (0.86-0.96)	0.42 (0.41-0.43)	0.46 (0.45-0.48)	7.00 (6.99-7.00)
<i>p</i> (TBI vs. HC)		<i>Including</i>	<0.0001	<0.0001	0.0009	0.042
		<i>Excluding</i>	<0.0001	<0.0001	0.001	0.055
TBI: favourable outcome	7	Including	1.07 (1.04-1.10)	0.48 (0.46-0.48)	0.44 (0.44-0.45)	7.02 (7.00-7.03)
		Excluding	1.07 (1.06-1.09)	0.47 (0.46-0.48)	0.44 (0.44-0.45)	7.02 (7.00-7.03)
TBI: unfavourable outcome	6	Including	1.14 (1.07-1.22)	0.47 (0.46-0.49)	0.41 (0.39-0.42)	7.07 (7.04-7.14)
		Excluding	1.14 (1.06-1.24)	0.48 (0.47-0.49)	0.41 (0.40-0.44)	7.07 (7.03-7.16)
<i>p</i> (Favourable vs. Unfavourable)		<i>Including</i>	0.3	0.9	0.04	0.03
		<i>Excluding</i>	0.3	0.9	0.06 [0.04]	0.057 [0.008]

³¹P MRS measurements of pH, phosphocreatine (PCr), adenosine triphosphate (γATP) and total-mobile-phosphate (PCr + γATP + inorganic phosphorus) ratios in 13 patients suffering from acute major traumatic brain injury (TBI) and 10 age-group matched healthy controls (HC). Results represent group medians of within-subject means, with interquartile ranges (IQR) in parentheses (curved brackets).

Voxels were considered injured if they contained ≥ 5 % radiological injury on FLAIR or SWI MR sequences. Favourable outcome (Fav) defined as 6-month Extended Glasgow Outcome Scale (GOS-E) ≥ 4, and unfavourable outcome (Unfav.) GOS-E ≤ 3. Statistical analysis performed using a linear mixed model in R (*nlme*), adjusting for voxel grey matter/white ratio. Inclusion of healthy controls and analysis of the linear model using *glht* (results in Fig. 4) found the difference in γATP/total-mobile-phosphate to be statistically significant (results in square [] brackets), but did not affect the significance of other measurements. *Abbreviations: see table in Precis; NA, not applicable.*

Table 5.2. ^{31}P MRS Data Acquired from TBI Patients and Healthy Controls

<i>Subject ID</i>	<i>PCr/γATP mean</i>	<i>PCr/γATP s.d.</i>	<i>PCr/total mean</i>	<i>PCr/total s.d.</i>	<i>γATP/total mean</i>	<i>γATP/total s.d.</i>	<i>pH mean</i>	<i>pH s.d.</i>	<i>no. Voxels</i>
TBI-01	1.06	0.11	0.47	0.03	0.45	0.02	7.03	0.09	7
TBI-02	1.10	0.17	0.48	0.04	0.44	0.03	7.02	0.03	7
TBI-03	1.41	0.13	0.52	0.04	0.37	0.03	7.29	0.07	7
TBI-04	1.00	0.12	0.42	0.06	0.42	0.04	7.15	0.09	7
TBI-05	1.09	0.23	0.46	0.06	0.42	0.04	7.10	0.07	4
TBI-06	1.07	0.14	0.48	0.04	0.45	0.02	7.01	0.07	6
TBI-07	1.03	0.13	0.45	0.03	0.45	0.02	6.98	0.02	8
TBI-08	1.21	0.13	0.48	0.04	0.40	0.04	7.02	0.06	8
TBI-09	1.20	0.04	0.47	0.02	0.39	0.02	7.05	0.05	6
TBI-10	1.23	0.09	0.49	0.03	0.40	0.03	7.04	0.02	7
TBI-11	1.04	0.05	0.46	0.01	0.44	0.02	7.04	0.02	7
TBI-12	1.04	0.08	0.46	0.03	0.44	0.01	7.04	0.07	8
TBI-13	1.10	0.28	0.50	0.06	0.46	0.05	6.96	0.06	8
HC-01	0.95	0.07	0.42	0.02	0.45	0.01	6.99	0.02	8
HC-02	0.74	0.07	0.37	0.02	0.50	0.02	7.00	0.02	8
HC-03	0.92	0.04	0.42	0.03	0.46	0.03	7.00	0.04	8
HC-04	0.98	0.05	0.44	0.02	0.45	0.01	7.00	0.01	8
HC-05	0.82	0.05	0.40	0.02	0.49	0.03	6.99	0.02	8
HC-06	0.99	0.04	0.45	0.01	0.45	0.01	6.97	0.03	8
HC-07	0.95	0.06	0.43	0.02	0.45	0.01	7.00	0.01	8
HC-08	0.88	0.04	0.42	0.02	0.48	0.01	6.99	0.04	8
HC-09	0.86	0.04	0.41	0.01	0.48	0.01	7.00	0.03	8
HC-10	0.97	0.04	0.43	0.03	0.45	0.03	7.03	0.03	8

Individual subject ^{31}P magnetic resonance spectroscopy (MRS) measurements of pH, phosphocreatine (PCr), adenosine triphosphate (γ ATP) and total-mobile-phosphate (PCr + γ ATP + inorganic phosphorus (Pi)) ratios derived from the central eight voxels of 13 TBI patients (TBI-01 – TBI-13) and 10 age-group matched healthy controls (HC-01 – HC-10). As part of a separate biochemical study, some patients had microdialysis catheters supplemented with either succinate or glucose so a voxel was excluded from analysis (TBI-01, TBI-02, TBI-03, TBI-04, TBI-05, TBI-06, TBI-10, TBI-11). Two subjects' CSI grids were positioned to capture superficially placed microdialysis catheters, excluding a further one (TBI-06 and TBI-09) and three (TBI-05) voxels that represented < 90 % brain tissue. *Abbreviations: see table in **Precis**.*

5.3.1 ³¹P MRS: metabolic changes in acute TBI

First, the high energy phosphate ratios and pH of TBI patients and age-group matched healthy controls were compared with Mann-Whitney U test, using each subject's mean value calculated from the central eight voxels of subjects' brains. PCr/ γ ATP was higher in TBI patients (**Figure 5.1A**): median (and interquartile range, IQR) PCr/ γ ATP was 1.09 (1.04-1.20) in TBI patients and 0.93 (0.86-0.96) in healthy controls ($p < 0.0001$). PCr/total-mobile-phosphate was also higher in TBI patients (**Figure 5.1C**): median PCr/total-mobile-phosphate was 0.47 (0.46-0.48) in TBI patients and 0.42 (0.41-0.43) in healthy controls ($p < 0.0001$); whereas γ ATP/total-mobile-phosphate was lower in TBI patients (**Figure 5.1D**): median γ ATP/total-mobile-phosphate was 0.44 (0.40-0.45) in TBI patients and 0.46 (0.45-0.48) in healthy controls ($p = 0.0003$). TBI patients' brain pH was more alkaline than that of healthy controls (**Figure 5.1B**): median 7.04 (7.02-7.05) in TBI patients; and 7.00 (6.99-7.00) in healthy controls ($p < 0.0001$).

Analysis was repeated using a linear mixed effects model that included all ($n = 170$) voxels. This again found a statistically significant difference in PCr/ γ ATP, PCr/total-mobile-phosphate, γ ATP/total-mobile-phosphate and pH between TBI patients and healthy controls, verifying Mann-Whitney U results (**Table 5.1, Figure 5.1**).

Intracellular pH correlated significantly with PCr/ γ ATP (**Figure 5.2A**). This association was not strong (Spearman's correlation coefficient $\rho = 0.27$), although it was highly statistically significant ($p = 0.0001$). There was a statistically significant inverse correlation between brain pH measured by ³¹P MRS and arterial blood pH measured by blood gas analyser (Spearman's $\rho = -0.61$, $p = 0.027$) (**Figure 5.2B**). Arterial pH ranged from 7.37 - 7.49: 9 patients' results were within accepted normal physiological range (7.35-7.45), 4 patients were slightly alkalotic. There was no statistically significant correlation between brain pH and arterial blood PaCO₂ (Spearman's $\rho = 0.42$, $p = 0.15$) (**Figure 5.C**).

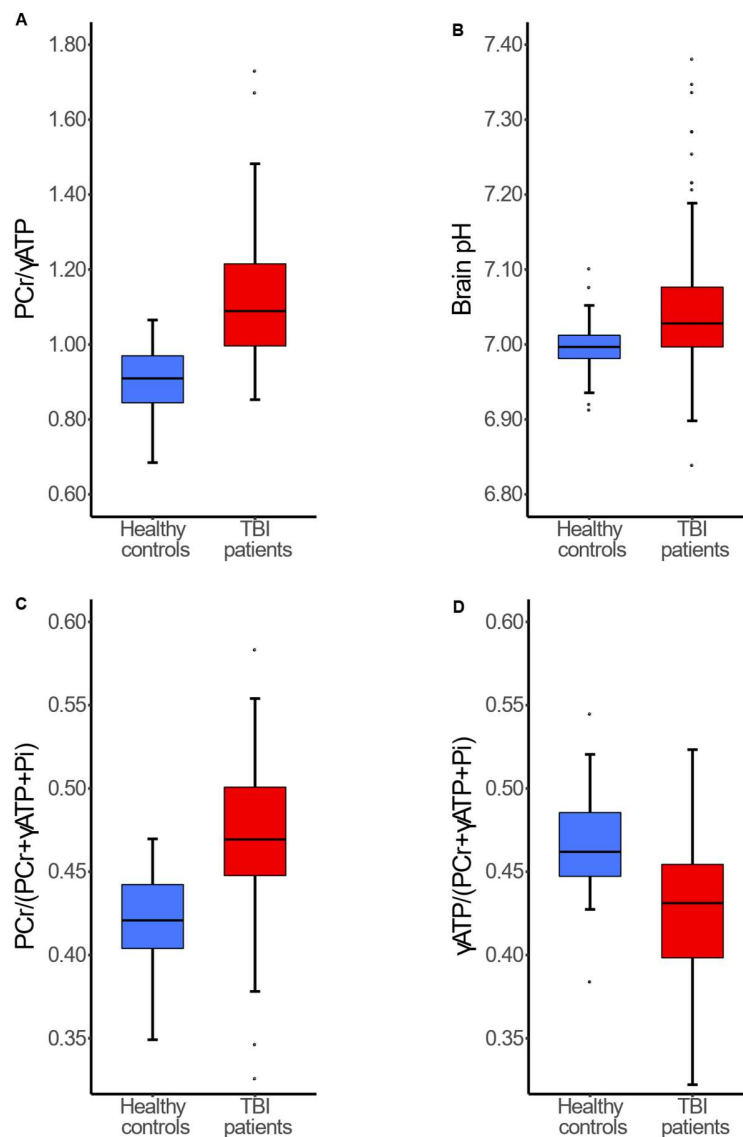


Figure 5.1. PCr/γATP, pH, PCr/total-mobile-phosphate and γATP/total-mobile-phosphate changes following TBI

Box-and-whisker plots of ^{31}P magnetic resonance spectroscopy measurements in the central eight voxels of healthy controls (in blue, 80 voxels) TBI patients (in red, 90 voxels: 'TBI patients'). There was a statistically significant difference in PCr/γATP ratio (*Panel A*; $p < 0.0001$), pH (*Panel B*; $p = 0.049$), PCr/total-mobile-phosphate (*Panel C*; $p < 0.0001$) and γATP/total-mobile-phosphate (*Panel D*; $p = 0.0009$). Statistical analysis performed using a linear mixed model (*lme* in R package *nlme*) that included voxel grey matter/white matter ratio as a covariate. *Abbreviations: see table in Precis.*

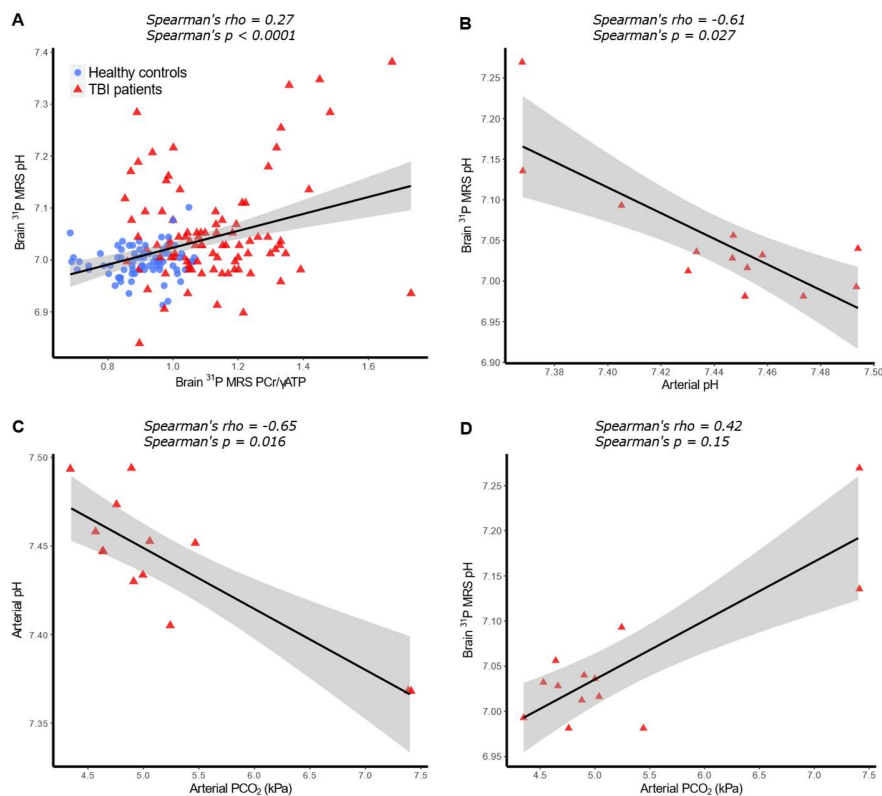


Figure 5.2 Scatter plots showing associations between brain pH, PCr/γATP, arterial pH and arterial PaCO₂ following TBI

Panel A: Brain pH and PCr/γATP ratio of combined voxels ($n = 170$) from healthy controls (blue circles) and TBI patients (red triangles) demonstrates a positive correlation between the two ($\rho = 0.27$, $p < 0.0001$). *Panel B:* Individual patient mean brain pH, measured using ³¹P MRS, is inversely correlated with patient arterial blood pH, measured with bedside blood gas analyser ($\rho = -0.61$, $p = 0.027$). *Panel C:* There was an inverse correlation between arterial pH and PaCO₂, as expected ($\rho = -0.65$, $p = 0.016$). *Panel D:* there was no statistically significant relationship between arterial blood PaCO₂ and brain pH. All correlations Spearman's ranked correlation coefficient with solid linear regression line, 95 % confidence interval denoted by grey-shaded area. *Abbreviations: see table in Precise.*

There was greater variation in pH and high energy phosphate ratios between TBI patients than between healthy controls (**Table 5.1**). The variability within each subject's eight voxels was also greater in TBI patients (**Table 5.2**). Exploration of potential confounding variables found no correlation between pH or PCr/γATP ratio and either patient age, or interval between injury and MRS scanning, nor was a difference found when patients were dichotomised into those less than or more than seven days after injury (Mann-Whitney U). Grey matter/white matter ratio was not significantly different between TBI patients and healthy controls ($p = 0.26$, Mann-Whitney), nor did it reach significance as a covariate in linear mixed model analysis of PCr/γATP, PCr/total-mobile-phosphate or pH. However, it was a

statistically significant covariate in linear mixed model analysis of γ ATP/total-mobile-phosphate ($p = 0.03$), and as it can affect ratios of high energy phosphates in the healthy brain (Mason *et al.*, 1998; Hetherington *et al.*, 2001), it was included in all mixed effects model analysis. Inclusion of scanner type (Siemens Trio or Verio) in the mixed effects models did not affect significance.

5.3.2 ^{31}P MRS: metabolic changes by outcome

To establish whether the above changes were a marker of cellular stress and injury, or an appropriate compensatory response representing repair and recovery, I compared PCr/ATP, PCr/total-mobile-phosphates, ATP/total-mobile-phosphates and pH of patients with favourable outcome to those with unfavourable outcome six months after scanning, using both Mann-Whitney U of subject means and linear mixed model of individual voxels. Patient outcome ranged between GOS-E 1-5 and was dichotomised into favourable and unfavourable outcome (see **Methods**). There was no statistically significant difference in PCr/ γ ATP between patients with favourable and unfavourable outcomes ($p > 0.2$) or PCr/total-mobile-phosphate ($p = 0.9$) by either method. There was a trend for patients with an unfavourable outcome to have a lower γ ATP/total-mobile-phosphate than patients with a favourable outcome, narrowly missing significance by Mann-Whitney U ($p = 0.051$), but significant by mixed model analysis ($p = 0.037$). Brain alkalosis (pH) was higher in patients with unfavourable outcome than patients with favourable outcome using both analytical methods ($p < 0.03$) (**Table 5.1**). Furthermore, to ascertain if the biochemical changes observed in TBI patients (relative to healthy controls) were present in both TBI outcome groups, I then included healthy controls in the model (**Figure 5.3**). Compared to healthy controls, PCr/ γ ATP and PCr/total-mobile-phosphate was elevated in patients with favourable outcome ($p < 0.001$) and patients with unfavourable outcome ($p < 0.0001$), with no difference between the two patient groups. γ ATP/total-mobile-phosphate was lower in patients both with favourable outcome ($p = 0.048$) and unfavourable outcome ($p < 0.0001$) compared to healthy controls, with a greater fall found in patients with unfavourable outcome ($p = 0.024$) using this method of analysis. Brain pH was found to only be alkalotic in patients with unfavourable outcome ($p = 0.0001$); and was not significantly different between patients with favourable outcome and healthy controls ($p = 0.9$). Adding healthy controls to the mixed effects model did not diminish the earlier differences that were significant between patients with favourable and unfavourable outcomes. A scatter plot of intracellular pH vs. PCr/ γ ATP with data-points differentiated for healthy controls and individual GOS-E patient outcomes (**Figure 5.4**) clearly shows that while PCr/ γ ATP elevation was a generality in patients, alkalosis was only in those with worst outcomes.

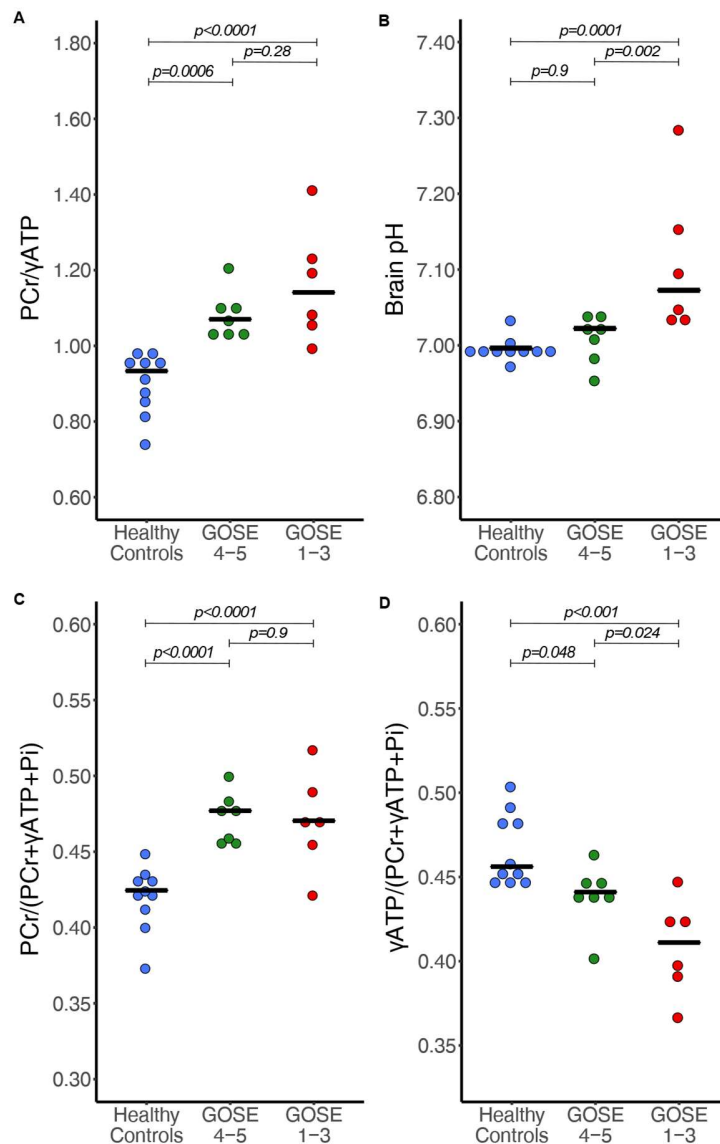


Figure 5.3. PCr/γATP, pH, PCr/total-mobile-phosphate and γATP/total-mobile-phosphate changes following TBI by patient outcome

Dot-plots of ^{31}P magnetic resonance spectroscopy measurements, with each point representing subject mean result, split by patient outcome at six months: healthy controls; favourable outcome (GOS-E ≥ 4); and unfavourable outcome (GOS-E 1-3). *Panel A*: PCr/γATP ratio was raised in both patient groups compared to healthy controls. *Panel B*: brain pH was significantly higher in patients with an unfavourable outcome than healthy controls and patients with a favourable outcome, who did not observe a change in their brain pH. *Panel C*: PCr/total-mobile-phosphate ratio was elevated in both patient outcome groups equally. *Panel D*: γATP/total-mobile-phosphate ratio was significantly lower in TBI patients potentially scaled to outcome, with a lower γATP/total-mobile-phosphate ratio being found in patients with a worse outcome. Statistical analysis was performed using a linear mixed model in R (package *nlme*) that included voxel grey matter/white matter ratio as a covariate, using generalised linear hypothesis tests (*glht*) with Bonferroni correction of the mixed effects model for inter-group comparisons. Statistical significance indicated by bars in figures. *Abbreviations: see table in Precis.*

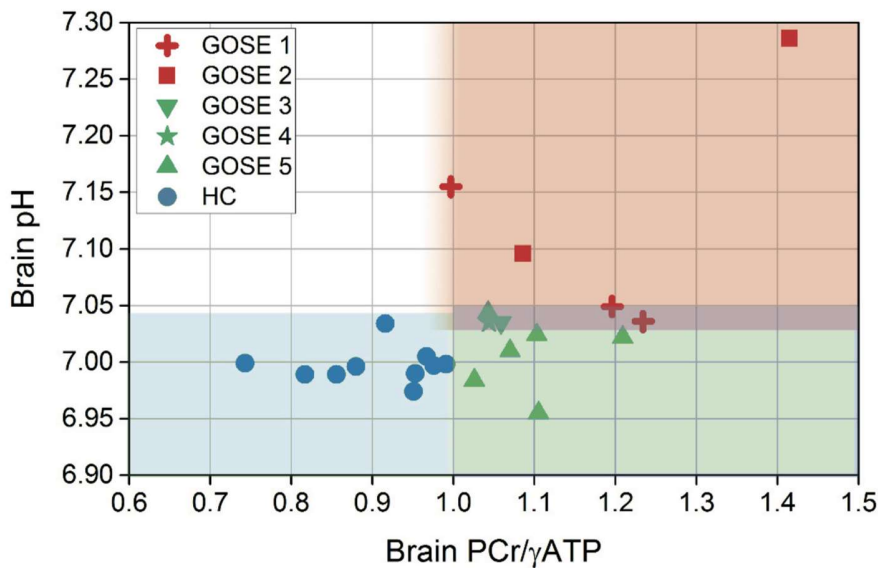


Figure 5.4. Scatter plot showing relationship between brain PCr/ATP, pH and patient outcome

Scatter plot of intracellular pH vs. PCr/γATP, with data-points differentiated for healthy controls and patients' GOS-E (GOSE) outcome scores. Each data-point represents the mean values for one subject.

Abbreviations: see table in Precis.

5.3.3 ³¹P MRS: metabolic changes in the absence of visible tissue injury

To ascertain whether brain alkalosis and elevated PCr/γATP occurred generally in the traumatised brain, rather than being limited to tissue visibly injured on MRI, data analysis was repeated excluding voxels with more than 5 % injury on FLAIR or SWI. This revealed the same pattern, although some statistical significance weakened (see **Figure 5.5** and **Table 5.1**): There was still a difference in within-subject mean PCr/γATP, PCr/total-mobile-phosphate and γATP/total-mobile-phosphate between all TBI patients and healthy controls by Mann-Whitney U and mixed effects model analysis ($p < 0.02$). The difference in pH between patients and healthy controls remained significant by Mann-Whitney ($p = 0.010$), but narrowly missed significance by mixed effects model ($p = 0.055$). Comparing patients with favourable and unfavourable outcomes, there was still no significant difference in PCr/γATP or PCr/total-mobile-phosphate. The difference in γATP/total-mobile-phosphate narrowly lost significance, both by *lme* ($p = 0.06$) and by Mann-Whitney ($p = 0.18$). The difference in pH between patients with favourable outcome and unfavourable outcome narrowly lost significance by Mann-Whitney ($p = 0.10$) and *lme* comparing only the two patient outcome groups ($p = 0.057$), but remained significant when healthy control subjects were included in the mixed effects model (**Figure 5.6**).

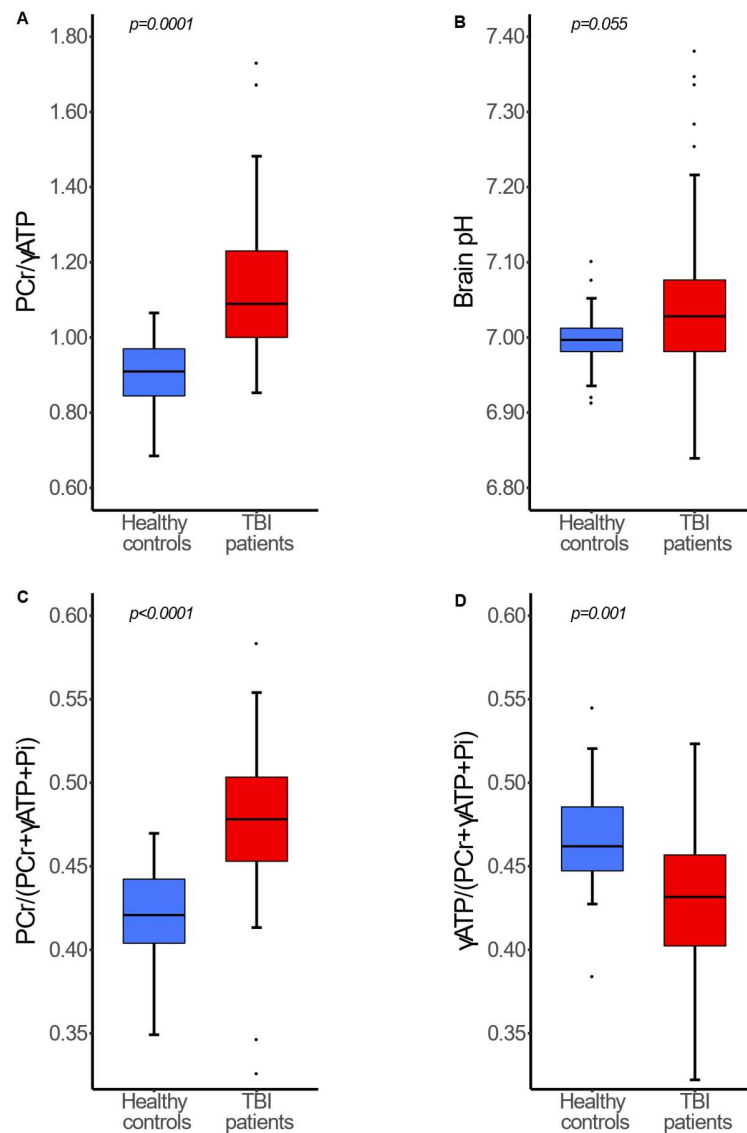


Figure 5.5. PCr/γATP, pH, PCr/total-mobile-phosphate and γATP/total-mobile-phosphate changes following TBI excluding voxels containing radiological evidence of injury

Box-and-whisker plots of ^{31}P magnetic resonance spectroscopy measurements in the central eight voxels of healthy controls and TBI patients, after excluding voxels that contained > 5 % radiological injury on FLAIR or SWI sequences (153 voxels). There statistically significant difference in PCr/γATP ratio (*Panel A*, $p = 0.0001$) remained, but the difference in pH was narrowly lost (*Panel B*; $p = 0.055$). There was a statistically significant difference in PCr/total-mobile-phosphate (*Panel C*; $p < 0.0001$) and γATP/total-mobile-phosphate (*Panel D*; $p = 0.001$) between TBI patients and healthy volunteers. Statistical analysis was performed using a linear mixed model (package *nlme* in R) that included voxel grey matter/white matter ratio as a covariate. *Abbreviations: see table in PreciS.*

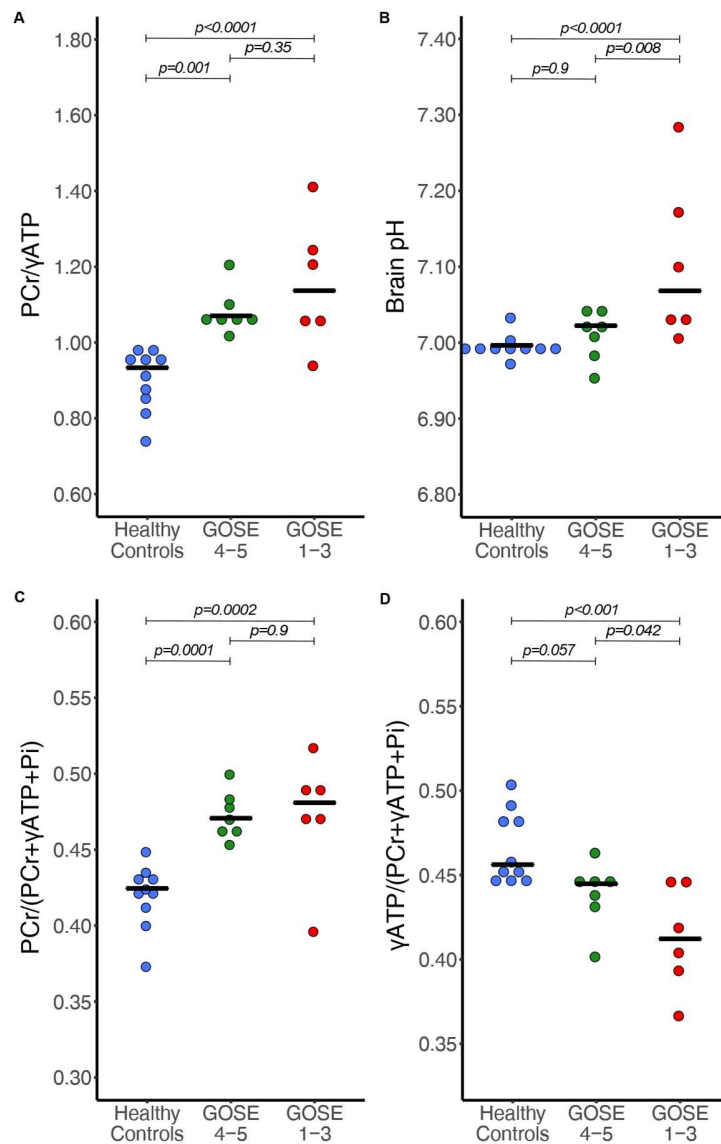


Figure 5.6. PCr/ γ ATP, pH, PCr/total-mobile-phosphate and γ ATP/total-mobile-phosphate changes following TBI by patient outcome excluding voxels containing radiological evidence of injury.

Dot-plots of ^{31}P magnetic resonance spectroscopy measurements, with each point representing subject mean result, split by patient outcome at six months: healthy controls; favourable outcome (GOS-E ≥ 4); and unfavourable outcome (GOS-E 1-3) after excluding voxels that contained $> 5\%$ radiological injury on FLAIR or SWI sequences. Statistical significance in PCr/ γ ATP ratio (Panel A), brain pH (Panel B), PCr/total-mobile-phosphate ratio (Panel C) and γ ATP/total-mobile-phosphate ratio (Panel D) indicated by bars in figures: analysis was performed using a linear mixed model in R (package *nlme*) that included voxel grey matter/white matter ratio as a covariate, using generalised linear hypothesis tests (*glht*) with Bonferroni correction of the mixed effects model for inter-group comparisons. Abbreviations see table in **Precis**.

5.4 Discussion

ATP, the fundamental unit of chemical energy in the brain, is principally produced by cerebral mitochondrial oxidative phosphorylation and cytosolic glycolysis. PCr acts as both a temporal and spatial buffer for ATP in the brain; donating its high-energy phosphate group to ADP for fast recycling of ATP to drive cellular processes in times of high demand, and diffusing from mitochondria to the cytoplasm, smoothing out spatial variations in cellular energy state (Schlattner *et al.*, 2006; Wallimann *et al.*, 2011). Here, significant changes in brain high energy phosphate metabolism (elevation of PCr/ATP) and brain pH (alkalosis) is demonstrated in acute-phase major TBI patients. These changes appear to be related to clinical outcome and persist when voxels containing structural abnormalities on MRI sequences sensitive for detecting injury following TBI were excluded – suggesting fundamental changes in energy state and acid-base balance occur in both visibly injured, and radiologically ‘uninjured’ acutely traumatised brain.

5.4.1 Change in PCr/ATP energy state following TBI

Quantification of absolute metabolite concentrations using *in-vivo* ^{31}P MRS is challenging, thus the PCr/ATP ratio is typically used to characterise cellular energy state. A high PCr/ATP ratio is interpreted as a tissue possessing greater energy reserve due to the relative abundance of the energy-replenishing PCr species relative to the active ATP species (Lodi *et al.*, 2001). Conventionally, when ATP synthesis is running normally, the cell’s PCr store is well-stocked; when ATP synthesis is struggling to meet demand, the PCr store runs down.

The higher PCr/ATP in acute phase TBI, at face value, implies a ‘better-stocked’ store of energy in patients than controls, which might seem counter-intuitive given findings of other studies of adverse brain metabolism following major TBI: including metabolic rate of glucose (Hattori *et al.*, 2003), extracellular L/P ratio (Timofeev *et al.*, 2011) and ^{31}P MRS experimental TBI models in animals (Vink *et al.*, 1988a). Indeed, findings of animal studies hyper-acutely after experimental injury show decreased PCr with unchanging ATP (therefore lower PCr/ATP ratio) (Mcintosh *et al.*, 1987; Vink *et al.*, 1988a, 1988b), whereas I found high PCr/total-mobile-phosphate and low ATP/total-mobile-phosphate, suggesting that both an increase in PCr and a fall in ATP occurred in the brains of these TBI patients.

The high PCr/ATP and PCr/total-mobile-phosphate in these TBI patients may be due to a change in their brains’ cell population (Hypothesis 1 in **Figure 5.7**). A neuroinflammatory cascade occurs after major TBI, with proliferation and migration of glia and inflammatory cells e.g. macrophages (Burda and Sofroniew, 2014). Maturation and activation of macrophages increases their PCr concentration; producing a PCr ‘reservoir’ not seen in non-activated monocytes in the systemic circulation (Loike *et al.*, 1984). Glia also

possess a naturally higher PCr/ATP ratio than neurons (Brand *et al.*, 1993; Alves *et al.*, 2000) and reserve capacity for ATP generation by increasing glycolysis of glycogen stores, or through autophagy (Hertz *et al.*, 2007, 2015; Glick *et al.*, 2010; Falkowska *et al.*, 2015). A higher PCr/ATP ratio (relative to healthy controls) was reported in white matter in the subacute period following TBI, attributed to glial proliferation ('reactive gliosis') (Garnett *et al.*, 2001). I propose that such upregulation of resident glial metabolism and activation and migration of inflammatory cells with higher PCr/ATP ratios, either from the bloodstream or through activation of resident microglia, are the most important contributors to the elevated PCr/ATP ratio in this study.

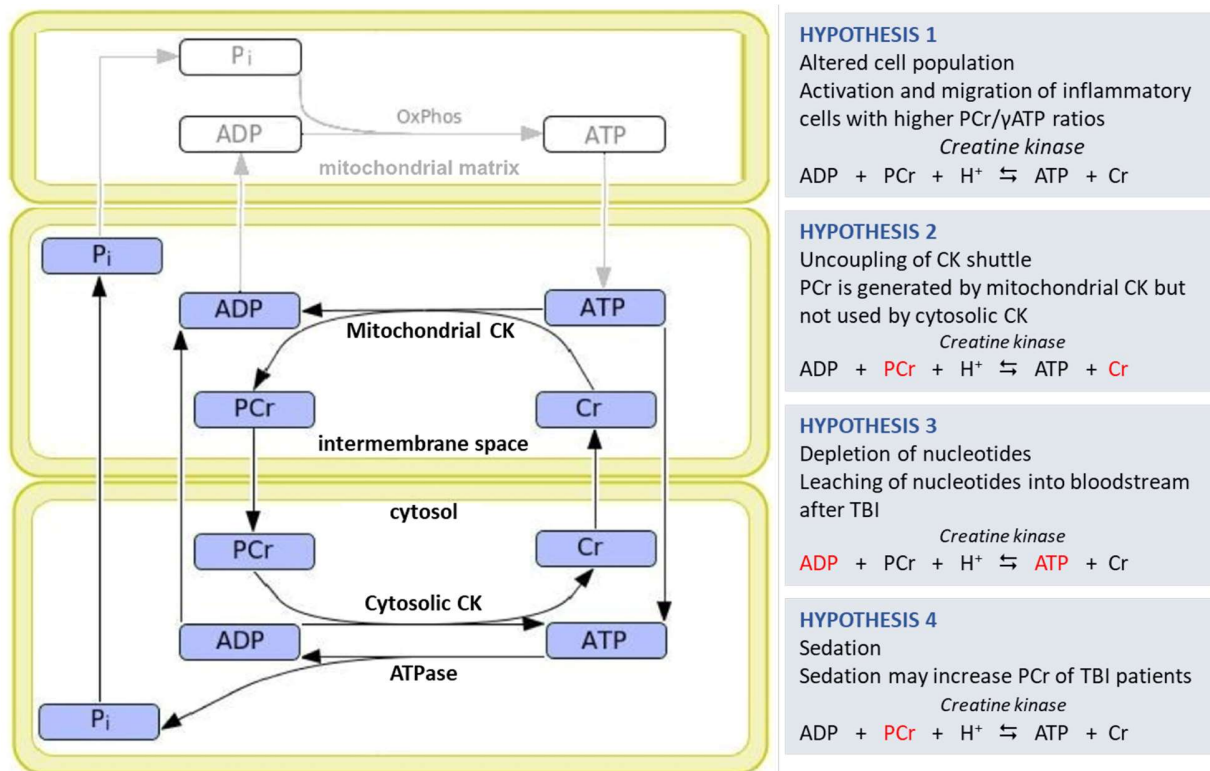


Figure 5.7. Hypotheses as possible explanations of ^{31}P MRS results.

Hypotheses for changes observed in TBI patients, that may coincide in these sedated TBI patients. *Abbreviations: see table in **Precis**.* The schematic of the compartmentalised creatine kinase system is adapted from Hettling and van Beek (2011, PLoS Comput Biol 7(8): e1002130, published Open Access © the Authors).

The rise in PCr/ATP and fall in ATP/total-mobile-phosphate may also represent a degree of neural tissue energy failure occurring independently of brain cell population changes and/or glial activation (Hypothesis 2, **Figure 5.7**). Mammalian cells work hard to maintain ATP homeostasis, even when stressed (Prichard *et al.*, 1983; Petroff *et al.*, 1984; Sauter and Rudin, 1993), so the apparent fall in ATP implied by a lower ATP/total-mobile-phosphate indicates more extreme metabolic dysfunction, and is most evident in patients with unfavourable outcomes. The high PCr/total-mobile-phosphate found is surprising, as PCr would be expected to regenerate ATP. However, elevated PCr/ATP may represent a combined result from two different cell populations in the traumatised brain: cells that are more sensitive to injury, such as neurons, experiencing energy failure with low ATP; and activated glia more resistant to injury, and inflammatory cells which may have a relatively higher concentration of PCr. Such concept of differentially viable cellular moieties was proposed in a subacute study of large-territory stroke (Zöllner *et al.*, 2015), which may share similar pathophysiology with patients who have sustained a major traumatic injury. Additionally, leaching of adenine bases from the injured brain (Weigand *et al.*, 1999; zur Nedden *et al.*, 2012) may contribute to the finding of low ATP together with elevated PCr; as if high energy phosphates were generated in the absence of sufficient adenine bases, the CK equilibrium may be shifted to a higher PCr/ATP ratio. However, this explanation less likely, as one would not expect selective ATP loss without loss of PCr and Cr from the traumatised brain.

Uncoupling of the mitochondrial-cytosolic CK system (Hypothesis 3 in **Figure 5.7**) may also contribute to high PCr/ATP in TBI patients. PCr is synthesised in the mitochondrial inter-membrane space by octameric mitochondrial CK (Mi-CK), and used in the cytosol by the dimeric, cytosolic form of CK (BB-CK). If TBI causes greater disruption or injury to cerebral BB-CK than to Mi-CK, or disruption of PCr and Cr shuttling between the two in the cytosol and mitochondria, PCr may be produced but not used, resulting in elevated PCr/ATP from accumulation of PCr and consumption of ATP. Although PCr (211 Daltons) is regarded as readily diffusible in cells due to its size and charge (Schlattner *et al.*, 2006; Wallimann *et al.*, 2011), the restricted diffusion of a similar sized molecule, N-acetylaspartate (NAA, 175 Daltons), has been demonstrated in animal models of pathology (Nicolay *et al.*, 2001), and has more recently been demonstrated in human pathology (Wood *et al.*, 2012). Gabr *et al.* reported in an advanced ³¹P MR diffusion spectroscopy study of human skeletal muscle that "In a time equal to the half-life of PCr in the CK reaction, PCr would diffuse an average distance of approximately 66 micrometres" (Gabr *et al.*, 2011). Although I could not find literature on such measurements in brain, I consider PCr as a diffusible, spatial buffer of energy reserve.

Unlike TBI, mitochondrial diseases demonstrate *below-normal* PCr/ATP ratios in brains (Eleff *et al.*, 1990) and heart muscle (Lodi *et al.*, 2001; Bates *et al.*, 2013). Also, physiological adaptation (rather than disease) can give ‘below-normal’ PCr/ATP ratios, e.g. Sherpa heart muscle (Hochachka *et al.*, 1996). In epilepsy, ipsilateral depression of PCr/ATP ratio occurred in the epileptogenic hippocampus, relative to contralateral ‘healthier’ hippocampus (Pan *et al.*, 2008). Like TBI, *elevated* brain PCr/ATP ratios (above healthy controls) were reported in Parkinson’s disease (Hu *et al.*, 2000), and in normal-appearing white matter in multiple sclerosis, attributed to diminished creatine kinase B activity (Steen *et al.*, 2010). This supports the idea that inflammation in TBI brain might at least partly contribute to the elevated PCr/ATP ratio observed.

5.4.2 Brain alkalosis following TBI

In the acute phase of TBI, patients’ brains overall were more alkaline compared to healthy controls (**Figure 5.1**). Sub-group analysis revealed this to be limited to patients who had unfavourable outcomes 6 months later (**Figure 5.3**). ^{31}P MRS measures predominantly intracellular pH (Ren *et al.*, 2015), estimated to represent 80 % of total brain volume (Syková *et al.*, 2008; Nicholson *et al.*, 2011). Of this, I am likely detecting a composite of cytosolic and mitochondrial pH, as the Pi peaks from each pool do not appear separately resolved in these *in-vivo* MR spectra. *Extracellular* acidification, measured with intracranial probes, is associated with metabolic derangement and increased TBI patient mortality (Gupta *et al.*, 2004; Timofeev *et al.*, 2013). *Intracellular* acidification is seen in rodent ^{31}P MRS studies of hyperacute major TBI (Vink *et al.*, 1987), followed by a period of intracellular alkalosis (Mcintosh *et al.*, 1987). A ^{31}P MRS study of recovering patients in the subacute/chronic phase of TBI found (intracellular) alkalosis of patients’ white matter (Garnett *et al.*, 2001). This finding of brain intracellular alkalosis in acute-phase TBI patients with unfavourable outcome 6 months later suggests that acute-phase alkalosis occurs when physiology is severely deranged, rather than simply being a feature of recovery after injury. Brain alkalosis was found experimentally in rats 24-48h after transient (8 minutes) forebrain ischaemia followed by reperfusion (Chopp *et al.*, 1990). In a clinical ^{31}P MRS study of large-territory ischaemic stroke, hyper-acute brain acidification was reported (within 18 hours of infarct), followed by brain alkalosis (by day 3) which persisted for 29 days (Levine *et al.*, 1992); these findings are supported by a later study of stroke patients 3-12 days after ictus (Zöllner *et al.*, 2015). Infarction is an extreme tissue injury, so concurs with my finding of brain alkalosis in TBI patients who proceed to unfavourable outcomes – although this study demonstrates alkalosis in normal-appearing tissue on conventional and advanced MR imaging.

The interrelationships among intracellular pH, extracellular pH, and their biological implications are complex and incompletely understood. Mammalian cells strive to maintain an optimal intracellular pH and actively transport H⁺ ions extracellularly by several regulatory mechanisms, as they can only survive when intracellular pH is neutral or slightly alkaline (McLean *et al.*, 2000; Chiche *et al.*, 2012). When astrocytes become alkalotic their rate of glycolysis increases, likely through increased activity of the rate-limiting enzyme phosphofructokinase (PFK) with an optimum around pH 7.2 – 7.3, and a steep pH dependence, falling dramatically at lower pH (Trivedi and Danforth, 1966; Theparambil *et al.*, 2016). Astrocyte glycolysis produces lactate; each lactate anion is co-transported by monocarboxylate transporters out of the cell accompanied by an H⁺ ion (McLean *et al.*, 2000) to 'feed' neurons in the model of the astrocyte-neuron lactate shuttle hypothesis (Pellerin and Magistretti, 1994; Bouzier-Sore *et al.*, 2003). Upregulation of brain glycolytic activity was shown in acute severe TBI (Glenn *et al.*, 2003; Marino *et al.*, 2007; Timofeev *et al.*, 2011; Carpenter *et al.*, 2015b). If an increase in astrocytic lactate/H⁺ export was not matched by increased lactate/H⁺ uptake by neurons, extracellular acidosis would occur in the presence of intracellular alkalosis. Given the greater vulnerability of neurons compared to glia, this may explain the intracellular alkalosis seen here, and the extracellular acidosis in other reports (Zygun *et al.*, 2004; Timofeev *et al.*, 2013).

Glial alkalosis may be self-regulated, or driven by neurons. Astrocytes can adapt their intracellular pH 'set-point' to be more alkaline (Swietach *et al.*, 2014), which increases their rate of glycolysis and synthesis of protein, DNA and RNA. This occurs in astrocytic tumours for cell division (Madhus, 1988; McLean *et al.*, 2000), and conceivably also for cellular repair in injured astrocytes. Several mechanisms regulate pH in astrocytes (McLean *et al.*, 2000). Intracellular alkalosis may arise from the cell exporting H⁺ ions – including those generated by glycolysis. This may be via monocarboxylate transporters (see above) that do not consume ATP. However, another H⁺-extrusion pathway is via H⁺-ATPase pumps that directly consume ATP. If this were necessary for cells to maintain glycolysis, it may significantly reduce the net efficiency of glycolytic ATP production if mitochondrial function were impaired in the traumatised brain (Timofeev *et al.*, 2011; DeVience *et al.*, 2017), as only two moles of ATP per mole of glucose are produced by 'isolated glycolysis'. If NADH shuttling (e.g. malate-aspartate shuttle) from the cytosol into mitochondria is operational then further ATP molecules can ensue from glycolysis. The yield per mole of glucose metabolised fully to CO₂ (by the combination of glycolysis, NADH shuttling and mitochondrial respiration) is theoretically 36-38 moles of ATP. However, the actual yield is considered somewhat lower (Lodish, 2000; Berg *et al.*, 2002). Upregulation of astrocyte glycolysis by intracellular alkalosis may also be activated by local neurons, as glial cytosolic alkalosis occurs in response to local

neuronal activity (Chesler and Kraig, 1989; Chesler, 2003). In TBI this may be a purposeful mechanism for neurons to induce additional metabolic support; or be a pathophysiological consequence of neuronal glutamate excitotoxic injury, associated with leakage of cytoplasmic elements from injured neurons (Farkas *et al.*, 2006; Kilinc *et al.*, 2008).

Alkali brain pH appears distinctive for patients who emerged with the worst clinical outcomes, concurring with association between brain hyperglycolytic state and TBI mortality (Glenn *et al.*, 2003). This implies that after TBI, alkalosis is either caused by energy perturbation proceeding in the worst cases to an adaptive state of alkaline pH associated with abnormal cell biology and biochemistry, or that alkalosis is a distinct product of more catastrophic neuronal injury. The significant change in pH in patients with unfavourable outcome, with no change in patients with favourable outcome, suggests that sedation did not affect brain pH, as all patients were treated effectively the same.

A change in cell population, a proposed explanation for elevation in PCr/ATP (see above), may also contribute to brain alkalinisation. White matter alkalosis was attributed to reactive gliosis because regions of pathology containing more glial cells (e.g. low-grade astrocytomas) typically have a higher pH (Garnett *et al.*, 2001). Reactive gliosis may thus contribute to elevation of both pH and PCr/ATP in this study.

5.4.3 Possible effects of sedation

Anaesthetising patients with propofol and midazolam sedation might have influenced these findings in TBI patients (Hypothesis 4, **Figure 5.7**). Powerful sedatives such as pentobarbitone (pentobarbital) (Nilsson and Siesjö, 1974) and high doses of diethyl ether, phenobarbital and sodium thiopentone (Nilsson and Siesjö, 1970) increased cerebral PCr in rodents (assayed biochemically after extraction, not MRS). Conversely, light sedatives and analgesics had no effect on rat brain PCr concentration, and no sedative/anaesthetic agents (at any concentration) influenced cerebral ATP concentration in those studies (Nilsson and Siesjö, 1970, 1974; Sauter and Rudin, 1993). Pentobarbitone also decreased the TCA cycle rate in rats (Sonnay *et al.*, 2017). Brain pH was not reported in those anaesthetic studies. The effects of propofol and midazolam on high-energy phosphates is unknown, but might resemble those of pentobarbitone and sodium thiopentone more than those of light sedation and analgesia. The elevation of PCr/total-mobile-phosphate was equivalent across the TBI outcome groups, so might be due to sedation. However, sedation/anaesthesia would not explain changes in ATP/total-mobile-phosphate (and pH, discussed below), as this decreased more in patients with unfavourable outcome, and all patients were treated essentially the same. Moreover, no changes in ATP were reported in the rodent

sedation studies (Nilsson and Siesjö, 1970, 1974; Sauter and Rudin, 1993), and changes in PCr/ATP and pH were reported in subacute TBI patients, including those mechanically-ventilated (without barbiturates, but presumably sedated) and those self-ventilating (Garnett *et al.*, 2001). Thus, although sedation may have influenced the changes in high energy phosphates that I observed, it is probably less important than the effect of brain injury in accounting for differences in high-energy phosphates and pH in this study. Interestingly, brain PCr/ATP and pH both increased in a ^{31}P MRS study of experimental (sheep) hypothermia (Swain *et al.*, 1991). Although hypothermia was not used in these patients, parallels may exist with TBI if ATP synthesis is faster than its utilisation and unused ATP increasingly transfers its high energy phosphate charge to the PCr store.

5.4.4 Ventilation and alkalosis

Increasing ventilation to lower PaCO₂ can cause brain alkalosis, as shown by ^{31}P MRS in self-hyperventilating healthy volunteers (Friedman *et al.*, 2007). In mechanically-hyperventilated TBI patients, intracranial probes detected *extracellular* alkalosis (Schneider *et al.*, 1998). However, the TBI management protocol in Addenbrooke's NCCU maintains arterial PaCO₂ > 4 kPa, and the mean PaCO₂ of these TBI patients was 4.8 kPa (range 4.3–7.4 kPa), equivalent to that expected in healthy subjects breathing normally. Interestingly, brain pH correlated inversely with arterial pH; apparently driven by arterial PaCO₂ (**Figure 5.2**). Brain alkalosis was absent in my ventilated patients with favourable outcome, who received similar treatment during MRS. Furthermore, brain alkalosis has been reported in TBI patients' white matter in both self-ventilating and mechanically-ventilated TBI patients sub-acutely post-injury (Garnett *et al.*, 2001).

5.4.5 Metabolic derangement in radiologically normal-appearing brain

When I excluded voxels with $\geq 5\%$ radiological injury, the pattern of elevated PCr/ATP and elevated pH persisted (**Figure 5.5**), suggesting diffuse metabolic derangement throughout the traumatised brain. The difference in brain pH between all TBI patients and healthy controls was narrowly lost statistically, attributable to lower 'n' and the absence of change in patients with a favourable outcome 'diluting' the effect seen in patients with unfavourable outcome. In a ^1H MRS TBI study, six months post-TBI, the marker of neuronal integrity and density NAA/Cr was lower, and the cell turnover marker Cho/Cr higher in radiologically-normal-appearing brain, with the magnitude of change predicting patient outcome (Garnett *et al.*, 2000). Similar ^1H MRS findings in another study appeared unrelated to abnormalities on conventional MR sequences (Marino *et al.*, 2007). In the chronic phase of TBI, abnormalities were reported using ^1H MRS in radiologically-normal-appearing patients' thalami (Uzan *et al.*, 2003), frontal

cortex (Ricci *et al.*, 1997) and occipito-parietal cortex (Friedman *et al.*, 1998). My ^{31}P MRS findings of early metabolic abnormality in radiologically-normal-appearing brain after major TBI thus concur with previous ^1H MRS reports, supporting the concept that microscopic whole-brain injury following TBI extends beyond macroscopic MRI-visible abnormalities.

5.4.6 ^{31}P MRS and clinical outcome

The relationship between the changes observed in brain ^{31}P MRS biochemistry and patient outcome suggests these changes represent underlying pathophysiology of brain injury, and that ^{31}P MRS may be an early predictor of 6-month outcome after major TBI. Patient outcome may correlate with some aspects of MRI-visible structural injury (Lee *et al.*, 2012), but MRI-visible injury is unreliable alone as a predictor (Coles, 2007) because of microscopic tissue damage without radiologically-identifiable injury (Garnett *et al.*, 2000; Coles, 2007; Marino *et al.*, 2011). ^1H MRS characteristics of microscopic tissue injury have been identified acutely and sub-acutely after injury that correlate with clinical outcome (Marino *et al.*, 2007): recovery of NAA (Signoretti *et al.*, 2008), NAA/Cr in the corpus callosum (Shutter *et al.*, 2006), and NAA/Cr in the brainstem (Carpentier *et al.*, 2006). This study is the first to demonstrate that acute-phase changes measured by ^{31}P MRS relate to clinical outcomes 6 months later. Brain alkalosis only occurred in patients with ultimately unfavourable outcomes. Importantly, this remained true when injured voxels were excluded, suggesting ^{31}P MRS utility in addition to ^1H MRS structural imaging. Of the three patients with unfavourable outcome and severe brain alkalosis (TBI-03, TBI-04, TBI-05), their predicted risks of unfavourable outcome at 6 months were respectively 31 %, 74 % and 86 %, using the CRASH head injury prognosis calculator (**Supplementary Table 5.1**) (Steyerberg *et al.*, 2008), suggesting that patient TBI-03 suffered metabolic injury unapparent to current predictive models. Early warning from ^{31}P MRS measurement of alkalosis that a patient may be heading towards unfavourable outcome will maximise opportunity for intervention to improve outcome. Furthermore, patient TBI-02 *without* pronounced brain alkalosis emerged with favourable (GOS-E 5) outcome, despite CRASH prediction of 90 % risk of unfavourable outcome. Although PCr/ATP did not reliably discriminate between TBI patient outcome groups, ATP/total-mobile-phosphate was lower in patients with unfavourable outcome than patients with favourable outcome. Again, this persisted when radiologically-injured voxel data were excluded (**Figure 5.6**). ^{31}P MRS may thus help early recognition of patients who will emerge better than conventionally predicted. These promising findings merit further, larger studies to confirm these relationships between acute ^{31}P MRS and 6-month outcome, and determine whether the technique might augment existing (non-MRS) outcome prognostication (Steyerberg *et al.*, 2008).

5.4.7 Strengths and limitations

^{31}P comprises 100 % of all naturally-occurring phosphorus atoms, so artificial enrichment is unnecessary for MR, which is non-invasive. Due to technical constraints of *in-vivo* MRS, absolute quantification of concentrations is very difficult to achieve accurately, so the ratio of PCr/ATP was used, enabling reliable comparisons for statistical analysis. For good sensitivity within a practicable scan duration, I used $2.5 \times 2.5 \times 2.5 \text{ cm}^3$ voxels (see **Chapter 4**). The central eight voxels were chosen as they represented a large volume of subjects' brains, whilst avoiding signal contamination from bone, muscle and scalp. Only 17 central eight voxels contained >5 % injury, too few for meaningful subgroup statistical analysis.

In-vivo MRI/MRS of sedated, ventilated patients in the acute phase of secondary brain injury following major TBI is challenging, and ^{31}P MRS, although non-invasive, safe, and not excessive on scan time, is not yet routinely used. The promising results in this modest cohort (13 patients, 10 controls) merit larger studies, including uninjured anaesthetised brain, to elucidate fundamental biochemical abnormalities following major TBI and establish the prognostic power of acute-phase ^{31}P MRS.

5.5 Conclusions

Here I have shown that clinical *in-vivo* ^{31}P MRS reveals significant changes in brain high-energy phosphate metabolism acutely after major TBI, indicating that a change in brain energy state accompanies known changes in brain metabolism (Timofeev *et al.*, 2011). The higher energy-store status (PCr/ATP) found in TBI patients compared to healthy controls is perhaps surprising, given the conventional view of 'energy crisis' in TBI, but appears to be due to both a relative increase in PCr and a relative fall in ATP, within the combined pool of total-mobile-phosphate. Among various hypotheses, upregulation of resident microglia and migratory influx of inflammatory cells with higher PCr/ATP ratio are likely, with possible variation in energy status dependent on cell type and susceptibility to injury. Acute TBI and inflammation are usually regarded as associated with "acidosis" extracellularly (Gupta *et al.*, 2004; Timofeev *et al.*, 2013) and intracellularly in hyper-acute animal TBI models (Mcintosh *et al.*, 1987; Vink *et al.*, 1988b). Acute TBI and inflammation are usually associated with acidosis of the extracellular space in patients' brains (Gupta *et al.*, 2004; Timofeev *et al.*, 2013), and the intracellular compartment in animal models (Mcintosh *et al.*, 1987; Vink *et al.*, 1988b). However, it appears that an intracellular *alkalosis* actually occurs in the acute phase of human TBI, but only in patient who emerge with unfavourable outcome after 6 months, suggesting acute-phase raised intracellular pH is important pathophysiologically in TBI. These changes in PCr/ATP and pH are present in radiologically-normal,

'uninjured' tissue on MR sequences sensitive for injury, suggesting widespread metabolic derangement occurs throughout the brain after major TBI, not just in lesions. Although patient outcome was primarily used to help understand these biochemical changes, brain pH shows potential as an early predictor of patient outcome after major TBI. No patient with a mean brain pH ≥ 7.05 had a favourable outcome. Combining voxel-based ^{31}P MRS brain pH measurement with existing predictive TBI outcome models may improve accuracy. Further study of ^{31}P MRS in TBI is merited to explore its full potential in evaluating brain injury, response to therapy, and how these correlate with outcome.

5.6 Declaration and specific acknowledgements

In-vivo ^{31}P MR spectroscopy sequences were acquired in collaboration with Dr M.O. Mada, diagnostic radiographer and MR physicist. MR Image and MR Spectroscopy co-registration was performed in collaboration with Dr J.L. Yan. Mr M.R. Guilfoyle provided statistical advice. This chapter has been published in the *Journal of Cerebral Blood Flow and Metabolism*, 2020 (Stovell *et al.*, 2020).

5.7 Supplementary Material

Supplementary Table 5.1. CRASH predictions for TBI patients

Subject number	CRASH prediction of unfavourable outcome
TBI-01	42 %
TBI-02	90 %
TBI-03	31 %
TBI-04	74 %
TBI-05	86 %
TBI-06	22 %
TBI-07	39 %
TBI-08	31 %
TBI-09	69 %
TBI-10	83 %
TBI-11	35 %
TBI-12	28 %
TBI-13	46 %

Risk of unfavourable outcome at six months calculated using online head injury prognosis calculator based on data from the CRASH trial (Corticosteroid Randomisation After Significant Head Injury).
<http://www.trialscoordinatingcentre.lshtm.ac.uk/Risk%20calculator/index.html>

Chapter 6

The effect of succinate on brain NADH/NAD⁺ redox state and high energy phosphate metabolism in acute traumatic brain injury

Contents

6.1	Introduction	125
6.2	Methods.....	125
6.2.1	Patient recruitment.....	125
6.2.2	Microdialysis	125
6.2.3	Magnetic resonance spectroscopy	127
6.2.4	Statistical analysis	129
6.3	Results.....	129
6.3.1	Patient demographics	129
6.3.2	Succinate supplementation resulted in an improved (lowered) lactate/pyruvate ratio..	130
6.3.3	³¹ P MRS revealed no difference in PCr/γATP ratio or intracellular pH in cohort overall ..	132
6.3.4	Decrease of Lactate/Pyruvate ratio was associated with an increased PCr/γATP ratio ...	133
6.4	Discussion.....	136
6.4.1	Succinate as a substrate in the brain	136
6.4.2	Effect of succinate on brain extracellular biochemistry after TBI.....	137
6.4.3	Effect of succinate on brain high energy phosphates after TBI.....	138
6.4.4	Strengths and limitations	142
6.5	Conclusions	143
6.6	Declaration and specific acknowledgements	144
6.7	Supplementary material	144

6.1 Introduction

It has recently been shown that succinate delivered by microdialysis to the injured brain lowers the lactate/pyruvate (L/P) ratio, which is understood to reflect an improvement in cellular NADH/NAD⁺ redox state (Williamson *et al.*, 1967; Jalloh *et al.*, 2017). It was suggested that succinate therapy achieves this by supporting mitochondrial TCA cycle function, which in turn can improve brain energy metabolism. However, it has not yet been demonstrated empirically that improved L/P ratio translates to better cellular energetics; and is associated with favourable changes in brain high energy phosphates – adenosine triphosphate (ATP) and its high-energy reserve species phosphocreatine (PCr).

In-vivo ³¹P MRS (see **Chapters 1, 2, 4 and 5**) allows measurement of these high energy phosphates in the living brain. In this study, I measured the ratio of brain PCr/ATP acutely (within the first 10 days following injury) in patients suffering from traumatic brain injury using *in-vivo* ³¹P Magnetic Resonance Spectroscopy (³¹P MRS) after microdialysis delivery of succinate, along with standard microdialysis measurements of extracellular chemistry, to establish if changes in L/P ratio are accompanied by changes in brain high energy phosphate metabolism. Brain intracellular pH was also evaluated using ³¹P MRS as an indicator of core physiology; and the ratios of PCr/total-mobile-phosphate and ATP/total-mobile-phosphate to indicate if any changes in PCr/ATP were primarily driven by changes in PCr or ATP. Total-mobile-phosphate was defined as the combined PCr + γ ATP + Pi signals, as in **Chapter 5**.

6.2 Methods

6.2.1 Patient recruitment

Eight adults (aged ≥ 16 years) who had sustained TBI and required intracranial monitoring, sedation, muscular paralysis, intubation and mechanical ventilation were recruited. Targeted depth of sedation was not changed over the study period. Sedation was achieved with propofol, with or without midazolam. Barbiturates were not used. Electroencephalography and bispectral index were not measured as they are not routinely used in Addenbrooke's NCCU.

6.2.2 Microdialysis

Microdialysis monitoring and succinate delivery were carried out as described in **Chapter 2 (Methods)**, using M Dialysis 71 microdialysis catheters (membrane length 10 mm, nominal molecular weight cut-off 100 kDa) (**Table 6.1**). The catheters were not directed into, nor adjacent to, lesions identified on computerized tomography (CT), e.g. contusions. Catheters were perfused at 0.3 μ L/min with CNS

Perfusion Fluid supplemented with 12 mmol/L disodium 2,3-¹³C₂ succinate for 24 hours before their MRS scans. Succinate perfusion was briefly suspended for MR scanning as the catheters' pump batteries are not MR compatible. The interval between pump disconnection and acquisition of ³¹P MR spectra was ca. ≈15 minutes. Before, during and after succinate perfusion, microdialysis collection vials were analysed hourly for glucose, lactate and pyruvate on a bedside ISCUS analyser. The microdialysis pumps were disconnected immediately before the patients went into the MRI scanner, although the catheters were kept in-situ.

Table 6.1 Patient demography

Patient	Age (years)	Sex	Injury Mechanism	Brain Injury	Admission	Days from	Catheter	Cath
					GCS	TBI	insertion	Latr
SUCC-01	62	M	Presumed assault	ASDH, brain contusions	10	7	R-CAD	Ipsi
SUCC-02	63	F	Fall from height	ASDH, ICH	7	3	R-T	Ipsi
SUCC-03	24	F	RTC	EDH, brain contusions	10	4	R-CAD	Cont
SUCC-04	65	M	RTC	brain contusions	6	6	L-T	Cont
SUCC-05	51	M	RTC	EDH, ICH	3	4	R-T	Ipsi
SUCC-06	42	M	Assault	DAI, early hypoxia*	8	10	L-CAD	Cont
SUCC-07	29	M	Assault	EDH, brain contusions	8	5	L-CAD	Cont
SUCC-08	42	F	RTC	ASDH, brain contusions	3	3	L-T	Ipsi

Catheter insertion denotes side (R/L) and whether via cranial access device (CAD) or tunnelled (T) at time of craniotomy/craniectomy. The catheters were not directed into, nor adjacent to, lesions identified on computerized tomography (CT). Cath Latr indicates whether microdialysis catheter was placed ipsilateral or contralateral to the cerebral hemisphere with greatest injury burden on CT. Patients SUCC-01 and SUCC-03 presented only moderately drowsy but then rapidly deteriorated; requiring sedation, intubation, ventilation and surgery for their TBI followed by a period of intracranial multimodality monitoring and treatment for intracranial hypertension. Patients SUCC-01 and SUCC-06 had persistently high ICP and were scanned as soon as they could tolerate lying flat. *Patient SUCC-06 had suspected hypoxia at the assault scene, but not while in neurocritical care unit. All patients received microdialysis perfusion with succinate and had ³¹P MRS; in one case (H) the ³¹P data were unusable due to low signal-to-noise. *Abbreviations: see table in **Precis**; RTC, road traffic collision; Ipsi, ipsilateral; Cont, contralateral; GCS denotes highest GCS at presentation to emergency services.*

6.2.3 *Magnetic resonance spectroscopy*

³¹P MRS Spectra were acquired using oblique 2-dimensional single slice chemical shift imaging (2D CSI) with 2.5 x 2.5 x 2.5 cm³ voxels, measuring pH, ATP, PCr, Pi and other phosphorus-containing species (see **Chapter 2, Methods**). Frontal voxels supplemented with succinate were compared with a contralateral partner voxel in each patient, exemplified by **Figure 6.1**. The contralateral frontal voxel was chosen as I deemed it the most relevant comparative volume of brain that would accommodate a 2.5 x 2.5 x 2.5 cm³ voxel. Voxels were inspected at time of grid positioning to ensure that they were equivalent on structural MRI sequences and free from significant injury. The microdialysis catheter tip (which contains a gold thread) is seen on CT, and its position is also apparent on MRI. Therefore, voxel grids were positioned around patients' catheters using their most recent CT scans co-registered to their MRI, then checked using susceptibility weighted MR sequences (SWI). ³¹P MRS spectra were filtered with a 200 ms Hanning filter, fitted, and peak areas computed using Siemens Syngo software (see **Chapter 4**). The γ ATP peak was chosen to represent the relative concentration of ATP (see **Chapter 5**). Patients also received standard ¹H clinical MR imaging.

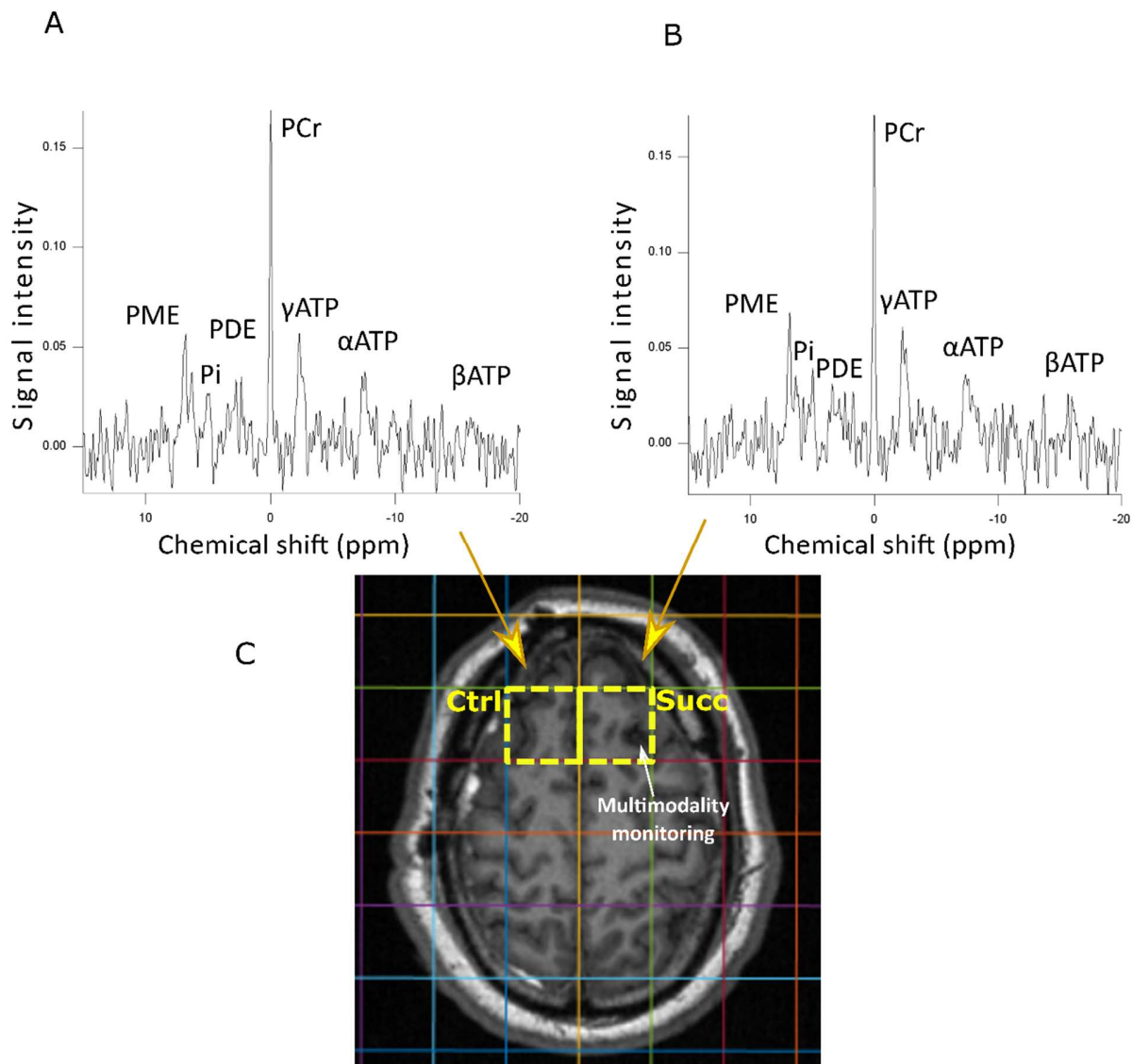


Figure 6.1. Example ^{31}P MRS spectra and voxel grid from a patient suffering from acute major TBI

Spectra (*Panels A and B*) and image (*Panel C*) acquired using a custom head-coil (Pulseteq Ltd) and 3T Siemens scanner. Axial magnetization-prepared rapid gradient-echo (MP-RAGE) MRI scan *Panel C* demonstrates voxel origin within the CSI grid. The patient's left frontal voxel (yellow border, marked 'Succ' for succinate, on the right of the image) contains a microdialysis catheter perfused with 12 mmol/litre disodium 2,3- $^{13}\text{C}_2$ succinate for 24 hours directly before the MR scan (spectrum shown in *Panel B*). The patient's right frontal voxel (yellow border, marked 'Ctrl' for control, on the left of the image) has no microdialysis catheter or supplementation and was used as the paired control (spectrum shown in *Panel A*). Key metabolites are annotated. *Abbreviations: see table in **Precis**.*

6.2.4 Statistical analysis

In this small study I investigated whether substantial differences in high energy phosphate metabolism resulted from delivery of succinate to the brain via microdialysis catheters, based on previous microdialysis studies from our group (12 % change (Jalloh *et al.*, 2017)). The difference in PCr/ γ ATP between ^{31}P MRS voxels perfused with succinate and their paired contralateral voxels was analysed using Wilcoxon signed rank test.

Microdialysis samples were defined as either being from a period of succinate supplementation, or from a preceding/succeeding period of baseline perfusion. The first two hours after starting or finishing succinate supplementation were considered a 'run-in period' or 'washout period' and results excluded, as in previous study of succinate microdialysis (Jalloh *et al.*, 2017). The period of succinate supplementation (mean 20 hours usable ISCUS data and after run-in/wash out exclusion) was compared with baseline perfusion (mean 15 hours usable ISCUS data and after run-in/washout exclusion) using a linear mixed effect model ('*lmer*' in R package *lme4* (Bates *et al.*, 2015)), which considers hourly data points rather than period mean/medians, whilst adjusting for 'clustering' of data, with a random γ -intercept (starting point) for each subject.

Correlation between percent difference in measured L/P ratio, and difference in inter-voxel PCr/ γ ATP was assessed using Spearman's correlation ('*cor.test*' function in R).

All statistical analysis was performed in R (www.r-project.org) and significance (alpha) for all tests set at 0.05.

6.3 Results

6.3.1 Patient demographics

Eight patients suffering from TBI received focal disodium succinate (12 mmol/L) perfusion for 24 hours via a frontal microdialysis catheter (**Table 6.1**) and a preceding/succeeding baseline period of microdialysis with normal CNS perfusion fluid. Of the 8 patients, 7 had *in-vivo* ^{31}P MRS that yielded spectra with acceptable signal-to-noise ratio for analysis. Example scan and spectra are shown in **Figure 6.1**.

6.3.2 Succinate supplementation resulted in an improved (lowered) lactate/pyruvate ratio

Comparing the period of baseline perfusion with the period of succinate perfusion, I found results similar to those of a previous patient cohort, studied by my group (Jalloh et al., 2017) (Table 6.2) (Figure 6.2). Following succinate supplementation, there was a statistically significant (by linear mixed effect model) mean 13 % decrease in L/P ratio ($p < 0.0001$, decrease in 6/8 patients and increase in 2/8), caused by a mean 25 % increase in pyruvate ($p < 0.0001$, increase in 7/8 patients and decrease in 1/8). There was no statistically significant change in lactate, with mean increase 6 % ($p = 0.08$, increase in 6/8 patients and decrease in 2/8) or glucose, with mean decrease 5 % ($p = 0.1$, decrease in 4/8 patients and increase in 2/8). In patients SUCC-01, SUCC-02 and SUCC-08 the decrease in L/P ratio was considerable (> 26 %), furthermore 2 of these patients (SUCC-02 and SUCC-08) had high baseline L/P ratios of 45.1 and 29 respectively. Brain tissue oxygen (PbtO₂) data were available for 4 patients, whose levels were all 25 mmHg or above, thus none of these 4 individuals suffered from brain hypoxia during the study. Three patients did not have PbtO₂ monitoring, and one patient's PbtO₂ data was not available. More detailed PbtO₂, intracranial pressure (ICP) and cerebral perfusion pressure (CPP) data can be found in Table 6.3.

Table 6.2. Results of microdialysis measured by ISCUS

Metabolite	Condition	SUCC-01	SUCC-02	SUCC-03	SUCC-04	SUCC-05	SUCC-06	SUCC-07	SUCC-08	Mean change
L/P ratio	Baseline	16.3	45.1	16.0	20.2	12.5	26.4	18.1	29.0	-13 %
	Succinate	11.5	28.4	14.1	18.4	11.8	26.5	20.6	21.4	
	% change	-29.6	-37.1	-12.1	-8.8	-5.2	+0.6	+14.0	-26.4	
Glucose (mM)	Baseline	2.7	1.3	1.9	2.6	3.4	1.5	1.6	1.5	-5 %
	Succinate	3.2	1.1	1.8	1.1	3.7	1.9	1.3	1.7	
	% change	+16.6	+11.3	-6.1	-58.1	+7.4	+23.9	-20.5	+10.3	
Lactate (mM)	Baseline	4.0	3.1	1.7	6.3	1.2	6.5	1.6	2.0	+6 %
	Succinate	3.6	3.2	1.8	2.9	1.4	7.1	2.2	2.7	
	% change	-9.9	+2.1	+6.2	-53.4	+13.0	+8.9	+41.6	+36.7	
Pyruvate (μM)	Baseline	244	70	105	313	99	247	81	76	+26 %
	Succinate	313	112	133	170	118	268	108	134	
	% change	+28.4	+60.9	+26.4	-45.6	+19.2	+8.1	+33.8	+75.9	

Mean results of microdialysis samples analysed with ISCUS during baseline perfusion with normal perfusion fluid or a period with succinate supplemented perfusion fluid. L/P ratio: lactate/pyruvate ratio, mM: millimole/litre, μM: micromole/litre. *p-values* from analysis of pooled results using the package *lmer* in R, (significance < 0.05 denoted by bold font) - see **Methods** subsection Statistical analysis for further details.

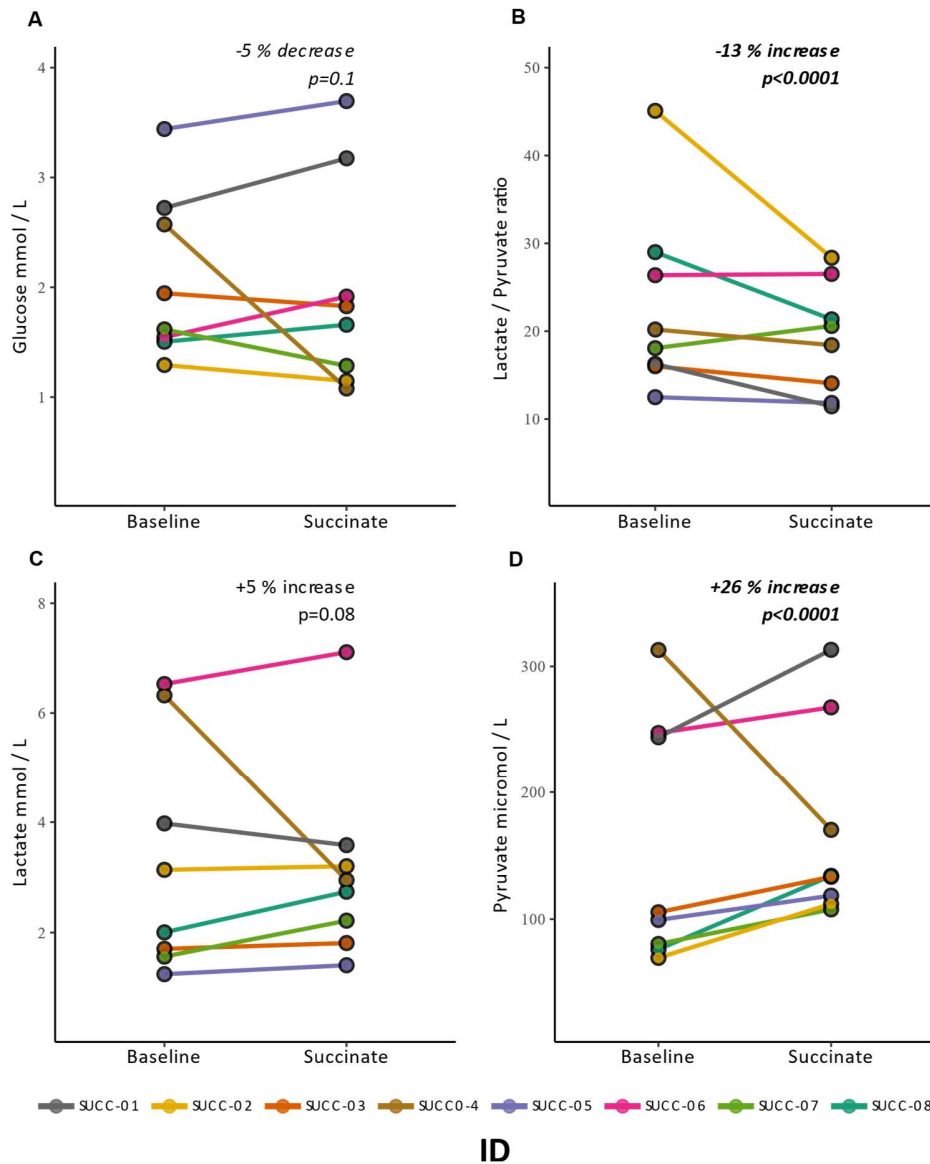


Figure 6.2. Line-plots of microdialysis measurements measured by bedside ISCUS.

Panel A glucose, *Panel B* lactate/pyruvate ratio (L/P ratio), *Panel C* lactate, *Panel D* pyruvate. Individual subject means from a period of 12 mmol/L succinate perfusion (24 hours) and preceding/succeeding baseline perfusion (24 hours) are represented. There was a statistically significant 13 % (mean of subject means) fall in lactate/pyruvate ratio ($p < 0.0001$) and a statistically significant 26 % (mean of subject means) rise in pyruvate ($p < 0.0001$) analysed using *lmer* in R (statistically significant results in bold italics).

Table 6.3. Patient mean multimodality monitoring results from baseline and supplementation period of microdialysis perfusion

Modality	Condition	SUCC-01	SUCC-02	SUCC-03	SUCC-04	SUCC-05	SUCC-06	SUCC-07	SUCC-08
ICP (mmHg)	Baseline period	9	12	14	10	14	18	19	12
	Succinate Supp.	9	13	15	10	16	19	15	14
CPP (mmHg)	Baseline period	81	76	75	77	74	75	74	75
	Succinate Supp.	83	71	73	78	82	75	74	80
PbtO ₂ (mmHg)	Baseline period	29	NA	NA	31	NA	37	25	34
	Succinate Supp.	28	NA	NA	27	NA	56	NA	31

Mean results of intracranial pressure (ICP), cerebral perfusion pressure (CPP) and brain tissue oxygen tension (PbtO₂) during baseline perfusion with normal CNS perfusion fluid and 12 mmol/L 2,3-¹³C₂ succinate perfusion (Succinate supp.), recorded using ICM+. *Abbreviations: see table in **Precis**.*

6.3.3 ³¹P MRS revealed no difference in PCr/γATP ratio or intracellular pH in cohort overall

The frontal voxels supplemented with succinate by their microdialysis catheters were compared with their adjacent contralateral equivalent frontal voxels that did not receive succinate supplementation (“partner” voxel) (Table 6.4). I did not detect a statistically significant overall difference in PCr/γATP ratio (Figure 6.3) between the voxels that received focal succinate perfusion and their contralateral equivalent frontal ‘partner’ voxel (Wilcoxon signed rank test, $p > 0.5$). While the group level did not show an overall significant difference, some of these patients had a markedly higher PCr/γATP levels following succinate supplementation, and demonstrated a statistically significant relationship between percentage increase in PCr/γATP and percentage decrease in extracellular L/P ratio (see below). Analysis of PCr/total-mobile-phosphate and γATP/total-mobile-phosphate similarly did not find a statistically significant difference in the cohort overall, but revealed that in those select patients, the apparent change in PCr/γATP ratio, and its correlation with change in L/P ratio, was predominantly due to a change in PCr rather than γATP (Figure 6.3 and 6.4). ³¹P MRS revealed no statistically significant difference in brain intracellular pH in the cohort overall as a result of succinate supplementation via microdialysis vs. contralateral ‘partner’ voxel without succinate (Wilcoxon signed rank test, $p = 1$) (Supplementary Table 6.1).

Table 6.4. PCr/ γ ATP ratio results from ^{31}P MRS analysis of frontal voxels supplemented with succinate, compared simultaneously to their contralateral unsupplemented voxels

Subject I.D.	PCr/ γ ATP ratio		Percentage difference
	Unsupplemented voxel	Succinate supplemented voxel	
SUCC-01	0.871	1.528	+ 75.5 %
SUCC-02	1.089	1.270	+ 16.6 %
SUCC-03	1.086	1.136	+ 4.6 %
SUCC-04	1.050	1.082	+ 3.1 %
SUCC-05	1.134	1.000	- 11.9%
SUCC-06	1.293	1.135	- 12.2 %
SUCC-07	0.967	0.963	- 0.4 %

^{31}P MRS measurements of PCr/ γ ATP in the frontal voxels of the seven patients who received succinate supplementation. Each voxel that received succinate was matched with a partner contralateral frontal voxel that did not receive supplementation, within the same patient. The difference in PCr/ γ ATP between supplemented and matched unsupplemented voxels was not statistically significantly different (two-tailed Wilcoxon signed rank test $p = 0.58$). An eighth patient (SUCC-08) also underwent ^{31}P MRS but yielded no useable data due to low signal-to-noise. *Abbreviations: see table in **Precis**.*

6.3.4 Decrease of Lactate/Pyruvate ratio was associated with an increased PCr/ γ ATP ratio

There was an inverse relationship between the improvement (lowering) in L/P ratio following succinate supplementation with the increase in PCr/ γ ATP, comparing the voxel receiving the succinate and its 'control' contralateral partner voxel that did not receive succinate, when these changes in PCr/ATP and L/P ratio were expressed as percentages (**Figure 6.4**) (Spearman's rank correlation, $\rho = -0.86$, $p = 0.024$). There was no statistically significant relationship between percentage change in extracellular L/P ratio and either percentage change in brain intracellular pH or absolute change in brain intracellular pH.

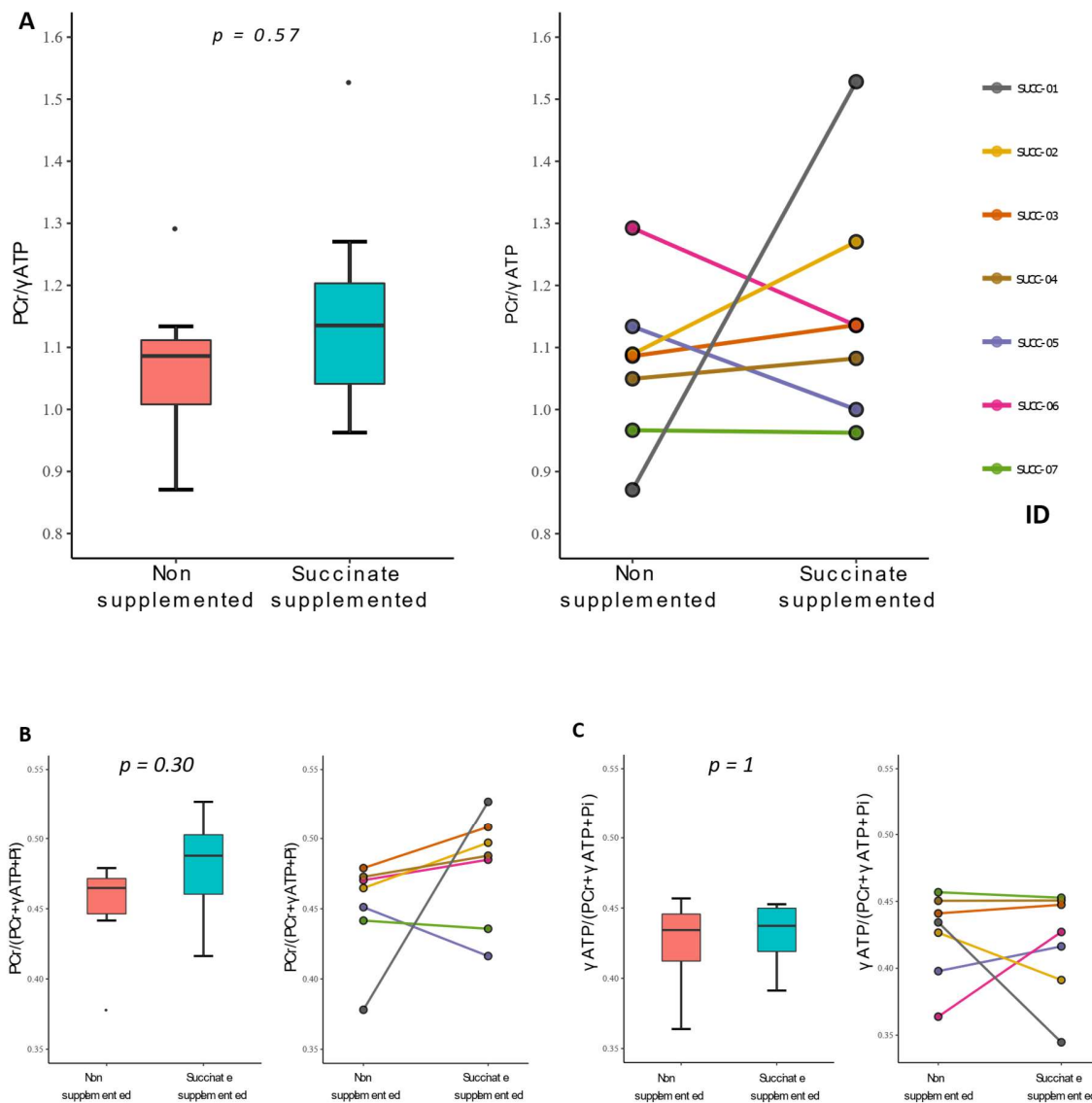


Figure 6.3 Boxplot and lineplot of difference in PCr/ATP between succinate supplemented and control voxels

Boxplots and lineplots of ^{31}P MRS *Panel A*: PCr/ γ ATP, *Panel B*: PCr/total-mobile-phosphate, and *Panel C*: γ ATP/total-mobile-phosphate; of frontal voxels that received microdialysis delivery of 12 mmol/L succinate and their corresponding partner (contralateral) frontal voxels that did not receive succinate. There were no significant differences in PCr/ γ ATP between succinate supplemented voxels and their contralateral voxel without succinate (paired comparison using Wilcoxon signed rank test, p-values in figure). The two voxels were analysed within the same MRI scan, in each patient. *Abbreviations: see table in Precis.*

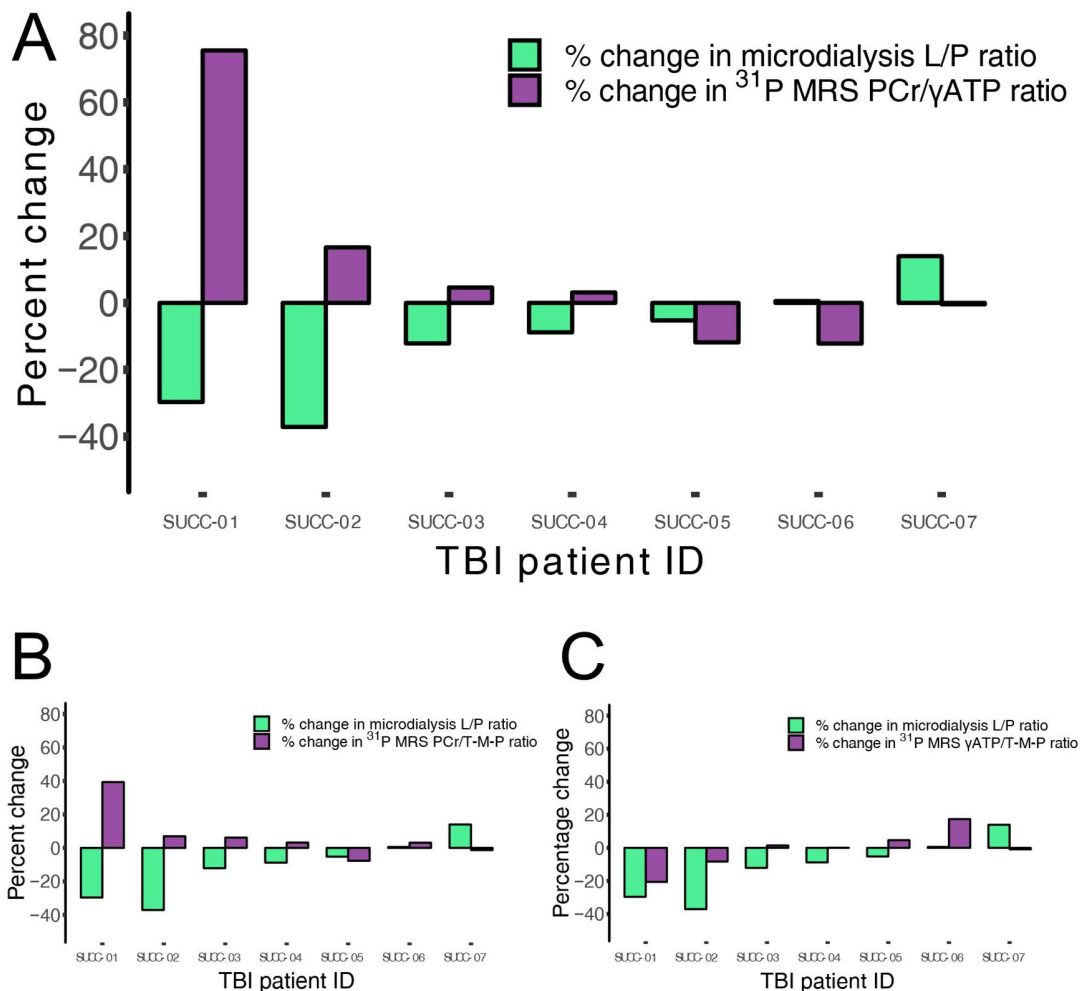


Figure 6.4. Bar charts showing relationships between changes in microdialysate L/P ratio and different ^{31}P MR spectroscopy ratios

Panel A: A negative correlation existed between percent change in cerebral microdialysate L/P ratio (green bars) and percent difference in ^{31}P MRS PCr/ATP ratio (purple bars) with succinate perfusion (Spearman's $\rho = -0.86$, $p = 0.024$): a greater percentage reduction in the L/P ratio correlates with a greater percentage increase in the PCr/ATP ratio.

Panel B: A negative correlation existed between percent change in cerebral microdialysate L/P ratio (green bars) and percent difference in ^{31}P MRS PCr/total-mobile-phosphate ratio (purple bars) with succinate perfusion (Spearman's $\rho = -0.86$, $p = 0.024$).

Panel C: An inverse relationship appeared to exist between percent change in cerebral microdialysate L/P ratio (green bars) and percent difference in ^{31}P MRS ATP/total-mobile-phosphate ratio (purple bars) with succinate perfusion, but this did not reach statistical significance (Spearman's $\rho = -0.57$, $p = 0.2$).

Percent change in microdialysate L/P ratio refers to difference during succinate perfusion compared with a baseline unsupplemented perfusion period in the same catheter. Percent difference in ^{31}P MRS ratios are the difference between a voxel that had received succinate perfusion via microdialysis catheter, and their 'partner' contralateral control voxel, without succinate. The findings of *Panel B* and *Panel C* suggest that the changes in *Panel A* (PCr/ATP) are predominantly driven by changes in PCr, rather than changes in ATP. **Abbreviations:** see table in *Precis*; **T-M-P:** total-mobile-phosphate.

6.4 Discussion

This is the first study of human brain metabolism in TBI that combines microdialysis and *in-vivo* ^{31}P MRS; comparing the effect of succinate supplementation on brain metabolism using both modalities, affirming that succinate improves NADH/NAD⁺ redox state (decreases L/P ratio) in the traumatised human brain. Whilst an overall statistically significant change in high energy phosphates (PCr/ATP) was not detected after succinate supplementation, those individuals who had the greatest improvement (decrease) in L/P ratio after succinate perfusion – i.e. those suffering from mitochondrial dysfunction – had considerable increases in their PCr/ATP ratio measured using ^{31}P MRS.

I suggest that the intrinsic heterogeneity of TBI may have been a factor leading to the absence of a clear-cut overall difference in PCr/ATP between a succinate-supplemented voxel and its paired contralateral unsupplemented voxel when measured simultaneously by ^{31}P MRS in this small cohort of patients. Microdialysis measurements, contrastingly, were performed within-voxel over a course of time and showed significant differences across the cohort between an unsupplemented baseline perfusion period and a succinate-supplemented perfusion period – notably improvement (lowering) of L/P ratio. Moreover, the finding of a significant correlation within the cohort between percentage decrease in L/P ratio and percentage increase in PCr/ATP reveals a link between cell NADH/NAD⁺ redox and high energy phosphate status; and suggests that succinate supplementation can increase cerebral high-energy phosphate status. This extends previous evidence that succinate delivered by microdialysis is metabolised by the TCA cycle (Jalloh *et al.*, 2017).

6.4.1 Succinate as a substrate in the brain

The oxidation of succinate to fumarate is unique as it is both a key step of the TCA cycle and the first step of the electron transport chain for the conversion of flavin adenine dinucleotide (FAD) to its reduced form FADH₂. It is catalysed by succinate dehydrogenase – which is Complex II of the electron transport chain. There is evidence that Complex II is less susceptible to injury than Complex I which oxidises nicotinamide adenine dinucleotide (NADH), so succinate has been proposed as a substrate that may support the TCA cycle and ATP generation by oxidative phosphorylation in stressed cells when mitochondrial function is impaired (Protti and Singer, 2006; Jalloh *et al.*, 2017).

Succinate is unlikely to benefit brain metabolism in cases of hypoxia or ischaemia. Without oxygen, the mitochondrial electron transport chain cannot function properly. In experimental ischaemia, succinate dehydrogenase (electron transport chain complex II and part of the TCA cycle) was reported to run ‘backwards’, building up succinate and reverse electron transport to complex I (Chouchani *et al.*, 2014).

In that study, reperfusion produced a surge in reactive oxygen species (via complex I) and cell death. The present study did not involve ischaemia–reperfusion. We have previously suggested that using succinate to support mitochondrial metabolism should be performed in the presence of adequate oxygenation, not during ischaemia–reperfusion (Jalloh *et al.*, 2017). None of the four patients in the present study with available Licox PbtO₂ data suffered from brain tissue hypoxia during the monitoring period, therefore we think it unlikely that this affected the other four patients in our study, as they received similar critical care management which specifically aims to avoid this. Furthermore, the ISCUS data suggests none of the 8 patients studied were ischaemic as microdialysate glucose levels were above 1 mmol/L in each case.

6.4.2 Effect of succinate on brain extracellular biochemistry after TBI

Previously it has been shown that 2,3-¹³C₂ succinate delivered via microdialysis enters the TCA cycle of the traumatised brain, demonstrated by the detection of downstream ¹³C labelled metabolites in the collected microdialysates using high-resolution ¹³C NMR (Jalloh *et al.*, 2017). Succinate uptake into cells can occur via the SLC13 family of Na⁺-coupled di-carboxylate and tri-carboxylate transporters (Kekuda *et al.*, 1999; Pajor, 1999; Schlessinger *et al.*, 2014). SLC13 occur widely, including in brain astrocytes and neurons where succinate uptake and metabolism were also shown using radiolabelling (Lamp *et al.*, 2011; Bergeron *et al.*, 2013; Pajor, 2014). Additionally, nonspecific uptake might occur in any cells with increased plasma membrane permeability. Appearance of metabolites with characteristic ¹³C NMR doublet signals clearly indicated uptake and mitochondrial metabolism of 2,3-¹³C₂ succinate (Jalloh *et al.*, 2017). The doubly ¹³C-labelled metabolites were unambiguous evidence the 2,3-¹³C₂ succinate molecules crossed from the perfusate into the brain extracellular space, entered the cells and were metabolised, exported into the extracellular fluid and recovered by the microdialysis catheter (Jalloh *et al.*, 2017). In that study, succinate potentiated several aspects of brain biochemistry: it significantly lowered extracellular L/P ratio, glutamate and glucose, trended towards elevating pyruvate, but did not significantly change the concentration of extracellular lactate (Jalloh *et al.*, 2017). Based on this, we proposed that succinate increases TCA cycle activity, thereby improving brain NADH/NAD⁺ redox state which aids glucose utilisation leading to increased pyruvate, and draws glutamate into the mitochondria to feed the TCA cycle.

The results from the present study support my group's previous findings and conclusions (Jalloh *et al.*, 2017) as again, succinate supplementation reduced extracellular L/P ratio and trended towards reducing brain extracellular glucose levels. I believe that these patients, especially those in which succinate

administration was associated with greatest decrease in L/P ratio (and in general, had the highest L/P ratio prior to supplementation) are suffering from more pronounced mitochondrial dysfunction, whereas those patients that demonstrate only modest changes in L/P ratio may not be so afflicted by disrupted mitochondria, but instead by the other pathophysiological processes of TBI. More recent cell culture studies of succinate supplementation to stressed mixed glia show similar findings of increased pyruvate and lowering of tissue L/P ratio after succinate administration in a model of mitochondrial dysfunction (Giorgi-Coll *et al.*, 2017). Through increasing TCA cycle activity, glycolysis may also be upregulated which would lead to an increase in pyruvate, a common condition in TBI patients (Bergsneider *et al.*, 1997; O'Connell *et al.*, 2005).

Another pathway by which succinate may in theory influence brain cells is via interaction with the succinate receptor (SUCNR1, also termed GPR91) which occurs in various tissues and cell types, including microglia, astrocytes and neurons (Gilissen *et al.*, 2016). SUCNR1 belongs to the G protein-coupled receptors (GPCRs) family, the largest group of human proteins involved in signal transduction across biological membranes (Fredriksson *et al.*, 2003). SUCNR1 shows pleiotropic effects (Gilissen *et al.*, 2016). Originally an “orphan” receptor with its actual ligand(s) unclear, the succinate-binding capability of GPR91 was subsequently discovered, although the actual range of ligands, their binding sites and their actions are still poorly understood. Due to the complexity of cell signalling, it is (as yet) difficult to categorise SUCNR1 (GPR91) roles. As one example, succinate binding to GPR91 has been reported to enhance post-hypoxia-ischaemia vascularization and reduce infarct size in a murine model of new-born hypoxia-ischaemia brain injury (Hamel *et al.*, 2014).

6.4.3 Effect of succinate on brain high energy phosphates after TBI

ATP is the universal molecule of chemical energy in the human body but PCr is only found in tissues that require energy in bursts, such as muscle and brain. PCr is considered a temporal “buffer” for ATP in the brain as it can donate its phosphate group to ADP via the action of creatine kinase. This rapidly regenerates ATP to allow continued cellular processes during periods of demand. PCr also diffuses more readily than ATP so acts as a spatial “buffer” for high energy phosphates, shuttling them from where they are generated in the mitochondria to where they are used in the cell cytoplasm and cell membrane (Wallimann *et al.*, 2011). The general perception in phosphorus biochemistry is that when ATP synthesis is running normally, the PCr store is well-stocked; when ATP synthesis is struggling to meet demand, the PCr store runs down. Absolute quantification of ³¹P species' concentrations are difficult to achieve

accurately with *in-vivo* ^{31}P MRS, whereas PCr/ATP ratio is readily measurable, facilitating inter-comparisons within subjects and between subjects.

I found that succinate supplementation was associated with a considerable increase in PCr/ATP in some of the TBI patients, but this did not occur across the group so did not translate to a change in mean PCr/ATP overall in this modest-sized cohort. I suggest that the intrinsic heterogeneity of TBI may have been a factor leading to the absence of a clear-cut overall difference in PCr/ATP between a succinate-supplemented voxel and its paired contralateral unsupplemented voxel when measured simultaneously by ^{31}P MRS in this small cohort of patients. Microdialysis measurements, contrastingly, were performed within-voxel over a course of time and showed significant differences across the cohort between an unsupplemented baseline perfusion period and a succinate-supplemented perfusion period – notably improvement (lowering) of L/P ratio. Moreover, the finding of a significant correlation within the cohort between percentage decrease in L/P ratio and percentage increase in PCr/ATP suggests that succinate supplementation can increase cerebral high-energy phosphate status. This extends previous evidence that succinate delivered by microdialysis is metabolised by the TCA cycle (Jalloh *et al.*, 2017). Many different pathophysiological processes contribute to secondary brain injury after TBI; including raised intracranial pressure, cerebral hypoperfusion, hypoxia, hypoglycaemia, neuroinflammation as well as mitochondrial dysfunction (Maas *et al.*, 2017). Conceivably, those patients whose PCr/ATP ratio was less responsive to succinate either suffered from more than one of these complex overlapping pathophysiological processes, or did not suffer from significant mitochondrial dysfunction, or suffered from mitochondrial dysfunction refractory to succinate supplementation. In those patients whose mitochondrial dysfunction is responsive to succinate, the metabolism of additional succinate to fumarate would generate FADH_2 , driving ATP generation via Complex II. Extra ATP produced (if not used) would be converted to the readily-mobilised store PCr, thereby elevating the PCr/ATP ratio (**Figure 6.5**). Importantly, those patients who did not respond to succinate at least had no significant deterioration in their metabolic profile.

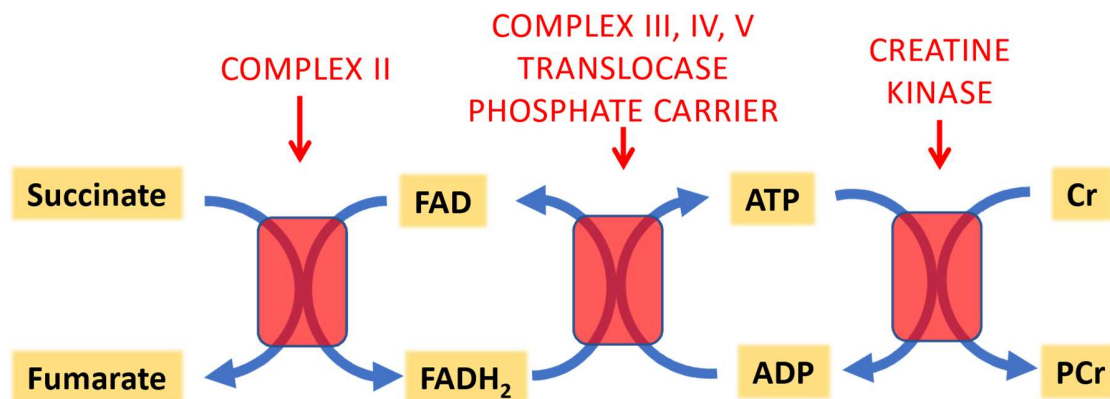


Figure 6.5. Simplified schematic showing potential mechanism of succinate's effect on PCr/ATP

Succinate misses out Complex I of the mitochondrial electron transport chain. Succinate's oxidation to fumarate by Complex II (succinate dehydrogenase) reduces FAD to FADH₂ – which is oxidized back to FAD – releasing electrons that pass through a chain of oxidation/reduction reactions, complex II to CoQ, complex III, Cytochrome C and complex IV with molecular oxygen as terminal electron acceptor, culminating in conversion of oxygen to water, while complexes III and IV export protons across the mitochondrial inner membrane creating a proton electrochemical potential gradient, driving ATP synthesis at complex V (ATP synthase), converting ADP to ATP. In the mitochondrial intermembrane space ATP donates its high energy phosphate to creatine, producing ADP and PCr, which diffuses into the cell cytoplasm for use by cellular machinery. *Abbreviations: see table in **Precis**.*

An elevated L/P ratio has been shown to be independently associated with poor outcome after TBI (Timofeev *et al.*, 2011), but it is not clear if this is because of brain energy failure. The extracellular L/P ratio is thought to reflect the L/P ratio in the cytoplasm – itself in equilibrium with cytoplasmic NADH/NAD⁺ (Williamson *et al.*, 1967). Lactate and NADH accumulate when generated by glycolysis; and also by the TCA cycle if the NADH cannot be used by Complex I of the electron transport chain – the principle mechanism for cellular generation of ATP. The strong association between percentage change in L/P ratio and percentage change in PCr/ATP in our small patient group (Spearman's $\rho = -0.86$, $p = 0.024$) (**Fig. 3a**) supports the proposal that L/P ratio is linked to downstream energy metabolism, as well as being a representative of NADH/NAD⁺ redox state. This is the first time that tissue NADH/NAD⁺ redox, as reflected by the extracellular L/P ratio, has been shown to be linked to tissue high energy phosphates (PCr and ATP) in the human brain.

The apparent change in PCr/ATP ratio in select patients appears to be driven primarily by an increase in PCr (PCr/total-mobile-phosphate), rather than by a change in ATP (ATP/total-mobile-phosphate) (**Figure 6.3**). However, an increase in cerebral PCr first requires increased production of ATP, as this is PCr's only precursor (**Figure 6.5**). It is possible that succinate metabolism supports ATP production to such an extent that the surplus phosphate energy potential is stored as PCr, thereby increasing cerebral PCr/ATP and PCr/total-phosphate ratios. Alternatively, there may be a disruption of patients' PCr-ATP shuttles, so that additional ATP generated is converted directly to PCr where it becomes 'trapped'. A potential mechanism for this is anaesthesia: short acting barbiturates and high doses of diethyl ether, phenobarbital and sodium thiopentone have been shown to increase PCr in sedated rats (Nilsson and Siesjö, 1970, 1971). My patients were deeply sedated with propofol and midazolam, which could conceivably have a similar effect causing shuttling of high energy phosphate charge into an unused PCr pool. These hypotheses are supported by the association between percentage improvement (decrease) in L/P ratio and percentage difference in PCr/total-mobile-phosphate ratio (**Figure 6.4**).

It is possible that elevated PCr seen in these patients (high PCr/ATP and PCr/total-mobile-phosphate) is due to a proinflammatory effect of succinate, as PCr/ATP has been shown to be elevated in activated monocytes in human blood (Loike *et al.*, 1984). Macrophages activated by lipopolysaccharide accumulate succinate and release it into the extracellular space (Littlewood-Evans *et al.*, 2016), which enhances Interleukin-1 beta (IL-1 β) production, a known pro-inflammatory mediator (Tannahill *et al.*, 2013; Peruzzotti-Jametti *et al.*, 2018). Thus, succinate may activate local cerebral inflammation, elevating the PCr/ATP ratio. However, this does not agree with the changes in inflammation is most commonly associated with an increase in L/P ratio, rather than the decrease found in this study (**Figure 6.4**).

The intracellular pH measured by ^{31}P MRS in this study did not correlate with succinate supplementation in the group as a whole. As this pH is intracellular, it is possible that these values might not necessarily closely reflect the L/P ratio change measured extracellularly. Intracellular pH has been shown by ^{31}P MRS in rat TBI models to decrease hyper-acutely following injury, followed by a period of intracellular alkalosis (Mcintosh *et al.*, 1987; Vink *et al.*, 1987). The study of intracellular pH changes in the acute phase of injury in **Chapter 5**, and a ^{31}P MRS study of recovering patients in the subacute/chronic phase of TBI found (intracellular) alkalosis of patients' white matter (Garnett *et al.*, 2001). The pH changes associated with succinate in Patients SUCC-01 and SUCC-07 could conceivably be indicating a return to more normal physiology, but this would need to be corroborated with further study. It is also possible

that the changes in pH reported in **Chapter 5** represent a degree of cell injury unrelated to energy metabolism.

I chose to administer succinate through microdialysis catheters because of my group's experience using this technique, and because it directly delivers succinate focally to the brain – avoiding issues with the blood-brain barrier or tissue hypoperfusion seen in the aftermath of TBI. However, the diffusion of succinate from a microdialysis catheter may have been insufficient to influence the whole of the chosen ^{31}P MRS voxel's metabolism. Thus, the effect of succinate will be diluted by the metabolism of unsupplemented tissue within the same voxel. The low gyromagnetic ratio of ^{31}P compared to ^1H (de Graaf, 2007) meant that the voxel size could not decrease any further than $2.5 \times 2.5 \times 2.5 \text{ cm}^3$ whilst maintaining an acceptable signal-to-noise ratio within a practical scan duration (35 minutes). Intravenous supplementation of succinate is an alternative delivery method, but needs to be further studied and compared with microdialysis brain delivery.

6.4.4 Strengths and limitations

Focal administration of succinate allows direct comparison between a region of succinate supplementation and an unsupplemented region in each patient's brain. However, a caveat to the correlation of L/P ratio and PCr/ATP is that changes in L/P ratio are related to baseline (unsupplemented) perfusion results from the same region of brain, whereas differences in PCr/ γ ATP are relative to an equivalent, paired frontal voxel that did not receive supplementation, scanned simultaneously. Due to clinical considerations, an acute-phase ventilated, sedated TBI patient is not scanned on consecutive days. It should be noted that the microdialysis pumps were disconnected immediately before entering the MR scanner as the pump batteries are non-MR-compliant. As microdialysis delivery of substrates occurs relatively slowly, I consider it unlikely the *ca.* 15-minute interval between pump disconnection and ^{31}P MRS acquisition diminished the effect of perfused succinate.

This study was designed to be able to detect sizeable changes in PCr/ γ ATP after microdialysis delivery of succinate to the injured brain. The apparent 10.8 % overall rise in PCr/ γ ATP in this cohort did not reach statistical significance but might achieve this in future with a larger number of patients. Nevertheless, I have demonstrated a significant correlation between changes observed on focal succinate perfusion, namely percentage decrease in extracellular L/P ratio, and percentage increase in brain (intracellular) PCr/ATP.

Sedation is an important part of patient management in neurocritical care during the acute phase of major traumatic brain injury. Sedation's effects include reduction in cerebral metabolic demand and reduction in intracranial pressure (Oddo *et al.*, 2016). Whereas I did not measure individual patients' depth of sedation, all were sedated sufficiently for endotracheal intubation, mechanical ventilation and control of intracranial hypertension. No changes were made to patients' targeted depth of sedation during the study period. As each patient acted as their own control the effects of sedation would be equivalent across all ^{31}P MRS voxels in that individual, and during their baseline and supplementation periods of microdialysis perfusion. Variability in time interval between patient injury and scan was due to some patients being initially less stable – so that they could not tolerate lying flat any sooner, despite optimal medical management. Thus, as all patients still required full sedation, they can be considered to be in the 'acute phase' of TBI, and any difference in brain metabolism due to interval from injury accounted for by each patient acting as their own internal control.

Due to the heterogeneity of TBI, it is difficult from the outset to anticipate which patients will suffer from mitochondrial dysfunction – the group I postulate will benefit most greatly from succinate supplementation. Such individuals can be identified by a combination of multimodality monitoring and advanced scanning technologies. I propose that a larger study is warranted, including intravenous infusion of succinate to address any concerns of limited diffusion from microdialysis catheters, and performing ^{31}P MRS measurement before and after succinate perfusion. For reasons mentioned above, an essential prerequisite for employment of succinate is the existence of adequate oxygenation and the absence of hypoxia or ischaemia.

6.5 Conclusions

Here, I have shown the effect of succinate delivery via microdialysis on the traumatised human brain's NADH/NAD⁺ redox state (microdialysate L/P ratio, using an ISCUS bedside analyser) and brain high energy phosphate metabolism (PCr/ATP ratio, using ^{31}P MRS of frontal voxels). I affirmed my group's previous findings that succinate improves (lowers) brain microdialysate L/P ratio, but have shown, for the first time, that this is associated with an increase in brain high energy phosphate ratio (PCr/ATP). This supports the interpretation that L/P ratio is linked to brain energy state, and suggests that succinate has potential to support brain energy metabolism in patients who are suffering from mitochondrial dysfunction.

6.6 Declaration and specific acknowledgements

In-vivo ^{31}P MR spectroscopy sequences were acquired in collaboration with Dr M.O. Mada, diagnostic radiographer and MR physicist. MR Image and MR Spectroscopy co-registration was performed in collaboration with Dr J.L. Yan. Mr M.R. Guilfoyle provided statistical advice. This chapter has been published in *Scientific Reports*, 2018 (Stovell *et al.*, 2018).

6.7 Supplementary material

Supplementary Table 6.1. Intracellular pH results from ^{31}P MRS analysis of frontal voxels supplemented with succinate, compared simultaneously to their contralateral unsupplemented voxels

Subject I.D.	pH Succ.	pH Unsupp.
SUCC-01	6.92	7.17
SUCC-02	7.06	7.03
SUCC-03	7.11	7.03
SUCC-04	7.01	6.98
SUCC-05	7.11	7.05
SUCC-06	7.17	7.18
SUCC-07	6.95	7.09
Wilcoxon rank	$p = 1$	

^{31}P MRS measurements of pH in the frontal voxels of the seven patients who received succinate supplementation. Each voxel that received succinate was matched to a partner contralateral frontal voxel that did not receive supplementation, within the same patient. The difference in pH between supplemented and matched non-supplemented voxels was not statistically significantly different (two-tailed Wilcoxon signed rank test, $p = 1$). *Abbreviations: Succ., succinate supplemented voxel; Unsupp., contralateral unsupplemented voxel.*

Chapter 7

The diffusion of small molecules delivered focally to the human brain via microdialysis catheters

Contents

7.1	Introduction	146
7.2	Methods.....	147
7.2.1	Patient recruitment.....	147
7.2.2	Microdialysis	147
7.2.3	Magnetic resonance imaging.....	148
7.2.4	Statistical analysis	149
7.3	Results.....	150
7.3.1	Patient demographics	150
7.3.2	Pattern of diffusion	150
7.3.3	Diffusion coefficient and maximum diffusion distance	150
7.3.4	Estimation of relaxivity and concentration.....	155
7.3.5	Effect on brain chemistry.....	156
7.4	Discussion.....	158
7.4.1	Summary	158
7.4.2	Diffusion of small molecules in the brain.....	158
7.4.3	Diffusion coefficient.....	160
7.4.4	Relaxivity and concentration	160
7.4.5	Effect of gadolinium on extracellular chemistry.....	162

7.4.6	Strengths, limitations and further work	163
7.5	Conclusions	164
7.6	Declaration and specific acknowledgements	164
7.7	Supplementary Material	165

7.1 Introduction

Despite its numerous clinical and research applications, cerebral microdialysis remains a developing technology. While it is used clinically to monitor the concentration of metabolites in the brain interstitium (extracellular fluid), it is unclear what volume of brain tissue and its metabolism these results represent - how far the small molecules recovered by catheters have diffused in the brain. Nor is it known how far small molecules delivered by retro-microdialysis for research studies, such as glucose in **Chapter 3**, or succinate in **Chapter 6**, diffuse through the brain.

Gadolinium-based MRI contrast agents are low molecular weight, water-soluble molecules that greatly shorten the T1 (time for MR spin-lattice relaxation) of tissue around them (in proportion to their concentration) to appear high signal or 'bright' on T1 weighted (T1W) MR images (see **Chapter 1, section 5.2**). In this study, I assessed the diffusion distance and pattern of the gadolinium contrast agent gadobutrol (Gadovist®) (**Figure 7.1**) delivered by microdialysis catheters into patients' cerebral white matter. Molar concentrations (10 mmol/L) were used that were equivalent to that of glucose in **Chapter 3** (4 mmol/L, 8 mmol/L) and succinate in **Chapter 6** (12 mmol/L).

Using this data, gadobutrol's diffusion coefficient (its propensity to freely diffuse through a specific medium) and relaxivity (how its T1 MR relaxation rate changes as a result of its concentration) were also estimated in human cerebral white matter – constants not reported in the literature to date.

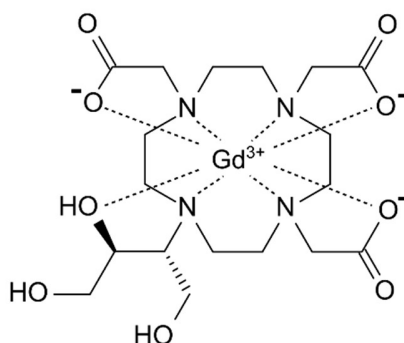


Figure 7.1 Gadobutrol

Gadobutrol, molecular weight 604.7 Daltons, is marketed as Gadovist®/Gadavist® by Bayer AG as a macrocyclic gadolinium MR contrast agent for intravenous administration.

7.2 Methods

7.2.1 Patient recruitment

Six adults (aged ≥ 16 years) who had sustained TBI and required sedation, muscular paralysis, intubation, mechanical ventilation and intracranial monitoring were recruited. Further details see **Chapter 2 (Generic Materials and Methods)**.

7.2.2 Microdialysis

Microdialysis monitoring and gadolinium (gadobutrol) perfusion were carried out as described in **Chapter 2**, using M Dialysis 71 microdialysis catheters (membrane length 10 mm, nominal molecular weight cut-off 100 kDa) (**Table 7.1**). The catheters were directed into cerebral white matter (in the region of the centrum semiovale), avoiding lesions identified on computerized tomography (CT), e.g. contusions. Following a period of perfusion with normal CNS Perfusion Fluid, perfusion fluid was changed to a new syringe that contained CNS perfusion fluid supplemented with 10 mmol/L gadobutrol. Automatic pump priming/flush sequences were run after fluid changeover, followed by 24 hours of gadobutrol perfusion at 0.3 $\mu\text{L}/\text{min}$ before acquisition of the MRI scans. The microdialysis pumps were disconnected immediately before the patients went into the MR scanner but catheters were kept in-situ. Before and during gadobutrol perfusion microdialysis collection vials were analysed hourly for concentration of glucose, lactate and pyruvate on a bedside ISCUSflex analyser.

Table 7.1 Subject demography

Patient	Age (years)	Sex	Injury Mechanism	Admission	Days from	Catheter
				GCS	TBI	insertion
GAD-01	65	M	RTC	3	3	RF-CAD
GAD-02*	37	F	Fall	8	5	LF-CAD
GAD-03	26	M	RTC	4	6	LF-CAD
GAD-04	46	M	Fall	8	4	RF-CAD
GAD-05	26	M	Fall	4	7	LF-CAD
GAD-06	68	F	Fall	11	9	RF-CAD

Catheter insertion denotes side (R/L) and insertion via cranial access device (CAD). The catheters were not directed into, nor adjacent to, lesions identified on computerized tomography (CT). Patient GAD-06 presented only moderately drowsy, but then deteriorated; requiring sedation, intubation, ventilation and intracranial multimodality monitoring. * Recovery of microdialysate failed for \approx 6 hours during patient GAD-02's perfusion, so the pump priming/flush sequence was re-run. GCS denotes highest GCS at presentation to emergency services.

7.2.3 Magnetic resonance imaging

Standard clinical sequences (MP-RAGE, FLAIR, SWI) and T1 maps were acquired with a 3 T Siemens Prismafit scanner and a 12-channel ^1H head/neck coil using Siemens Syngo MapIt software to construct T1 maps at 1 mm isotropic resolution. MapIt uses 3 flip angles (5° , 15° , 26°), with a TE of 2 ms, TR of 15 ms, field of view (FOV) 224 x 224 mm, 88 slices in the axial plane, and 2 averages, requiring a total scan time of 28 minutes. B1 maps were acquired to allow correction of B1 inhomogeneity, and signal acquired fitted to Equation 2.4 (further details see **Chapter 2**).

T1 map volumes were reformatted such that they were perpendicular to the microdialysis catheter trajectory and ≥ 4 tissue T1 profiles were drawn in the reformatted slices using MATLAB (MathWorks, USA) through the central point of maximum gadolinium perfusion, avoiding grey matter and CSF spaces. Each subject's profiles were averaged and plotted. The lowest (shortest) T1 of a subject's average profile represented maximum gadolinium concentration at the catheter. The flat horizontal 'tail' of each subject's average profile (ignoring random noise) was used as a measure of white matter baseline T1. The position of the start of this 'tail' on the x-axis was used to define maximum diffusion distance of gadobutrol. To establish the potential effect of variability determining baseline T1, the individual profiles with the highest and lowest 'tail' in each subject were recorded (see **Supplementary Figure 7.1**).

Additional tissue T1 profiles were plotted through patient GAD-05's grey-white matter interface to characterise diffusion across the grey-white matter boundary. Whereas other patients' perfusion

regions occasionally approached grey matter, only GAD-05's catheter centre passed adjacent to and perpendicular to an area of sulcal grey matter (on one side).

Using Equation 2.5 the concentration of gadobutrol immediately adjacent to the catheters was approximated using the difference between its tissue T1, and the baseline tissue T1. This approximation relied on the relaxivity of gadobutrol in human blood plasma at 37 °C as a surrogate for gadobutrol in human cerebral white matter (Pintaske *et al.*, 2006). Then, assuming the relaxivity of gadobutrol in cerebral white matter is *not* exactly equal to that in human blood plasma, and assuming that a steady-state maximum concentration of gadolinium is achieved close to the catheter after 24 hours continuous perfusion, Equation 2.5 was used to estimate the relaxivity (R) of gadobutrol in human cerebral white matter. Relaxivity is a measure of how the concentration of a substrate affects its medium's T1 and T2 NMR relaxation rate. It is magnetic field (B_0) dependent and has independent T1 and T2 values – in this chapter 'relaxivity' refers to effect on white matter's T1 relaxation.

Equation 2.5

$$C = \frac{\left(\frac{1}{T1_{observed}} - \frac{1}{T1_{tissue}} \right)}{R}$$

Where $T1_{observed}$ is the T1 of the voxel (in seconds (s)), $T1_{tissue}$ is the baseline T1 of each subject's cerebral white matter (s) and R is the relaxivity of gadobutrol ($3.6 \text{ L.mmol}^{-1}\text{s}^{-1}$) (Pintaske *et al.*, 2006). Subjects' $T1_{tissue}$ was defined as the shortest value of T1 in their their mean white matter profile (see **Supplementary Figure 7.1**).

7.2.4 Statistical analysis

Averages of all axial profiles of each subject's gadolinium diffusion profiles were calculated in MATLAB and compared qualitatively. Average profiles, excluding subject GAD-02, were exported into R and fitted using a nonlinear least squares method (R package *nls2*) (see **Results**) to estimate the diffusion coefficient of gadobutrol in human cerebral white matter.

Cerebral extracellular chemistry directly before gadolinium supplementation (baseline) was compared with that during gadolinium supplementation: hourly ISCUSflex measurements of glucose, pyruvate, lactate and L/P ratio in recovered microdialysate using plain unsupplemented microdialysis perfusion fluid were compared to the following period of perfusion supplemented with gadobutrol using Wilcoxon signed rank tests of subject mean data, and a linear mixed effects model ('lmer' in R) of subject individual hourly data. The first two vials after changeover from baseline to gadolinium perfusion were

excluded as 'run-in' vials, as per other studies (**Chapters 3 and 6**). Further details see description in **Chapters 2 and 3**.

7.3 Results

7.3.1 Patient demographics

Six patients suffering from TBI had gadolinium (10 mmol/L) perfusion for 24 hours via a frontal microdialysis catheter. Patient demographics are in **Table 7.1**.

7.3.2 Pattern of diffusion

In human cerebral white matter gadolinium diffused in a spheroidal pattern; or an ellipsoid of revolution whose central long axis was the microdialysis catheters' semipermeable membranes; resulting in a uniform circular pattern of diffusion perpendicularly from the catheter centre (**Figure 7.2**). At white-grey matter boundaries the difference in tissue T1 appeared to be predominantly due to tissue type, but there was a difference in the T1 of grey matter adjacent to the catheters compared to the T1 of grey matter remote from the catheters (see **Figure 7.3**). This shows that gadolinium diffused across the white-grey matter boundary and then through grey matter. It was not possible to measure the relative difference in diffusion through grey matter and white matter as diffusion through grey matter could only be reliably characterised perpendicularly from a catheter centre in a single patient.

7.3.3 Diffusion coefficient and maximum diffusion distance

There was evidence of gadobutrol diffusion up to 14 mm from the centre of GAD-03 and GAD-05's catheters, with a mean maximum radial diffusion distance (up to where the T1 profile 'tail' reached the tissue baseline T1; see **Methods**) of 12.3 mm (s.d. 2.7 mm, range 7 – 14 mm) across the whole patient group. Patient GAD-02 had failure of microdialysate recovery for \approx 6 hours; either due to a failure of perfusion fluid delivery or microdialysate return. A failure of delivery is more likely as gadobutrol diffused over a shorter distance compared to the other patients (**Figure 7.4**) and microdialysate recovery was restored when the pump flush sequence was re-run. When subject GAD-02 was excluded from analysis, the mean maximum diffusion distance of gadolinium was 13.4 mm (s.d. 0.5 mm, range 13 – 14 mm).

There was little variation between different profiles *within* each subject suggesting a consistent, reproducible pattern of diffusion occurs radially from a catheter's centre in all directions (**Figure 7.4**). Excluding subject GAD-02, there was little variation between the average profiles of each patient, suggesting gadobutrol diffuses reproducibly through different subjects' white matter.

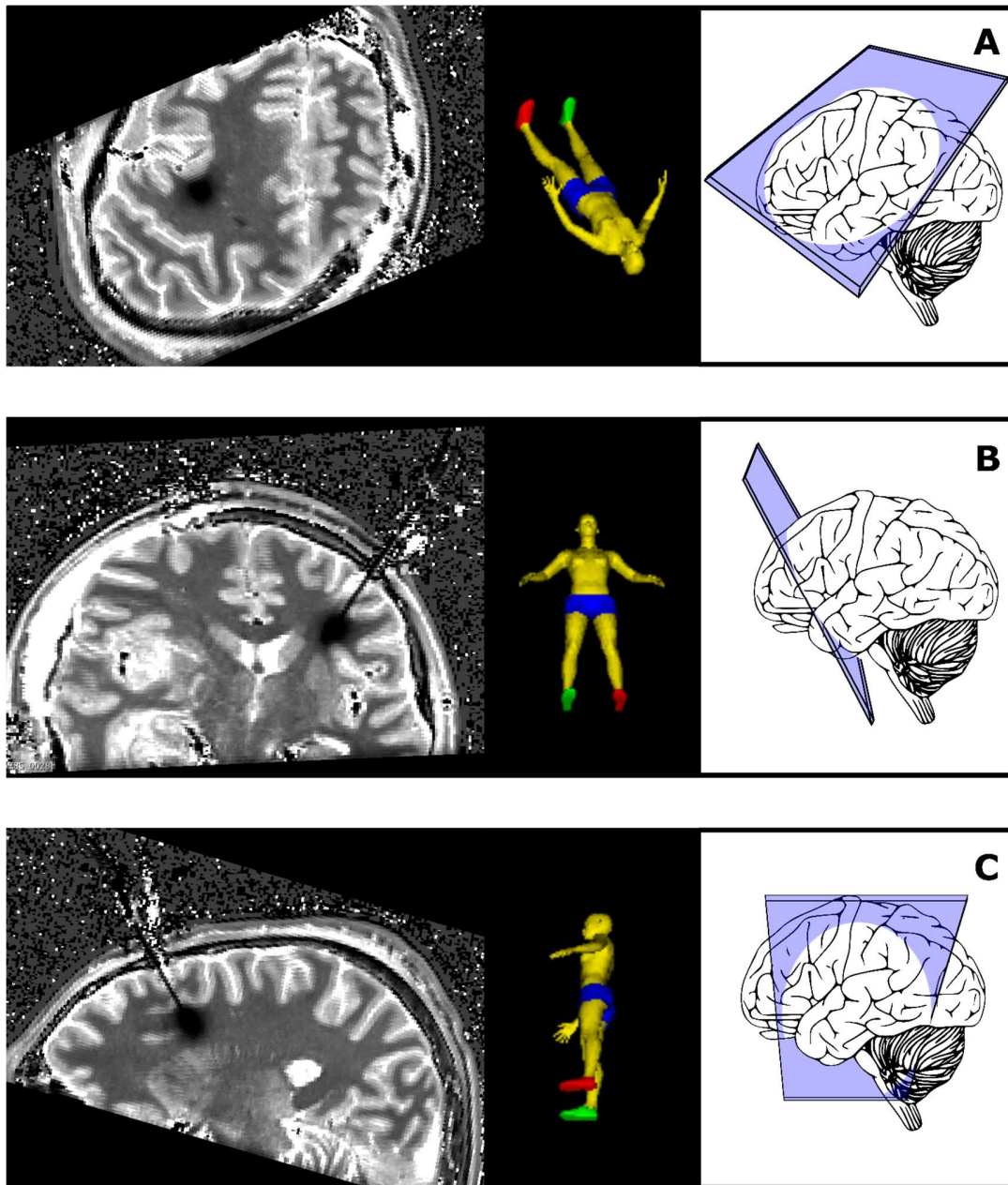


Figure 7.2 Pattern of gadolinium diffusion in human cerebral white matter

On the left, example T1 maps (1 mm isotropic) from patient GAD-05 demonstrating gadolinium (gadobutrol) perfusion from a 100 kDa cut-off microdialysis catheter in three orthogonal planes oriented to align with the catheter; catheters were not inserted at 90 degrees to the standard axial, coronal and sagittal anatomical orientation. In the centre, model homunculi demonstrate image orientation relative to patient position. On the right, orientation of respective viewing planes in respect to the patient's brain. *Panel A* represents axial plane of the catheter, *Panel B* coronal plane, and *Panel C* sagittal plane.

Cerebral grey matter appears light-grey and white matter appears darker-grey. Gadolinium in the catheter (*Panel B* and *C*) and its diffusion through the brain in a broad ellipse of revolution from the catheter membrane (*Panels A, B* and *C*) appears dark-grey/black.

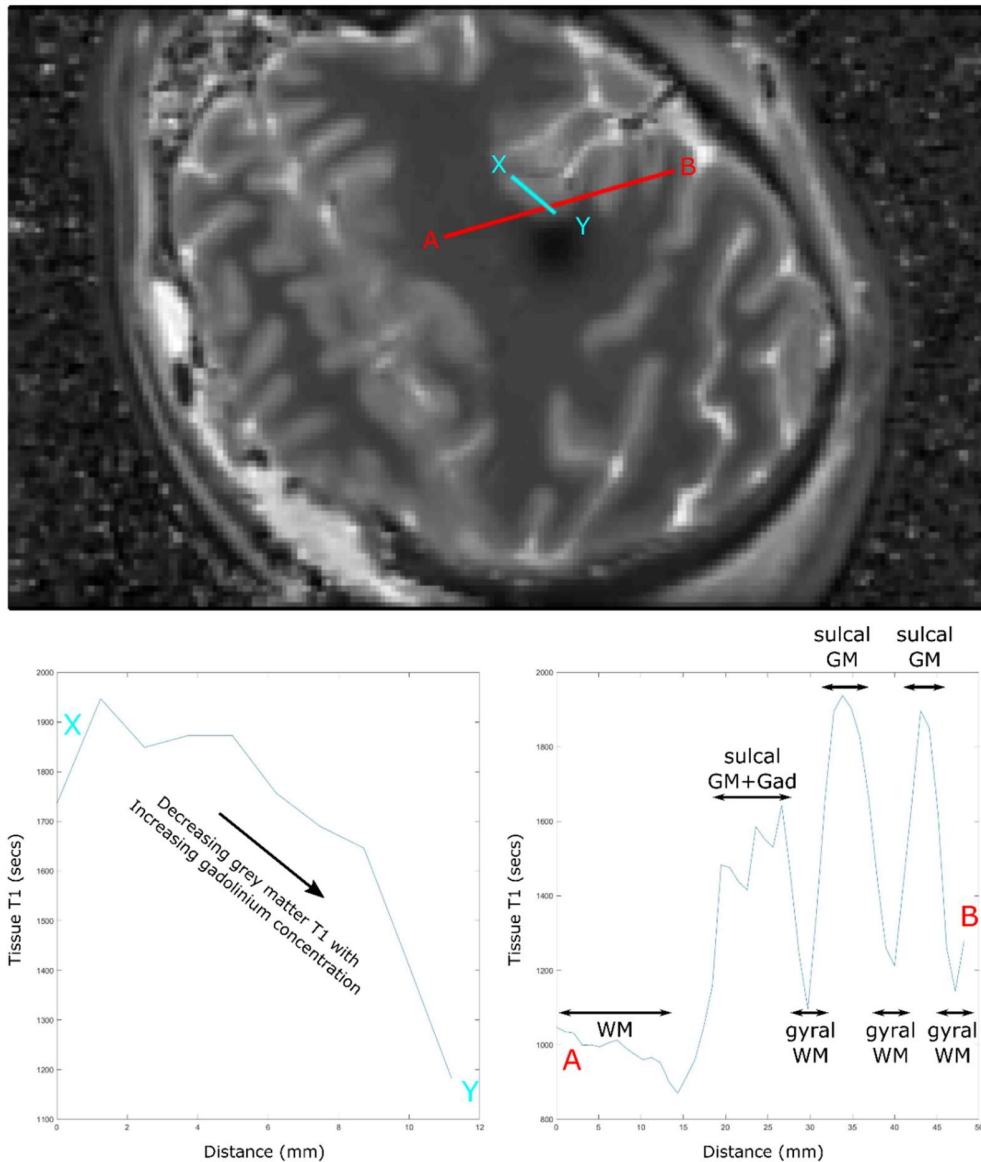


Figure 7.3 Pattern of gadolinium diffusion at grey matter-white matter boundary

Example T1 map of 100 kDa cut-off microdialysis catheter demonstrating gadolinium (gadobutrol) diffusion across GM-WM boundary into GM of sulcus in patient GAD-05. Cyan coloured profile 'X-Y' across the base of a cerebral sulcus demonstrates falling GM T1 approaching the catheter due to increasing concentration of gadolinium. Red coloured profile 'A-B' demonstrates tissue T1 through the WM of the centrum semiovale, then successive regions of sulcal GM and gyral WM. The first 'peak' of GM T1 in the profile is lower than the two subsequent peaks due to gadobutrol diffusion from the adjacent catheter. GM regions are anatomically equivalent. *Abbreviations: see table in **Precis**.*

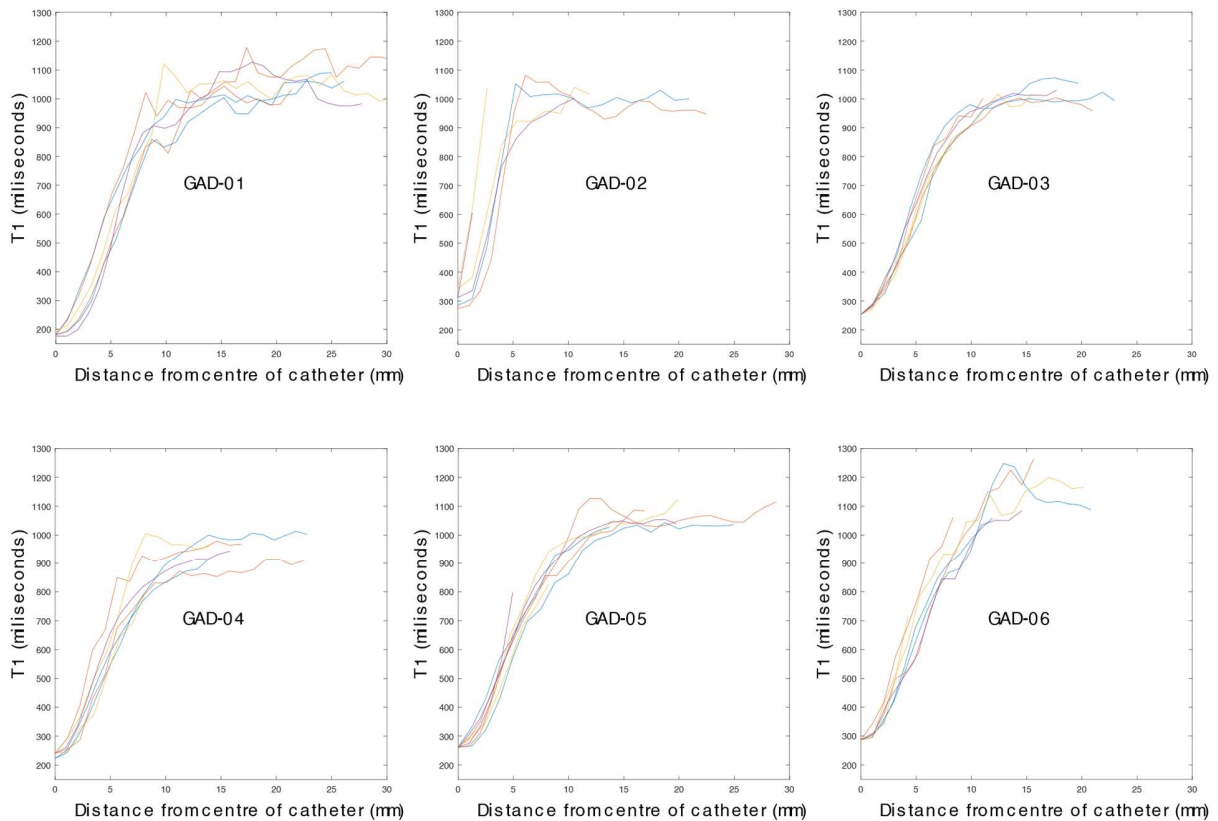


Figure 7.4 Individual subject profiles of tissue T1 from the centre of microdialysis catheters

Profiles drawn perpendicularly to the catheter trajectories through the centre of the microdialysis membrane length. Little variation is observed within patients, with modest variability between patients. Gadolinium perfusion from subject GAD-02's catheter failed for ≈ 6 hours during the perfusion period.

Mean diffusion profiles, expressing gadobutrol concentration as percentage of maximum calculated from Equation 2.5 for each subject is shown in **Figure 7.5**. Despite evidence of gadobutrol up to a 13-14 mm from the catheters there was a steep concentration drop off with $\leq 50\%$ of maximum concentration achieved beyond ≈ 4 mm and $\leq 10\%$ of maximum achieved beyond ≈ 7 mm from the catheters' centre.

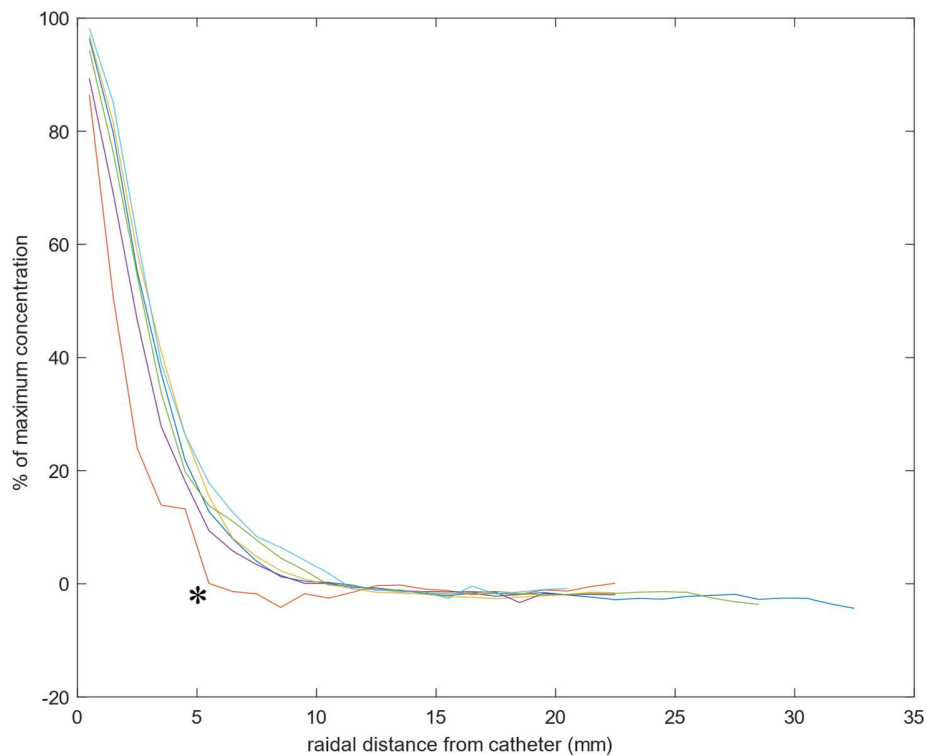


Figure 7.5 Gadobutrol concentration from catheter as % maximum

Subject-average percent maximum concentration profiles of gadobutrol at increasing radial distance from the centre of microdialysis catheters, demonstrating $\leq 50\%$ of maximum concentration ≥ 4 mm from the catheters. *Average diffusion profile of subject GAD-02 (beige-orange profile) demonstrates reduced, irregular diffusion due to failure of microdialysate recovery (and likely gadobutrol delivery) for ≈ 6 hours.

Gadobutrol concentration drop-off from the microdialysis catheters followed that of Brownian motion: creating a gaussian probability distribution with a percentage of maximum concentration “%C”, at distance “x” from the catheter, at time “t”:

Equation 7.1 (Pattle, 1959)

$$\%C = \frac{1}{\sqrt{4\pi Dt}} e\left(-\frac{x^2}{4Dt}\right)$$

Where D is the diffusion coefficient of a small molecule. Assuming a diffusion time (t) of 24 hours (86,400 seconds), the radial diffusion distance (mm) and relative concentration (percentage of maximum) data (**Figure 7.5**) was fitted to estimate the diffusion coefficient of gadobutrol in human cerebral white matter to be $9.9 \times 10^{-7} \text{ mm}^2\text{s}^{-1}$.

7.3.4 Estimation of relaxivity and concentration

Using Equation 2.5 and the relaxivity of gadobutrol in human blood plasma ($3.6 \text{ L}\cdot\text{mmol}^{-1}\cdot\text{s}^{-1}$ (Pintaske *et al.*, 2006)) as an approximation for gadobutrol in human cerebral white matter, the maximum concentration of gadobutrol achieved around the microdialysis catheters was approximated to be 0.84 mmol/L . However, the relaxivity of gadobutrol in cerebral white matter is unlikely to be equal to that of blood plasma. Besides, after 24 hours of continuous perfusion, the concentration of gadobutrol in the brain's interstitial fluid immediately adjacent to the catheters might be expected to reach equilibrium with the perfusion fluid. Assuming this equilibrium was achieved and interstitial fluid (the extracellular space) occupies 20 % of cerebral tissue volume (Syková *et al.*, 2008) where the gadobutrol is limited to (Aime and Caravan, 2009), the whole-tissue concentration of gadobutrol would be 2 mmol/L . Using this value and Equation 2.5, the relaxivity of gadobutrol in human cerebral white matter can be estimated as $1.61 \pm 0.38 \text{ L}\cdot\text{mmol}^{-1}\cdot\text{s}^{-1}$ (mean \pm s.d.). Individual subject results in **Table 7.2**.

Table 7.2 Subject estimated relaxivity and concentration approximation

Subject	Maximum distance (mm)	Minimum T1 (s)	Baseline T1 (s)	Estimated Relaxivity (L.mmol ⁻¹ s ⁻¹)	Concentration Approximation (mmol/L)*
GAD-01	13	0.183	1.05 [0.98-1.17]	2.26 [2.22-2.31]	1.25 [1.23-1.28]
GAD-02	7	0.303	0.98 [0.93-1.03]	1.14 [1.11-1.16]	0.63 [0.62-0.65]
GAD-03	14	0.253	1.01 [0.96-1.07]	1.48 [1.45-1.51]	0.82 [0.81-0.84]
GAD-04	13	0.236	0.96 [0.85-1.01]	1.60 [1.53-1.63]	0.89 [0.85-0.90]
GAD-05	14	0.262	1.05 1.01-1.12]	1.43 [1.41-1.46]	0.80 [0.79-0.81]
GAD-06	13	0.287	1.12 [1.05-1.26]	1.29 [1.27-1.35]	0.72 [0.70-0.75]
<i>Mean (s.d.)</i>	<i>12.3</i>	<i>0.254</i>	<i>1.03</i>	<i>1.53 (0.39)</i>	<i>0.85 (0.22)</i>
Mean (s.d.)	13.4	0.244	1.04	1.61 (0.38)	0.90 (0.21)

Maximum distance effect of gadobutrol observed from catheter, minimum T1 representing maximum gadobutrol concentration around the catheter, baseline white matter T1, relaxivity of gadobutrol estimated from Equation 2.5, and approximation of concentration using relaxivity of gadobutrol in blood serum (3.6 L.mmol⁻¹s⁻¹ (Pintaske *et al.*, 2006)) for each subject, with mean. Range in baseline T1 and resultant estimated relaxivity in square brackets [] (see Methods). *Mean (s.d.)* in italics includes all subjects, whereas **Mean (s.d.)** in bold indicates all subjects excluding subject GAD-02 whose perfusion failed for ≈ 6 hours.

7.3.5 Effect on brain chemistry

Compared to baseline perfusion, microdialysis with CNS perfusion fluid containing 10 mmol/L gadobutrol was associated with the following changes, measured in brain microdialysates on an ISCUSflex analyser: There was a 10 % decrease in extracellular glucose (decrease in 4/5 subjects, increase in 1/5). There was a 6 % increase in overall extracellular lactate caused by an increase in 3/5 subjects, minimal change in 1/5, and a decrease in 1/5. Pyruvate increased 17 % overall due to a substantial increase in 2/5 subjects, a more modest decrease in 2/5 and minimal change in 1/5. There was a small, 6 % overall decrease in L/P ratio with an increase in 2/5 subjects, decrease in 2/5 (1 substantially) and no change in 1/5. Summary of results and statistical significance in **Table 7.3** and **Figure 7.6**, individual results in **Supplementary Figure 7.1**.

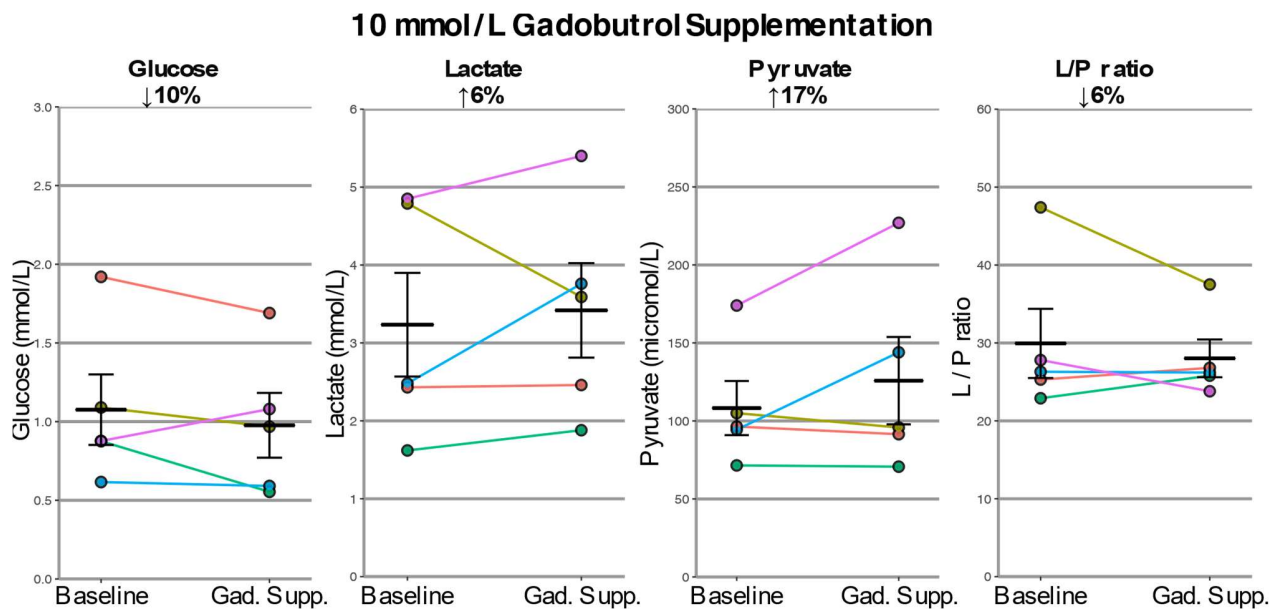


Figure 7.6 ISCUSflex bedside analyser measurements of brain extracellular chemistry at baseline and during microdialysis supplementation with 10 mmol/L gadobutrol

Each pair of data-points indicates mean levels at baseline and during gadobutrol perfusion, respectively, for that patient. Supplementation was for ≈ 24 hours. Baseline denotes ≈ 30 hours of pre-supplementation. Black crossbars on graphs denote averages of patient means with one standard error of the mean standard error. *Abbreviations: see table in Precis; Gad. Supp., gadobutrol supplementation.*

Table 7.3 Summary ISCUSflex bedside analyser measurements of brain extracellular chemistry at baseline and during microdialysis supplementation with 10 mmol/L gadobutrol.

	Baseline mean	Supp. mean	% change mean	<i>Imer</i> <i>p</i>	<i>Wilcoxon</i> <i>p</i>
Glucose	1.08	0.98	↓10 %	0.0006	0.3
Lactate	3.23	3.42	↑6 %	0.017	0.4
Pyruvate	108	126	↑17 %	0.0001	0.8
L/P ratio	29.9	28.0	↓6 %	0.0001	0.6

Group means of each subject's mean value during baseline perfusion and perfusion during supplementation with gadolinium (gadobutrol). Significance determined by linear mixed effects model (*Imer*) of un-averaged data, and Wilcoxon signed rank of patient's means using R. Arrows \uparrow/\downarrow denote direction and % change increases/decreases respectively.

7.4 Discussion

7.4.1 Summary

In this study I have demonstrated that CNS perfusion fluid containing 10 mmol/L gadobutrol diffuses up to 13.4 mm (measured radially) from microdialysis catheters in human cerebral white matter – but with a sharp concentration drop off so that $\leq 50\%$ of maximum concentration is found ≥ 4 mm; and $\leq 10\%$ of maximum concentration is found ≥ 7 mm from the catheter centres.

Using the pattern of diffusion over 24 hours continuous perfusion I have estimated gadobutrol's diffusion coefficient in human cerebral white matter and estimated the relaxivity of gadobutrol in human cerebral white matter – assuming equilibrium of microdialysis perfusate and brain interstitium is achieved immediately adjacent to the catheter.

7.4.2 Diffusion of small molecules in the brain

The diffusion coefficient of small molecules depends on their size, temperature and viscosity in a free diffusion medium. The brain extracellular environment is thought to represent only $\approx 20\%$ of brain volume and contains subsequent barriers of diffusion meaning the diffusion coefficient of small molecules is often 2-3 times less than it would be in a free diffusion medium (Syková *et al.*, 2008). This is due to several factors including: (1) the volume of extracellular fluid, (2) tortuosity of the extracellular fluid channels, (3) loss into the systemic bloodstream, (4) obstruction by extracellular tubules and matrices, (5) binding to cell membranes, and (6) active cellular uptake (Syková *et al.*, 2008).

Gadobutrol (molecular weight 605 g/mol) is a larger molecule than Glucose (**Chapter 3**, molecular weight 180 g/mol) and succinate (**Chapter 6**, molecular weight 118 g/mol), meaning its free diffusion in the human brain should be less than the other substrates studied in this thesis. However, as an extracellular contrast agent, gadobutrol is not taken up by cells (6), nor does it bind to them (5) (Bellin and Van Der Molen, 2008; Aime and Caravan, 2009); whereas glucose and succinate are actively taken up by cells via GLUT and SLC13 transporters (respectively) – thus gadobutrol's free diffusion may in fact be greater. Furthermore, gadobutrol does not cross the intact blood-brain barrier (BBB) (Montagne *et al.*, 2016); unlike glucose and succinate (GLUT and SLC13 transporters) (3). The BBB was thought to be grossly intact in the subjects in this study as no evidence of radiological injury in the brain surrounding the catheters was found on imaging before or after insertion of catheters.

It is expected that brain temperature, obstruction by extracellular matrix (4), tortuosity of fluid channels (2), and extracellular fluid volume would be equivalent across patients who received perfusion with

gadolinium, glucose and succinate. Anisotropy of diffusion, with diffusion distance in this study measured transversely to the main cerebral white matter tracts is likely to be similar in patients across studies as catheters were inserted using equivalent trajectories to those in **Chapters 3 and 6 (Figure 7.2)**.

Excluding patient GAD-02 whose gadobutrol perfusion was interrupted for ≈ 6 hours (see **Results**), there was great consistency within a subject's individual profiles, between different subjects' mean profiles, and the maximum distance that the effect of gadobutrol was noted from the catheters. This suggests that the diffusion of gadobutrol in human cerebral white matter is uniform within human cerebral white matter of the region of the centrum semiovale.

In a similar study using animal models the gadolinium contrast agent Gadodiamide (592 g/mol) was found to permeate a similar 'core' distance of ≈ 4 mm around opened ended catheters (i.e. not semipermeable microdialysis catheters) in porcine cerebral white matter, with evidence of low concentration gadolinium further from the catheter (Chen *et al.*, 2004). However, Chen *et al.* actively pumped contrast agent using convection enhanced delivery with a perfusion rate of 0.5-1 $\mu\text{L}/\text{min}$ for 2 hours; whereas in my study gadobutrol was delivered at 0.3 $\mu\text{L}/\text{min}$ and allowed to passively diffuse for 24 hours. In another study, the gadolinium contrast agent gadopentetic acid pumped from convection enhanced delivery catheters at a rate of 0.1-0.5 $\mu\text{L}/\text{min}$ into non-human primate striatum (grey matter) reached a core volume of 3 mm from the catheters, with a sharp concentration drop-off similar to the profiles achieved in **Figure 7.5** (Heiss *et al.*, 2010). A study comparing results from concurrent microdialysis and positron emission tomography (PET) found that the oxygen extraction fraction of a 10 mm (radial) region of interest around a microdialysis catheter correlated with cerebral lactate/pyruvate ratio measured by microdialysis (Hutchinson *et al.*, 2002). Another study, comparing FDG-PET and microdialysis readings in TBI patients revealed positive linear correlations between PET cerebral metabolic rate of glucose (CMR_{glc}) and microdialysate lactate concentration, and between CMR_{glc} and pyruvate, using a spherical region of interest (ROI) of 20 mm diameter, thus a radius of 10 mm (Hutchinson *et al.*, 2009).

The transition between grey matter and white matter did not appear to be a significant barrier to diffusion in this study. Although the interface is readily visible to the naked eye and on MR imaging, there is no physical 'barrier' between cortical layer VI and the subcortical white matter, such as a

basement membrane, to expect such an interruption of diffusion (Thomson, 2010). However, the diffusion of metabolites (glutamate, glutamine, N-acetyl aspartate, creatinine and choline) was shown to be less in human grey matter than white matter in a 7T MRI study (Kan *et al.*, 2012), as was the diffusion of tetramethylammonium (TMA) in rat brain grey matter compared to white matter in a direct diffusion study (Syková *et al.*, 1996).

7.4.3 Diffusion coefficient

The diffusion coefficient of gadobutrol – its propensity to diffuse through a medium relative to its concentration gradient – is not well reported in living tissue. MR studies of *water's* diffusion in the living human brain find the apparent diffusion coefficient may vary from $0.75 - 2.48 \times 10^{-3} \text{ mm}^2\text{s}^{-1}$; more specifically in frontal white matter between $0.75 - 1.95 \text{ mm}^2\text{s}^{-1}$ (Pierpaoli *et al.*, 1996; Toft *et al.*, 1996; Shimony *et al.*, 1999; Engelter *et al.*, 2000). The diffusion coefficient of gadobutrol in human cerebral white matter in this study is estimated to be 3 orders of magnitude lower, at $9.9 \times 10^{-7} \text{ mm}^2\text{s}^{-1}$. This difference is likely to be predominantly due to gadobutrol being a much larger molecule than water (604.7 Daltons vs. 18 Daltons). However, its diffusion is also limited to the brain's extracellular matrix (Bellin and Van Der Molen, 2008; Aime and Caravan, 2009) whereas water diffuses across cell membranes so may diffuse *via* both the extracellular and intracellular compartment. However, the estimated diffusion coefficient in human cerebral white matter is still 2 orders of magnitude lower ($9.9 \times 10^{-7} \text{ mm}^2\text{s}^{-1}$) than that of the gadolinium contrast agent gadoterate meglumine (Dotarem) in human cancer xenografts implanted into mice ($2.08 \times 10^{-4} \text{ mm}^2\text{s}^{-1}$ (Koh *et al.*, 2013)). Although gadobutrol is not thought to readily cross the BBB, a proportion would be expected to be absorbed into the systemic circulation over a 24-hour perfusion period, reducing the estimate of diffusion coefficient in this study. Moreover, the effective diffusion coefficient of the brain extracellular fluid is generally accepted to be 2-3 times smaller than that its free diffusion coefficient due to the reasons described above. In the presence of cytotoxic oedema associated with TBI, an increase in cell volume relative to extracellular volume may decrease the measured diffusion coefficient of the brain through tighter junctions between cells (Syková *et al.*, 2008). To more accurately ascertain the diffusion coefficient of gadobutrol in human cerebral white matter T1 maps could be acquired at additional time points of gadolinium perfusion.

7.4.4 Relaxivity and concentration

Using Equation 2.5, either gadobutrol's concentration can be estimated if its relaxivity is known, or its relaxivity estimated if its concentration is known.

Using gadobutrol's (T1) relaxivity in human blood plasma as an approximation for cerebral white matter, the absolute concentration of gadobutrol achieved at the centre of the microdialysis catheter was approximated to be 0.84 mmol/L; only 8 % of the perfusion fluid concentration (10 mmol/L). The principal cause for this discrepancy is the extracellular distribution of gadolinium: gadobutrol is a cyclical extracellular contrast agent that does not readily cross cell membranes (Bellin and Van Der Molen, 2008; Aime and Caravan, 2009). As the human brain extracellular space represents only $\approx 20\%$ of total brain volume (Syková *et al.*, 2008; Nicholson and Hrabětová, 2017) the expected maximum tissue concentration is 2 mmol/L, much closer to the approximated 0.84 mmol/L calculated from Equation 2.5. Moreover, the extracellular space may represent less than 20 % of brain volume in the acute phase of TBI due to increased cell volume associated with potential cytotoxic oedema (Syková *et al.*, 2008; Nicholson and Hrabětová, 2017).

Although the relaxivity of gadobutrol in human blood plasma is the closest surrogate for relaxivity in cerebral white matter reported in the literature, it is unlikely to be accurate. The T1 of an MR-detectible nucleus in a tissue is dependent on its temperature, viscosity, molecular weight, its Larmor frequency and distance from other magnetic dipoles (see **Supplementary Equation 1**). Cerebral white matter has a greater abundance of high molecular weight macromolecules (e.g. cell membranes) than plasma, which also increases its viscosity, making its baseline T1 shorter. This means that the absolute difference between tissue baseline T1 and T1 observed on addition of gadolinium is less. The T1 of plasma at 3T is reportedly around 2.3 seconds (Rohrer *et al.*, 2005), whereas the average T1 of human cerebral white matter in this study was found to be 1.03 seconds.

After a sufficiently long period of continuous perfusion, the concentration of gadobutrol in the extracellular fluid adjacent to the microdialysis catheter will match that of the perfusion fluid. After 24 hours of continuous perfusion at 10 mmol/L this might be expected to be achieved. Assuming this is the case, the relaxivity of gadobutrol in human cerebral white matter is estimated to be $1.6 \text{ L}\cdot\text{mmol}^{-1}\cdot\text{s}^{-1}$ (from Equation 2.5). This estimate assumes gadolinium is limited to the brain's extracellular space occupying 20 % of brain volume (Syková *et al.*, 2008) and achieving an effective tissue concentration of 2 mmol/L (20 % of 10 mmol/L). Patient GAD-02 was excluded from this calculation as their gadobutrol perfusion was interrupted for 6 hours. The estimate of $1.6 \text{ L}\cdot\text{mmol}^{-1}\cdot\text{s}^{-1}$ is comparable to the relaxivity of other gadolinium contrast agents in water and plasma, reported in the literature (Rohrer *et al.*, 2005; Pintaske *et al.*, 2006).

7.4.5 Effect of gadolinium on extracellular chemistry

Free elemental gadolinium is toxic at nano-molar and micro-molar concentrations due to it blocking voltage-gated calcium channels and enzymes (Bellin and Van Der Molen, 2008). By chelating gadolinium in a linear (acyclic), or macrocyclic ligand, or 'wrapper' (**Figure 7.1**) it becomes non-toxic, remaining in the systemic circulation and extracellular fluid before being renally excreted (Bellin and Van Der Molen, 2008; Gulani *et al.*, 2017). In the absence of pathology, gadolinium preparations do not readily cross the BBB (Montagne *et al.*, 2016); but with repeated exposure gadolinium can deposit, or accumulate in patients' globus pallidi and dentate nuclei. This may be through some of the administered gadolinium contrast agent losing its protective chelating wrapper (Gulani *et al.*, 2017), then potentially becoming harmful. However, this occurs much more readily in linear acyclic preparations than the macrocyclic preparations such as gadobutrol used in this study (Gulani *et al.*, 2017). Moreover, no harm or behavioural change has been found in animal studies involving repeated exposure to gadolinium contrast agents (Gulani *et al.*, 2017).

This study was neither designed nor powered to detect the effect of gadobutrol on cerebral extracellular metabolism, and there are no reports of studies using microdialysis to study the effect of gadobutrol in this fashion. Nonetheless, gadobutrol perfusion was potentially associated with a decrease in extracellular glucose concentration. Despite this reaching statistical significance with linear mixed model analysis (*lmer*), it is difficult to confidently attribute this effect to gadobutrol using such a small sample size with the known potential variability of microdialysis results (Timofeev *et al.*, 2011). Furthermore, there was no change when analysed by Wilcoxon signed rank analysis. Low extracellular glucose may be caused by either insufficiency of glucose supply, or an increase in glucose uptake and metabolism. The associated increase in extracellular lactate and pyruvate suggests that the measured change is due to increased glucose metabolism, but whether it is related to gadobutrol supplementation is difficult to determine.

A retrospective FDG-PET/CT study found that chronic exposure to a variety of gadolinium contrast agents was associated with a reduced maximum standardised uptake value (of fludeoxyglucose, FDG) when compared to controls (Bauer *et al.*, 2017), but this study was criticised for a number of confounding variables (Naganawa, 2017). A subsequent animal study found that chronic exposure to gadolinium (Gadodiamide) was not associated with changes in the cerebral metabolic rate of glucose in the deep brain nuclei (grey matter) measured by FDG-PET. Most importantly, in the current study, there was no increase in the ratio of lactate to pyruvate (L/P ratio) that would suggest mitochondrial

dysfunction: indeed, the L/P ratio was slightly lower during gadobutrol perfusion. Besides, any toxic effect of gadobutrol would require disassociation of gadolinium from its chelating compound – a process that is thought to take longer than the 24 hours measured in this study (Frenzel *et al.*, 2008).

7.4.6 Strengths, limitations and further work

Gadolinium (gadobutrol) is an appropriately similarly-sized small molecule surrogate for glucose and succinate visible on MRI scans at low concentration with high spatial resolution that can be used to model the diffusion pattern of such small molecules in the living human brain. By using T1 maps instead of 'classic' T1 weighted imaging, quantitative analysis that includes estimation of diffusion and relaxivity constants is possible. The commercial software MapIt uses the multiple spoiled gradient echo technique to automatically acquire T1 maps with great time efficiency.

A caveat to using gadobutrol as a surrogate for glucose and succinate are the likely differences between their pharmacokinetics. Glucose and succinate are metabolically active compounds taken up and metabolised by cells, whereas gadobutrol remains predominantly inert in the extracellular space (Bellin and Van Der Molen, 2008; Gulani *et al.*, 2017). Although all will be lost to some degree into the systemic circulation, this again may be less rapid for gadobutrol due to its low BBB permeability (Montagne *et al.*, 2016). It is difficult to address this problem with phantom studies as they are non-dynamic, and animal models using tissue extraction techniques require mammals with sufficiently large cerebral white matter and grey matter regions to be comparable to humans (Chen *et al.*, 2004).

Estimation of gadobutrol's diffusion coefficient could be improved by acquiring T1 maps at earlier timepoints and fitting Equation 7.1 using data with other measurements of time, " t ". This would also aid the measurement of gadobutrol's relaxivity in human cerebral white matter as it would ascertain whether a constant concentration of gadobutrol had been achieved adjacent to the catheters after 24 hours of perfusion, or if there was a change in observed T1 at later timepoints.

Increasing the number of subjects studied would improve the estimation accuracy of both constants, but most importantly give weight to analysis of changes in extracellular chemistry measured by ISCUSflex analysis of the recovered microdialysate; a measurement which appeared to possess the greatest variability. By measuring both a pre-gadobutrol and post-gadobutrol perfusion baseline (as in **Chapter 3**) an account of underlying trends in subject physiology could have been accounted for. However, it is likely that any theoretical effect of gadobutrol on tissue physiology would persist into the

post-gadobutrol perfusion period. Furthermore, the process of transferring a patient to the MR suite itself may cause confounding changes in microdialysis results.

7.5 Conclusions

The gadolinium contrast agent Gadobutrol diffuses in an ellipsoid pattern up to 13 mm from the centre of a microdialysis catheter in human cerebral white matter (the distance from centre of catheter up to where the T1 profile 'tail' reaches tissue baseline T1; see **Methods**); with a sharp concentration drop achieving $\leq 50\%$ concentration ≥ 4 mm from the catheter centre. The grey-white matter junction and grey matter do not appear to be significant barriers to diffusion.

The estimated T1 relaxivity of gadobutrol in human cerebral white matter is $1.61 \text{ L.mmol}^{-1}\text{s}^{-1}$; comparable to gadobutrol's relaxivity in water and human plasma. The diffusion coefficient of gadobutrol in human cerebral white matter was approximated to be $9.9 \times 10^{-7} \text{ mm}^2\text{s}^{-1}$.

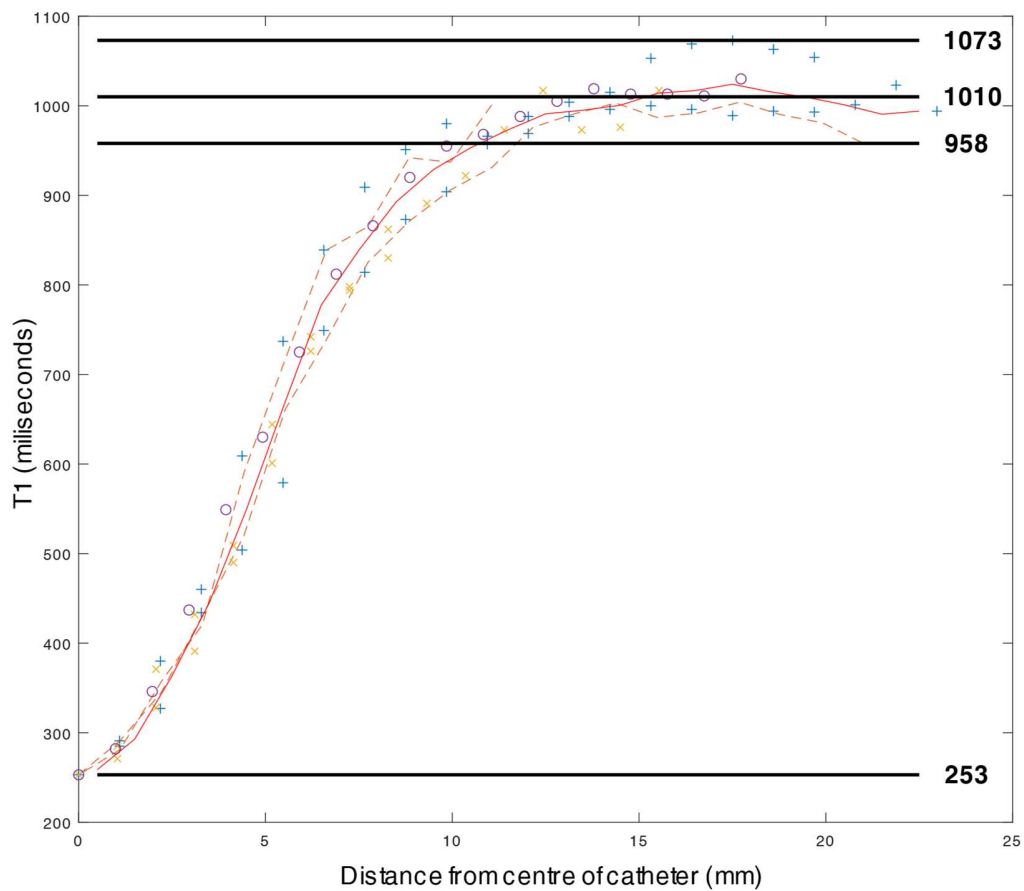
Assuming the diffusion of gadobutrol is a suitable model for the diffusion of succinate from microdialysis catheters in the human brain, 25 mm ^{31}P MRS voxels are an acceptable size for the experiments performed in **Chapter 6**.

Furthermore, microdialysis has potential to deliver treatments to focal pathologies of the human brain; such as cerebral contusions after head injury, intrinsic brain tumour chemotherapy delivery, and neurodegenerative conditions that affect the basal ganglia. This study provides a platform for future development of new catheters optimally designed to treat such conditions.

7.6 Declaration and specific acknowledgements

In-vivo T1 maps were acquired in collaboration with Dr D. Tozer, MR physicist and Mr P.P.R. Ruetten, PhD student. Orientating the acquired T1 maps' workspace into the axial plane of the microdialysis catheters was performed in collaboration with Dr D. Tozer. Creation of T1 profiles through the centre of microdialysis catheters in MATLAB was performed in collaboration with Mr P.P.R. Ruetten.

7.7 Supplementary Material



Supplementary Figure 7.1 Baseline T1 variability

Individual profiles from subject GAD-03 showing the minimum T1 value (253 ms) representing maximum gadobutrol concentration and the baseline T1 value (1,010 ms) representing normal white matter from where the average of the profiles becomes unchanging. Maximum variability in determining the baseline is represented by the individual profile with the greatest (1,073 ms) and lowest (958 ms) T1 values.

Profile created in MATLAB.

Supplementary Table 7.1 ISCUSflex clinical microdialysis analyser individual results

ID	Age	Sex	Baseline	Gadolinium	Baseline	Gadolinium	Baseline	Gadolinium	Baseline	Gadolinium
			perfusion	perfusion	perfusion	perfusion	perfusion	perfusion	perfusion	perfusion
			Glucose	Glucose	Lactate	Lactate	Pyruvate	Pyruvate	L/P ratio	L/P ratio
			(mmol/L)	(mmol/L)	(mmol/L)	(mmol/L)	(μ mol/L)	(μ mol/L)		
GAD-01	65	M	1.92	1.69	2.43	2.46	96	92	25.3	26.8
			(\pm 0.49)	(\pm 0.296)	(\pm 0.75)	(\pm 0.41)	(\pm 30)	(\pm 8)	(\pm 2.9)	(\pm 3.7)
GAD-02	42	F	NA	NA	NA	NA	NA	NA	NA	NA
GAD-03	26	M	1.09	0.97	4.79	3.59	105	96	47.4	37.5
			(\pm 0.29)	(\pm 0.21)	(\pm 0.78)	(\pm 0.28)	(\pm 16)	(\pm 6)	(\pm 5.2)	(\pm 2.9)
GAD-04	46	M	0.88	0.55	1.62	1.88	72	71	22.9	25.8
			(\pm 0.11)	(\pm 0.08)	(\pm 0.18)	(\pm 0.18)	(\pm 6)	(\pm 4)	(\pm 3.1)	(\pm 4.0)
GAD-05	25	M	0.62	0.59	2.48	3.76	94	144	26.3	26.2
			(\pm 0.22)	(\pm 0.23)	(\pm 0.34)	(\pm 0.62)	(\pm 13)	(\pm 20)	(\pm 2.0)	(\pm 2.0)
GAD-06	66	F	0.88	1.08	4.85	5.40	174	227	27.8	23.8
			(\pm 0.24)	(\pm 0.25)	(\pm 0.67)	(\pm 0.66)	(\pm 17)	(\pm 18)	(\pm 1.7)	(\pm 2.3)

Table shows each subject's mean results and standard deviations (\pm sd) from baseline perfusion and perfusion supplemented with gadolinium (gadobutrol) via the microdialysis catheter. *Abbreviations: see table in **Precis**.*

Supplementary Equation 7.1

Expression for T_1 of a nucleus affected by a magnetic dipole that is a distance R away:

$$\frac{1}{T_1} = \frac{9}{8} \frac{\gamma^4 \hbar}{R^6} \left(\frac{\tau_c}{1 + \omega_0^2 \tau_c^2} + \frac{4\tau_c}{1 + 4\omega_0^2 \tau_c^2} \right)$$

Where γ is the gyromagnetic ratio, \hbar is Planck's constant/ 2π , ω is the Larmor frequency of the nucleus, and $1/\tau_c$ is the frequency of molecular motion. A molecule that tumbles rapidly has a short τ_c , due to low viscosity, low molecular weight, or high temperature.

Chapter 8

Conclusions

Contents

8.1	Overview	168
8.2	Summary of results	169
8.2.1	Chapter 3 – Glucose supplementation to the traumatised human brain.....	169
8.2.2	Chapter 4 – Development of in-vivo ³¹ P MRS for human traumatic brain injury patients	170
8.2.3	Chapter 5 – ³¹ P MRS study of brain energetics and pH in the acutely traumatised human brain	170
8.2.4	Chapter 6 – Succinate supplementation to the traumatised human brain	171
8.2.5	Chapter 7 – Diffusion of small molecules from microdialysis catheters in human brain .	172
8.3	General Discussion	172
8.3.1	The application of in-vivo ³¹ P MRS and quantitative MRI T1 maps to acute human traumatic brain injury	172
8.3.2	Changes in brain energy state and pH in the acute phase of human major traumatic brain injury	173
8.3.3	Brain metabolic fuels after Traumatic Brain Injury.....	175
8.4	Future work.....	177
8.4.1	Study of brain metabolism kinetics.....	177
8.4.2	Characterising the effect of sedation.....	177
8.4.3	Gadolinium diffusion.....	178

8.1 Overview

Severe traumatic brain injury in humans causes a constellation of pathological processes in the brain that result in significant patient morbidity. Challenges of studying cerebral energy metabolism in human severe TBI includes the heterogeneity of the patient population, individuals' clinical instability, their unplanned emergency presentation, and the complexity of the organ (the brain).

In this thesis I have studied the acutely traumatised human brain's 'upstream' metabolism of glucose and its products (i.e. glycolysis and the TCA cycle) using microdialysis and ^{13}C high resolution NMR, as well as the 'downstream' end-products of metabolism, the high energy phosphates (i.e. oxidative phosphorylation), using *in-vivo* ^{31}P MR spectroscopy (**Figure 8.1**).

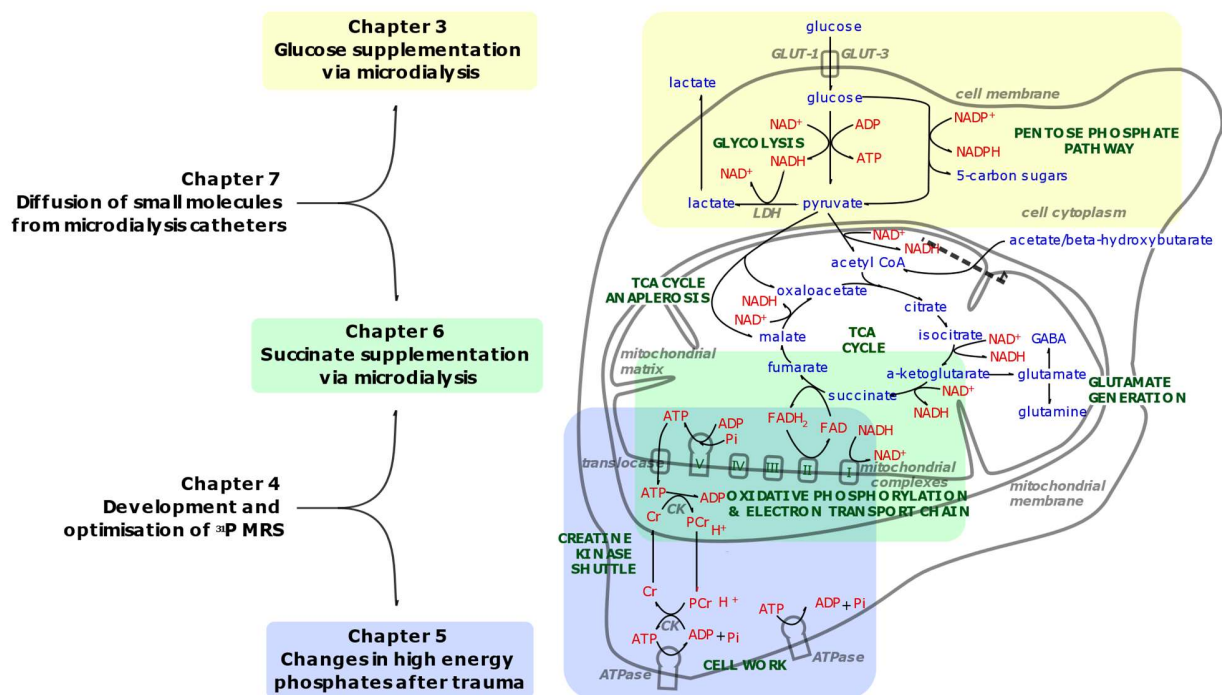


Figure 8.1. Significance of studies to cerebral metabolism after TBI

Chapter 3 studied 'upstream metabolism' by supplementing glucose to the traumatised brain. **Chapter 5** studied 'downstream metabolism' by measuring high energy phosphate ratios. **Chapter 6** explored the efficacy of succinate in TBI as a link between 'upstream metabolism' and 'downstream metabolism'.

Chapter 4 developed the *in-vivo* ^{31}P MRS technique, supporting **Chapters 5** and **6**, whilst **Chapter 7** explored diffusion of study substrates in the brain, supporting **Chapters 3** and **6**. Figure adapted from

Figure 1.6, simplified; further details see **Chapter 1**. Abbreviations: see table in **Precis**.

8.2 Summary of results

8.2.1 Chapter 3 – Glucose supplementation to the traumatised human brain

Hypothesis 1: *“Supplementing the brain with glucose directly will increase extracellular lactate and pyruvate as a sign of increased glycolytic metabolism, with evidence of further metabolism by the tricarboxylic acid cycle.*

- High-physiological concentration direct supplementation of glucose appeared to modestly support traumatised brain metabolism by increasing glycolysis – evident by increasing extracellular lactate and pyruvate.
- High-physiological concentration direct supplementation of glucose did not appear to significantly affect traumatised brain extracellular L/P ratio.
- Supra-physiological concentration direct supplementation of glucose did not appear to support brain metabolism in the same way as high-physiological supplementation; either through toxicity, negative feedback, or because of heterogeneity between patient groups.
- Direct glucose supplementation to the neuroglycopenic brain appeared to modestly support traumatised brain metabolism by increasing glycolysis – evident by increasing extracellular lactate and pyruvate.
- Directly supplementing the traumatised brain with high concentration ^{13}C labelled glucose led to only modest ^{13}C enrichment of lactate, suggesting exchange of glucose or lactate with an external pool, such as the systemic circulation, diluting the ^{13}C pool.
- Directly supplementing the brain with high concentration ^{13}C labelled glucose led to no detectable ^{13}C labelling in glutamine (a TCA cycle spin-out product), suggesting significant ^{13}C label dilution occurs during glutamine’s synthesis from glucose.
- In the traumatised human brain, glycolysis appears responsible for 88.5 % of lactate produced by metabolism of local glucose, with 11.5 % of lactate produced by pentose phosphate pathway metabolism of local glucose.
- A close correlation existed between the concentration of lactate produced by glycolysis, and the concentration of lactate produced by the pentose phosphate pathway in the traumatised human brain.

These findings support the hypothesis that supplementing the brain with glucose directly will increase extracellular lactate and pyruvate as a sign of increased glycolytic metabolism, but do not

support evidence of further metabolism by the tricarboxylic acid cycle. A likely explanation of the apparent lack of evidence of TCA cycle metabolism is dilution of ^{13}C label.

8.2.2 Chapter 4 – Development of in-vivo ^{31}P MRS for human traumatic brain injury patients

- ^{31}P MR spectra of the living human brain could be acquired using 2D chemical shift imaging with an 8 x 8 grid of 25 mm x 25 mm x 25 mm (isotropic) voxels employing weighted sampling of k-space for 18 to 35 minutes.
- In-vivo ^{31}P MRS data can be analysed with either Siemens Syngo software, or alternatively with LCMoDel software. LCMoDel analysis required a ^{31}P ‘basis set’ kindly supplied by a third party (Dr Dinesh Deelchand, University of Minnesota).
- The advantages of LCMoDel were its automated output of voxel data, and its quantitative assessment of spectra quality and fit. A disadvantage of LCMoDel is the potential uncertainty of spectra-voxel co-registration, as LCMoDel is third party software.
- The advantages of Syngo were its ability to identify individual peak widths, the option to customise fitting parameters, its dedicated workflow that overlays the voxel grid on structural sequences, and the lower noise/variance of computed results compared to LCMoDel

8.2.3 Chapter 5 – ^{31}P MRS study of brain energetics and pH in the acutely traumatised human brain

Hypothesis 2: *“The PCr/ATP ratio of the acutely traumatised brain is lower than that of healthy controls, signifying a lower energy reserve.”*

Hypothesis 3: *“The pH of the acutely traumatised brain is lower (more acidic) than that of healthy controls due to impairment of mitochondrial respiration and accumulation of lactate and H^+ ions.”*

- In-vivo ^{31}P MRS, measuring combined intracellular and extracellular ^{31}P metabolites, detected changes in high energy phosphate metabolism (PCr/ATP, PCr/total-mobile-phosphates, ATP/total-mobile-phosphates) in the acutely traumatised human brain after a significant injury. These changes appeared to be related to patients’ clinical outcomes assessed six months after the scan.
- Cerebral PCr/ATP was higher in patients suffering from acute severe traumatic brain injury than age-group matched healthy volunteers. ATP, the universal unit of chemical energy, fell after major TBI (ATP/total-mobile-phosphate) depending on patients’ outcome – and thus likely injury severity. The greatest fall in ATP occurred in patients with an unfavourable outcome at six months.

- PCr (a high-energy phosphate reserve for ATP synthesis) increased after moderate-severe TBI (PCr/total-mobile-phosphate and PCr/ATP) independently of patient outcome – and thus likely independently of injury severity.
- Cerebral pH was higher (more alkali) in patients suffering from acute severe traumatic brain injury than age-group matched healthy volunteers.
- Alkalosis of the traumatised human brain (high pH) appeared to be a predictor that a patient will have an unfavourable outcome.
- The addition of brain PCr/ATP and pH data to TBI prognostic models may improve their accuracy.

These findings do not support the hypotheses that the PCr/ATP ratio and pH of the acutely traumatised brain is lower than that of healthy controls. It must be noted that although ^{31}P MRS measures total intracellular and extracellular ^{31}P species, the intracellular compartment dominates.

8.2.4 Chapter 6 – Succinate supplementation to the traumatised human brain

Hypothesis 4: “Succinate improves (lowers) the L/P ratio of the traumatised human brain”

Hypothesis 5: “Succinate leads to an increase in brain PCr/ATP ratio, measured by in-vivo ^{31}P MRS, signifying it improves brain energy store state.”

- Direct supplementation of disodium succinate to the traumatised human brain lowered (improved) extracellular L/P ratio around its local environment.
- Direct supplementation of disodium succinate to the traumatised brain increased the cerebral PCr/ATP ratio of select patients, apparently by increasing their PCr stores.
- Direct supplementation of disodium succinate to the traumatised brain did not appear to change PCr/ATP in patients overall – but this may be due to insufficient numbers of subjects.
- After direct supplementation of disodium succinate to the traumatised human brain, an inverse correlation was found between percentage decrease in L/P ratio and percentage increase in PCr/ATP; implying a link between the parameters, and suggesting that succinate may improve cerebral energetic state in select patients.

These findings support the hypothesis that succinate lowers the L/P ratio of the traumatised human brain, and may support the hypothesis that succinate leads to an increase in brain PCr/ATP ratio, as measured by ^{31}P MRS.

8.2.5 Chapter 7 – Diffusion of small molecules from microdialysis catheters in human brain

Hypothesis 6: “Small molecules perfused via microdialysis catheters for 24 hours will diffuse in the human brain to infiltrate a 25 mm x 25 mm x 25 mm voxel of tissue (used in preceding studies).”

- Gadolinium contrast agent (gadobutrol) diffused in a broad ellipsoid of revolution up to 12 mm radially (along short axis) from the centre of microdialysis catheters in human cerebral white matter over 24 hours.
- A sharp concentration drop-off in concentration was apparent so that $\leq 50\%$ of maximum concentration could be found ≥ 4 mm away, and around 1% of maximum concentration was found 10 mm away.
- The grey matter and the grey-white matter boundary did not appear to be significant barriers to diffusion from a catheter placed in white matter.
- The relaxivity of gadobutrol in human cerebral white matter was estimated to be $1.61 \text{ L}\cdot\text{mmol}^{-1}\text{s}^{-1}$.
- The diffusion coefficient of gadobutrol in human cerebral white matter was estimated to be $9.9 \times 10^{-7} \text{ mm}^2\text{s}^{-1}$.

These findings partially support the hypothesis that small molecules perfused via microdialysis catheters for 24 hours will diffuse in the human brain to infiltrate a 25 mm x 25 mm x 25 mm voxel of tissue, but the concentration drop-off with radial distance outwards from the microdialysis catheter likely renders their effect at the periphery of such voxels negligible ($< 1\%$ of maximum concentration).

8.3 General Discussion

8.3.1 The application of in-vivo ^{31}P MRS and quantitative MRI T1 maps to acute human traumatic brain injury

In the acute phase of major traumatic brain injury, cerebral metabolic state can be interrogated with tools that provide single ‘snapshots’ of metabolism such as MRS, PET, and CT perfusion – or techniques that allow continuous assessment such as microdialysis and arteriovenous difference measurements (Carpenter *et al.*, 2015a).

^{31}P MRS is non-invasive, does not involve ionizing radiation, and directly measures whole brain tissue: encompassing the extracellular *and* intracellular components (although the intracellular compartment dominates). It can be used to measure ratios of free high energy phosphates including ATP, PCr and Pi produced by oxidative phosphorylation and the creatine kinase system – representing the brain’s

fundamental energy state. Most other modalities assess the more 'upstream' energy metabolism of glycolysis and the TCA cycle (Stovell *et al.*, 2017).

A limitation of using ^{31}P MRS in TBI is the need to transfer critically ill patients to an MR scanner. I have shown that spectra can be safely acquired and assessed simultaneously from multiple voxels in the acutely traumatised human brain, allowing both focal assessment of brain metabolism by voxel, and general assessment of brain metabolic state by summation of voxels (**Chapter 4**). It appears that *in-vivo* ^{31}P MR 2D CSI performed with 25 mm isotropic voxels is the ideal trade-off between spatial and spectral resolution for the timeframe afforded.

Microdialysis allows continuous assessment of the brain's extracellular space; thought to be linked to intracellular and thus whole-brain metabolism. Key limitations of microdialysis are its invasiveness and its focal nature; with uncertainty how its results can be extrapolated to whole brain metabolism (Carpenter *et al.*, 2015a). By using a gadolinium-based contrast agent and quantitative MR imaging I have expanded our understanding of the likely region within the human brain that microdialysis results represent (**Chapter 7**). More directly, I have characterised how agents diffuse in the brain when delivered by microdialysis that will support the study of metabolic pathways and explore potential therapeutic targets. When retromicrodialysis is used in conjunction with analytic techniques that rely on voxels or regions of interest, I found that although a 25 mm voxel is an acceptable size, a smaller 8-10 mm sized voxel would more appropriately represent cerebral tissue 'dosed' with study substrate delivered by microdialysis. However, whereas a 10 mm voxel is feasible with ^1H MRS, the signal-to-noise ratio expected from a 10 mm ^{31}P MRS voxel would be inadequate, even at 7 Tesla. In the future, extending this study to include other neuroanatomical structures, such as the deep cerebral nuclei, may allow the development of retromicrodialysis as a therapy to deliver therapeutic agents to focal pathologies found in delicate structures sensitive to the pressure and fluid shift effects of open-ended or convection-enhanced delivery catheters. This assumes that the diffusion of gadolinium contrast agent is comparable to that of other low molecular weight, water-soluble, study substrates.

8.3.2 Changes in brain energy state and pH in the acute phase of human major traumatic brain injury

Significant changes in the metabolism of glucose, lactate and oxygen that underlie cell energy generation are well reported in major traumatic brain injury (Timofeev *et al.*, 2011; Prins *et al.*, 2013; Glenn *et al.*, 2015b; Veenith *et al.*, 2016; Okonkwo *et al.*, 2017); and a high cerebral L/P ratio is

interpreted as a failure of the brain's NADH/NAD⁺ redox system, thought to be linked to brain energy state (Williamson *et al.*, 1967; Stovell *et al.*, 2018). However, this is the first time that changes in ATP – the universal biological unit of chemical energy – and its associated high energy phosphates have been demonstrated in the acute phase of major traumatic brain injury in humans.

Using ³¹P MRS, I have shown that cerebral PCr/ATP is *higher* in the acute phase of TBI than age-group matched healthy controls due to both a fall in ATP and an increase in PCr when they were expressed as percentages of total mobile phosphate (where total mobile phosphate = ATP + PCr + Pi) (**Chapter 5**). Processes that may elevate PCr/ATP include upregulation of resident microglia and migration of inflammatory cells with higher PCr/ATP ratio, and uncoupling of the CK shuttle that exchanges high energy phosphates between separate PCr and ATP pools. Whereas the increase in cerebral PCr appears independent of tissue injury severity and may be at least partly a phenomenon of anaesthesia, the fall in ATP after trauma depends on injury severity (indicated by patient outcome) and so likely represents pathology. Furthermore, changes in high energy phosphate PCr/ATP ratio appear to be linked to changes in extracellular L/P ratio, supporting the importance of L/P ratio in clinical care (**Chapter 6**) (Hutchinson *et al.*, 2015).

A disturbance of cerebral pH resulting in brain tissue alkalinisation was found in patients who had an unfavourable outcome (**Chapter 5**). This finding is in contrast to existing studies that report acidosis of the brain's extracellular interstitium (Zygun *et al.*, 2004; Timofeev *et al.*, 2013). Brain alkalosis may be due to an upregulation of inflammatory cells linked to changes in PCr/ATP ratio, or be a mechanism that astrocytes use to increase their glycolytic activity. However, the strong association between pH derangement and unfavourable outcome suggests it is an important metabolic phenomenon.

Changes in high energy phosphate metabolism and pH in radiologically uninjured brain imply a generalised derangement of brain metabolism occurs after major TBI, rather than pathophysiology limited to focal macroscopic areas of radiological injury (**Chapter 5**), as they persisted when voxels with significant injury were excluded from analysis.

Furthermore, these findings suggest that *in-vivo* ³¹P MRS has clinical potential, to identify patients with occult metabolic injury forecasting unfavourable outcome, so attempts can be made to avert their course with alternative metabolic support, as well as supporting more accurate prognostication. A larger study designed and powered to predict outcome is required to help discern the clinical role of ³¹P MRS in the acute phase of major TBI. By studying non-TBI controls who happen to be undergoing sedation for

non-neurological pathology, any influence of sedation on PCr/ATP ratio and pH can also be ascertained, or excluded as a confounder. A more automated acquisition and analysis of ^{31}P spectra is also required, using multi-slice CSI technology that acquires multiple voxel grids with a modest increase in acquisition time.

8.3.3 Brain metabolic fuels after Traumatic Brain Injury

Glucose is conventionally regarded as the primary substrate for brain energy metabolism (**Chapter 1**) (Prins *et al.*, 2013; Jalloh *et al.*, 2015b). However, it remains unclear how cerebral glucose metabolism in the acute phase of TBI can be optimised, and what the brain does with the glucose delivered to it: whether individual cells fully metabolise each molecule of glucose by glycolysis followed by the TCA cycle, or if this process is shared between cells, or cell types, as proposed by the astrocyte-neuron lactate shuttle hypothesis.

Direct glucose supplementation to the traumatised human brain may modestly support metabolism by increasing cellular glycolysis, evident by an increase in its extracellular products lactate and pyruvate; particularly evident in the neuroglycopenic brain (**Chapter 3**). Supplementing glucose at supra-physiological concentrations may conversely cause metabolic inhibition – although this trend may be due to heterogeneity between patients and their brains' underlying ability to metabolise glucose due to injury severity. Glycolytic lactate production was found to be the dominant local metabolic fate of glucose metabolism, with a much smaller proportion of lactate produced via the PPP. However, changes in glycolysis and PPP appeared co-ordinated, as there was a close positive linear correlation between glycolysis-derived lactate and PPP-derived lactate with a molecular ratio of 2,3- $^{13}\text{C}_2$ lactate to 3- ^{13}C lactate of 6.8 : 1.

In addition to glucose, the brain can directly metabolise lactate as a fuel. The modest ^{13}C enrichment of lactate despite such high ^{13}C glucose enrichment (**Chapter 3**) suggests significant exchange of the brain's extracellular lactate pool with the systemic circulation. Furthermore, the absence of ^{13}C enrichment in glutamine in the 1,2- $^{13}\text{C}_2$ glucose supplementation studies, in contrast to the production of ^{13}C -glutamine when ^{13}C lactate is supplemented (Gallagher *et al.*, 2009; Jalloh *et al.*, 2018) implies that this extracellular lactate pool is integral to glutamine synthesis, and possibly that of its related neurotransmitters glutamate and GABA.

Succinate is unique as both a TCA cycle intermediate and step in the electron transport chain of oxidative phosphorylation (**Chapter 1**). Succinate supplementation to the traumatised human brain appears to support cerebral metabolism by promoting mitochondrial function through complex II; thereby reducing the extracellular L/P ratio, a marker of cell NADH/NAD⁺ redox state (Williamson *et al.*, 1967). Although succinate supplementation did not change cerebral PCr/ATP ratio overall (**Chapter 7**), there was a trend towards an increase in PCr/ATP and PCr/total-mobile-phosphates which may reach significance in a larger study. Moreover, there was a significant inverse relationship between percentage change in PCr/ATP ratio and percentage change in L/P ratio, resulting from succinate supplementation, i.e. PCr/ATP increase was associated with L/P decrease (Stovell *et al.*, 2018).

Supporting cerebral metabolism in patients in the acute phase of a major TBI may include intravenous supplementation of glucose in patients whose glycolytic function is not impaired – realised by a corresponding rise in extracellular lactate and pyruvate measured by microdialysis. However, the importance of extracellular lactate as a metabolic intermediate promotes hypertonic lactate infusion as an additional metabolic supplement to glucose (Quintard *et al.*, 2016). Succinate appears to have a varied metabolic response in different individuals, so identifying patients who are most likely to benefit appears key. This may involve multimodality monitoring with microdialysis to identify patients with a high L/P ratio in the absence of tissue hypoxia and cerebral hypoperfusion that suggests primary mitochondrial dysfunction. The use of succinate as a metabolic rescue therapy in major TBI patients would require systemic administration at a dose sufficient to penetrate the brain and influence its metabolism without causing systemic or cerebral side effects

Given the intrinsic heterogeneity of major TBI and its patient population, relatively large sample sizes are required to draw confident conclusions. The number of subjects recruited to these studies were acceptable for exploratory microdialysis studies but would require greater numbers for a clinical trial. Furthermore, expanding the use of ³¹P MRS to studies of glucose supplementation would ascertain whether the apparent glycolytic support was associated with changes in brain high energy phosphates.

8.4 Future work

8.4.1 Study of brain metabolism kinetics

In this thesis the changes in the concentrations of cerebral metabolites imply a change in metabolic flux, but do not measure such rates directly.

Dynamic *in-vivo* ^{13}C MRS studies can measure rates of cerebral glucose uptake, glycolysis, the TCA cycle and glutamine/glutamate cycling by intravenously infusing ^{13}C glucose and measuring the concentration of ^{13}C in the metabolites over time (de Graaf *et al.*, 2011; Rothman *et al.*, 2011). These studies are challenging due to the high cost of large amounts of ^{13}C isotopes, as well as the need for tight control of hyperglycaemia in MR scanners whilst avoiding dangerous overshoots into hypoglycaemia and extreme hyperglycaemia.

The benefit of administering ^{13}C glucose intravenously instead of via microdialysis is minimising contamination by systemic circulating glucose as its mobilisation is suppressed. Furthermore, using *in-vivo* MRS measures whole-tissue metabolism, rather than *in-vitro* NMR analysis of extracellular samples 'off-line'.

I have designed an experiment to measure the rate of cerebral 1) glucose uptake, 2) glycolysis, 3) the TCA cycle, and 4) glutamate-glutamine cycling in patients in the acute phase of major TBI, and comparing them to awake and sedated age-group matched healthy controls.

I hypothesise that, when compared to sedated healthy brain, TBI:

- Impedes brain metabolic function, particularly the TCA cycle, in both neurones and glia.
- Disrupts normal glutamate/glutamine cycling.
- Influences the proportion of glucose entering the TCA cycle via anaplerosis.

I hypothesise that, when compared to awake healthy volunteers, sedation:

- Reduces the metabolic rate of the TCA cycle, in both neurones and glia.
- Reduces the rate of glutamate/glutamine cycling.

The clinical study protocol and successful application for ethical approval is in **Chapter 10 (Appendix)**.

8.4.2 Characterising the effect of sedation

Existing studies of cerebral metabolism in acute, sedated TBI patients have typically used awake, healthy volunteers as controls. The effects of sedation and anaesthesia in patients is either ignored or has to be accepted as a potential confounder. By including subjects who have been sedated for pathology unrelated to cerebral metabolism in a future *in-vivo* dynamic ^{13}C MRS study (see 8.4.1 above, and

Appendix 2 & 3), a more meaningful comparison can be made to attribute changes directly to TBI, rather than the combined effects of TBI, sedation, and mechanical ventilation. The addition of *in-vivo* 'static' ^{31}P MRS to the imaging protocol (**Appendix 2**) allows further analysis and comparison of **Chapter 5's** results. Furthermore, the mechanism of action of sedation and general anaesthetic drugs and their effect on the human brain can be explored. Understanding the effects of sedation on both 'upstream metabolism' using *in-vivo* ^{13}C MRS and 'downstream metabolism' of high energy phosphates using *in-vivo* ^{31}P MRS in healthy volunteers is also relevant to clinicians who use sedative and anaesthetic agents.

I hypothesise that, when compared to sedated healthy brain, TBI:

- Impedes exchange of high energy phosphate species in the human brain.
- Reduces the pool of available adenosine nucleotide bases resulting in a change in the PCr / ATP ratio.

I hypothesise that, when compared to awake healthy volunteers, sedation:

- Reduces exchange of high energy phosphate species in the human brain.
- Has no effect on the PCr/ATP ratio in the human brain.

8.4.3 Gadolinium diffusion

The diffusion pattern of gadolinium contrast agent (gadobutrol) from microdialysis catheters was measured in two dimensions using multiple linear profiles perpendicular to the catheters. This could be extended to measure a three-dimensional diffusion volume. It would be difficult to accurately ascertain the diffusion distance of very low concentrations of gadobutrol due to subtle variation in the baseline T1 of white matter and grey matter, but it is expected that anything greater than 10 % of maximum concentration could be adequately modelled. Repeating the experiment perfusing gadobutrol for 48 hours and confirming no further shortening of tissue T1 beyond the results of **Chapter 7** would determine that a steady state gadobutrol concentration had been achieved; and that the relaxivity of gadobutrol in human white matter was accurately estimated. Furthermore, by studying the diffusion of catheters directed into cortical grey matter and the deep cerebral nuclei would characterise diffusion in structures that are potential targets for new pharmacological trials. Thus, microdialysis could be developed into a method of targeted therapy delivery. This experiment will require a 'substantial amendment' to the existing ethical approval and study protocol.

Chapter 9

References

- Aime S, Caravan P. Biodistribution of gadolinium-based contrast agents, including gadolinium deposition. *J. Magn. Reson. Imaging* 2009; 30: 1259–1267.
- Alves PM, Fonseca LL, Peixoto CC, Almeida AC, Carrondo MJ, Santos H. NMR studies on energy metabolism of immobilized primary neurons and astrocytes during hypoxia, ischemia and hypoglycemia. *NMR Biomed.* 2000; 13: 438–48.
- Aries MJH, Czosnyka M, Budohoski KP, Steiner LA, Lavinio A, Koliak AG, et al. Continuous determination of optimal cerebral perfusion pressure in traumatic brain injury. *Crit. Care Med.* 2012; 40: 2456–63.
- Bartnik BL, Lee SM, Hovda DA, Sutton RL. The fate of glucose during the period of decreased metabolism after fluid percussion injury: a ¹³C NMR study. *J. Neurotrauma* 2007; 24: 1079–92.
- Bartnik BL, Sutton RL, Fukushima M, Harris NG, Hovda D a, Lee SM. Upregulation of pentose phosphate pathway and preservation of tricarboxylic acid cycle flux after experimental brain injury. *J. Neurotrauma* 2005; 22: 1052–65.
- Bates D, Mächler M, Bolker B, Walker S. Fitting Linear Mixed-Effects Models Using lme4. *J. Stat. Softw.* 2015; 67
- Bates MGD, Hollingsworth KG, Newman JH, Jakovljevic DG, Blamire AM, MacGowan GA, et al. Concentric hypertrophic remodelling and subendocardial dysfunction in mitochondrial DNA point mutation carriers. *Eur. Heart J. Cardiovasc. Imaging* 2013; 14: 650–8.
- Bauer K, Lathrum A, Raslan O, Kelly P V., Zhou Y, Hewing D, et al. Do Gadolinium-Based Contrast Agents Affect ¹⁸F-FDG PET/CT Uptake in the Dentate Nucleus and the Globus Pallidus? A Pilot Study. *J. Nucl. Med. Technol.* 2017; 45: 30–33.
- Becher B, Spath S, Goverman J. Cytokine networks in neuroinflammation. *Nat. Rev. Immunol.* 2017; 17: 49–59.
- Bellin M-F, Van Der Molen AJ. Extracellular gadolinium-based contrast media: an overview. *Eur. J. Radiol.* 2008; 66: 160–7.
- Berg JM (Jeremy M, Tymoczko JL, Stryer L, Stryer L. *Biochemistry*. 5th ed. New York: W.H. Freeman; 2002.
- Bergeron MJ, Cléménçon B, Hediger MA, Markovich D. SLC13 family of Na⁺-coupled di- and tri-carboxylate/sulfate transporters. *Mol. Aspects Med.* 2013; 34: 299–312.
- van den Berghe G, Wouters P, Weekers F, Verwaest C, Bruyninckx F, Schetz M, et al. Intensive insulin therapy in critically ill patients. *N. Engl. J. Med.* 2001; 345: 1359–67.
- Bergsneider M, Hovda D a, Shalmon E, Kelly DF, Vespa PM, Martin N a, et al. Cerebral hyperglycolysis following severe traumatic brain injury in humans: a positron emission tomography study. *J. Neurosurg.* 1997; 86: 241–251.
- Bouzat P, Sala N, Suys T, Zerlauth J-B, Marques-Vidal P, Feihl F, et al. Cerebral metabolic effects of exogenous lactate supplementation on the injured human brain. *Intensive Care Med.* 2014; 40: 412–421.
- Bouzier-Sore A-K, Voisin P, Canioni P, Magistretti PJ, Pellerin L. Lactate is a preferential oxidative energy substrate over glucose for neurons in culture. *J. Cereb. Blood Flow Metab.* 2003; 23: 1298–306.
- Brand A, Richter-Landsberg C, Leibfritz D. Multinuclear NMR studies on the energy metabolism of glial and neuronal cells. *Dev. Neurosci.* 1993; 15: 289–98.
- Brant-Zawadzki M, Gillan GD, Nitz WR. MP RAGE: a three-dimensional, T1-weighted, gradient-echo sequence—initial experience in the brain. *Radiology* 1992; 182: 769–75.
- Burda JE, Sofroniew M V. Reactive gliosis and the multicellular response to CNS damage and disease. *Neuron* 2014; 81: 229–48.
- Cantaert T, Baeten D, Tak PP, van Baarsen LGM. Type I IFN and TNF α cross-regulation in immune-mediated inflammatory disease: basic concepts and clinical relevance. *Arthritis Res. Ther.* 2010; 12: 219.
- Carpenter KLH, Czosnyka M, Jalloh I, Newcombe VFJ, Helmy A, Shannon RJ, et al. Systemic, local, and imaging biomarkers of brain injury: more needed, and better use of those already established? *Front. Neurol.* 2015a; 6: 26.

- Carpenter KLH, Jalloh I, Gallagher CN, Grice P, Howe DJ, Mason A, et al. 13C-labelled microdialysis studies of cerebral metabolism in TBI patients. *Eur. J. Pharm. Sci.* 2014; 57: 87–97.
- Carpenter KLH, Jalloh I, Hutchinson PJ. Glycolysis and the significance of lactate in traumatic brain injury. *Front. Neurosci.* 2015b; 9: 112.
- Carpentier A, Galanaud D, Puybasset L, Muller J-C, Lescot T, Boch A-L, et al. Early Morphologic and Spectroscopic Magnetic Resonance in Severe Traumatic Brain Injuries Can Detect “Invisible Brain Stem Damage” and Predict “Vegetative States”. *J. Neurotrauma* 2006; 23: 674–685.
- Cavassila S, Deval S, Huegen C, van Ormondt D, Graveron-Demilly D. Cramér-Rao Bound Expressions for Parametric Estimation of Overlapping Peaks: Influence of Prior Knowledge. *J. Magn. Reson.* 2000; 143: 311–320.
- Cavassila S, Deval S, Huegen C, van Ormondt D, Graveron-Demilly D. Cramér-Rao bounds: an evaluation tool for quantitation. *NMR Biomed.* 2001; 14: 278–83.
- Chance B, Eleff S, Leigh JS. Noninvasive, nondestructive approaches to cell bioenergetics. *Proc. Natl. Acad. Sci. U. S. A.* 1980; 77: 7430–7434.
- Chen Z-J, Gillies GT, Broaddus WC, Prabhu SS, Fillmore H, Mitchell RM, et al. A realistic brain tissue phantom for intraparenchymal infusion studies. *J. Neurosurg.* 2004; 101: 314–322.
- Cheng H-LM, Wright GA. Rapid high-resolution T(1) mapping by variable flip angles: accurate and precise measurements in the presence of radiofrequency field inhomogeneity. *Magn. Reson. Med.* 2006; 55: 566–74.
- Chesler M. Regulation and modulation of pH in the brain. *Physiol. Rev.* 2003; 83: 1183–221.
- Chesler M, Kraig RP. Intracellular pH transients of mammalian astrocytes. *J. Neurosci.* 1989; 9: 2011–9.
- Chiche J, Le Fur Y, Vilmen C, Frassinetti F, Daniel L, Halestrap AP, et al. In vivo pH in metabolic-defective Ras-transformed fibroblast tumors: key role of the monocarboxylate transporter, MCT4, for inducing an alkaline intracellular pH. *Int. J. cancer* 2012; 130: 1511–20.
- Chopp M, Chen H, Vande Linde AMQ, Brown E, Welch KMA. Time course of postischemic intracellular alkalosis reflects the duration of ischemia. *J. Cereb. Blood Flow Metab.* 1990; 10: 860–5.
- Chouchani ET, Pell VR, Gaude E, Aksentijević D, Sundier SY, Robb EL, et al. Ischaemic accumulation of succinate controls reperfusion injury through mitochondrial ROS. *Nature* 2014; 515: 431–435.
- Coles JP. Imaging after brain injury. *Br. J. Anaesth.* 2007; 99: 49–60.
- Das KC. Hyperoxia Decreases Glycolytic Capacity, Glycolytic Reserve and Oxidative Phosphorylation in MLE-12 Cells and Inhibits Complex I and II Function, but Not Complex IV in Isolated Mouse Lung Mitochondria. *PLoS One* 2013; 8: e73358.
- Deelchand DK, Nguyen TM, Zhu XH, Mochel F, Henry PG. Quantification of in vivo ³¹P NMR brain spectra using LCModel. *NMR Biomed.* 2015; 28: 633–641.
- DeVience SJ, Lu X, Proctor J, Rangghran P, Melhem ER, Gullapalli R, et al. Metabolic imaging of energy metabolism in traumatic brain injury using hyperpolarized [1-¹³C]pyruvate. *Sci. Rep.* 2017; 7: 1907.
- Dienel GA, Rothman DL, Nordström C-H. Microdialysate concentration changes do not provide sufficient information to evaluate metabolic effects of lactate supplementation in brain-injured patients. *J. Cereb. Blood Flow Metab.* 2016; 36: 1844–1864.
- DiSabato DJ, Quan N, Godbout JP. Neuroinflammation: the devil is in the details. *J. Neurochem.* 2016; 139 Suppl: 136–153.
- Donnelly J, Czosnyka M, Sudhan N, Varsos G V., Nasr N, Jalloh I, et al. Increased blood glucose is related to disturbed cerebrovascular pressure reactivity after traumatic brain injury. *Neurocrit. Care* 2015; 22: 20–5.
- Eleff SM, Barker PB, Blackband SJ, Chatham JC, Lutz NW, Johns DR, et al. Phosphorus magnetic resonance spectroscopy of patients with mitochondrial cytopathies demonstrates decreased levels of brain phosphocreatine. *Ann. Neurol.* 1990; 27: 626–30.
- Engelter ST, Provenzale JM, Petrella JR, DeLong DM, MacFall JR. The effect of aging on the apparent diffusion coefficient of

- normal-appearing white matter. *AJR. Am. J. Roentgenol.* 2000; 175: 425–30.
- Erecinska M, Silver IA. ATP and Brain Function. *J. Cereb. Blood Flow Metab.* 1989; 2–19.
- Falkowska A, Gutowska I, Goschorska M, Nowacki P, Chlubek D, Baranowska-Bosiacka I. Energy Metabolism of the Brain, Including the Cooperation between Astrocytes and Neurons, Especially in the Context of Glycogen Metabolism. *Int. J. Mol. Sci.* 2015; 16: 25959–25981.
- Farkas O, Lifshitz J, Povlishock JT. Mechanoporation induced by diffuse traumatic brain injury: an irreversible or reversible response to injury? *J. Neurosci.* 2006; 26: 3130–40.
- Fredriksson R, Lagerström MC, Lundin L-G, Schiöth HB. The G-protein-coupled receptors in the human genome form five main families. Phylogenetic analysis, paralogon groups, and fingerprints. *Mol. Pharmacol.* 2003; 63: 1256–72.
- Frenzel T, Lengsfeld P, Schirmer H, Hütter J, Weinmann H-J. Stability of gadolinium-based magnetic resonance imaging contrast agents in human serum at 37 degrees C. *Invest. Radiol.* 2008; 43: 817–28.
- Friedman SD, Brooks WM, Jung RE, Hart BL, Yeo R a. Proton MR spectroscopic findings correspond to neuropsychological function in traumatic brain injury. *AJNR. Am. J. Neuroradiol.* 1998; 19: 1879–85.
- Friedman SD, Jensen JE, Frederick BB, Artru AA, Renshaw PF, Dager SR. Brain Changes to Hypocapnia Using Rapidly Interleaved Phosphorus-Proton Magnetic Resonance Spectroscopy at 4 T. *J. Cereb. Blood Flow Metab.* 2007; 27: 646–653.
- Gabr RE, El-Sharkawy A-MM, Schär M, Weiss RG, Bottomley PA. High-energy phosphate transfer in human muscle: diffusion of phosphocreatine. *Am. J. Physiol. Cell Physiol.* 2011; 301: C234-41.
- Gallagher CN, Carpenter KLH, Grice P, Howe DJ, Mason a., Timofeev I, et al. The human brain utilizes lactate via the tricarboxylic acid cycle: a ¹³C-labelled microdialysis and high-resolution nuclear magnetic resonance study. *Brain* 2009; 132: 2839–2849.
- Garnett MR, Blamire AM, Corkill RG, Cadoux-Hudson T a, Rajagopalan B, Styles P. Early proton magnetic resonance spectroscopy in normal-appearing brain correlates with outcome in patients following traumatic brain injury. *Brain* 2000; 123 (Pt 1: 2046–54.
- Garnett MR, Corkill RG, Blamire a M, Rajagopalan B, Manners DN, Young JD, et al. Altered cellular metabolism following traumatic brain injury: a magnetic resonance spectroscopy study. *J. Neurotrauma* 2001; 18: 231–240.
- Gilissen J, Jouret F, Pirotte B, Hanson J. Insight into SUCNR1 (GPR91) structure and function. *Pharmacol. Ther.* 2016; 159: 56–65.
- Giorgi-Coll S, Amaral AI, Hutchinson PJA, Kotter MR, Carpenter KLH. Succinate supplementation improves metabolic performance of mixed glial cell cultures with mitochondrial dysfunction. *Sci. Rep.* 2017; 7: 1003.
- Glenn TC, Kelly DF, Boscardin WJ, McArthur DL, Vespa P, Oertel M, et al. Energy dysfunction as a predictor of outcome after moderate or severe head injury: indices of oxygen, glucose, and lactate metabolism. *J. Cereb. Blood Flow Metab.* 2003; 23: 1239–50.
- Glenn TC, Martin N a., McArthur DL, Hovda D a., Vespa P, Johnson ML, et al. Endogenous Nutritive Support after Traumatic Brain Injury: Peripheral Lactate Production for Glucose Supply via Gluconeogenesis. *J. Neurotrauma* 2015a; 32: 811–819.
- Glenn TC, Martin N, Horning M., McArthur DL, Hovda D, Vespa P, et al. Lactate: brain fuel in human traumatic brain injury: a comparison with normal healthy control subjects. *J. Neurotrauma* 2015b; 32: 820–32.
- Glick D, Barth S, Macleod KF. Autophagy : cellular and molecular mechanisms. *J. Pathol.* 2010; 221: 3–12.
- de Graaf R, Rothman DL, Behar KL. State of the art direct ¹³C and indirect ¹H-[¹³C] NMR spectroscopy in vivo. A practical guide. *NMR Biomed.* 2011; 24: 958–72.
- de Graaf RA. *In Vivo NMR Spectroscopy*. 2nd ed. Chichester, UK: John Wiley & Sons, Ltd; 2007.
- de Graaf RA, Mason GF, Patel AB, Behar KL, Rothman DL. In vivo ¹H-[¹³C]-NMR spectroscopy of cerebral metabolism. *NMR Biomed.* 2003; 16: 339–357.
- Gulani V, Calamante F, Shellock FG, Kanal E, Reeder SB, International Society for Magnetic Resonance in Medicine. Gadolinium deposition in the brain: summary of evidence and recommendations. *Lancet. Neurol.* 2017; 16: 564–570.

- Gupta AK, Zygun DA, Johnston AJ, Steiner LA, Al-Rawi PG, Chatfield D, et al. Extracellular Brain pH and Outcome following Severe Traumatic Brain Injury. *J. Neurotrauma* 2004; 21: 678–84.
- Hamel D, Sanchez M, Duhamel F, Roy O, Honoré J-C, Noueihed B, et al. G-protein-coupled receptor 91 and succinate are key contributors in neonatal postcerebral hypoxia-ischemia recovery. *Arterioscler. Thromb. Vasc. Biol.* 2014; 34: 285–93.
- Hanson LG. Is quantum mechanics necessary for understanding magnetic resonance? *Concepts Magn. Reson. Part A* 2008; 32A: 329–340.
- Harish G, Mahadevan A, Pruthi N, Sreenivasamurthy SK, Puttamallesh VN, Keshava Prasad TS, et al. Characterization of traumatic brain injury in human brains reveals distinct cellular and molecular changes in contusion and pericontusion. *J. Neurochem.* 2015; 134: 156–72.
- Hartree W, Hill A V. The anaerobic processes involved in muscular activity. *J. Physiol.* 1923; 58: 127–37.
- Hattori N, Huang S, Wu H, Yeh E, Glenn TC, Vespa PM, et al. Correlation of Regional Metabolic Rates of Glucose with Glasgow Coma Scale After Traumatic Brain Injury. *J. Nucl. Med.* 2003; 44: 1709–1716.
- Havsteen I, Ohlhues A, Madsen KH, Nybing JD, Christensen H, Christensen A. Are Movement Artifacts in Magnetic Resonance Imaging a Real Problem?-A Narrative Review. *Front. Neurol.* 2017; 8: 232.
- Heiss JD, Walbridge S, Asthagiri AR, Lonser RR. Image-guided convection-enhanced delivery of muscimol to the primate brain. *J. Neurosurg.* 2010; 112: 790–5.
- Helmy A, Carpenter KLH, Menon DK, Pickard JD, Hutchinson PJ a. The cytokine response to human traumatic brain injury: temporal profiles and evidence for cerebral parenchymal production. *J. Cereb. Blood Flow Metab.* 2011; 31: 658–670.
- Helmy A, Carpenter KLH, Skepper JN, Kirkpatrick PJ, Pickard JD, Hutchinson PJ. Helmy et al. - 2009 - Microdialysis of cytokines methodological considerations, scanning electron microscopy, and determination of relative recovery.pdf. 2009; 13: 1–13.
- Hermanides J, Plummer MP, Finnis M, Deane AM, Coles JP, Menon DK. Glycaemic control targets after traumatic brain injury: a systematic review and meta-analysis. *Crit. Care* 2018; 22: 11.
- Hertz L, Peng L, Dienel GA. Energy Metabolism in Astrocytes: High Rate of Oxidative Metabolism and Spatiotemporal Dependence on Glycolysis/Glycogenolysis. *J. Cereb. Blood Flow Metab.* 2007; 27: 219–249.
- Hertz L, Xu J, Song D, Du T, Li B, Yan E, et al. Astrocytic glycogenolysis: mechanisms and functions. *Metab. Brain Dis.* 2015; 30: 317–333.
- Hetherington HP, Spencer DD, Vaughan JT, Pan JW. Quantitative ³¹P spectroscopic imaging of human brain at 4 Tesla: Assessment of gray and white matter differences of phosphocreatine and ATP. *Magn. Reson. Med.* 2001; 45: 46–52.
- Hillered L, Valtysson J, Enblad P, Persson L. Interstitial glycerol as a marker for membrane phospholipid degradation in the acutely injured human brain. *J. Neurol. Neurosurg. Psychiatry* 1998; 64: 486–91.
- Hillman J, Aneman O, Anderson C, Sjögren F, Säberg C, Mellergård P. A microdialysis technique for routine measurement of macromolecules in the injured human brain. *Neurosurgery* 2005; 56: 1264–8; discussion 1268–70.
- Hlatky R, Valadka AB, Goodman JC, Contant CF, Robertson CS. Patterns of energy substrates during ischemia measured in the brain by microdialysis. *J. Neurotrauma* 2004; 21: 894–906.
- Hochachka PW, Clark CM, Holden JE, Stanley C, Ugurbil K, Menon RS. ³¹P magnetic resonance spectroscopy of the Sherpa heart: a phosphocreatine/adenosine triphosphate signature of metabolic defense against hypobaric hypoxia. *Proc. Natl. Acad. Sci. U. S. A.* 1996; 93: 1215–20.
- Hoult DI. The Origins and Present Status of the Radio Wave Controversy in NMR. *Concepts Magn. Reson. Part A* 2009; 34: 193–216.
- Hu MT, Taylor-Robinson SD, Chaudhuri KR, Bell JD, Labbé C, Cunningham VJ, et al. Cortical dysfunction in non-demented Parkinson's disease patients: a combined (³¹P)-MRS and (¹⁸F)FDG-PET study. *Brain* 2000; 123 (Pt 2: 340–52.
- Hui S, Ghergurovich JM, Morscher RJ, Jang C, Teng X, Lu W, et al. Glucose feeds the TCA cycle via circulating lactate. *Nature* 2017; 551: 115–118.

- Hutchinson PJ, Gupta AK, Fryer TF, Al-Rawi PG, Chatfield D a, Coles JP, et al. Correlation between cerebral blood flow, substrate delivery, and metabolism in head injury: a combined microdialysis and triple oxygen positron emission tomography study. *J. Cereb. Blood Flow Metab.* 2002; 22: 735–745.
- Hutchinson PJ, Jalloh I, Helmy A, Carpenter KLH, Rostami E, Bellander B-M, et al. Consensus statement from the 2014 International Microdialysis Forum. *Intensive Care Med.* 2015; 41: 1517–28.
- Hutchinson PJ, Koliass AG, Timofeev IS, Corteen EA, Czosnyka M, Timothy J, et al. Trial of Decompressive Craniectomy for Traumatic Intracranial Hypertension. *N. Engl. J. Med.* 2016; 375: 1119–30.
- Hutchinson PJ, O'Connell MT, Seal A, Nortje J, Timofeev I, Al-Rawi PG, et al. A combined microdialysis and FDG-PET study of glucose metabolism in head injury. *Acta Neurochir. (Wien).* 2009; 151: 51–61.
- Ichai C, Armando G, Orban J-C, Berthier F, Rami L, Samat-Long C, et al. Sodium lactate versus mannitol in the treatment of intracranial hypertensive episodes in severe traumatic brain-injured patients. *Intensive Care Med.* 2009; 35: 471–9.
- Ichai C, Payen J-F, Orban J-C, Quintard H, Roth H, Legrand R, et al. Half-molar sodium lactate infusion to prevent intracranial hypertensive episodes in severe traumatic brain injured patients: a randomized controlled trial. *Intensive Care Med.* 2013; 39: 1413–1422.
- Italiani P, Boraschi D. From Monocytes to M1/M2 Macrophages: Phenotypical vs. Functional Differentiation. *Front. Immunol.* 2014; 5: 514.
- Jacobus WE. Theoretical support for the heart phosphocreatine energy transport shuttle based on the intracellular diffusion limited mobility of ADP. *Biochem. Biophys. Res. Commun.* 1985; 133: 1035–1041.
- Jäkel S, Dimou L. Glial Cells and Their Function in the Adult Brain: A Journey through the History of Their Ablation. *Front. Cell. Neurosci.* 2017; 11: 24.
- Jalloh I, Carpenter KLH, Grice P, Howe DJ, Mason A, Gallagher CN, et al. Glycolysis and the pentose phosphate pathway after human traumatic brain injury: microdialysis studies using 1,2-(13)C2 glucose. *J. Cereb. Blood Flow Metab.* 2015a; 35: 111–20.
- Jalloh I, Carpenter KLH, Helmy A, Carpenter TA, Menon DK, Hutchinson PJ. Glucose metabolism following human traumatic brain injury: methods of assessment and pathophysiological findings. *Metab. Brain Dis.* 2015b; 30: 615–632.
- Jalloh I, Helmy A, Howe DJ, Shannon RJ, Grice P, Mason A, et al. Focally perfused succinate potentiates brain metabolism in head injury patients. *J. Cereb. Blood Flow Metab.* 2017; 37: 2626–2638.
- Jalloh I, Helmy A, Howe DJ, Shannon RJ, Grice P, Mason A, et al. A Comparison of Oxidative Lactate Metabolism in Traumatically Injured Brain and Control Brain. *J. Neurotrauma* 2018; 35: 2025–2035.
- Jalloh I, Helmy A, Shannon RJ, Gallagher CN, Menon DK, Carpenter KLH, et al. Lactate Uptake by the Injured Human Brain: Evidence from an Arteriovenous Gradient and Cerebral Microdialysis Study. *J. Neurotrauma* 2013; 30: 2031–2037.
- Jauch-Chara K, Oltmanns KM. Glycemic control after brain injury: boon and bane for the brain. *Neuroscience* 2014; 283: 202–9.
- Jennett B, Bond M. Assessment of outcome after severe brain damage. *Lancet (London, England)* 1975; 1: 480–4.
- Jennett B, Snoek J, Bond MR, Brooks N. Disability after severe head injury: observations on the use of the Glasgow Outcome Scale. *J. Neurol. Neurosurg. Psychiatry* 1981; 44: 285–93.
- Kan HE, Techawiboonwong A, van Osch MJP, Versluis MJ, Deelchand DK, Henry P-G, et al. Differences in apparent diffusion coefficients of brain metabolites between grey and white matter in the human brain measured at 7 T. *Magn. Reson. Med.* 2012; 67: 1203–9.
- Keevil SF. Spatial localization in nuclear magnetic resonance spectroscopy. *Phys. Med. Biol.* 2006; 51: R579-636.
- Kekuda R, Wang H, Huang W, Pajor AM, Leibach FH, Devoe LD, et al. Primary structure and functional characteristics of a mammalian sodium-coupled high affinity dicarboxylate transporter. *J. Biol. Chem.* 1999; 274: 3422–9.
- Kilinc D, Gallo G, Barbee KA. Mechanically-induced membrane poration causes axonal beading and localized cytoskeletal damage. *Exp. Neurol.* 2008; 212: 422–30.
- Killen MJ, Giorgi-Coll S, Helmy A, Hutchinson PJA, Carpenter KLH. Metabolism and inflammation: implications for traumatic

- brain injury therapeutics. *Expert Rev. Neurother.* 2019; 19: 227–242.
- Kimelberg HK. Functions of mature mammalian astrocytes: a current view. *Neuroscientist* 2010; 16: 79–106.
- Koh TS, Hartono S, Thng CH, Lim TKH, Martarello L, Ng QS. In vivo measurement of gadolinium diffusivity by dynamic contrast-enhanced MRI: a preclinical study of human xenografts. *Magn. Reson. Med.* 2013; 69: 269–76.
- Komoroski RA, Pearce JM, Mrak RE. 31P NMR spectroscopy of phospholipid metabolites in postmortem schizophrenic brain. *Magn. Reson. Med.* 2008; 59: 469–474.
- Lamp J, Keyser B, Koeller DM, Ullrich K, Bräulke T, Mühlhausen C. Glutaric Aciduria Type 1 Metabolites Impair the Succinate Transport from Astrocytic to Neuronal Cells. *J. Biol. Chem.* 2011; 286: 17777–17784.
- Lee S-Y, Kim SS, Kim C-H, Park S-W, Park JH, Yeo M. Prediction of outcome after traumatic brain injury using clinical and neuroimaging variables. *J. Clin. Neurol.* 2012; 8: 224–9.
- Levine SR, Helpert JA, Welch KM, Vande Linde AM, Sawaya KL, Brown EE, et al. Human focal cerebral ischemia: evaluation of brain pH and energy metabolism with P-31 NMR spectroscopy. *Radiology* 1992; 185: 537–44.
- Liesz A, Dalpke A, Mracsko E, Antoine DJ, Roth S, Zhou W, et al. Erratum: Liesz et al., ‘DAMP Signaling Is a Key Pathway Inducing Immune Modulation after Brain Injury’. *J. Neurosci.* 2019; 39: 5419.
- Lin EC. Glycerol utilization and its regulation in mammals. *Annu. Rev. Biochem.* 1977; 46: 765–95.
- Littlewood-Evans A, Sarret S, Apfel V, Loesle P, Dawson J, Zhang J, et al. GPR91 senses extracellular succinate released from inflammatory macrophages and exacerbates rheumatoid arthritis. *J. Exp. Med.* 2016; 213: 1655–62.
- Lodi R, Rajagopalan B, Blamire AM, Cooper JM, Davies CH, Bradley JL, et al. Cardiac energetics are abnormal in Friedreich ataxia patients in the absence of cardiac dysfunction and hypertrophy: an in vivo 31P magnetic resonance spectroscopy study. *Cardiovasc. Res.* 2001; 52: 111–9.
- Lodish HF. *Molecular cell biology.* W.H. Freeman; 2000.
- Loike JD, Kozler VF, Silverstein SC. Creatine kinase expression and creatine phosphate accumulation are developmentally regulated during differentiation of mouse and human monocytes. *J. Exp. Med.* 1984; 159: 746–57.
- Maas AIR, Menon DK, Adelson PD, Andelic N, Bell MJ, Belli A, et al. Traumatic brain injury: integrated approaches to improve prevention, clinical care, and research. *Lancet. Neurol.* 2017; 16: 987–1048.
- Maas AIR, Menon DK, Steyerberg EW, Citerio G, Lecky F, Manley GT, et al. Collaborative European NeuroTrauma Effectiveness Research in Traumatic Brain Injury (CENTER-TBI): a prospective longitudinal observational study. *Neurosurgery* 2015; 76: 67–80.
- Maas AIR, Murray GD, Roozenbeek B, Lingsma HF, Butcher I, McHugh GS, et al. Advancing care for traumatic brain injury: findings from the IMPACT studies and perspectives on future research. *Lancet. Neurol.* 2013; 12: 1200–10.
- Madhus I. Regulation of intracellular pH in eukaryotic cells. *Biochem. J.* 1988; 250: 1–8.
- Magnoni S, Tedesco C, Carbonara M, Pluderer M, Colombo A, Stocchetti N. Relationship between systemic glucose and cerebral glucose is preserved in patients with severe traumatic brain injury, but glucose delivery to the brain may become limited when oxidative metabolism is impaired. *Crit. Care Med.* 2012; 40: 1785–1791.
- Mannion RJ, Cross J, Bradley P, Coles JP, Chatfield D, Carpenter A, et al. Mechanism-Based MRI Classification of Traumatic Brainstem Injury and Its Relationship to Outcome. *J. Neurotrauma* 2007; 24: 128–135.
- Marchi N, Bazarian JJ, Puvanna V, Janigro M, Ghosh C, Zhong J, et al. Consequences of repeated blood-brain barrier disruption in football players. *PLoS One* 2013; 8: e56805.
- Marino S, Ciurleo R, Bramanti P, Federico A, De Stefano N. 1H-MR spectroscopy in traumatic brain injury. *Neurocrit. Care* 2011; 14: 127–133.
- Marino S, Zei E, Battaglini M, Vittori C, Buscalferri A, Bramanti P, et al. Acute metabolic brain changes following traumatic brain injury and their relevance to clinical severity and outcome. *J. Neurol. Neurosurg. Psychiatry* 2007; 78: 501–7.
- Martinez FO, Gordon S. The M1 and M2 paradigm of macrophage activation: time for reassessment. *F1000Prime Rep.* 2014; 6:

13.

- Mason GF, Chu W-J, Vaughan JT, Ponder SL, Twieg DB, Adams D, et al. Evaluation of ^{31}P metabolite differences in human cerebral gray and white matter. *Magn. Reson. Med.* 1998; 39: 346–353.
- Mcintosh TK, Faden AI, Bendall MR, Vink R. Traumatic Brain Injury in the Rat - Alterations in Brain Lactate and Ph as Characterized by H-1 and P-31 Nuclear-Magnetic-Resonance. *J. Neurochem.* 1987; 49: 1530–1540.
- McLean LA, Roscoe J, Jorgensen NK, Gorin FA, Cala PM. Malignant gliomas display altered pH regulation by NHE1 compared with nontransformed astrocytes. *Am. J. Physiol. Cell Physiol.* 2000; 278: C676-88.
- Menon DK, Ercole A. Critical care management of traumatic brain injury. *Handb. Clin. Neurol.* 2017; 140: 239–274.
- Montagne A, Toga AW, Zlokovic B V. Blood-Brain Barrier Permeability and Gadolinium: Benefits and Potential Pitfalls in Research. *JAMA Neurol.* 2016; 73: 13–4.
- Naganawa S. Effect of Gadolinium Deposition on ^{18}F -FDG PET/CT of Dentate Nucleus and Globus Pallidus. *J. Nucl. Med. Technol.* 2017; 45: 173.1-173.
- zur Nedden S, Doney AS, Frenguelli BG. The Double-Edged Sword: Gaining Adenosine at the Expense of ATP. How to Balance the Books. In: Masino S, Boison D, editor(s). *Adenosine*. New York, NY: Springer New York; 2012. p. 109–129.
- Newcombe VFJ, Hawkes RC, Harding SG, Willcox R, Brock S, Hutchinson PJ, et al. Potential heating caused by intraparenchymal intracranial pressure transducers in a 3-tesla magnetic resonance imaging system using a body radiofrequency resonator: assessment of the Codman MicroSensor Transducer. *J. Neurosurg.* 2008; 109: 159–164.
- Nguyen NHT, Gonzalez SV, Hassel B. Formation of glycerol from glucose in rat brain and cultured brain cells. Augmentation with kainate or ischemia. *J. Neurochem.* 2007; 101: 1694–1700.
- NICE-SUGAR Study Investigators, Finfer S, Chittock DR, Su SY-S, Blair D, Foster D, et al. Intensive versus conventional glucose control in critically ill patients. *N. Engl. J. Med.* 2009; 360: 1283–97.
- Nicholson C, Hrabětová S. Brain Extracellular Space: The Final Frontier of Neuroscience. *Biophys. J.* 2017; 113: 2133–2142.
- Nicholson C, Kamali-Zare P, Tao L. Brain extracellular space as a diffusion barrier. *Comput. Vis. Sci.* 2011; 14: 309–325.
- Nicolay K, Braun KP, Graaf RA, Dijkhuizen RM, Kruiskamp MJ. Diffusion NMR spectroscopy. *NMR Biomed.* 2001; 14: 94–111.
- Nilsson L, Siesjö BK. The effect of anesthetics upon labile phosphates and upon extra- and intracellular lactate, pyruvate and bicarbonate concentrations in the rat brain. *Acta Physiol. Scand.* 1970; 80: 235–48.
- Nilsson L, Siesjö BK. The effect of deep halothane hypotension upon labile phosphates and upon extra- and intracellular lactate and pyruvate concentrations in the rat brain. *Acta Physiol. Scand.* 1971; 81: 508–16.
- Nilsson L, Siesjö BK. Influence of anaesthetics on the balance between production and utilization of energy in the brain. *J. Neurochem.* 1974; 23: 29–36.
- Nortje J, Coles JP, Timofeev I, Fryer TD, Aigbirhio FI, Smielewski P, et al. Effect of hyperoxia on regional oxygenation and metabolism after severe traumatic brain injury: Preliminary findings*. 2008; 36: 273–281.
- O’Connell MT, Seal A, Nortje J, Al-Rawi PG, Coles JP, Fryer TD, et al. Glucose metabolism in traumatic brain injury: a combined microdialysis and $[^{18}\text{F}]\text{-2-fluoro-2-deoxy-D-glucose-positron emission tomography (FDG-PET)}$ study. *Acta Neurochir. Suppl.* 2005; 95: 165–8.
- Oddo M, Crippa IA, Mehta S, Menon D, Payen J-F, Taccone FS, et al. Optimizing sedation in patients with acute brain injury. *Crit. Care* 2016; 20: 128.
- Oddo M, Schmidt JM, Carrera E, Badjatia N, Connolly ES, Presciutti M, et al. Impact of tight glycemic control on cerebral glucose metabolism after severe brain injury: a microdialysis study. *Crit. Care Med.* 2008; 36: 3233–8.
- Okonkwo DO, Shutter LA, Moore C, Temkin NR, Puccio AM, Madden CJ, et al. Brain Oxygen Optimization in Severe Traumatic Brain Injury Phase-II: A Phase II Randomized Trial. *Crit. Care Med.* 2017; 45: 1907–1914.
- Pajor AM. Sodium-coupled transporters for Krebs cycle intermediates. *Annu. Rev. Physiol.* 1999; 61: 663–82.

- Pajor AM. Sodium-coupled dicarboxylate and citrate transporters from the SLC13 family. *Pflügers Arch. - Eur. J. Physiol.* 2014; 466: 119–130.
- Pan JW, Williamson A, Cavus I, Hetherington HP, Zaveri H, Petroff OAC, et al. Neurometabolism in human epilepsy. *Epilepsia* 2008; 49: 31–41.
- Pardo B, Contreras L, Satrústegui J. De novo Synthesis of Glial Glutamate and Glutamine in Young Mice Requires Aspartate Provided by the Neuronal Mitochondrial Aspartate-Glutamate Carrier Aralar/AGC1. *Front. Endocrinol. (Lausanne)*. 2013; 4: 149.
- Patel AB, Lai JCK, Chowdhury GMI, Hyder F, Rothman DL, Shulman RG, et al. Direct evidence for activity-dependent glucose phosphorylation in neurons with implications for the astrocyte-to-neuron lactate shuttle. *Proc. Natl. Acad. Sci.* 2014; 111: 5385–5390.
- Pattle RE. DIFFUSION FROM AN INSTANTANEOUS POINT SOURCE WITH A CONCENTRATION-DEPENDENT COEFFICIENT. *Q. J. Mech. Appl. Math.* 1959; 12: 407–409.
- Pellerin L, Magistretti PJ. Glutamate uptake into astrocytes stimulates aerobic glycolysis: a mechanism coupling neuronal activity to glucose utilization. *Proc. Natl. Acad. Sci. U. S. A.* 1994; 91: 10625–9.
- Pellerin L, Magistretti PJ. Sweet sixteen for ANLS. *J. Cereb. Blood Flow Metab.* 2012; 32: 1152–1166.
- Peruzzotti-Jametti L, Bernstock JD, Vicario N, Costa ASH, Kwok CK, Leonardi T, et al. Macrophage-Derived Extracellular Succinate Licenses Neural Stem Cells to Suppress Chronic Neuroinflammation. *Cell Stem Cell* 2018; 22: 355-368.e13.
- Petroff O a, Prichard JW, Behar KL, Alger JR, den Hollander J a, Shulman RG. Cerebral intracellular pH by 31P nuclear magnetic resonance spectroscopy. *Neurology* 1985; 35: 781–8.
- Petroff OA, Prichard JW, Behar KL, Alger JR, Shulman RG. In vivo phosphorus nuclear magnetic resonance spectroscopy in status epilepticus. *Ann. Neurol.* 1984; 16: 169–77.
- Petroff OAC. GABA and glutamate in the human brain. *Neuroscientist* 2002; 8: 562–573.
- Pierpaoli C, Jezzard P, Basser PJ, Barnett A, Di Chiro G. Diffusion tensor MR imaging of the human brain. *Radiology* 1996; 201: 637–48.
- Pinheiro J, Bates D, DebRoy S, Sarkar D, Team RC. *nlme: Linear and Nonlinear Mixed Effects Models.* 2018
- Pintaske J, Martirosian P, Graf H, Erb G, Lodemann K-P, Claussen CD, et al. Relaxivity of Gadopentetate Dimeglumine (Magnevist), Gadobutrol (Gadovist), and Gadobenate Dimeglumine (MultiHance) in Human Blood Plasma at 0.2, 1.5, and 3 Tesla. *Invest. Radiol.* 2006; 41: 213–221.
- Plummer MP, Notkina N, Timofeev I, Hutchinson PJ, Finnis ME, Gupta AK. Cerebral metabolic effects of strict versus conventional glycaemic targets following severe traumatic brain injury. *Crit. Care* 2018; 22: 16.
- Prichard JW, Alger JR, Behar KL, Petroff OA, Shulman RG. Cerebral metabolic studies in vivo by 31P NMR. *Proc. Natl. Acad. Sci.* 1983; 80: 2748–2751.
- Prichard JW, Shulman RG. NMR spectroscopy of brain metabolism in vivo. *Annu. Rev. Neurosci.* 1986; 9: 61–85.
- Prins M, Greco T, Alexander D, Giza CC. The pathophysiology of traumatic brain injury at a glance. *Dis. Model. Mech.* 2013; 6: 1307–15.
- Protti A, Singer M. Bench-to-bedside review: potential strategies to protect or reverse mitochondrial dysfunction in sepsis-induced organ failure. *Crit. Care* 2006; 10: 228.
- Provencher SW. Estimation of metabolite concentrations from localized in vivo proton NMR spectra. *Magn. Reson. Med.* 1993; 30: 672–9.
- Provencher SW. Automatic quantitation of localized in vivo 1H spectra with LCModel. *NMR Biomed.* 2001; 14: 260–264.
- Provencher SW. *LCModel & LCMgui User's Manual.* 2018
- Quintard H, Patet C, Zerlauth J-B, Suys T, Bouzat P, Pellerin L, et al. Improvement of Neuroenergetics by Hypertonic Lactate Therapy in Patients with Traumatic Brain Injury Is Dependent on Baseline Cerebral Lactate/Pyruvate Ratio. *J. Neurotrauma*

2016; 33: 681–687.

R Core Team. R: A Language and Environment for Statistical Computing. 2018

Redpath TW. Signal-to-noise ratio in MRI. *Br. J. Radiol.* 1998; 71: 704–7.

Reinstrup P, Ståhl N, Mellergård P, Uski T, Ungerstedt U, Nordström CH. Intracerebral microdialysis in clinical practice: baseline values for chemical markers during wakefulness, anesthesia, and neurosurgery. *Neurosurgery* 2000; 47: 701–709; discussion 709–710.

Ren J, Sherry AD, Malloy CR. 31 P-MRS of healthy human brain: ATP synthesis, metabolite concentrations, pH, and T 1 relaxation times. *NMR Biomed.* 2015; 28: 1455–1462.

Ricci R, Barbarella G, Musi P, Boldrini P, Trevisan C, Basaglia N. Localised proton MR spectroscopy of brain metabolism changes in vegetative patients. *Neuroradiology* 1997; 39: 313–9.

Rohrer M, Bauer H, Mintorovitch J, Requardt M, Weinmann HJ. Comparison of magnetic properties of MRI contrast media solutions at different magnetic field strengths. *Invest. Radiol.* 2005; 40: 715–724.

Rose CF, Verkhratsky A, Parpura V. Astrocyte glutamine synthetase: pivotal in health and disease. *Biochem. Soc. Trans.* 2013; 41: 1518–24.

Rosenfeld J V, Maas AI, Bragge P, Morganti-Kossmann MC, Manley GT, Gruen RL. Early management of severe traumatic brain injury. *Lancet* 2012; 380: 1088–1098.

Rostami E, Bellander B-M. Monitoring of glucose in brain, adipose tissue, and peripheral blood in patients with traumatic brain injury: a microdialysis study. *J. Diabetes Sci. Technol.* 2011; 5: 596–604.

Rothman DL, de Feyter HM, de Graaf RA, Mason GF, Behar KL. 13C MRS studies of neuroenergetics and neurotransmitter cycling in humans. *NMR Biomed.* 2011; 24: 943–957.

Le Roux P, Menon DK, Citerio G, Vespa P, Bader MK, Brophy G, et al. The International Multidisciplinary Consensus Conference on Multimodality Monitoring in Neurocritical Care: Evidentiary Tables. *Neurocrit. Care* 2014; 21: 297–361.

Saeed N, Menon DK. A knowledge-based approach to minimize baseline roll in chemical shift imaging. *Magn. Reson. Med.* 1993; 29: 591–8.

Salim T, Sershen CL, May EE. Investigating the Role of TNF- α and IFN- γ Activation on the Dynamics of iNOS Gene Expression in LPS Stimulated Macrophages. *PLoS One* 2016; 11: e0153289.

Salway JG. *Metabolism at a glance.* Blackwell Pub; 2004.

Sauter A, Rudin M. Determination of creatine kinase kinetic parameters in rat brain by NMR magnetization transfer: Correlation with brain function. *J. Biol. Chem.* 1993; 268: 13166–13171.

Schlattner U, Tokarska-Schlattner M, Wallimann T. Mitochondrial creatine kinase in human health and disease. *Biochim. Biophys. Acta* 2006; 1762: 164–80.

Schlenk F, Graetz D, Nagel A, Schmidt M, Sarrafzadeh AS. Insulin-related decrease in cerebral glucose despite normoglycemia in aneurysmal subarachnoid hemorrhage. *Crit. Care* 2008; 12: R9.

Schlessinger A, Sun NN, Colas C, Pajor AM. Determinants of substrate and cation transport in the human Na⁺/dicarboxylate cotransporter NaDC3. *J. Biol. Chem.* 2014; 289: 16998–7008.

Schmidt JM, Claassen J, Ko S-B, Lantigua H, Presciutti M, Lee K, et al. Nutritional support and brain tissue glucose metabolism in poor-grade SAH: a retrospective observational study. *Crit. Care* 2012; 16: R15.

Schneider GH, Sarrafzadeh AS, Kiening KL, Bardt TF, Unterberg AW, Lanksch WR. Influence of hyperventilation on brain tissue-PO₂, PCO₂, and pH in patients with intracranial hypertension. *Acta Neurochir. Suppl.* 1998; 71: 62–5.

Shimony JS, McKinstry RC, Akbudak E, Aronovitz JA, Snyder AZ, Lori NF, et al. Quantitative diffusion-tensor anisotropy brain MR imaging: normative human data and anatomic analysis. *Radiology* 1999; 212: 770–84.

Shutter L, Tong KA, Lee A, Holshouser BA. Prognostic role of proton magnetic resonance spectroscopy in acute traumatic brain

injury. *J. Head Trauma Rehabil.* 2006; 21: 334–49.

Sidek S, Ramli N, Rahmat K, Ramli NM, Abdulrahman F, Kuo TL. In vivo proton magnetic resonance spectroscopy (1H-MRS) evaluation of the metabolite concentration of optic radiation in primary open angle glaucoma. *Eur. Radiol.* 2016; 26: 4404–4412.

Signoretti S, Marmarou A, Aygok GA, Fatouros PP, Portella G, Bullock RM. Assessment of mitochondrial impairment in traumatic brain injury using high-resolution proton magnetic resonance spectroscopy. *J. Neurosurg.* 2008; 108: 42–52.

Simon DW, McGeachy MJ, Bayir H, Clark RSB, Loane DJ, Kochanek PM. The far-reaching scope of neuroinflammation after traumatic brain injury. *Nat. Rev. Neurol.* 2017; 13: 171–191.

Simpson IA, Carruthers A, Vannucci SJ. Supply and demand in cerebral energy metabolism: the role of nutrient transporters. *J. Cereb. Blood Flow Metab.* 2007; 27: 1766–91.

Singhal A, Baker AJ, Hare GMT, Reinders FX, Schlichter LC, Moulton RJ. Association between cerebrospinal fluid interleukin-6 concentrations and outcome after severe human traumatic brain injury. *J. Neurotrauma* 2002; 19: 929–37.

Skoch A, Jiru F, Bunke J. Spectroscopic imaging: basic principles. *Eur. J. Radiol.* 2008; 67: 230–9.

Smielewski P, Czosnyka M, Steiner L, Belestri M, Piechnik S, Pickard JD. ICM+: software for on-line analysis of bedside monitoring data after severe head trauma. *Acta Neurochir. Suppl.* 2005; 95: 43–9.

Sonnay S, Duarte JMN, Just N, Gruetter R. Energy metabolism in the rat cortex under thiopental anaesthesia measured In Vivo by 13 C MRS. *J. Neurosci. Res.* 2017; 95: 2297–2306.

Sonneville R, den Hertog HM, Güiza F, Gunst J, Derese I, Wouters PJ, et al. Impact of hyperglycemia on neuropathological alterations during critical illness. *J. Clin. Endocrinol. Metab.* 2012; 97: 2113–23.

Steen C, Wilczak N, Hoogduin JM, Koch M, De Keyser J. Reduced creatine kinase B activity in multiple sclerosis normal appearing white matter. *PLoS One* 2010; 5: e10811.

Stefan D, Cesare F Di, Andrasescu A, Popa E, Lazariev A, Vescovo E, et al. Quantitation of magnetic resonance spectroscopy signals: the jMRUI software package. *Meas. Sci. Technol.* 2009; 20: 104035.

Stein NR, McArthur DL, Etchepare M, Vespa PM. Early Cerebral Metabolic Crisis After TBI Influences Outcome Despite Adequate Hemodynamic Resuscitation. *Neurocrit. Care* 2012; 17: 49–57.

Steiner LA, Czosnyka M, Piechnik SK, Smielewski P, Chatfield D, Menon DK, et al. Continuous monitoring of cerebrovascular pressure reactivity allows determination of optimal cerebral perfusion pressure in patients with traumatic brain injury. *Crit. Care Med.* 2002; 30: 733–8.

Steyerberg EW, Mushkudiani N, Perel P, Butcher I, Lu J, McHugh GS, et al. Predicting outcome after traumatic brain injury: development and international validation of prognostic scores based on admission characteristics. *PLoS Med.* 2008; 5: e165; discussion e165.

Stocchetti N, Taccone FS, Citerio G, Pepe PE, Le Roux PD, Oddo M, et al. Neuroprotection in acute brain injury: an up-to-date review. *Crit. Care* 2015; 19: 186.

Stovell MG, Mada MO, Carpenter TA, Yan J-L, Guilfoyle MR, Jalloh I, et al. Phosphorus spectroscopy in acute TBI demonstrates metabolic changes that relate to outcome in the presence of normal structural MRI. *J. Cereb. Blood Flow Metab.* 2020; 40: 67–84.

Stovell MG, Mada MO, Helmy A, Carpenter TA, Thelin EP, Yan J-L, et al. The effect of succinate on brain NADH/NAD+ redox state and high energy phosphate metabolism in acute traumatic brain injury. *Sci. Rep.* 2018; 8: 11140.

Stovell MG, Yan J-L, Sleigh A, Mada MO, Carpenter TA, Hutchinson PJA, et al. Assessing Metabolism and Injury in Acute Human Traumatic Brain Injury with Magnetic Resonance Spectroscopy: Current and Future Applications. *Front. Neurol.* 2017; 8: 426.

Stubbs M, Freeman D, Ross BD. Formation of n.m.r.-invisible ADP during renal ischaemia in rats. *Biochem. J.* 1984; 224: 241–6.

Swain J a., McDonald TJ, Balaban RS, Robbins RC. Metabolism of the heart and brain during hypothermic cardiopulmonary bypass. *Ann. Thorac. Surg.* 1991; 51: 105–109.

- Sweeney MD, Ayyadurai S, Zlokovic B V. Pericytes of the neurovascular unit: key functions and signaling pathways. *Nat. Neurosci.* 2016; 19: 771–83.
- Swietach P, Vaughan-Jones RD, Harris AL, Hulikova A. The chemistry, physiology and pathology of pH in cancer. *Philos. Trans. R. Soc. Lond. B. Biol. Sci.* 2014; 369: 20130099.
- Syková E, Nicholson C, Sykova, Eva; Nicholson C. Diffusion in brain extracellular space. *Physiol. Rev.* 2008; 88: 1277–340.
- Syková E, Svoboda J, Simonová Z, Lehmenkühler A, Lassmann H. X-irradiation-induced changes in the diffusion parameters of the developing rat brain. *Neuroscience* 1996; 70: 597–612.
- Takami H, Furuya E, Tagawa K, Seo Y, Murakami M, Watari H, et al. NMR-invisible ATP in rat heart and its change in ischemia. *J. Biochem.* 1988; 104: 35–9.
- Tannahill GM, Curtis AM, Adamik J, Palsson-McDermott EM, McGettrick AF, Goel G, et al. Succinate is an inflammatory signal that induces IL-1 β through HIF-1 α . *Nature* 2013; 496: 238–42.
- Teasdale G, Jennett B. Assessment of coma and impaired consciousness: A practical scale. *Lancet* 1974; 304: 81–84.
- Thelin EP, Tajsic T, Zeiler FA, Menon DK, Hutchinson PJA, Carpenter KLH, et al. Monitoring the Neuroinflammatory Response Following Acute Brain Injury. *Front. Neurol.* 2017; 8: 1–14.
- Theparambil SM, Weber T, Schmälzle J, Ruminot I, Deitmer JW. Proton fall or bicarbonate rise: Glycolytic rate in mouse astrocytes is paved by intracellular alkalinization. *J. Biol. Chem.* 2016; 291: 19108–19117.
- Thomson AM. Neocortical layer 6, a review. *Front. Neuroanat.* 2010; 4: 13.
- Timofeev I, Carpenter KLH, Nortje J, Al-Rawi PG, O'Connell MT, Czosnyka M, et al. Cerebral extracellular chemistry and outcome following traumatic brain injury: a microdialysis study of 223 patients. *Brain* 2011; 134: 484–94.
- Timofeev I, Nortje J, Al-Rawi PG, Hutchinson PJA, Gupta AK. Extracellular brain pH with or without hypoxia is a marker of profound metabolic derangement and increased mortality after traumatic brain injury. *J. Cereb. Blood Flow Metab.* 2013; 33: 422–7.
- Toft PB, Leth H, Peitersen B, Lou HC, Thomsen C. The apparent diffusion coefficient of water in gray and white matter of the infant brain. *J. Comput. Assist. Tomogr.* 1996; 20: 1006–11.
- Tomlinson DR, Gardiner NJ. Glucose neurotoxicity. *Nat. Rev. Neurosci.* 2008; 9: 36–45.
- Trivedi B, Danforth WH. Effect of pH on the kinetics of frog muscle phosphofructokinase. *J. Biol. Chem.* 1966; 241: 4110–2.
- Ulrich EL, Akutsu H, Doreleijers JF, Harano Y, Ioannidis YE, Lin J, et al. BioMagResBank. *Nucleic Acids Res.* 2008; 36: 402–408.
- Uzan M, Albayram S, Dashti SGR, Aydin S, Hanci M, Kuday C. Thalamic proton magnetic resonance spectroscopy in vegetative state induced by traumatic brain injury. *J. Neurol. Neurosurg. Psychiatry* 2003; 74: 33–8.
- Veenith T V., Carter EL, Geeraerts T, Grossac J, Newcombe VFJ, Outtrim J, et al. Pathophysiologic Mechanisms of Cerebral Ischemia and Diffusion Hypoxia in Traumatic Brain Injury. *JAMA Neurol.* 2016; 73: 542–50.
- Vespa P, Boonyaputthikur R, McArthur DL, Miller C, Etchepare M, Bergsneider M, et al. Intensive insulin therapy reduces microdialysis glucose values without altering glucose utilization or improving the lactate/pyruvate ratio after traumatic brain injury*. *Crit. Care Med.* 2006; 34: 850–856.
- Vespa P, McArthur DL, Stein N, Huang S-C, Shao W, Filippou M, et al. Tight glycemic control increases metabolic distress in traumatic brain injury: a randomized controlled within-subjects trial. *Crit. Care Med.* 2012; 40: 1923–9.
- Vink R, Faden a I, McIntosh TK. Changes in cellular bioenergetic state following graded traumatic brain injury in rats: determination by phosphorus 31 magnetic resonance spectroscopy. *J. Neurotrauma* 1988a; 5: 315–30.
- Vink R, McIntosh TK, Weiner MW, Faden a I. Effects of traumatic brain injury on cerebral high-energy phosphates and pH: a 31P magnetic resonance spectroscopy study. *J. Cereb. Blood Flow Metab.* 1987; 7: 563–571.
- Vink R, McIntosh TK, Yamakami I, Faden AI. 31P NMR characterization of graded traumatic brain injury in rats. *Magn. Reson. Med.* 1988b; 6: 37–48.

- Wallimann T, Tokarska-Schlattner M, Schlattner U. The creatine kinase system and pleiotropic effects of creatine. *Amino Acids* 2011; 40: 1271–1296.
- Wallimann T, Wyss M, Brdiczka D, Nicolay K, Eppenberger HM. Intracellular compartmentation, structure and function of creatine kinase isoenzymes in tissues with high and fluctuating energy demands: the 'phosphocreatine circuit' for cellular energy homeostasis. *Biochem. J.* 1992; 281: 21–40.
- Wang KKW, Yang Z, Yue JK, Zhang Z, Winkler EA, Puccio AM, et al. Plasma Anti-Glial Fibrillary Acidic Protein Autoantibody Levels during the Acute and Chronic Phases of Traumatic Brain Injury: A Transforming Research and Clinical Knowledge in Traumatic Brain Injury Pilot Study. *J. Neurotrauma* 2016; 33: 1270–7.
- Weigand MA, Michel A, Eckstein HH, Martin E, Bardenheuer HJ. Adenosine: a sensitive indicator of cerebral ischemia during carotid endarterectomy. *Anesthesiology* 1999; 91: 414–421.
- Williamson DH, Lund P, Krebs HA. The redox state of free nicotinamide-adenine dinucleotide in the cytoplasm and mitochondria of rat liver. *Biochem. J.* 1967; 103: 514–27.
- Wishart DS, Tzur D, Knox C, Eisner R, Guo AC, Young N, et al. HMDB: The human metabolome database. *Nucleic Acids Res.* 2007; 35: 521–526.
- Wood ET, Ronen I, Techawiboonwong A, Jones CK, Barker PB, Calabresi P, et al. Investigating axonal damage in multiple sclerosis by diffusion tensor spectroscopy. *J. Neurosci.* 2012; 32: 6665–9.
- Yoshizaki K, Watari H, Radda GK. Role of phosphocreatine in energy transport in skeletal muscle of bullfrog studied by ³¹P-NMR. *Biochim. Biophys. Acta* 1990; 1051: 144–50.
- Zaitsev M, Maclaren J, Herbst M. Motion artifacts in MRI: A complex problem with many partial solutions. *J. Magn. Reson. Imaging* 2015; 42: 887–901.
- Zetterling M, Hillered L, Enblad P, Karlsson T, Ronne-Engström E. Relation between brain interstitial and systemic glucose concentrations after subarachnoid hemorrhage. *J. Neurosurg.* 2011; 115: 66–74.
- Zhang Q, Raoof M, Chen Y, Sumi Y, Sursal T, Junger W, et al. Circulating mitochondrial DAMPs cause inflammatory responses to injury. *Nature* 2010; 464: 104–7.
- Zhu X-H, Qiao H, Du F, Xiong Q, Liu X, Zhang X, et al. Quantitative imaging of energy expenditure in human brain. *Neuroimage* 2012; 60: 2107–2117.
- Ziebell JM, Morganti-Kossmann MC. Involvement of pro- and anti-inflammatory cytokines and chemokines in the pathophysiology of traumatic brain injury. *Neurotherapeutics* 2010; 7: 22–30.
- Zöllner JP, Hattingen E, Singer OC, Pilatus U. Changes of pH and energy state in subacute human ischemia assessed by multinuclear magnetic resonance spectroscopy. *Stroke* 2015; 46: 441–6.
- Zygun DA, Steiner LA, Johnston AJ, Hutchinson PJ, Al-Rawi PG, Chatfield D, et al. Hyperglycemia and brain tissue pH after traumatic brain injury. *Neurosurgery* 2004; 55: 877–882.

Chapter 10

Appendices

Contents

10.1	Appendix 1 - Co-registration of MR imaging data	191
10.1.1	Data preparation.....	191
10.1.2	Co-registration of image sets acquired with ³¹ P coil and ¹ H coil.....	192
10.1.3	Creation of grey matter, white matter and cerebrospinal fluid masks	193
10.1.4	Creation of FLAIR and SWI injury masks	193
10.1.5	Create individual voxel masks for each voxel in MatLab	194
10.2	Appendix 2 – Interrogating Metabolism Kinetics in the Human Brain Clinical Study Protocol	194
10.3	Appendix 3 – Interrogating Metabolism Kinetics in the Human Brain Research Ethics Application	228

10.1 Appendix 1 - Co-registration of MR imaging data

Image co-registration was performed in collaboration with Dr Jiun-Lin Yan, using scripts developed by Mr Stephen Price's group, Department of Clinical Neuroscience, University of Cambridge:

10.1.1 Data preparation

- ³¹P MRS CSI data acquired with the ³¹P head coil were imported from the WBIC terminal in **.dicom10** format using the script:

```
dcmconv.pl remoteae <<protocol number>> -id <<subject ID>> -info -outtype
dicom10
```

Then renamed using a standard format **CSI.dcm**.

- ¹H T2W scans acquired with the ³¹P head coil and ¹H MP-RAGE, FLAIR and SWI scans acquired with the 12-channel ¹H coil were imported from the WBIC terminal in **.nifti** format using the script:

dcmconv.pl remoteae <<protocol number>> -id <<subject ID>> -info
Scans were renamed using a standard format, **Reference.nii**, **MPRAGE_orig.nii**, **FLAIR.nii** and **SWI.nii**.

- Header information was extracted from **CSI.dcm**, and named **header.txt**, using the script:

```
print_tags.pl CSI.dcm > header.txt
```

- A screenshot of the Siemen's terminal was taken and downloaded as an image, showing the T2W axial slice in the centre of the CSI voxel grid, for later comparison.

10.1.2 Co-registration of image sets acquired with ³¹P coil and ¹H coil

- **MPRAGE2.nii**, **FLAIR.nii** and **SWI.nii** were co-registered to **Reference.nii** using the FSL script FLIRT (FMRIB's Linear Image Registration Tool) (example for **MPRAGE2.nii**):

```
flirt -ref <<Reference.nii>> -in <<MPRAGE_orig.nii>> -out  
<<FL_MPRAGE2_2_Reference>> -omat <<FL_MPRAGE2_2_Reference.mat>> -cost normmi  
-searchrx -90 90 -searchry -90 90 -searchrz -90 90 -dof 12 -interp trilinear
```

- The co-registration was checked in FslView by comparing the ventricular system and gyral/sulcal pattern of **Reference.nii** and the co-registered image. If less than ≈ 2 mm error, the co-registered images were renamed **FL_MPRAGE.nii**, **FL_FLAIR.nii** and **FL_SWI.nii**.
- If co-registration was unacceptable, the following steps were taken:
 - The neck was excluded from the **MPRAGE_orig.nii** sequence, then co-registered to the reference image using the FSL script fslroi (Appropriate voxel cut offs were determined by opening the image in FslView):
fslroi <<MPRAGE_orig.nii>> <<MPRAGE.nii>> 0 256 0 256 0 192
 - The co-registration was attempted using the PD sequence from the ³¹P coil as **Reference.nii**, rather than the T2W sequence.
 - The brain was either manually or automatically extracted (see below) from **MPRAGE_orig.nii** and **Reference.nii**, then co-registration attempted.

- A successfully co-registered sequence was used as a ‘bridge’ if one of the sequences (***FL_MPRAGE.nii*** for example) was successful, then the unsuccessful sequence co-registered to the successful sequence.

10.1.3 Creation of grey matter, white matter and cerebrospinal fluid masks

- The brain was extracted from the co-registered MP-RAGE using FSL’s automatic brain extraction script bet:

```
bet <<FL_MPRAGE.nii>> <<FL_MPRAGE_BE.nii>> -f 0.5 -B
```

- The brain extraction was checked in 3D slicer (<https://www.slicer.org/>).
- If unsuccessful, 3D slicer was used to manually draw a mask of the brain using the ‘Editor tool’, which was saved as ***FL_MPRAGE_BE_mask-label.nii***. This mask was then applied to ***FL_MPRAGE.nii*** using the FSL script fslmaths:

```
fslmaths <<FL_MPRAGE.nii>> -mul <<FL_MPRAGE_BE_mask-label.nii>> <<FLMPRAGE_BEm.nii>>
```

- Segmentation of grey matter, white matter and cerebrospinal fluid (CSF) was performed using FSL’s script fast:

```
fast -t 1 -n 4 -o <<Segmentation.nii.gz>> <<FLMPRAGE_BEm.nii>>
```

- Segmentation was made binary using FSL’s script fslmaths:

```
fslmaths Segmentation_pve_0.nii.gz -div Segmentation_pve_1.nii.gz CSF.nii.gz
```

```
fslmaths Segmentation_pve_2.nii.gz -div Segmentation_pve_2.nii.gz GM.nii.gz
```

```
fslmaths Segmentation_pve_3.nii.gz -div Segmentation_pve_3.nii.gz WM.nii.gz
```

- Each of these was checked in FSL’s FslView, to ensure it is labelled correctly.

10.1.4 Creation of FLAIR and SWI injury masks

- ***FL_FLAIR.nii*** was opened in 3D slicer and a mask of regions of injury (***FL_FLAIR-label.nii***) was manually defined with the Editor tool, using the criteria:

Abnormal signal (typically high) relative to surrounding brain that is a result of TBI. Blood in ventricles, blood in subarachnoid space, subdural blood and artifacts related to external ventricular drains and multimodal monitoring were excluded.

- *FL_SWI.nii* was opened in 3D slicer and a mask of regions of injury (*FL_SWI-label.nii*) was manually defined with the Editor tool, using the criteria:

Abnormal signal (typically low) relative to adjacent brain tissue that is a result of TBI. Low signal found in known vascular anatomy and Signal artefact from metallic invasive monitoring was not included. For regions of brain with nexuses of multiple small low signal regions separated by only a small amount of normal appearing brain, such as might occur in contusions, the whole volume was taken as injured.

10.1.5 Create individual voxel masks for each voxel in MatLab

Using scripts in MatLab (The MathWorks, Inc., MA, USA), developed by Dr Tim Larkin and Dr Jiun-Lin Yan:

- The CSI voxel grid was overlaid on the Reference.nii sequence, using the extracted header information in *header.txt*. The position of the grid, and the level of its centre slice, was compared to the screenshot from the Siemen's terminal, acquired in **Data Preparation**. If the central slice did not match that of the screenshot, the central slice was adjusted.
- Individual voxel masks were created for each of the 25 mm x 25 mm x 25 mm voxels in the selected central 8 x 8 grid (see **Selection of voxels**).
- The amount of grey matter, white matter, CSF, FLAIR injury and SWI injury in each voxel 3D space was calculated using intersection of the respective masks. The data was combined and exported as a *Voxel_Percent_<<subject>>.csv*, for each subject.

10.2 Appendix 2 – Interrogating Metabolism Kinetics in the Human Brain Clinical Study Protocol

Cambridge Neurotrauma Research Group.

Clinical Study Protocol

Study Title: Interrogating Metabolism Kinetics in the Human Brain

Protocol Version: Version 1.2 06.12.2018

Sponsor reference: A094334

Funder's reference:

REC Reference Number: 17/EE/0075

IRAS I.D.: 221640

Chief Investigator: **Prof Peter J Hutchinson**

Professor and Honorary Consultant Neurosurgeon

Box 167, Department of Neurosurgery, Addenbrooke's Hospital, Hills Road, Cambridge, CB2 0QQ, UK.

Tel: +44(0)1223 336946 Fax: +44(0)1223 216926

Email: pjah2@cam.ac.uk

Lead Investigator: **Mr Matthew G Stovell**

Clinical Research Associate (Neurosurgery) and Honorary Neurosurgery Registrar

Box 167, Department of Neurosurgery, Addenbrooke's Hospital, Hills Road, Cambridge, CB2 2QQ, UK.

Tel: +44(0)1223 217842 Fax: +44(0)1223 414396

Email: mgs48@cam.ac.uk

Co-investigators:

Dr Keri Carpenter

Dr Graeme Mason

Dr Alison Sleight

Mr Adel Helmy

Dr Adrian Carpenter

Dr Marius Mada

Prof David Menon

Mr Ivan Timofeev

Dr Ram Adapa

Mr Mathew Guilfoyle

Mr Ibrahim Jalloh

Mr Christopher Wickens

Study Sponsor:

Cambridge University Hospitals NHS Foundation Trust and University of Cambridge

R & D Office, Box 277, Addenbrooke's Hospital

Hills Road, Cambridge CB2 0QQ

Study Synopsis

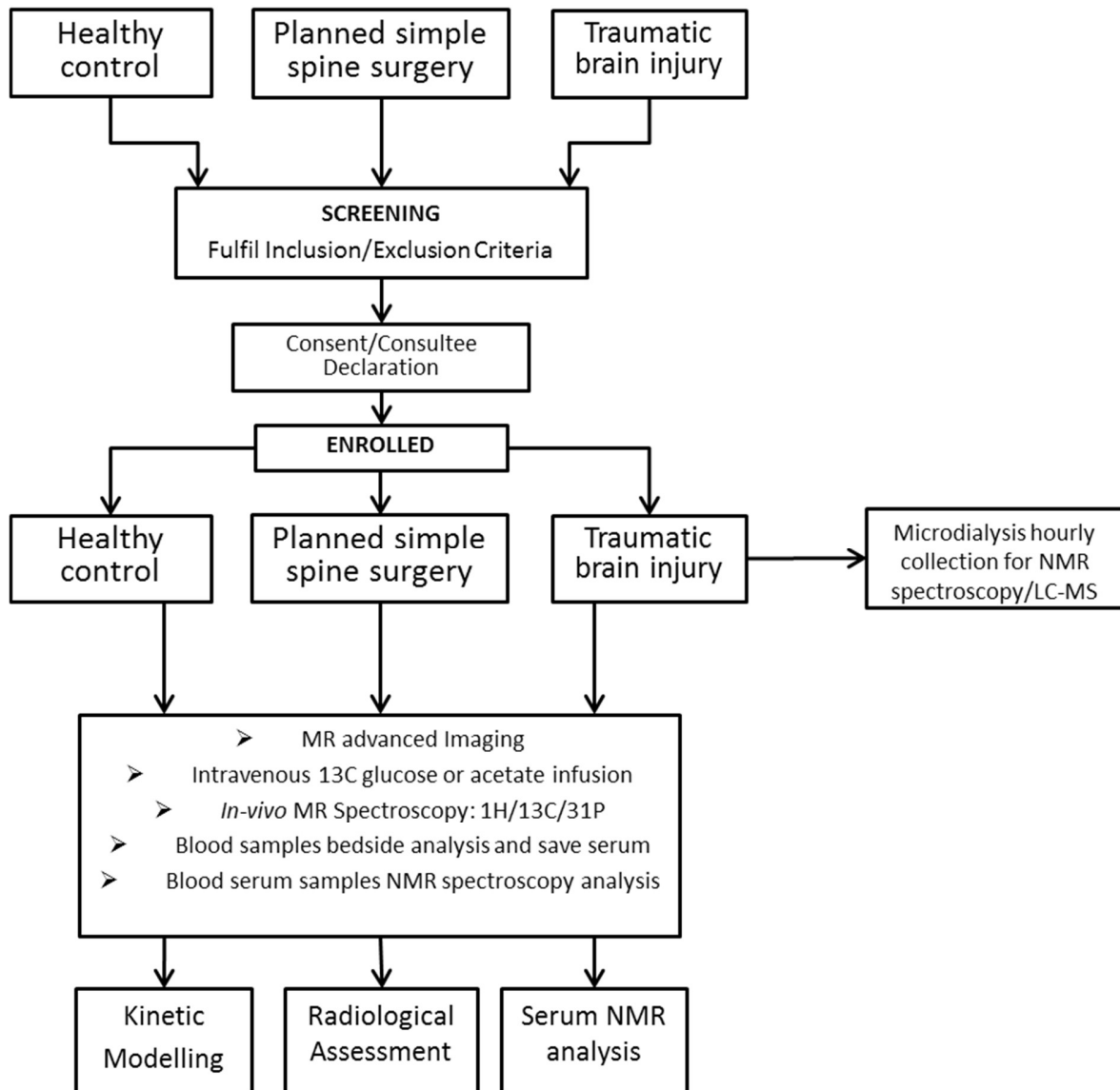
Title of clinical study	Interrogating Metabolism Kinetics in the Human Brain
Sponsors names	a) Cambridge University Hospitals NHS Foundation Trust b) University of Cambridge
Medical condition or disease under investigation	Traumatic Brain Injury General Anaesthesia
Purpose of study	Characterise kinetics of brain energy metabolism in injured and normal brain.
Primary objectives	Characterise the effect of traumatic brain injury and anaesthesia on the kinetics of energy metabolism in human brain.
Secondary objectives	Assess microdialysis and MRS assessment of energy generation. Assess the therapeutic effect of metabolism supplementation.
Study Design	Observational
Sample Size	60
Summary of eligibility criteria	a) TBI requiring ventilation b) Healthy adult controls requiring simple spine surgery c) Healthy adult controls
Investigational techniques	^{13}C -labelled intravenous infusion In vivo MR Spectroscopy High resolution NMR LC-MS Conventional microdialysis

Abbreviations

^{13}C	13-carbon
^{31}P	31-phosphorous
APACHE II	Acute Physiology and Chronic Health Evaluation II
AST	Aspartate transaminase
ATP	Adenosine triphosphate
BMI	Body Mass Index
CNS	Central nervous system
CSF	Cerebrospinal Fluid
DQFCOSY	Double-quantum filtered correlation spectroscopy
HSQC	Heteronuclear single-quantum correlation
ICP	Intracranial pressure

ISS	Injury Severity Score
IV	Intravenous
L/P	Lactate/pyruvate
LC-MS	Liquid chromatography-Mass spectrometry
MRI	Magnetic resonance imaging
MRS	Magnetic resonance spectroscopy
NCCU	Neurosciences Critical Care Unit
NMR	Nuclear magnetic resonance
PCr	Phosphocreatine
Pi	Inorganic phosphate
PPP	Pentose phosphate pathway
TBI	Traumatic brain injury
TCA	Tricarboxylic acid
WBIC	Wolfson Brain Imaging Centre

1 Study Flow Chart



2 Table of Contents

Study Synopsis.....	Error! Bookmark not defined.
Abbreviations	Error! Bookmark not defined.
1 Study Flow Chart	Error! Bookmark not defined.
2 Table of Contents	Error! Bookmark not defined.
3 Introduction	Error! Bookmark not defined.
3.1 Overview	Error! Bookmark not defined.
3.2 Background.....	Error! Bookmark not defined.
4 Rationale for Study	Error! Bookmark not defined.
5 Research objective and purpose.....	Error! Bookmark not defined.
6 Study Design	Error! Bookmark not defined.
6.1 Overall statement of design.....	Error! Bookmark not defined.
6.2 Subject selection.....	Error! Bookmark not defined.
6.3 Overall number of subjects.....	Error! Bookmark not defined.
6.4 Sample size determination.....	Error! Bookmark not defined.
7 Individual Studies.....	Error! Bookmark not defined.
7.1 Study 1 – Measuring the TCA cycle rate (V_{TCA}), glutamate/glutamine cycling (V_{cycle}) and the appearance of lactate ($V_{lactate}$) in TBI and general anaesthesia. ..	Error! Bookmark not defined.
7.2 Study 2 – The proportion of TCA cycle anaplerosis in TBI	Error! Bookmark not defined.
7.3 Study 3 – Measuring the TCA cycle rate (V_{TCA}) and glutamate/glutamine cycling (V_{cycle}) in glia under general anaesthesia and TBI.....	Error! Bookmark not defined.
7.4 Study 4 – Measuring high energy phosphorus flux in TBI and General Anaesthesia	Error! Bookmark not defined.
7.5 Study duration	Error! Bookmark not defined.
8 Selection and withdrawal of subjects.....	Error! Bookmark not defined.
8.1 Subject withdrawal criteria.....	Error! Bookmark not defined.
9 Infusion, MRS and microdialysis regimes	Error! Bookmark not defined.
9.1 IV infusion & sampling regime	Error! Bookmark not defined.
9.2 Microdialysis & NMR analysis	Error! Bookmark not defined.
9.3 MRS.....	Error! Bookmark not defined.
9.4 Data analysis.....	Error! Bookmark not defined.
10 Other study procedures and assessments.....	Error! Bookmark not defined.
10.1 Patient recruitment.....	Error! Bookmark not defined.
10.2 Baseline data.....	Error! Bookmark not defined.
11 Assessment of Safety	Error! Bookmark not defined.
11.1 Definitions	Error! Bookmark not defined.
11.2 Evaluation of adverse event.....	Error! Bookmark not defined.
11.3 Reporting Procedure.....	Error! Bookmark not defined.
12 Statistics	Error! Bookmark not defined.
12.1 Study Statistician.....	Error! Bookmark not defined.
12.2 Statistical methods to be employed for analysis of endpoints	Error! Bookmark not defined.
13 Direct access to source data / documents	Error! Bookmark not defined.
14 Ethical considerations	Error! Bookmark not defined.
14.1 Consent.....	Error! Bookmark not defined.
14.2 Ethical committee review	Error! Bookmark not defined.
14.3 Declaration of Helsinki and ICH Good Clinical Practise	Error! Bookmark not defined.
15 Data handling and record keeping	Error! Bookmark not defined.
16 Financing and Insurance	Error! Bookmark not defined.
17 Publications policy.....	Error! Bookmark not defined.
18 References	Error! Bookmark not defined.

Introduction

2.1 Overview

While the fundamental metabolic processes glycolysis, the tricarboxylic acid (TCA) cycle and oxidative phosphorylation are well characterised, energy metabolism and its kinetics in human brain remains poorly understood in trauma and anaesthesia. We aim to explore the kinetics of human cerebral metabolism using a combination of in vivo ^{13}C MRS, ^{31}P MRS and ^1H MRS during intravenous infusion of ^{13}C -labelled substrates, identify disruptions of energy production and ways of ameliorating them.

2.2 Background.

2.2.1 *Fundamental biochemistry of energy metabolism*

Energy metabolism is the overall process through which living systems acquire and utilise the energy they need to carry out various functions. Humans, like all chemotrophs, obtain this energy by oxidising organic compounds, notably carbohydrates, lipids and proteins. This energy is coupled to endergonic reactions resulting in the synthesis of high-energy phosphate compounds, specifically adenosine triphosphate (ATP). The most fundamental organic compound utilised by humans is glucose. ATP is generated by three well-recognised processes (Figure 1).

a) Glycolysis – the linear pathway by which glucose is converted (via several intermediates) to pyruvate, thereby generating 2 mol of ATP per mol of glucose. There is a continuous back-and-forward exchange between pyruvate and lactate by the enzyme lactate dehydrogenase, but under normal, aerobic conditions most carbon from this pool of pyruvate and lactate is converted to acetyl and enters the tricarboxylic acid (TCA) cycle. However, under anaerobic conditions, lactate may accumulate, raising the relative proportion of lactate. lactate/pyruvate (L/P) ratio can therefore be used as an indicator of the comparative degree of aerobic vs. anaerobic metabolism.

b) Tricarboxylic acid (TCA) cycle (also termed citric acid cycle or Krebs cycle) – cyclical pathway comprises a series of 8 reactions that oxidise the acetyl group of acetyl-CoA producing 3 molecules of nicotinamide adenine dinucleotide

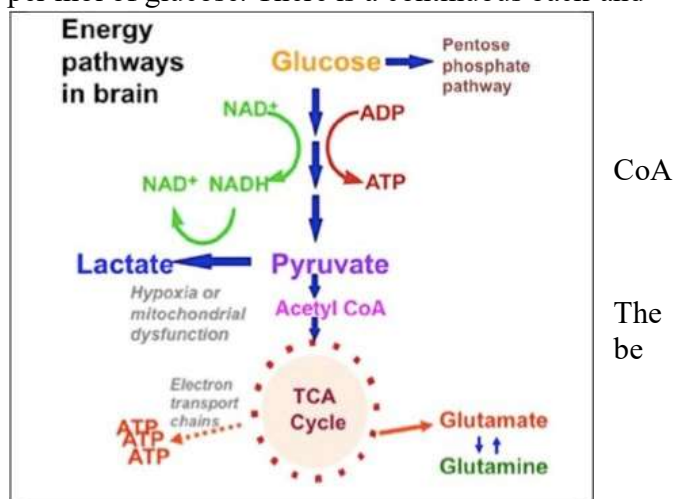


Figure 1. Major energy pathways in the brain include glycolysis, which takes place in the cytosol and produces pyruvate, which enters mitochondria and is converted into acetyl CoA that enters the TCA cycle. Alternatively, pyruvate can stay in the cytosol and is converted into lactate that is exported out of the cell. The pentose phosphate pathway takes place in the cytosol and is an alternative energy pathway that can be up-regulated after injury; it is an important source of NADPH used in the reduction of glutathione for preventing oxidative stress.

(NADH), one molecule of flavin adenine dinucleotide (FADH₂), and one molecule of guanosine triphosphate (GTP). When glucose is the substrate the acetyl group is generated by the oxidation of pyruvate from glycolysis.

c) Oxidative phosphorylation – the process occurring in mitochondria through which NADH and FADH₂ from the TCA cycle are oxidised by oxygen in the electron transport chain resulting in the synthesis of further molecules of ATP. Overall, one molecule of glucose, in the presence of oxygen, processed via this three-stage pathway (glycolysis, TCA cycle and oxidative phosphorylation), yields a net production of 36 molecules of ATP. Until recently, understanding of these processes has arisen through laboratory investigations, and the concepts applied to humans. Advances in technology are now enabling direct, detailed exploration of metabolism in man. Techniques available include microdialysis, nuclear magnetic resonance (NMR) spectroscopy and *in vivo* magnetic resonance spectroscopy (MRS) - see below.

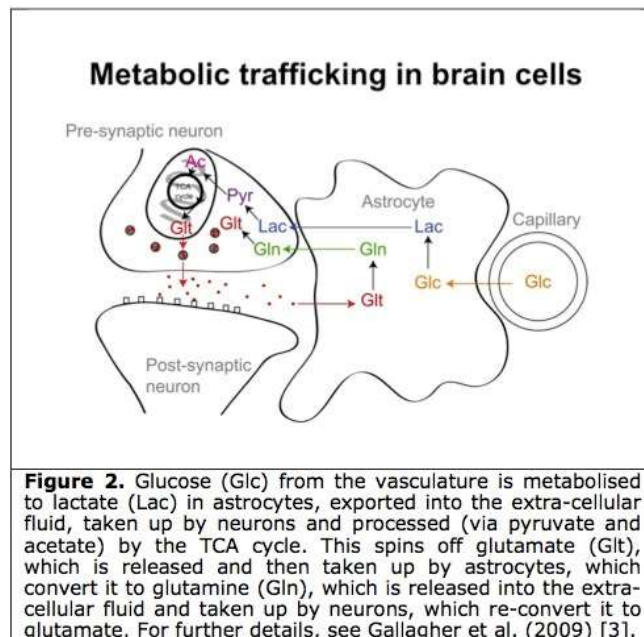
2.2.2 Brain energy metabolism as a special case

While glucose is recognised as the primary substrate in most organs, including muscle, recent evidence suggests that the situation in the brain is considerably more complex, particularly in relation to the main cell types. Traditionally it has been believed that both glia and neurones metabolise glucose as the preferred substrate via glycolysis to pyruvate, which is converted to acetyl CoA and enters the TCA cycle resulting in the generation of ATP by oxidative phosphorylation. It is increasingly evident that neurones utilise lactate (classically perceived as a waste product) as an energy substrate (Figure 2). A scheme of metabolic trafficking between astrocytes and neurons has been proposed by Pellerin and Magistretti¹ as a result of *in vitro* studies and has been later supported by studies in animals (e.g.²) and our recent microdialysis studies using ¹³C-labelling have demonstrated that the injured human brain can metabolise lactate via the TCA cycle³. Conversely glia (astrocytes and oligodendrocytes) are able to metabolise acetate directly into the TCA cycle^{4,5}, whereas neurones do not under normal conditions. Thus studies using acetate as a substrate allow the metabolism of the glial population of the brain to be investigated independently from the neuronal population. We have also demonstrated that the traumatised human brain is able to metabolise exogenously administered succinate, resulting in an improvement in the L/P ratio⁶, but it is unclear whether this favours one cell population over the other.

MRS studies of healthy humans demonstrate that the majority of energy metabolism in the brain (80 %) is to support glutamate neurotransmission and hence signalling and only 15 – 20 % of glucose oxidation supports non-functional processes. In both rat and human brains increments in glutamate cycling (release and uptake then conversion to glutamine) and glucose oxidation are closely coupled in a one-to-one ratio⁷.

The brain, like other tissue with excitable cells (muscle, renal) possess an additional high energy phosphate Phosphocreatine (PCr). PCr acts as both a temporal and spatial buffer for ATP so that a high ratio of PCr to ATP is classically thought to demonstrate a situation of energy reserve⁸.

Cerebral metabolism following injury appears to differ from that in normal brain, although the full extent and nature of these changes are poorly understood, especially in man. The best-known metabolic characteristic of injured brain is a high L/P ratio (greater than 25 regarded as indicative of ischaemia mitochondrial dysfunction) and our study of microdialysate L/P ratio in 233 TBI patients, demonstrated that L/P ratio > 25 predicted unfavourable outcome in a multivariate analysis in addition to previously known predictors of outcome^{9,10}. There is a greater flux of glucose through the glycolysis¹¹ in human TBI, and we have demonstrated the potential metabolically beneficial effect of succinate when administered via retromicrodialysis in the traumatised human brain⁶.



brain
is
or
study
TBI

in

PPP

2.2.3 *In vivo Magnetic Resonance Spectroscopy in the evaluation of cerebral metabolism*

In vivo magnetic resonance spectroscopy (MRS) is a non-invasive radiation free technique that uses magnetic fields to detect chemical species in tissues. Certain nuclei possessing 'spin' such as ¹H, ¹³C and ³¹P are detectible using MRS. Both the position of these nuclei within a metabolite, and what metabolite that is can be ascertained from their position relative to each other (causing J-coupling / scalar coupling), and the surrounding chemical environment (causing chemical shift on the spectra).

³¹P MRS allows the study of high energy phosphorous species through the natural isotopic abundance of ³¹P (100 %) in ATP, PCr and Pi. Through measuring these species the ratio of PCr to ATP and pH of tissues can be elucidated. Kinetics of transfer of phosphorus from PCr to ATP can be estimated using the magnetization transfer technique¹². We have demonstrated differences in brain pH and the PCr / ATP ratio between patients with severe TBI and awake, healthy volunteers [*unpublished data*].

¹³C MRS allows the study of a variety organic compounds containing carbon. The majority of naturally occurring carbon is ¹²C; with ¹³C making up 1.1 %. For this reason ¹³C MRS is often performed after supplementation with ¹³C enriched substrates. By continually acquiring MRS data whilst infusing a ¹³C enriched metabolite, such as glucose, both its metabolic fate, and the rate of flux between its intermediates can be tracked¹³. Using this technique the rate of glucose uptake, glycolysis, the TCA cycle and glutamate-glutamine cycling has been calculated in healthy awake man, but never in sedated humans or those suffering from acute severe TBI.

^1H MRS is used both as a research tool and in specific clinical applications such as brain tumour characterisation. By using ^1H MRS some species with similar chemical spectra on ^{31}P MRS and ^{13}C MRS can be distinguished from each other.

2.2.4 *Cerebral Microdialysis and high resolution NMR*

Monitoring of severe TBI and high grade subarachnoid patients in neuro-critical care may include intracranial pressure monitoring, brain tissue oxygen monitoring and extracellular chemistry monitoring using microdialysis. Microdialysis catheters possess a semi-permeable membrane that is continuously perfused with fluid, allowing molecules to diffuse across the membrane, to and from the brain's extracellular space. Clinically, the catheter is perfused with a physiological salt solution and the returning fluid (microdialysate) is analysed at the bedside using automated enzymatic colorimetric assays to measure endogenous glucose, lactate, pyruvate, glutamate and glycerol. In this way microdialysis has been used to monitor glucose delivery and the balance between aerobic and anaerobic metabolism using the ratio of lactate to pyruvate (L/P ratio). When exogenous ^{13}C labelled substrates have been administered to the patient via retromicrodialysis or intravenously the surplus microdialysate in the vial left after bedside analysis can be pooled and analysed via high resolution NMR to detect concentrations of substrates that are not detectable by *in-vivo* MRS.

3 Rationale for Study

A need for better understanding of energy metabolism in the injured human brain.

Energy metabolism in the human brain is still incompletely understood. ^{13}C MRS infusion studies have elucidated the kinetics of glucose uptake, glycolysis and the TCA cycle in the healthy brain, and recently in aging ¹⁴. However, following acute severe traumatic brain injury, a complex (and variable) sequence of pathological processes arise, in which cerebral energy perturbations appear to play a major role. These pathologies evolve over the scale of hours and days, and, despite treatment, may lead to a range of clinical outcomes from good recovery to varying degrees of disability or even death. Historically, attention focussed on raised pressure and ischaemia, i.e. a deficiency in supply of oxygen, glucose and other blood-borne nutrients, falling short of the metabolic demands of the injured brain. Now with protocol driven therapy gross ischaemia and raised intracranial pressure is managed so that adequate cerebral perfusion is maintained. Despite this, a failure of brain metabolism is often seen in patients with acute severe TBI manifested as a high L/P ratio despite adequate brain perfusion. There is some evidence to suggest that the metabolic dysfunction may centre around mitochondrial function. Our study will determine how TBI affects different stages of metabolism – flux through glycolysis and the TCA cycle using ^{13}C MRS and the exchange of high energy phosphates using ^{31}P MRS – allowing future therapies to target metabolic dysfunction and optimise clinical outcome.

Previous studies of brain metabolism in acute severe TBI have used awake, healthy volunteers as comparisons. The significant confounding factor of sedative/anaesthetic use in these patients has had to be accepted or ignored. By studying healthy volunteers under the effects of general anaesthesia a more meaningful comparison and better understanding of brain metabolism perturbation in acute severe TBI can be made. Additionally, the mechanism of action of general

anaesthetics and their effects on the human brain are not well understood. Using ^{31}P MRS and ^{13}C MRS to identify changes in metabolic flux caused by general anaesthesia in healthy volunteers is in itself relevant to all surgery and anaesthesia.

4 Research objective and purpose

The objective of the proposed study is to use *in vivo* magnetic resonance spectroscopy (MRS) to study the kinetics of the fundamental processes of metabolism; namely glycolysis, the TCA cycle and oxidative phosphorylation / high energy phosphate turnover. Firstly, ^{13}C MRS with concurrent intravenous infusion of ^{13}C labelled substrates will allow the rate of lactate production, the TCA cycle rate and the rate of glutamate/glutamine cycling. ^{31}P MRS will allow changes in the ratios of high energy phosphates PCr and ATP and the flux between these pools to be elucidated. ^1H MRS will complement ^{13}C MRS and ^{31}P MRS allowing further distinction of spectra.

a) Metabolism in uninjured brain

^{13}C MRS and ^{31}P MRS studies on the uninjured brain have only been performed on healthy, awake patients. By performing this study we will discover for the first time how general anaesthesia affects the kinetics of metabolism (rate of glycolysis, the TCA cycle and glutamate-glutamine cycling and high energy phosphate flux) in the human brain. This will also allow, for the first time, a more meaningful comparison for sedated patients with acute severe TBI.

b) Metabolism in the injured brain

Following acute severe TBI we will perform ^{13}C MRS infusion and ^{31}P MRS studies on patients admitted to our neuro-critical care unit. We will identify the pathophysiological effect of TBI on specific steps in brain metabolism, namely changes in the rate of glycolysis, the TCA cycle rate and changes to the coupling of neurons and glia in the rate at which they cycle glutamate and glutamine. We will identify pathophysiological changes in the ratios of high energy phosphates in the traumatised brain and a breakdown in exchange between PCr and ATP. We will compare our findings to age group matched healthy controls in the uninjured brain group.

5 Study Design

5.1 Overall statement of design

This is to be an uncontrolled, non-randomised, observational investigation split into 4 studies that will satisfy the overall objectives described above. Studies will run concurrently.

5.2 Subject selection

60 subjects will be recruited; 20 patients with TBI, 20 patients undergoing surgery for simple spine surgery and 20 healthy controls.

5.2.1 *TBI Patients – metabolism in the injured brain*

TBI patients form a heterogeneous group with different mechanisms of injury resulting in variable intracranial lesions. However, the energy perturbations associated with evolving injury take place at the cellular level and are likely to share common mechanisms. We will study the occipital lobe of patients as this region is often spared from large haematomas, but will be affected by global metabolic dysfunction.

5.2.1.1 *Inclusion and exclusion criteria*

Inclusion Criteria

- Traumatic Brain Injury (moderate–severe) requiring ventilation and intracranial pressure monitoring
- Aged 17 years or over

Exclusion Criteria

- Bleeding diathesis
- Patient unlikely to survive more than 24 hours
- Diabetes mellitus

5.2.2 *Simple Spine Surgery Patients – metabolism in uninjured anaesthetised brain*

We regularly perform elective cranial and spine surgery in our department and our team have extensive experience transferring anaesthetised patients to our adjacent MRI suite for advanced imaging. We will choose young patients with no significant co-morbidities who are already having a general anaesthetic for simple spine surgery so that the total anaesthetic time will remain short. Patients will be recruited from outpatient clinic: the treating neurosurgeon will offer the patient a discussion with the research team, if they agree a research team member will discuss the study with them for potential recruitment.

5.2.2.1 *Inclusion and exclusion criteria*

Inclusion Criteria

- Simple spine surgery (lumbar or cervical).
- Simple peripheral nerve surgery.
- Aged 17 to 70 years old.

Exclusion Criteria

- Significant co-morbidities including diabetes mellitus
- ASA grade > II.
- All female patients of child bearing age will undergo pregnancy testing and will be excluded from the imaging arm of the study if the test is positive
- Subjects with non-MR compatible implants
- Patients with previous significant head injury requiring hospitalisation or other CNS pathology

5.2.3 *Healthy control subjects – metabolism in uninjured awake brain*

We have experience recruiting and performing MRI & MRS scans on healthy volunteers at the WBIC. Volunteers will be recruited from our local department using email advertisements, and from known healthy volunteers who have contributed to previous studies and made known they are happy to be approached again in the future for new studies.

5.2.3.1 *Inclusion and exclusion criteria*

Inclusion Criteria

- Aged 17 years or over

Exclusion Criteria

- Significant co-morbidities including diabetes mellitus
- All female patients of child bearing age will undergo pregnancy testing and will be excluded from the imaging arm of the study if the test is positive
- Subjects with non-MR compatible implants
- Patients with previous significant head injury requiring hospitalisation or other CNS pathology

5.3 Overall number of subjects

Patients will be allocated, non-randomly, to the following groups depending on their clinical presentation with either TBI as an emergency or for simple spine surgery (most commonly electively). The individual study groups are overlapping such that data collected from some of the subjects will be used in the testing of more than one hypothesis (see specific study objectives in section 7).

Table 1. Subject allocation

	Traumatic brain injury patients	Healthy controls under general anaesthesia (spinal surgery)	Awake healthy controls
Study 1	10	10	10
Study 2	10 [§]		
Study 3	10	10	10
Study 4	20*	20*	20*
Total no. of subjects	20	20	20

[§]The patients from study 2 will be the same patients that are part of study 1.

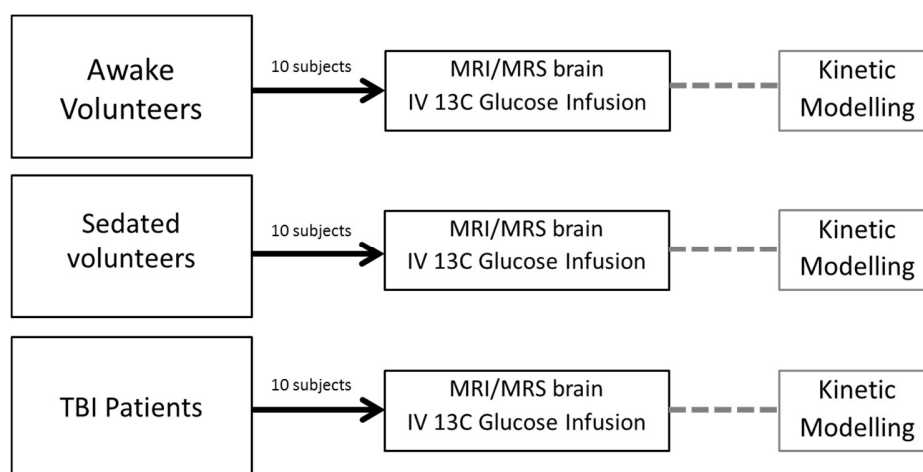
*The subjects from study 4 will comprise of the patients recruited to Study 1 and Study 3.

5.4 Sample size determination

As this is an observational, non-interventional study, a formal sample size calculation is not appropriate. The proposed sample size is based on pilot studies and previous studies performed in this unit and elsewhere. The sample sizes selected here will allow robust inferences about the mechanisms under investigation without confounding from individual variability.

6 Individual Studies

6.1 Study 1 – Measuring the TCA cycle rate (V_{TCA}), glutamate/glutamine cycling (V_{cycle}) and the appearance of lactate ($V_{lactate}$) in TBI and general anaesthesia.



6.1.1 Hypotheses

TBI impedes brain metabolic function, particularly the TCA cycle, and disrupts normal glutamate/glutamine cycling when compared to sedated healthy brain. The metabolic rate and glutamate/glutamine cycling is reduced in healthy brain under general anaesthesia.

6.1.2 Primary Objectives

Assess V_{TCA} , V_{cycle} and $V_{lactate}$ in patients suffering from acute severe TBI, healthy volunteers under general anaesthesia and awake volunteers using ^{13}C MRS during an infusion of ^{13}C enriched glucose.

6.1.3 Primary Endpoint

The primary endpoints will be measures of lactate, glutamate and glutamine peaks on continuously acquired ^{13}C MRS spectra.

6.1.4 Selection of subjects

30 subjects will be recruited; divided equally between injured brain, uninjured sedated brain and uninjured awake brain groups.

6.1.5 Infusion and Sampling Schedule

Uninjured Brain Groups

Healthy patients undergoing planned simple spine surgery will be anaesthetised and taken for surgery as usual. Immediately post-operatively they will be taken for an MRI in the WBIC (in the same department). Awake healthy volunteers will have peripheral intravenous catheters placed by medically trained personnel for infusion and blood sampling.

Subjects will have an infusion of ^{13}C enriched glucose for 2 hours, during which MRS and MRI data will be acquired. They will have a small volume of blood taken serially during the infusion to track blood glucose and calculate the ^{13}C glucose enrichment in the blood (sample analysed

afterwards using high resolution NMR). Baseline insulin and cortisol will also be performed with a save serum that will be kept in the academic neurosurgery department. A Bispectral index (BIS) recording will be performed to calibrate depth of anaesthesia and brain electrical activity in sedated patients and awake volunteers. Patients will be recovered from anaesthesia as standard in our hospital. Further specification see **IV Infusion Regime** and **IV sampling**.

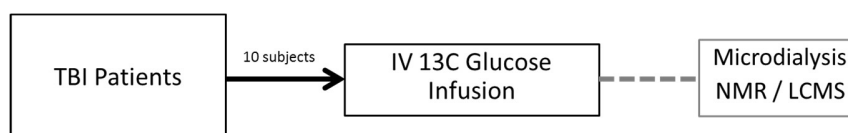
TBI Group

Patients admitted with TBI will be transferred to the WBIC adjacent to the NCCU where they will have an infusion of ^{13}C enriched glucose for 2 hours, during which MRS and MRI data will be acquired. They will have a small volume of blood taken serially during the infusion to track blood glucose and calculate the ^{13}C glucose enrichment in the blood (sample analysed afterwards using high resolution NMR). Baseline insulin and cortisol will also be performed with a save serum that will be kept in the academic neurosurgery department. During anaesthesia a Bispectral index (BIS) recording will be performed to calibrate depth of anaesthesia and brain electrical activity. Any clinically relevant MR imaging that is required will also be performed. Patients will then be returned to the NCCU for continued clinical care.

6.1.6 Assessment at 6 months

TBI patients will be followed up at 6 months. A standard questionnaire survey will be employed utilising standardised outcome measures (SF-36 and Glasgow Outcome Score).

6.2 Study 2 – The proportion of TCA cycle anaplerosis in TBI



6.2.1 Hypothesis

TBI influences the proportion of glucose entering the TCA cycle via anaplerosis.

6.2.2 Primary Objectives

Determine the proportion of glucose entering the TCA cycle via acetyl CoA and that entering via anaplerosis as oxaloacetate ‘top up’ using high resolution NMR spectroscopy and LC-MS of pooled microdialysis samples after IV infusion with ^{13}C enriched glucose for **Study 1**.

6.2.3 Primary Endpoint

The primary endpoints will be measures of the relative proportions of 4,5- $^{13}\text{C}_2$ glutamine to 2,3- $^{13}\text{C}_2$ glutamine in recovered microdialysis during and after IV ^{13}C glucose infusion using high resolution NMR spectroscopy of recovered samples.

6.2.4 Selection of subjects

10 patients with TBI will be recruited.

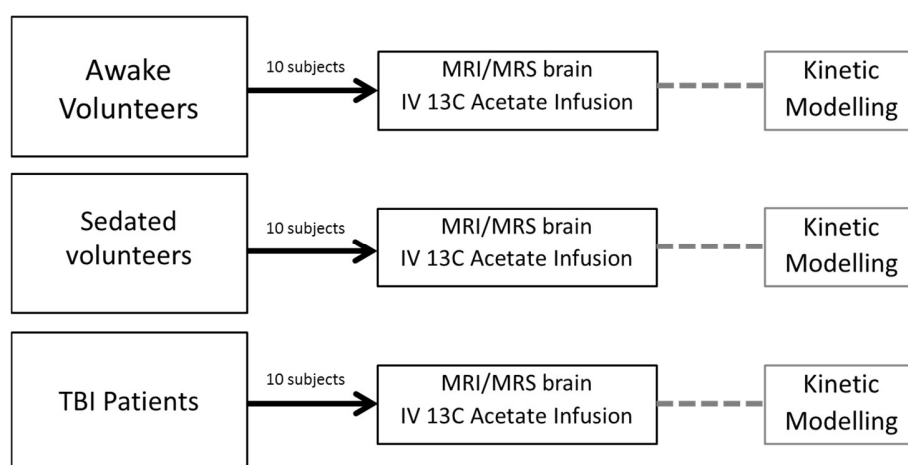
6.2.5 *Microdialysis schedule*

Patients admitted with TBI will have a microdialysis catheter inserted into non-contused brain either at the time of surgery for a traumatic lesion or through cranial access devices inserted on the NCCU. The catheter will be connected to perfusion pumps on the NCCU and perfused with standard CNS perfusion fluid. During and after ^{13}C enriched glucose IV infusion the recovered microdialysis samples will be pooled for NMR/LC-MS analysis.

6.2.6 *Assessment at 6 months*

TBI patients will be followed up at 6 months. A standard questionnaire survey will be employed utilising standardised outcome measures (SF-36 and Glasgow Outcome Score).

6.3 Study 3 – Measuring the TCA cycle rate (V_{TCA}) and glutamate/glutamine cycling (V_{cycle}) in glia under general anaesthesia and TBI.



6.3.1 *Hypotheses*

TBI impedes brain metabolic function of both neurons and glia, particularly the TCA cycle, and disrupts normal glutamate/glutamine cycling when compared to sedated healthy brain. Glutamate/glutamine cycling is reduced in healthy brain under general anaesthesia.

6.3.2 *Primary Objectives*

Assess V_{TCA} and V_{cycle} of glia in patients suffering from acute severe TBI, healthy volunteers under general anaesthesia and awake volunteers using ^{13}C MRS during an infusion of ^{13}C enriched acetate; a glia specific substrate.

6.3.3 *Primary Endpoint*

The primary endpoints will be measures of glutamate and glutamine peaks on continuously acquired ^{13}C MRS spectra.

6.3.4 *Selection of subjects*

30 patients will be recruited; divided equally between injured brain, uninjured sedated brain and uninjured awake brain groups.

6.3.5 *Infusion and Sampling Schedule*

Uninjured Brain Groups

Healthy patients undergoing planned simple spine surgery will be anaesthetised and taken for surgery as usual. Immediately post-operatively they will be taken for an MRI in the WBIC (in the same department). Awake healthy volunteers will have peripheral intravenous catheters placed by medically trained personnel for infusion and blood sampling.

Subjects will have an infusion of ^{13}C enriched acetate for 2 hours, during which MRS and MRI data will be acquired. They will have a small volume of blood taken serially during the infusion to calculate the ^{13}C acetate enrichment in the blood (sample analysed afterwards using high resolution NMR). Baseline insulin and cortisol will also be performed with a save serum that will be kept in the academic neurosurgery department. A Bispectral index (BIS) recording will be performed to calibrate depth of anaesthesia and brain electrical activity in sedated patients and awake volunteers. Patient will then be recovered from anaesthesia as standard in our hospital. Further specification see **IV Infusion Regime** and **IV sampling**.

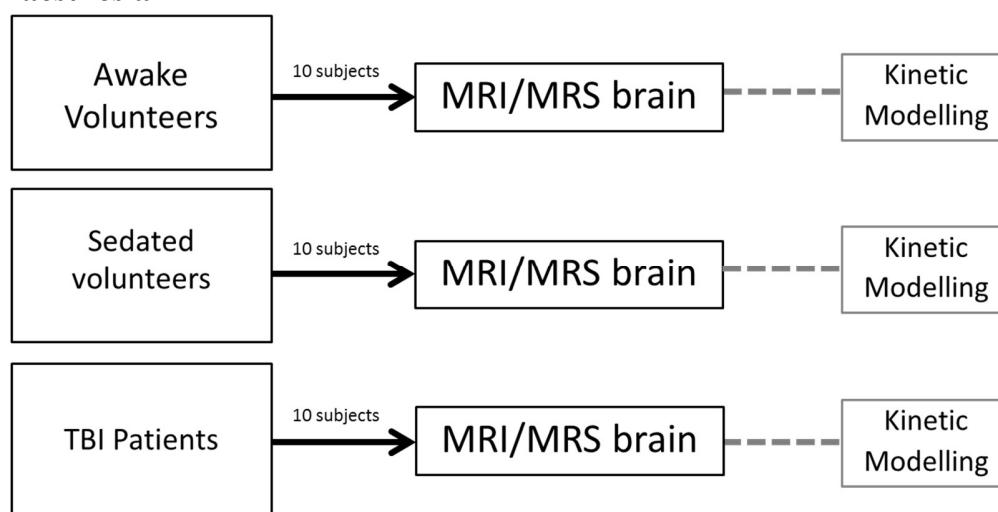
TBI Group

Patients admitted with TBI will be transferred to the WBIC adjacent to the NCCU where they will have an infusion of ^{13}C enriched acetate for 2 hours, during which MRS and MRI data will be acquired. They will have a small volume of blood taken serially during the infusion to calculate the ^{13}C acetate enrichment in the blood (sample analysed afterwards using high resolution NMR). Baseline insulin and cortisol will also be performed with a save serum that will be kept in the academic neurosurgery department. During anaesthesia a Bispectral index (BIS) recording will be performed to calibrate depth of anaesthesia and brain electrical activity. Any clinically relevant MR imaging that is required will also be performed. Patients will then be returned to the NCCU for continued clinical care. Further specification see **IV Infusion Regime** and **IV sampling**.

6.3.6 *Assessment at 6 months*

TBI patients will be followed up at 6 months. A standard questionnaire survey will be employed utilising standardised outcome measures (SF-36 and Glasgow Outcome Score).

6.4 Study 4 – Measuring high energy phosphorus flux in TBI and General Anaesthesia



6.4.1 Hypothesis

TBI impedes the high energy phosphates exchange in the human brain and reduces the pool of available adenosine nucleotide bases resulting in a change in the PCr / ATP ratio and flux of phosphate between PCr and ATP when compared to healthy sedated volunteers. General anaesthesia of healthy brain results in a reduction in flux between PCR and ATP when compared to awake, healthy brain.

6.4.2 Primary Objectives

Determine differences in the PCr / ATP and PCr / Pi ratio and flux between these three species in the brains of patients suffering from acute severe TBI, healthy volunteers under general anaesthesia and awake volunteers using ^{31}P MRS and the magnetisation transfer technique.

6.4.3 Secondary Objectives

Determine differences in the pH of the brain of patients suffering from acute severe TBI, healthy volunteers under general anaesthesia and awake volunteers using ^{31}P MRS and blood gas analysis.

6.4.4 Primary Endpoint

The primary endpoints will be measures of PCr, ATP and Pi peaks using in vivo ^{31}P MRS and ^1H MRS.

6.4.5 Secondary Endpoint

The secondary endpoint will be measuring of chemical shift of the Pi peak using in vivo ^{31}P MRS and blood gas analysis of arterial/venous blood from intravascular catheters of subjects.

6.4.6 Selection of subjects

30 subjects will be recruited; divided equally between injured brain, uninjured sedated brain and uninjured awake brain groups.

6.4.7 *Imaging Schedule*

Uninjured Brain Groups

Healthy patients undergoing planned simple spine surgery will be anaesthetised and taken for surgery as usual. Immediately post-operatively they will be taken for an MRI in the WBIC (in the same department) as part of **Study 1** and **Study 3**. Awake healthy volunteers will have peripheral intravenous catheters placed by medically trained personnel for infusion and blood sampling.

Subjects will have a ^{31}P MRS scan performed to interrogate high energy phosphates including ATP in the brain either prior to, or after infusion of ^{13}C enriched glucose or acetate. A Bispectral index (BIS) recording will be performed to calibrate depth of anaesthesia and brain electrical activity in sedated patients and awake volunteers, as described earlier in **Study 1** and **Study 3**. A blood gas analysis of PCO_2 and pH will be performed from indwelling venous catheters, or arterial catheters when present. Patients will be recovered from anaesthesia as standard in our hospital.

TBI Group

Patients admitted with TBI will be transferred to the WBIC adjacent to the NCCU where they will have a ^{31}P MRS scan performed to interrogate high energy phosphates including ATP in the brain either prior to, or after infusion of ^{13}C enriched glucose or acetate. A blood gas analysis of PCO_2 and pH will be performed from indwelling venous catheters or arterial catheters where available. During anaesthesia a Bispectral index (BIS) recording will be performed to calibrate depth of anaesthesia and brain electrical activity. Any clinically relevant MR imaging that is required will also be performed. Patients will then be returned to the NCCU for continued clinical care.

6.4.8 *Assessment at 6 months*

TBI patients will be followed up at 6 months. A standard questionnaire survey will be employed utilising standardised outcome measures (SF-36 and Glasgow Outcome Score).

6.5 Study duration

Uninjured brain group

'Healthy brain' patients recruited undergoing simple spine surgery will be recovered from their general anaesthetic as normal in our hospital and then return to the ward. They will have continuous blood glucose monitoring after cessation of the glucose infusion to prevent any hypoglycaemic episodes occurring in the immediate period after the study. After discharge they will have no further involvement in the study. These patients will receive routine clinical follow-up for their primary spinal pathology.

Awake healthy volunteers will be offered a meal/snack after cessation of their glucose infusion and blood glucose monitoring for a brief period. They will not require further follow up unless significant unexpected pathology is identified on structural MR imaging. If this occurs they will be seen in a dedicated clinic by a Neurologist for discussion and advice for further investigations or management.

TBI group

TBI patients with microdialysis catheters will undergo a period of microdialysis monitoring for however long their clinical monitoring is required. All TBI patients will be followed up in the

neurotrauma (PJ Hutchinson/I Timofeev) or Neurosciences Critical Care Unit (DK Menon) follow-up clinics at 6 months. A standard questionnaire survey will be employed utilising standardised outcome measures (SF-36 and Glasgow Outcome Score).

7 Selection and withdrawal of subjects

The patient population in the study includes those suffering a moderate-severe TBI, those undergoing surgery for simple spine pathology (such as degenerative disc disease) and healthy volunteer controls. Specific inclusion and exclusion criteria are described above for each of the groups.

7.1 Subject withdrawal criteria

A subject may choose to withdraw from the study at any point. Identifiable data already collected with consent would be retained and used in the study. No further data or tissue would be collected or any other research procedures carried out on or in relation to the participant. TBI patients and spine patients would still be invited to attend their routine clinical follow up appointment but any data collected here would not be used in the study.

8 Infusion, MRS and microdialysis regimes

8.1 IV infusion & sampling regime

Healthy volunteers will have two intravenous cannulas inserted for sampling and infusion of ubiquitously labelled ($^{13}\text{C}_6$) glucose or 1- ^{13}C acetate. Patients undergoing spinal surgery or suffering from TBI will already have sufficient intravascular access for the study. However, if a patient undergoing spinal surgery does not have an arterial line one will be inserted.

Acetate or glucose will be infused to achieve sufficient fractional enrichment in subjects and then maintained for the duration of the study. Total serum glucose will be measured during the study to guide the infusion rate and ensure safety. As acetate is normally found in the blood at trace concentrations and there is no real-time bedside test for serum acetate it will be measured after the scan using high resolution NMR of processed samples.

A blood test to measure baseline cortisol and endogenous insulin will also be performed and a save serum sample stored for future analysis, as required.

8.2 Microdialysis & NMR analysis

TBI patients who already have microdialysis catheters for clinical monitoring will continue their normal microdialysis regime, but the excess microdialysate will be pooled and sent for high resolution NMR analysis to determine the labelling pattern of glutamate and glutamine in the extracellular space in the University Chemistry Laboratory. To quantify ^{13}C signals of glutamine (C4, C3 and C2 positions as markers of TCA cycle activity) we will integrate them relative to an internal standard, with reference to calibration curves for each ^{13}C signal of standard glutamine (plus internal standard) run under identical NMR conditions. Similarly, we will quantify ^{13}C signals from other metabolites (e.g. lactate), with individual calibration for each ^{13}C signal within each species. Additional molecular structural characterisation will, where appropriate, be obtained by powerful 2-dimensional NMR techniques (e.g. HSQC and DQFCOSY), which we have successfully tested on microdialysates (unpublished). Spin echo difference NMR will also be employed to distinguish between ^{13}C labelled and unlabelled species where appropriate. We will take into account natural abundance of ^{13}C (1.1% of all carbon atoms).

8.3 MRS

In vivo Magnetic Resonance Spectroscopy (^1H , ^{13}C , ^{31}P MRS) and MRI studies will be performed in the Wolfson Brain Imaging Centre on a 3T Siemens system to measure metabolic kinetics in an appropriately selected region of subjects' brains. We will use ^{13}C MRS to measure the flux of glucose through glucose uptake and glycolysis by measuring the appearance of lactate, the TCA cycle by the appearance of glutamate, and the rate of glutamate/glutamine cycling by the relative appearance of glutamine and glutamate. We will use in vivo ^{31}P MRS to determine the oxidative phosphorylation status by measuring the ratios of phosphocreatine, ATP and inorganic phosphate, and calculate the pH of the brain parenchyma. We will also use the magnetization transfer technique to measure the kinetics of exchange between these high energy phosphorus species¹⁵. ^1H MRS will be used to help delineate species that share similar ^{13}C spectra such as the fifth carbon position in glutamate and the first carbon position in lactate. Routine WBIC clinical MRI will be performed in all patients to select regions of interest, resolve white matter and grey matter proportions within these regions and burden of radiological injury.

8.4 Data analysis

MRS spectra data will be processed and analysed using standard methods. The peak heights of glutamate and several other metabolites in the spectrum will be measured and compared to the peak height of creatine for purposes of quantification. Time courses of glutamate/glutamine cycling will be fitted using a 2-compartment metabolic model of brain metabolism that includes glutamatergic neurons, and astrocytes. The model will be expressed as differential equations by Cwave software¹⁶ and fitted to the data. Cwave is a package to interface between metabolic flow schemes and the equations of mass and isotope balance that are used to determine isotopic labeling time courses, including statistical considerations of non-normal parameter distributions.

9 Other study procedures and assessments

9.1 Patient recruitment

Treating clinicians employed by Cambridge University Hospitals NHS Foundation Trust will identify patients who are eligible for this study and notify research team members. Once identified, research team members will approach patients to seek informed consent or, when appropriate, a relative, friend or carer to act as a personal consultee. In the case where no relative, friend or carer can be identified during the patient's admission to NCCU despite reasonable steps to do so, a clinician responsible for the patient who is prepared to be consulted but has no connection to the study will be consulted in their stead (As per Section 32 of the Mental Capacity Act 2005).

9.2 Baseline data

All subjects will have medical history, clinical examination and routine investigation details recorded from the medical notes. The following are to be recorded:

- a) Sex
- b) Age and date of birth
- c) Weight and BMI
- d) Any significant past medical history

- e) For TBI patients their clinical presentation including presenting Glasgow Coma Scale and pupillary abnormalities
- f) TBI clinical parameters including intracranial pressure, cerebral perfusion pressure, mean arterial pressure, oxygenation
- g) For patients their full blood count (including platelets and differential white cell count), biochemical series (including glucose, urea, creatinine, uric acid, electrolytes, calcium, alkaline phosphatase, AST)
- i) Radiological information – e.g. traumatic lesion size and location in TBI
- j) Trauma scoring system data for TBI patients (APACHE II, Rotterdam, ISS)

10 Assessment of Safety

As a team with extensive experience performing MRI scans on critically ill patients and managing intravenous infusions the risks of the study to subjects will be kept to a minimum. Nonetheless, four specific areas of risks include general anaesthesia and patient transfer, infusion of glucose/acetate, and vascular access/blood taking.

TBI patients will be under general anaesthesia/sedated during and after our study as part of their treatment for acute severe TBI so this will not be influenced by our study. Patients undergoing simple spinal surgery will already require a general anaesthetic for their primary pathology in our department; which is the reason for choosing this subject group. The study will prolong the duration of their overall anaesthetic, but to no more than to the duration of modestly complex spinal procedures that we frequently perform in our department. Nonetheless, we will only recruit healthy patients with no significant past medical history and considered to be low risk of anaesthetic so that they are not affected by the increased duration of anaesthesia. The Wolfson Brain Imaging Centre is adjacent to NCCU and directly below neurotheatres to facilitate the transfer of patients between these places.

Glucose infusion will be performed by a physician with close monitoring of blood sugar. A standardised initial higher infusion rate will be employed (see Study Guidelines) to obtain sufficient blood fractional enrichment followed by a more modest hyperglycaemia for the majority of the study. At the end of the study blood sugar monitoring will continue and the glucose infusion will be gradually decreased to avoid rebound hypoglycaemia. TBI patients will have continued intensive monitoring of their blood sugar and other parameters as part of their routine clinical care. Otherwise healthy patients undergoing simple spinal surgery and awake volunteers will have continued monitoring of blood sugar for a 2 hours after normoglycaemia has been achieved. Once a steady state of normoglycaemia has been achieved there should be no further effects of the glucose infusion. Short term acetate infusion at a low dose in our study is generally considered safe and does not require any specific additional monitoring^{17,18}. Nonetheless we will employ the same monitoring regime of patients receiving acetate as those receiving glucose.

A small volume of blood will be taken from all subjects to monitor blood glucose and analyse fractional enrichment of labelled substrate in the blood. This will be in the order of ~ 30 mls; a volume that will not have any deleterious effect on patients with TBI, those undergoing simple spine surgery, or awake healthy volunteers. Blood sampling and the infusion of glucose/acetate

will require the insertion of two peripheral intravenous catheters in healthy awake subjects but TBI patients and those undergoing simple spine surgery will already have sufficient vascular access no further vascular catheters will be required.

Given the critical condition of the TBI patients recruited to this study there is an expectation that a proportion of participants will die despite treatment, and that those who survive will have a range of neurological deficits that may be highly disabling. Furthermore, adverse events (e.g. sepsis) are common in this patient group. Reflecting this, an extended period of treatment in the Neurosciences Critical Care Unit and as a ward inpatient is likely. Therefore we will record and report adverse events relevant to the study procedures (transfer to MR, infusion of glucose/acetate and blood taking) and any serious adverse events that occur within 24 hours of the study occurring.

Patients having a general anaesthetic for simple spine surgery will be recruited if they are otherwise healthy so very low risk for all aspects of the study. Occasionally complications as a result of spine surgery unrelated to our study may occur. Only adverse events that may be related to our study will be reported. Any adverse effect of our study would occur straight away so serious adverse events that occur within 48 hours of our study intervention will be reported.

The additional risk to awake healthy volunteers includes discomfort and potential (but unlikely) superficial infection as a result of intravenous cannulation. If any adverse events that are relevant to the study procedure occur they will be reported, but serious adverse events will be reported if they occur within the first 24 hours of the study.

10.1 Definitions

10.1.1 Adverse event

The following adverse events will be reported:

- Respiratory complications as a consequence of prolonged anaesthesia in spinal surgery patients
- Clinically significant hypoglycaemia as a result of glucose / acetate infusion
- Infection from intravenous catheter inserted for the purposes of the study

10.1.2 Serious Adverse Event (SAE)

A SAE will be defined as any event that

- results in death within 48 hours of the study intervention
- leads to a serious deterioration in the health of the patient, user or others and includes:
 - a life threatening illness or injury
 - a permanent impairment to a body structure or function that is not considered to be due to a complication of TBI or spine surgery
 - a condition requiring hospitalisation or increased length of existing hospitalization that is not considered to be due to a complication of TBI or spine surgery
 - a condition requiring otherwise unnecessary medical or surgical intervention and which might have led to death or serious deterioration in health had suitable action or intervention not taken place that is not

considered to be due to a complication of TBI or spine surgery.

- might have led to any of the above

10.2 Evaluation of adverse event

Patients will have regular surveillance as part of normal daily clinical care, and adverse events will be identified as part of this process. Individual adverse events will be evaluated by the Chief Investigator to determine severity and causality, and reported as detailed below.

10.2.1 *Assessment of Severity*

- Mild: The subject is aware of the event or symptom, but the event or symptom is easily tolerated.
- Moderate: The subject experiences sufficient discomfort to interfere with or reduce his or her usual level of activity.
- Severe: Significant impairment of functioning; the subject is unable to carry out usual activities and / or the subject's life is at risk from the event.

10.2.2 *Assessment of Causality*

- Probable: A causal relationship is clinically / biologically highly plausible and there is a plausible time sequence between onset of the AE and the study procedures.
- Possible: A causal relationship is clinically / biologically plausible and there is a plausible time sequence between onset of the AE and the study procedures.
- Unlikely: A causal relation is improbable and another documented cause of the AE is most plausible.
- Unrelated: A causal relationship can be definitely excluded and another documented cause of the AE is most plausible.

10.3 Reporting Procedure

10.3.1 *Adverse Events and Serious Adverse Events*

The Chief Investigator will report adverse events to the Sponsor every 3 months.

The Chief Investigator will report Serious Adverse Events related or probably related to the study interventions, that occur within 24 hours of the study intervention occurring (48 hours in case of simple spine patients), along with the assessment of severity and causality, to the Sponsor as soon as possible within 24 hours of the matter coming to their attention.

10.3.2 *Breaches of Study Protocol*

The Chief Investigator will report serious breaches of the study protocol and/or Good Clinical Practice to the Sponsor within 7 days of the matter coming to their attention.

11 Statistics

11.1 Study Statistician

Statistical analysis will be carried out by the study team, including those at the Magnetic Resonance Research Center, Yale University, CT, USA.

11.2 Statistical methods to be employed for analysis of endpoints

The ^{13}C MRS and ^{31}P MRS measures of metabolic kinetics will be compared between groups. We have little idea of how much these parameters will change in general anaesthesia or TBI.

Kinetic modelling of ^{13}C MRS will be performed in Cwave to simulate a two-compartment model of brain glutamate and glutamine.

Independent t-test and Chi-Square test will be used to determine the difference between awake and sedated healthy volunteers; and sedated healthy volunteers and patients suffering from TBI. Spearman's rank order will be used for correlational analyses. All tests will have significance level set at $p \leq 0.05$.

12 Direct access to source data / documents

The investigators will permit study related monitoring, audits, REC review, and regulatory inspections. The conduct of the research will be reviewed at regular departmental research meetings.

13 Ethical considerations

13.1 Consent

If appropriate, healthy volunteers and patients undergoing simple spine surgery will be asked for their informed consent following full discussion of the protocol and provision of the written information sheet. It is envisaged that patients in the TBI group will not have the mental capacity to consent because of their injury. In this situation advice will be sought from a relative, carer or friend who will act as a personal consultee. If no relative, friend or carer can be identified during the patient's admission to NCCU despite reasonable steps to do so, a clinician responsible for the patient who is prepared to be consulted but has no connection to the study will be nominated as a personal consultee in their stead, as per Section 32 of the Mental Capacity Act (2005). The personal consultee will be asked to consider whether the patient should take part in the study or whether doing so might upset them. They will also be asked about the patient's expressed wishes and attitude towards participation in research. A written information sheet will be provided. If there is agreement that the patient would wish to participate the personal consultee will be asked to sign and date the Declaration Form.

Should the patient later recover capacity to consent a full discussion of the study will be had and written information provided. If the patient wishes to continue follow-up and is willing for any samples collected to be retained for analysis they will sign the Consent Form.

13.2 Ethical committee review

The study protocol is to be seen and approved by the appropriate ethical review committee of Cambridgeshire. Copies of the letters of approval are to be filed in the study file.

13.3 Declaration of Helsinki and ICH Good Clinical Practise

The study is to be carried out in conformation with the spirit and the letter of the declaration of Helsinki, and in accord with the ICH Good Clinical Practice Guidelines

14 Data handling and record keeping

Patient demographics, analysed data and appropriate clinical data will be stored securely on computers within the University Division of Neurosurgery, Department of Clinical Neuroscience, University of Cambridge in a password-protected format in a locked facility. Hard records and copies will also be stored securely in this locked facility. No one outside the direct study team will have access to this data.

Anonymised study samples (eg. Microdialysis and save-serum) will be stored in the Neurochemistry Laboratory, Division of Neurosurgery, University of Cambridge but be identifiable using a unique code.

MRI, MRS and basic patient data will be stored electronically at the WBIC. All information held at the WBIC remains identifiable. It is held securely on password protected servers with access restricted to the relevant research team working in association with members of the WBIC. Data can be downloaded in an anonymised format using the unique WBIC identifier.

Data that is sent to our collaborators in the Magnetic Resonance Research Center, Yale School of Engineering & Applied Science, New Haven, USA will be anonymised so that it is no longer 'patient data', but will still be identifiable by a unique code.

The Principal and Lead investigators will ultimately be responsible for storing all data (electronic and paper) securely in compliance with The Data Protection Act 1998. The WBIC's System Level Security Policy is appended.

15 Financing and Insurance

The study is supported by the Medical Research Council. NHS and University of Cambridge indemnity schemes will apply.

16 Publications policy

Results will be published in the peer reviewed scientific literature and presented at local, national and international scientific conferences.

17 References

1. Pellerin, L. & Magistretti, P. J. Glutamate uptake into astrocytes stimulates aerobic glycolysis: a mechanism coupling neuronal activity to glucose utilization. *Proc. Natl. Acad. Sci. U. S. A.* **91**, 10625–9 (1994).
2. Tyson, R. L., Gallagher, C. & Sutherland, G. R. ¹³C-Labeled substrates and the cerebral metabolic compartmentalization of acetate and lactate. *Brain Res.* **992**, 43–52 (2003).
3. Gallagher, C. N. *et al.* The human brain utilizes lactate via the tricarboxylic acid cycle: a ¹³C-labelled microdialysis and high-resolution nuclear magnetic resonance study. *Brain*

- 132**, 2839–2849 (2009).
4. Muir, D., Berl, S. & Clarke, D. D. Acetate and fluoroacetate as possible markers for glial metabolism in vivo. *Brain Res.* **380**, 336–40 (1986).
 5. Waniewski, R. A. & Martin, D. L. Preferential Utilization of Acetate by Astrocytes Is Attributable to Transport. *J. Neurosci.* **18**, 5225–5233 (1998).
 6. Jalloh, I. *et al.* Focally perfused succinate potentiates brain metabolism in head injury patients. *J. Cereb. Blood Flow Metab.* 0271678X16672665 (2016). doi:10.1177/0271678X16672665
 7. Sibson, N. R. *et al.* Stoichiometric coupling of brain glucose metabolism and glutamatergic neuronal activity. *Neurobiology* **95**, 316–321 (1998).
 8. Wallimann, T., Wyss, M., Brdiczka, D., Nicolay, K. & Eppenberger, H. M. Intracellular compartmentation, structure and function of creatine kinase isoenzymes in tissues with high and fluctuating energy demands: the ‘phosphocreatine circuit’ for cellular energy homeostasis. *Biochem. J.* **281**, 21–40 (1992).
 9. Bellander, B.-M. *et al.* Consensus Meeting on Microdialysis in Neurointensive Care. *Intensive Care Med.* **30**, 2166–2169 (2004).
 10. Timofeev, I. *et al.* Cerebral extracellular chemistry and outcome following traumatic brain injury: a microdialysis study of 223 patients. *Brain* **134**, 484–494 (2011).
 11. Jalloh, I. *et al.* Glycolysis and the pentose phosphate pathway after human traumatic brain injury: microdialysis studies using 1,2-¹³C₂ glucose. *J. Cereb. Blood Flow Metab.* **35**, 111–120 (2015).
 12. Du, F., Cooper, A., Lukas, S. E., Cohen, B. M. & Öngür, D. Creatine kinase and ATP synthase reaction rates in human frontal lobe measured by ³¹P magnetization transfer spectroscopy at 4T. *Magn. Reson. Imaging* **31**, 102–108 (2013).
 13. de Graaf, R. a., Rothman, D. L. & Behar, K. L. State of the art direct ¹³C and indirect ¹H- [¹³C] NMR spectroscopy in vivo. A practical guide. *NMR Biomed.* **24**, 958–972 (2011).
 14. Lin, A.-L. & Rothman, D. L. What have novel imaging techniques revealed about metabolism in the aging brain? *Future Neurol.* **9**, 341–354 (2014).
 15. Befroy, D. E., Rothman, D. L., Petersen, K. F. & Shulman, G. I. ³¹P-Magnetization Transfer Magnetic Resonance Spectroscopy Measurements of In Vivo Metabolism. *Diabetes* **61**, 2669–2678 (2012).
 16. Mason, G. F. CWave: Software for the Design and Analysis of ¹³C Labeling Studies Performed In Viva. *Proc. Intl. Sot. Mag. Reson. Med.* **8**, 1870 (2000).
 17. Chioléro, R. *et al.* Effects of infused sodium acetate, sodium lactate, and sodium beta-hydroxybutyrate on energy expenditure and substrate oxidation rates in lean humans. *Am. J. Clin. Nutr.* **58**, 608–13 (1993).
 18. Suarez, J. I. *et al.* Administration of hypertonic (3%) sodium chloride/acetate in hyponatremic patients with symptomatic vasospasm following subarachnoid hemorrhage. *J. Neurosurg. Anesthesiol.* **11**, 178–84 (1999).

- Appendix 3 – Interrogating Metabolism Kinetics in the Human Brain Research Ethics Application